Villanova University

The Graduate School

Department of Civil and Environmental Engineering

AN INFILTRATION ANALYSIS OF THE VILLANOVA POROUS CONCRETE INFILTRATION BASIN BMP

A Thesis in

Civil Engineering

by

Andrea M. Braga

Submitted in partial fulfillment

of the requirements

for the degree of

Master of Science in Water Resources

and Environmental Engineering

September 2005

AN INFILTRATION ANALYSIS OF THE

VILLANOVA POROUS CONCRETE INFILTRATION BASIN BMP

By

Andrea M. Braga

September 2005

Robert G. Traver, Ph.D., P.E. Faculty Advisor Associate Professor of Civil and Environmental Engineering	Date
Ronald A. Chadderton, Ph.D., P.E. Chairman, Department of Civil and Environmental Engineering	Date
Barry C. Johnson, Ph.D., P.E. Dean, College of Engineering	Date

Acknowledgements

I would like to begin by thanking my mother and father for their continued faith, love and support throughout my collegiate endeavors, without which this could not have been possible. I would also like to thank my siblings, Steven, Christina, Cynthia, and Kevin for the competitive nature taken in all activities, scholastic among others, and from which I attained the drive and determination to perform to my highest potential. To my family, I love you, and cannot begin to express my gratitude for all you have provided for me.

I would like to extend my thanks to the EPA and the PaDEP for making this project financially possible. The project was funded by a grant from the EPA Section 319 Non-point Source Pollution Program through the PaDEP.

I owe a great deal to everyone in the Civil Engineering Department at Villanova University who have guided me throughout both my undergraduate and graduate time here at Villanova and who, through their own research, comments and questions have encouraged, supported and enlightened me. Specifically I would like to offer the utmost appreciation to Dr. Robert Traver, my advisor, for giving me this opportunity and whose knowledge and guidance have been invaluable throughout my college experience.

I would like to extend a special thank you to Clay Emerson and Michael Horst for their discussions and advice during this process and to Erika Dean, Jordan Emilio, Erika Tokarz, Gregg Woodroof, and Megan Vanacore for all of their assistance throughout graduate school. You have all made my last year at Villanova one to remember.

Abstract

The objective of this study is to find and evaluate what factors influence the infiltration process that occurs in subsurface infiltration basins and to develop a model to predict the process. In the summer of 2002, the common area between two dormitories at Villanova University was retrofitted to create a Porous Concrete Infiltration Basin BMP. The system consists of porous concrete and three infiltration beds filled with coarse aggregate, wrapped in a geotextile filter fabric, and underlain by undisturbed silty sand.

The infiltration performance of the site is the focus of the study. A model was developed using Green-Ampt formula to characterize the infiltration occurring in the basin for both small and large events. The effectiveness and accuracy of the model was measured by comparing the model outputs with observed water surface elevation data recorded from instrumentation on site. It was found that the when the bed depth is shallow (< 4 in) the governing factor affecting hydraulic conductivity and infiltration rate is temperature, with higher rates during warmer temperatures. For events with higher bed depths, the governing factor is the maximum bed depth, although it is proposed that temperature also plays an important role in hydraulic conductivity and infiltration rate. It was also shown during shorter antecedent dry time when the soil has not drained completely between events, the infiltration rates tend to be higher than otherwise expected.

Table of Contents

List of Figures

List of Tables

Chapter 1: Project Overview

1.0 Project Statement

This study focuses on the results of field data collected from the Villanova University Stormwater Partnership's (VUSP) Porous Concrete Infiltration Basin BMP. The objective of this study is to find and evaluate what factors influence the infiltration process that occurs in subsurface infiltration basins and to develop a model to predict the process.

1.1 Introduction

Urbanization has a significant effect on the water quality and quantity of both the ground water sources and the surface water sources of the environment in which it is introduced. With increasing developmental progress, there is a quantifiable decrease in area free to allow stormwater infiltration and recharge into the groundwater table. Instead of entering normally back into the hydrologic cycle through infiltration into the soil, stormwater is forced to bypass this critical step and flow over impervious areas such as parking lots, rooftops, and roadways. This results in a drastic increase in direct runoff into nearby surface waters. These elevated volumes of runoff carry sediments, suspended and dissolved solids, metals, and other toxins to the surface waters. Not only does this adversely affect the ecology and health of the local rivers and streams, but it also has a regional effect, with the potential to cause flooding and erosion and sedimentation miles downstream from the source.

During rain storms and snow melting events the decreased pervious land cover, such as grasslands and wooded areas, and consequent increase in runoff volume, sends stormwater directly to rivers at such high rates that the river systems are unable to

balance the flows. This results in flood events, stream bank erosion, sedimentation, and the ultimate destruction of the natural habitat and overall water quality of the river systems. Infiltrating stormwater locally into the ground instead of discharging it through conventional pipe sewers is increasingly considered as a means of controlling urban stormwater runoff, thereby reducing runoff peaks and volumes, and returning the urban hydrological cycle to a more natural state (Mikkelsen, 1996).

Stormwater Best Management Practices (BMPs) include the concept of source control which establishes a passive system that intercepts pollutants at the source and disposes of stormwater close to the point of the rainfall (Barbosa et al., 2001). These systems are an innovative way to minimize the adverse effects of urbanization by reducing or eliminating runoff from the site. BMPs include detention systems, such as wetlands and wet detention ponds, and infiltration systems. Specifically, there are two types of infiltration systems: surface infiltration and sub-surface infiltration. Surface infiltration systems allow stormwater to permeate green surfaces, such as rain/recharge gardens, swales, and grass trenches. This type of infiltration system is a practice that comes closest to natural infiltration of rainwater, allowing runoff to slowly soak into the soil, thus removing most of the toxins present in the stormwater before it reaches the groundwater table. However, collecting stormwater from impermeable surfaces and spreading it out onto green areas puts high restrictions on the design and land use of urban space, which is often highly limited (Mikkelsen, 1996). Therefore, sub-surface infiltration is the most common type of system used in highly urbanized areas.

Sub-surface infiltration systems typically consist of large cavities dug out of the ground that are then filled with clean stone. Stormwater is stored temporarily in these

cavities in the voids between the stone while it slowly percolates into the surrounding soil. Water can enter the system in a number of ways. Roof drains and inlets directly convey water from the rooftops and surrounding impervious pavement into the bed bottom through perforated piping. However, a new and innovative way to get stormwater runoff into these underground infiltration beds is to have it directly infiltrate through porous pavement. Special mixes of asphalt or concrete are used in these systems to allow the water to soak directly into the underlying bed minimizing the use of inlets and pipes and maximizing the volume of stormwater captured and infiltrated into the ground.

Porous pavement systems with underlying infiltration beds present a new way of looking at development. Instead of limiting the effects of urbanization, porous pavement systems incorporate it into the design while, simultaneously, continuing the process of recharging the groundwater table and returning the water back to its natural place in the hydrological cycle.

Villanova University voluntarily retrofitted an existing paved area on campus with a subsurface structural infiltration BMP. The site functions as a demonstration and research project. Funding for this project was provided by the 319 NPS Grant Program. The site is currently a United States Environmental Protection Agency Non Point Source (NPS) National Monitoring Site, and is providing important data on both the water quality and water quantity aspects for infiltration BMP's (Kwiatkowski, 2004).

1.2 Site Description

The Porous Concrete Infiltration Basin BMP is located on the campus of Villanova University in southeastern Pennsylvania. Villanova University is located in Radnor Township approximately 20 miles west of Philadelphia, PA. The site underlies a

pedestrian area on Villanova's Main Campus between the dormatories of Sheehan Hall and Sullivan Hall (Figure 1).

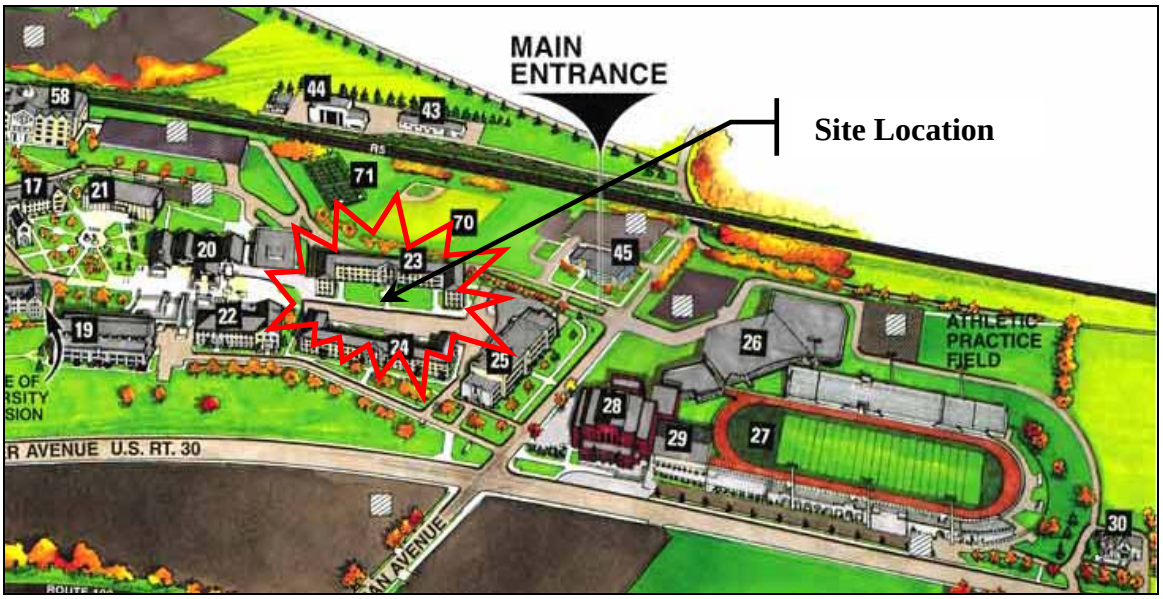

Figure 1. Porous concrete infiltration basin BMP location map

The location was found to be highly suitable for this type of project due to its low level of road traffic, resulting in a low level of potential pollutants and risk of spills. This area of campus is used mainly for foot traffic and recreational use during the year, with the majority of vehicular traffic occurring during the days of move-in and move-out from the Sheehan and Sullivan Hall dormitories.

Geologically, the site is situated on a mix of sand and silty sand, which has a high potential for infiltration. An attempt was made to determine the elevation of the groundwater table in this area, but was unsuccessful. The groundwater table was not encountered within the first 12 ft (3.7 m) below ground surface. Therefore, the attempt to determine the water table elevation was discontinued, because at these depths the site was not seen as a threat for groundwater contamination.

Prior to retrofitting the site with the BMP, the area consisted primarily of a very light traffic road/walking path, several concrete walkways, two dormitories, and assorted grass areas. The general layout of the drainage basin remained essentially the same following the retrofit; however, some surfaces were altered. The impervious surfaces on the site were crowned to direct runoff toward the porous concrete or, in some cases, directly connected to infiltration beds through a system of pipes, as is the case for the roof tops. Figure 2 shows the site prior to, and following, the retrofit (Kwiatkowski, 2004).

Figure 2. Pre (left) and post (right) construction photograph of the porous concrete site

The total drainage area for the BMP is 57,700 square feet, 62% of which (35,850 sq. ft.) is impervious. The impervious areas consist of portions of the dormitory rooftops, concrete walkways, part of an asphalt driveway at the upper end of the watershed, the paving stone border around the porous concrete, and the traditional concrete areas surrounded by the porous concrete. Table 1 summarizes the watershed by surface cover and respective contributing area.

Table 1. Post-construction surface cover areas

Surface Cover	Porous Concrete	Standard Concrete/ Asphalt	Grass/ Mulch Beds	Roof	Total Area	% Impervious
Area (ft^2)	2150	18850	19700	17000	57700	62
Area (m^2)	200	1750	1830	1580	5360	62

Of the remaining 21,850 square feet of the drainage area, 90% or 19,700 square feet is pervious. This area consists of the grass areas located in front of and along the sides of Sheehan and Sullivan Halls. Porous concrete comprises the remaining 10% or 2,150 square feet. Figure 3 is an aerial schematic of the drainage area for the site illustrating the areas that drain to each bed.

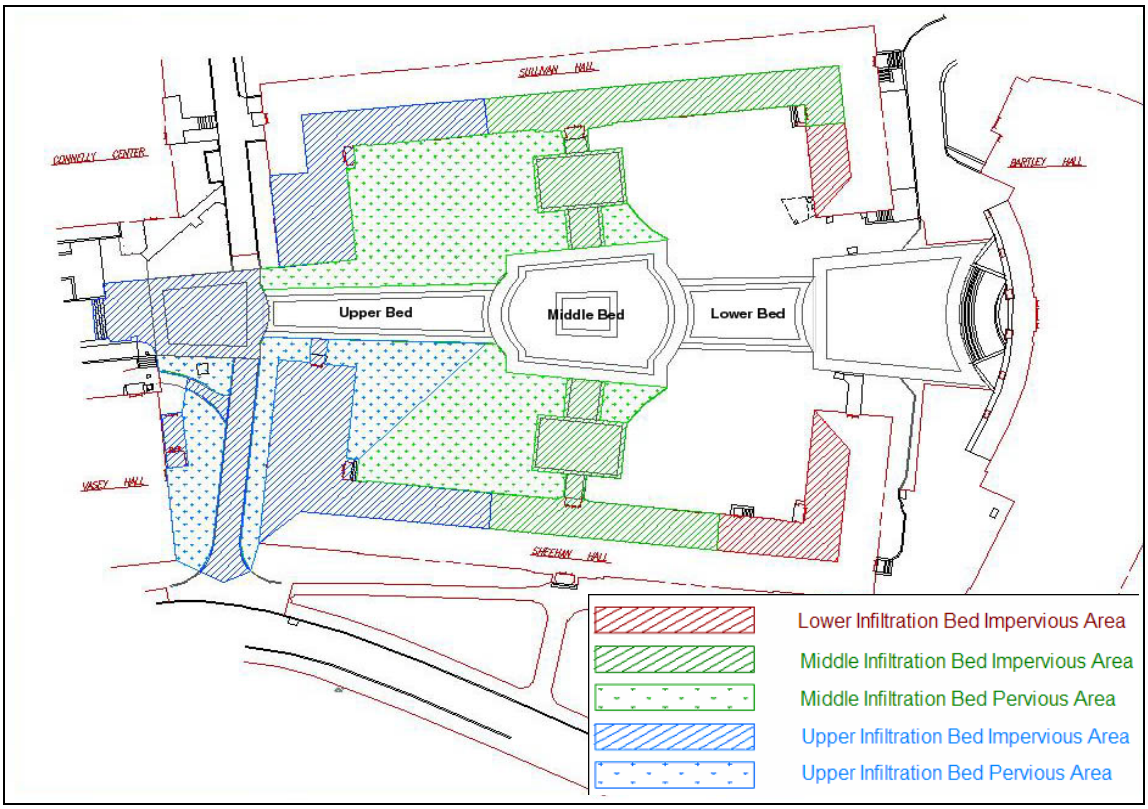

Figure 3. Drainage area schematic of the site

The site is divided into three separate drainage areas, one for each of the underlying infiltration beds. The three drainage areas shown in Figure 3 are divided into impervious and pervious areas contributing to each of the infiltration beds. These contributing areas were established by an evaluation of the grading and sloping of the region in and around the location of the site, and from the location of the roof drains running off of each of the dormitories. During a storm event, water will run off of the impervious walkways and, depending on the magnitude of the storm, the pervious grassland, in addition to being piped directly into the beds via the roof drains and perforated piping. The rain that falls directly onto the porous pavement will soak directly into the bed that it falls upon. It is necessary to note that although there is pervious grassland around the lower infiltration bed, it does not contribute to the stormwater infiltrating the bed. Due to the grading of that region of the site, stormwater is diverted away from the porous concrete and towards the impervious pavement located past the site's drainage area, in front of Bartley Hall. Therefore, the drainage area that contributes to the lower infiltration bed consists solely of the direct runoff from the pavement onsite in addition to the roof drains on Sheehan and Sullivan Halls.

1.3 Porous Concrete Infiltration BMP

The Villanova Porous Concrete Infiltration Basin BMP utilizes porous concrete in conjunction with underlying infiltration beds effectively to return the retrofitted site to its pre-development hydrologic status in terms of both water quality and water quantity. The site is composed of porous concrete, brick pavers, and conventional concrete pavement. The area composed of porous concrete is highlighted in Figure 4.

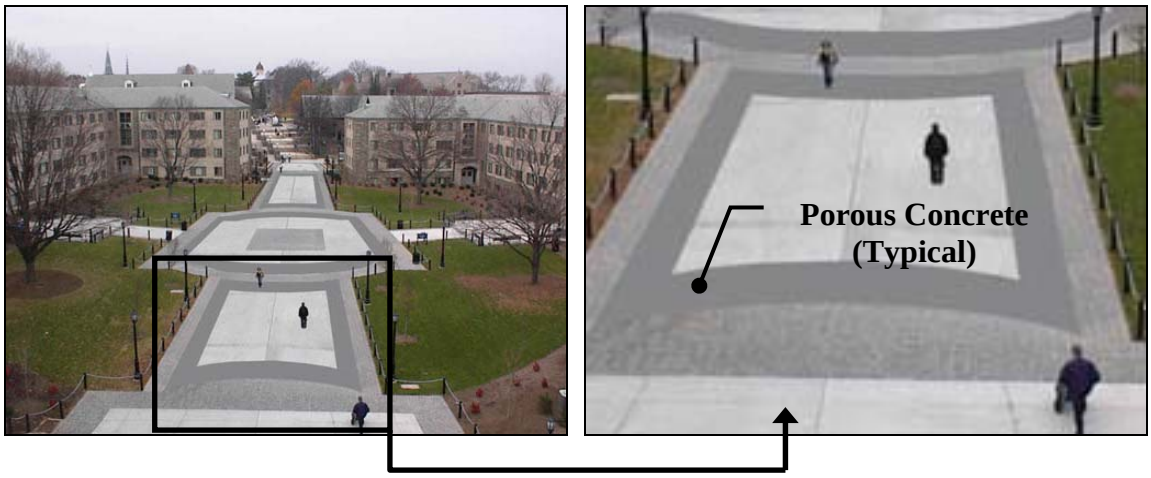

Figure 4. Porous concrete BMP highlighting the porous concrete (dark grey color)

There are two main types of porous pavement, porous asphalt and porous concrete. Porous asphalt consists of an open-graded coarse aggregate bonded together by asphalt cement, while porous concrete consists of a specially formulated mixture of Portland cement, uniform, open-graded coarse aggregate, and water. Since the fine-graded aggregate is removed, both mixtures have sufficient interconnected voids to make them highly permeable to water and allow rapid percolation of water through the pavement (USEPA, 1999). The Villanova BMP utilizes porous concrete in its design due to its gray color and high aesthetic appeal, making it a closer match than porous asphalt to the buildings surrounding the site.

As highlighted in Figure 4, the porous concrete is used only as an outline for the site, under which three infiltration beds lie. The high permeability of the material made it necessary to convert only a small fraction of the area to porous concrete to attain the desired infiltration (Kwiatkowski, 2004). Inside the area outlined by the porous concrete is conventional impervious concrete pavement, with brick pavers laid along the outside border and within the center of the site. The site is crowned at a 1% slope so that during a storm event, stormwater will run off the brick pavers and standard pavement and

permeate the porous pavement, allowing for flow into the infiltration beds and, ultimately, into the underlying soil.

Water passes directly through the porous concrete almost immediately after reaching it. Figure 5 illustrates the ability of the material to convey the water. Once through the porous concrete, the runoff enters one of three infiltration beds, identified in Figure 6 as the upper, middle and lower bed (Kwiatkowski, 2004).

Figure 5. Illustration of the ability of porous concrete to convey water

Figure 6. Infiltration bed locations during and after construction

Cahill Associates of West Chester, PA (Cahill, 2003) completed the hydrologic design for this site in 2001. Cahill conducted percolation tests in mid-September with the finalized design completed shortly thereafter.

The Porous Concrete BMP consists of three large rock infiltration beds arranged in a cascading structure down the center of the site. A profile of the three infiltration beds is shown in Figure 7. In addition to the porous concrete, which acts primarily as a transportation medium allowing runoff on the surface to find its way into the infiltration beds underneath, the rooftop gutters of the adjacent dormitories also drain to the infiltration beds. The downspouts from these gutters are connected to 4-inch (10 cm) High Density Polyethylene (HDPE) pipes which are, in turn, connected directly to the three infiltration beds via perforated piping (Ladd, 2004).

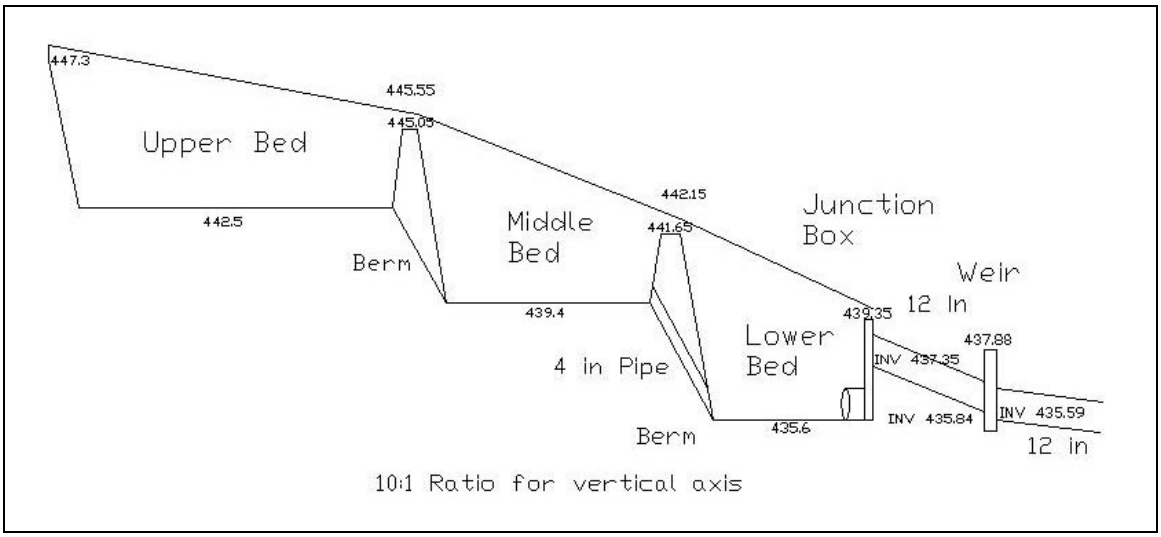

Figure 7. Profile of infiltration beds and overflow pipes

A slot drain located near the top of the site, and a storm drain inlet near Sheehan Hall connect to the upper infiltration bed through a series of 8 in (20 cm) HDPE pipes. The slot drain captures runoff from the concrete area at the top of the site while the storm

drain inlet was designed to capture runoff from the driveway and areas adjacent to the building (Ladd, 2004).

Each of the beds is approximately 3-4 ft (0.9-1.2 m) deep and filled with 3-4 in (7.6-10 cm) diameter clean washed American Association of State Highway and Transportation Officials (AASHTO) No. 2 clean-washed course stone aggregate. The aggregate produces a void space of approximately 40% within the infiltration beds and allows quick percolation to the soil layer beneath. The void space also allows for some storage during events when the infiltration rate from the beds is slower than the rate of stormwater runoff inflow (Kwiatkowski, 2004). At the base of the infiltration beds, directly above the undisturbed native soil and below the stone, is a layer of geotextile filter fabric. This layer provides separation between the stones and soil to prevent any upward migration of fines into the infiltration bed. Allowing fines to migrate upward could eventually lead to a decrease in void space within the beds and alter the effectiveness of the system from a water quantity perspective (Kwiatkowski, 2004). Figure 8 shows the course aggregate stones above the filter fabric for the middle infiltration bed.

Located above the course aggregate is 3 inches (7.6 cm) of AASHTO No. 57 choker stone. These smaller diameter, 2-4 in (5-10 cm), stones provide a solid base for the porous concrete and prevent the porous concrete from seeping into the void spaces of the larger stones during placement. The uppermost, visible layer consists of 6 in (15 cm) of porous concrete. A 4 in (10 cm) HDPE pipe located in the berm between the beds connects the bottoms of the lower two infiltration beds. This allows water to travel down from the middle bed to the lower bed, maximizing the infiltration area.

Figure 8. Middle infiltration bed under construction

Additionally, there are two 6 in (15 cm) HDPE pipes which run along the top of all three beds directly below the choker course. These pipes allow excess water, once bed capacity is reached, to travel down to the bottom of the site and into the existing storm sewer system. This reduces the risk of stormwater rising up through the porous concrete (Ladd, 2004). Figure 9 shows a cross section sketch of an infiltration bed.

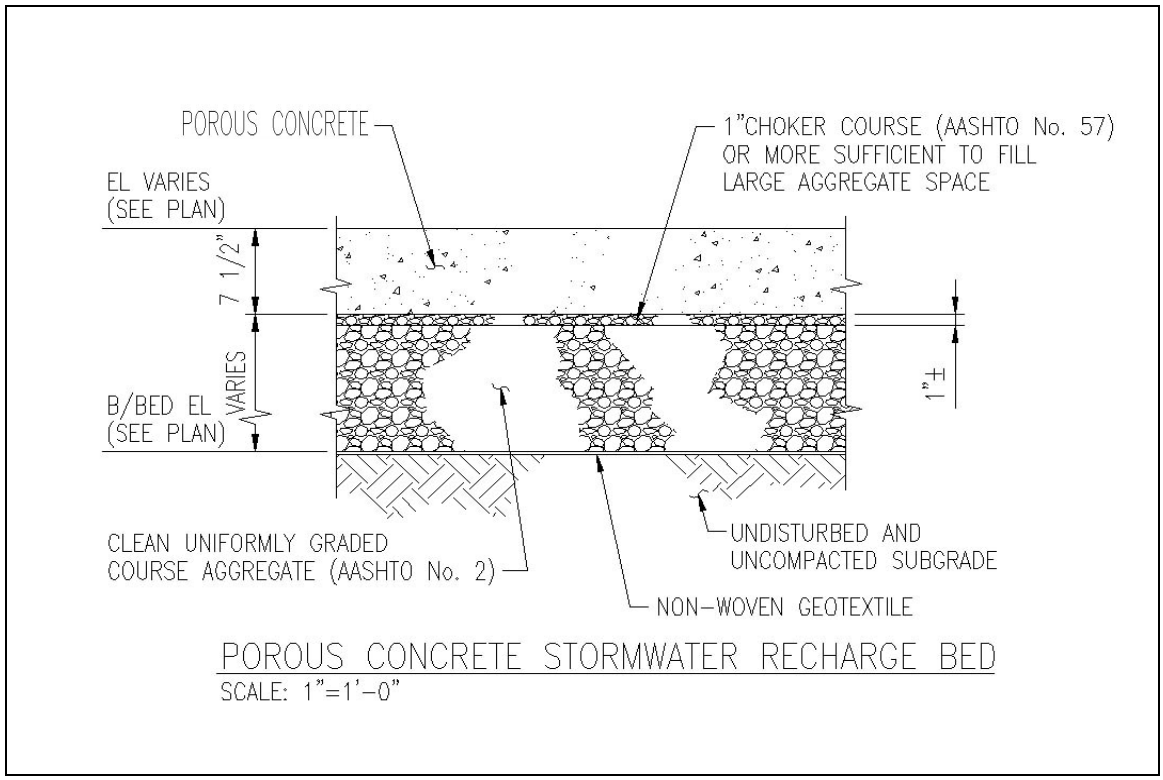

Figure 9. Cross section of an infiltration bed (Cahill, 2003)

The site was designed to store and infiltrate runoff from the first 2 in (5 cm) of a storm event through the use of the three infiltration beds. Storms of this size represent approximately 80% of the annual storm events for this region (Prokop, 2003). Storms with a volume of runoff greater than the design capture volume would still have the first portion captured during the storm event. Once the design capture volume is exceeded, excess stormwater would leave the site through the existing storm sewer system by means of an overflow pipe. This pipe is located in a junction box that is directly adjacent to the bottom corner of the lower infiltration bed. The junction box, Figure 10, serves as an intersecting point for pipes coming from the rooftop gutters and the lower infiltration bed. Overflow from the beds leaves through the overflow pipe that discharges the water into the existing storm sewer system (Ladd, 2004).

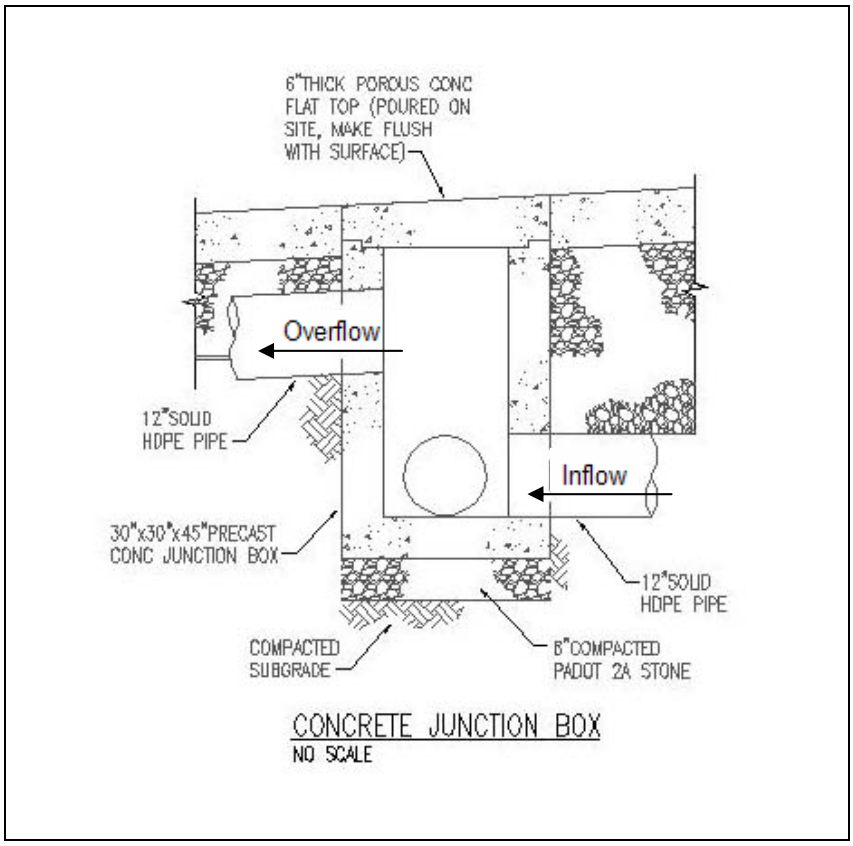

Figure 10. Sketch of junction box (Cahill, 2003)

It is essential to understand how the water moves through the system after it enters the infiltration beds. When a rainstorm or snowstorm occurs, stormwater or snowmelt will be piped from the rooftops and inlets or soak through the porous concrete and collect in the infiltration beds beneath. Infiltration into the soil will then begin; however, this is a slow process. During larger storms, runoff may begin to fill the beds at a rate higher than that of infiltration. The system is specifically designed to handle the excess runoff of larger storms without allowing the beds to fill to capacity and overflow back up through the porous concrete and onto the ground surface. This is accomplished through the construction of the infiltration beds and the outlet structure that discharges excess water from the site.

As shown in Figure 7, the beds are staggered at different depths due to the natural slope of the site. The beds are separated by earthen berms, which prevent continuous flow from bed to bed and allow the water to remain in each bed for infiltration purposes. However, the 4 in (10 cm) diameter pipe placed through the berm connecting the middle and lower beds prevents water from remaining in the middle bed for infiltration. Instead, any runoff that soaks into this bed will immediately be diverted via the pipe to the lower infiltration bed. Contrary to the design plans, the upper bed was not constructed with this overflow pipe, thus forcing all water that is collected through this section of porous concrete and contributing impervious piping to remain in the upper bed for infiltration. The only way for water to exit the upper bed is through the two 6 in (15 cm) HDPE pipes, which run along the top of each bed, directly below the choker course.

In the case of a larger storm event, stormwater will fill the lower bed and begin to discharge through the overflow pipes located in the junction box (Figure 10) to an outlet control structure. The outlet control structure, shown in Figure 11, is connected to the junction box through a 12 in (30 cm) diameter overflow pipe. The outlet structure is controlled by a V-notch weir, which begins to discharge after the lower bed is filled to a depth of 18 in (46 cm). Once the bed fills to the elevation of the overflow pipe, the water enters the pipes and is ultimately discharged into the existing campus storm sewer system.

Figure 11. Weir outlet control structure

1.4 Construction[1]

The initial construction of the Porous Concrete BMP occurred during the summer of 2002. N. Abbonizio Contractors, Inc. of Conshohocken, PA were the contractors for the project. The first phase of construction began on May 20th and involved removing the existing asphalt pavement roadway, curbing, and concrete sidewalks and entrance walkways or the original site, shown in Figure 12.

[1] Portions of this section are taken from Kwiatkowski (2004) and Ladd (2004) Masters Thesis and from Lessons Learned II – Porous Concrete Demonstration Site (Traver et. al, 2005).

Figure 12. Original site before construction

Construction then continued in a sequential order starting at the lower bed closest to Bartley Hall and ending with the upper bed. The boundaries of the infiltration beds were first marked out and the beds were excavated to the required depth and dimensions. A 4 in (10 cm) HDPE pipe was run through the berm connecting the lower and middle infiltration beds and the geotextile filter fabric was laid across the bottom and sides of the beds. The junction boxes, as mentioned in the previous section, were installed in the lower corners of the bottom infiltration bed. Two 12 in (30 cm), 10 in (25.4 cm), and 8 in (20.3 cm) perforated HDPE pipes were laid along the bottom of lower, middle and upper beds, respectively and ultimately connected to the junction boxes. These pipes are used to disperse the water across the whole area of the bed. The beds were then filled with

AASHTO No. 2 clean-washed stone to a depth of approximately 4 ft (1.2 m). The upper infiltration bed, shown in Figure 13, was excavated and filled in the same manner as the lower and middle beds, the only major difference being that there was no pipe placed in the berm connecting the upper and middle beds.

Figure 13. Upper infiltration bed mid-way through construction

Construction of the beds was sequenced so that no heavy equipment came in contact with the undisturbed soil, thus protecting it and preserving its infiltration capacity. The beds were excavated from the sides and no equipment passed over the bottom until each bed had been filled with aggregate. These stones absorbed and dispersed the weight of the vehicles in such a way that no compaction of the underlying soil is expected (Ladd, 2004).

During the construction of the infiltration beds, work was also underway to connect all of the building's downspouts to the infiltration beds. Trenches were dug in front of the two dormitories and 4 in (10.2 cm) HDPE pipes were connected directly to all of the downspouts and ran the length of the buildings, as shown in Figure 14. These pipes were then directly connected to the larger pipes already covered by stone in the infiltration beds by 6 in (15.2 cm) and 8 in (20.3 cm) pipes (Ladd, 2004).

Figure 14. HDPE pipes connecting downspouts

Pouring of the porous concrete began on June 30th 2002. Wooden bracing was laid to act as a framework for the concrete. The original design called for the entire area between the paving stones to be porous concrete. To help strengthen the concrete, an additive called Eco-Creto was used (Eco-Creto, 2004). The Eco-Creto was mixed with

the porous concrete while it was still in the truck. Approximately 3 gallons of Eco-Creto was added to each yard of concrete. After the concrete was compacted, large sheets of plastic were laid over the surface, as shown in Figure 15. These sheets were used to allow the porous concrete to properly hydrate while it was curing (Ladd, 2004).

Figure 15. Plastic sheets covering the porous concrete

There were delays throughout the pour due to problems with the porous concrete material. On some days there were minor problems and work progressed satisfactorily. On others, bad truckloads meant that only a small area could be successfully poured. Pouring of all the porous concrete areas was completed by the middle of August 2002. Some patching was required for areas that did not cure properly. These areas were

removed and replaced with a fresh batch of porous concrete (Ladd, 2004). The completed site is shown in Figure 16.

Figure 16. Completed initial site construction

1.4.1 Reconstruction I

The original site design consisted of three large porous surfaces bordered with decorative pavers, as shown in Figure 16. Unfortunately, the surface of the porous concrete failed shortly after the completion of construction. The failure was caused by a number of elements, the most significant being a lack of understanding of the impact the porous concrete material properties had on construction practice. At the time of construction, this site was the first to use this material in the region. Considerable

knowledge was gained in the initial construction, which would be used in the reconstruction of the surface (Kwiakowski, 2004).

Due to the surface failure, the porous concrete site was redesigned and resurfaced in the spring of 2003, incorporating the lessons learned from the original construction and information from visits to other sites (Traver et al., 2003). Interestingly, despite the poor cosmetic appearance of the failed porous concrete surface, review of initial data and field observations suggested the original site had more than enough porous concrete surface. As a result, it was determined the porous area could be reduced without affecting the site's performance.

The new design was altered to include narrow strips of porous concrete around the perimeter of each bed with conventional concrete replacing the porous concrete in the middle as illustrated Figure 17. The pavers would remain along the perimeter. The conventional impervious concrete in the middle was crowned to promote drainage towards the porous strips along the perimeter. The excellent ability of the porous concrete to transmit water suggested it could handle runoff from areas in addition to that occurring on the porous concrete surface itself. The completed site is shown in Figure 18.

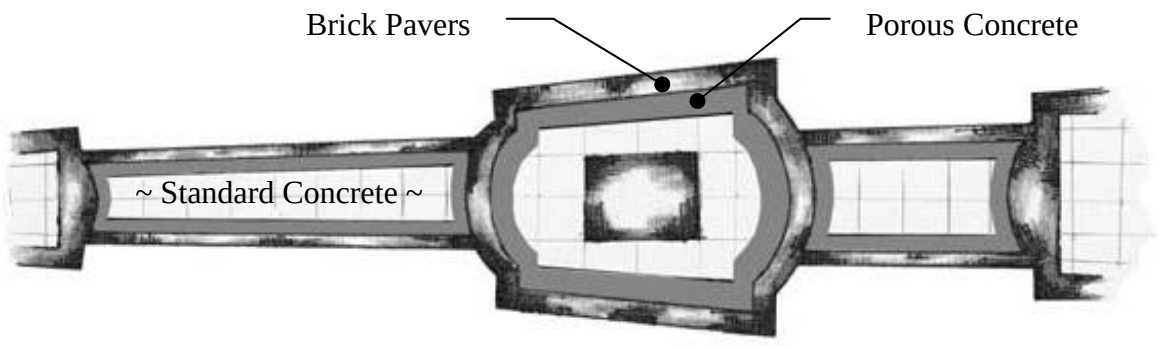

Figure 17. Illustration of new surface design

Figure 18. Completed re-construction

It appeared as if the second attempt would be successful until the onset of the winter of 2003/2004 and the associated snow/ice events. Slowly, multiple small areas across the site began to deteriorate. The surface of the porous concrete began to flake and crumble, as evidenced by the loose gravel. Current speculation suggests freeze thaw may be responsible for the deterioration due to clogged pathways in the porous concrete; however, no definite conclusions have been drawn. Despite its poor esthetic appearance, the porous concrete is still functioning.

1.4.2 Reconstruction II

In October of 2004, during Villanova University's Fall Break, construction was performed once again at the site to replace sections of the porous concrete that had failed or were not functioning properly, approximately 40% of the reconstructed surface. It was observed that the areas of porous concrete that had failed in the 2003 reconstruction were from the later parts of each individual pour, and that the first portion of each pour was in acceptable to good condition. It was also observed during the original reconstruction that the end of each pour was less malleable, and extremely hard to work. As only the top layer of the porous concrete had failed, it is speculated that impermeable layers were formed at the end of the pours allowing freeze thaw to occur.

Demolition began on site on October 12th 2004 and a total of twelve sections of porous concrete were removed from the site (Figure 19). The sections to be replaced had been marked prior to demolition by Villanova's Facilities Management Office.

Figure 19. Sections of removed porous concrete

Each section was saw cut and subsequently jack hammered to break up the porous concrete. The large chunks that were removed appeared to be in good condition other than at the surface. The large pieces were removed by hand and some of the gravel was shoveled out. This process did produce some fines and gravel, but the amount was not substantial enough to clog the pores and prevent water from infiltrating into the bed.

Four test pads had been poured on Villanova's campus prior to the reconstruction in 2003 and were reevaluated prior to this renovation. Two of these pads were formed with the same proprietary additive used in the original and the 2003 pour, while the remaining pads used the "Florida Mix", a standard porous concrete mixture, with no proprietary strength additive. As all four pads had remained in good condition and had maintained their porosity, it was decided that the strength additive was not necessary.

Placement began on October 13th 2004. The mixture was poured 1.5 in (3.8 cm) above the surrounding surface, as opposed to 0.5 in (1.3 cm) higher as in the re-construction in 2003, so that a roller with higher compaction could be used. The higher compaction also allowed the workers to get the porous concrete flush to the standard concrete already in place, without the elevation difference that was noted during the previous construction. Additionally, a hand trowel was used after the porous concrete was raked into place to ensure the pour was even and filled all gaps (Figure 20). The concrete sections were then quickly compacted with the roller which was hosed down with water each time before passing over the concrete to prevent it from sticking to the roller.

Paving was completed on the second day of pouring. It was observed that the "Florida Mix" was much easier to pour than the previous mixture, and no problems with stiffening occurred during the pours.

Figure 20. Rolling (left) and hand trowelling (right) of new porous concrete

After compaction, each section poured was covered with wet burlap strips as shown in Figure 21. This material is heavier than the plastic that had been used in the previous construction so it remained in place over the concrete throughout the recommended 48 hour period and provided for better hydration.

Figure 21. Wet burlap covering porous concrete

Once the porous concrete had cured, the burlap strips were removed. The color of the new sections was fairly consistent and close to the existing color (Figure 22). Over time, it is believed that the color will become more uniform. A few small sections do look less pervious where the different compaction techniques were attempted, but overall the new sections appear to be acceptable and their effectiveness is promising.

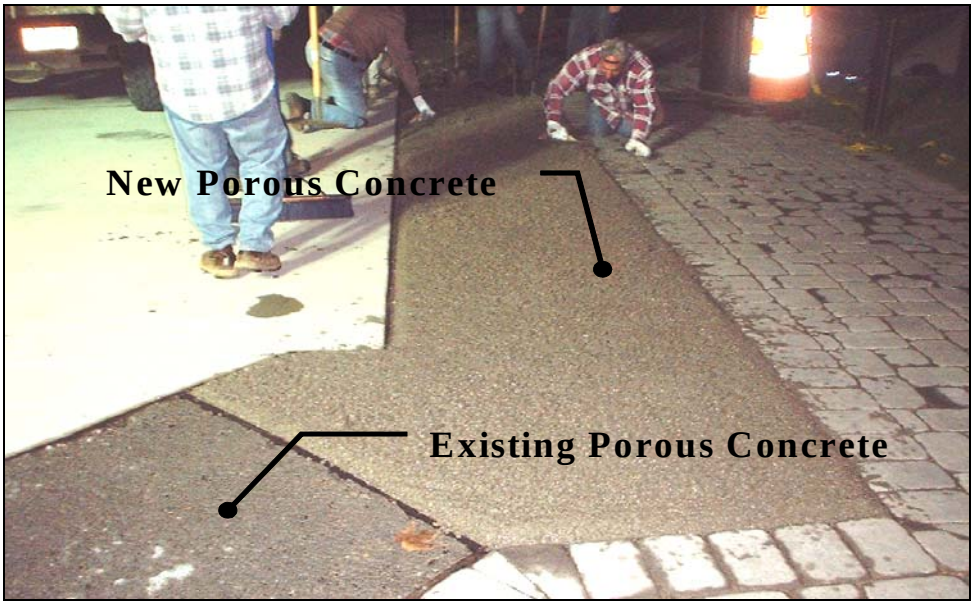

Figure 22. New porous concrete adjacent to existing porous concrete

1.5 Research Objectives

The primary goal of this research is to evaluate the hydraulic capabilities of infiltration basin BMP's with overlying stone bed and porous concrete or asphalt lots. Infiltration BMP's are becoming more readily acceptable as a means of reducing post-development runoff volumes and peak flow rates to pre-construction levels, while simultaneously increasing recharge of the groundwater table. However, the design, construction, and operation of infiltration basins to this point have not been standardized due to a lack of understanding of the infiltration processes that occur in these structures.

The companions to this thesis are Kwiatkowski (2004), which considered the study site from a water quantity aspect, and Ladd (2004) which developed and assessed a model characterizing the site from a water quantity perspective.

The objective of this study is to evaluate and understand the infiltration process that occurs in subsurface infiltration basins to aid in improved design of such structures. Additionally, factors affecting infiltration rate such as antecedent dry time, ponding depth, and temperature will be evaluated. The research will concentrate entirely on the results of field data collected from the Villanova University Stormwater Partnership's (VUSP) Porous Concrete Infiltration Basin BMP. Data from instrumentation on site relay the depth and temperature of the stormwater in the basin, moisture content at three given depths under the basin bottom and at corresponding depths outside the basin vicinity, overflow from site, and rainfall on site. This approach to monitoring will give researchers and engineers a better understanding of the rainfall inputs and outputs of infiltration and overflow from the site so that more effective and efficient design and implementation of these systems as standard stormwater best management practices will be possible.

Chapter 2: Literature Review

2.1 Introduction

Stormwater infiltration structures, such as basins and trenches, are designed and constructed to capture runoff and allow it to percolate slowly into the underlying soil (Akan, 2002). The porous concrete infiltration site was designed, in the same way, to capture and infiltrate stormwater runoff from the impervious surfaces created by development of the site. Site location is an important factor when determining whether an infiltration structure can be utilized. The infiltration capacity of the soil and location of the seasonal high groundwater table are some of the site-specific characteristics which must be investigated before plans for infiltration basin design can begin. Unlike detention basins, infiltration basins do not have widely accepted design standards and procedures (Akan, 2002). The variables that present the most concern in the design process are the infiltration properties of the soils on site. The sections to follow are a review of infiltration models used on similar sites as well as a review of known factors affecting infiltration rates and the importance of the control volume in design.

2.2 Modeling Infiltration

Groundwater recharge is composed of two main functions, infiltration and percolation. Infiltration is defined as “the physical process of water entry into the soil” and involves the displacement of air into the soil matrix by water (Al-Muttair and Al-Turbak, 1991). Soil water movement or percolation is the process of water flow from one point within the soil to another. Infiltration and percolation must both be taken into consideration when modeling water flow into the soil because the rate of infiltration is controlled by the rate of percolation (Hsu et al., 2002).

The process of infiltration of water into soil and movement of that water through the soil profile have been studied and characterized using many different equations, both empirically and physically based. Richard's equation, which was derived from Darcy's Law, was one of the first equations to describe both infiltration and percolation in unsaturated soil (Hsu et al., 2002). Two of the most famous and widely used infiltration models to determine infiltration capacities of subsurface soils are the Green and Ampt formula and Horton's formula, both derivatives of Richard's Equation.

2.2.1 Green and Ampt Method

The Green-Ampt formula is a physically approximative and mathematically exact solution to surface infiltration (Hsu et al., 2002). The original formula,

$$f_p = K_s \frac{(S - L)}{L} \tag{1}$$

where f_p = infiltration rate [L/T], K_s = saturated hydraulic conductivity [L/T], S = capillary suction at the wetting front [L] and L = distance from the ground surface to the wetting front [L]; assumes that the soil surface is covered by ponded water of negligible depth and that the water is infiltrated into a homogeneous soil with uniform water content (Viessman and Lewis, 2003).

During the infiltration process, it is assumed that water enters the soil uniformly to create a discrete "wetting front" a distance, L from the surface, separating the saturated soil above from the unsaturated soil below. This value can be determined by the following equation:

$$L = \frac{F}{IMD} = \frac{F}{(\theta_s - \theta_i)} \tag{2}$$

in which F = cumulative infiltrated water [L] and IMD = initial moisture deficit or the saturated soil moisture content less the initial soil moisture content (Viessman and Lewis, 2003). Figure 23 illustrates the Green-Ampt variables using a sample soil profile.

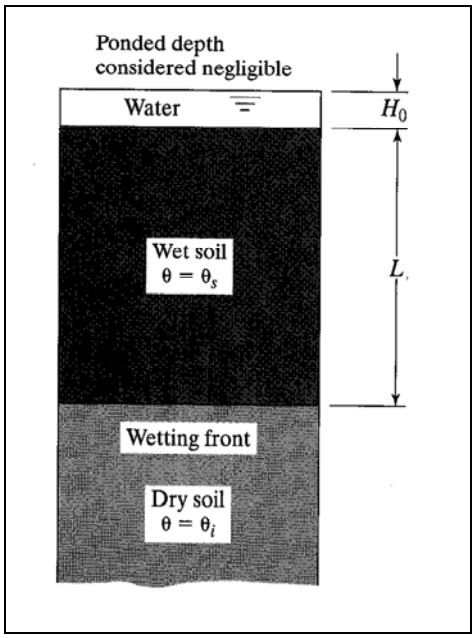

Figure 23. Definition sketch for Green-Ampt model (Viessman and Lewis, 2003)

Additionally, by combining equations (1) and (2):

$$f_p = \frac{dF}{dt} = K_s(1 + \frac{S(\theta_s - \theta_i)}{F}) \tag{3}$$

All variables in equation (3) are measurable soil properties, which is why Green-Ampt formula is characterized as "physically approximative." Additionally, equation (3) can be integrated with control bounds of F = 0 at t = 0 to obtain equation (4).

$$F - S(\theta_s - \theta_i)\ln(\frac{F + S(\theta_s - \theta_i)}{S(\theta_s - \theta_i)}) = K_s t \tag{4}$$

This form of the Green-Ampt equation is more suitable for use in watershed modeling processes than equations (1) or (3) because it relates the cumulative infiltration, F to the time at which infiltration began. This equation assumes a ponded surface so that the

actual infiltration rate is equal to the infiltration capacity at all times; therefore, the equation does not deal with the potential for rainfall intensity to be less than the infiltration rate (Viessman and Lewis, 2003).

In a study done by Al-Muttair and Al-Turbak (1991) the Green and Ampt model was used to characterize the infiltration process in an artificial recharge basin with a decreasing ponded depth, as illustrated in Figure 24. Using an equation similar to that derived in equation (4) they were able to conduct a continuous system infiltration model and determine the cumulative infiltration at set time intervals using equation (5) in a trial and error method.

$$K_s(t_j - t_{j-1}) = F_j - F_{j-1} - S_{fj} \ln\left(\frac{S_{fj} + F_j}{S_{fj} + F_{j-1}}\right) \tag{5}$$

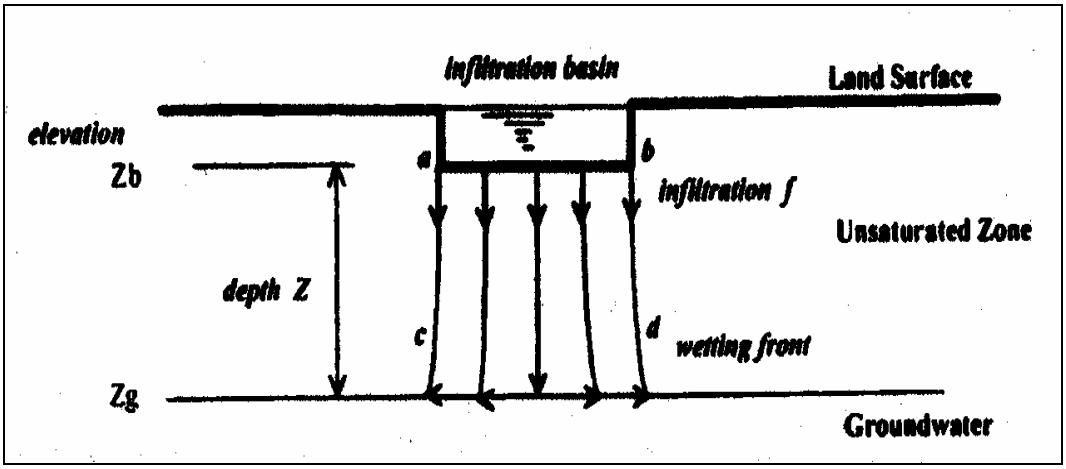

Figure 24. I-D infiltration basin sketch for Green-Ampt model (Guo and Hughes, 2001)

Like all equations, some assumptions were made in this model. The first assumption, comparable to equation (4), is that behind the wetting front, the soil is uniformly saturated with a constant hydraulic conductivity corresponding to that of natural saturation. The second assumption is that at the wetting front, the water pressure

head remains constant (Al-Muttair and Al-Turbak, 1991). Unlike equation (4), in which a negligible amount of constant ponded water is assumed to exist on the ground surface, equation (5) deals instead with the infiltration occurring in a basin, and thus must take into account the depth of ponded water in that basin. In order to accomplish this, and to model the decreasing ponded depth in the infiltration basin, another term was added to the equation. This is done by using storage suction factor, equation (6),

$$S_f = (S + H)(\theta_s - \theta_i) \tag{6}$$

which consists of the change in moisture content between the saturated wetting front and the initial conditions, capillary suction at the wetting front, as well as a new term, H, which is equal to the ponded depth of water in the basin (Al-Muttair and Al-Turbak, 1991). The average stepwise infiltration rate can then be calculated using equation (7).

$$I_j = \frac{F_j - F_{j-1}}{t_j - t_{j-1}} \tag{7}$$

The study consisted of five experimental runs conducted in a 24.76 X 14.47 X 0.4 meter deep artificial recharge basin. The walls of the basin were composed of cement blocks covered by a heavy-duty plastic sheet to prevent lateral infiltration to get a clear representation of 1-D flow through the basin bottom. Soil samples were taken from different locations and depths in the basin before each test was run and average initial moisture content was calculated and recorded. The basin was then filled to a specific elevation and at set time intervals the level of water in the bed was recorded. Due to the high variability of infiltration rate during the beginning of each run, readings were taken at short intervals, and as time proceeded the interval between readings was increased (Al-Muttair and Al-Turbak, 1991). Table 2 shows the details for each run. Also, as Figure

25 illustrates, the results of the model for the first run match very well to what was actually seen and recorded in the field. The same trend was seen in the four other runs, validating the effectiveness of this model.

Table 2. Details for infiltration runs (Al-Muttair and Al-Turbak, 1991)

Run No.	Initial Depth (cm)	Initial Moisture Content (% by volume)	Depth of Water Table (m)	Duration (hr)
1	23.24	0.504	8.06	43.00
2	22.85	2.856	3.69	53.15
3	20.76	3.912	8.98	46.13
4	21.45	2.892	13.11	45.50
5	27.04	9.468	1.60	53.52

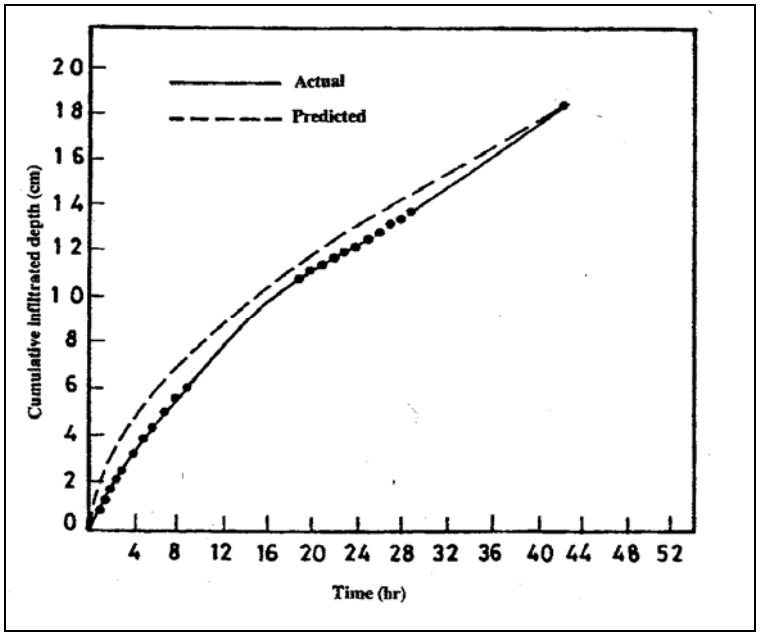

Figure 25. Cumul. infiltration depth vs. time for run 1 (Al-Muttair and Al-Turbak, 1991)

The Green and Ampt equation is one of the most widely used equations for modeling one-dimensional vertical flow of water into soil. It was developed from an integration of Darcy's Law by assuming infiltration from a ponded surface into a deep homogeneous soil of uniform antecedent water content (Risse et al., 1994). What makes

this model ideal is its reliance on physical parameters, most of which can be evaluated from properties of the soils identified through field-testing. Sensitivity analyses on the Green-Ampt equation parameters have indicated that infiltration amounts were most sensitive to porosity and hydraulic conductivity and less sensitive to capillary suction (Risse et al., 1994). Therefore, it is important to take soil samples that are most representative of the site and to pay attention to detail when performing site and soil tests.

2.2.2 Horton's Equation

One of the most widely used empirical equations for infiltration is Horton's equation with exponential decay,

$$f(t) = f_c + (f_o - f_c)e^{(-kt)} \tag{8}$$

in which f(t) = infiltration rate at any time t [L/T]; f_o and f_c = initial and final infiltration rates [L/T]; and k = exponential decay coefficient [1/T]. Using this equation, infiltration of water is modeled through surface soil. However, the values for the initial and final infiltration rates and the exponential decay coefficient can be difficult to determine. Even more limiting is the fact that Horton's equation "expresses infiltration capacity as a function of time and has no provision for the recovery of soil storage capacity during dry periods" (Aron, 1992).

In order to account for the change in soil storage capacity during wet and dry periods Bauer (1974) proposed an equation for soil drainage and recovery of its infiltration capacity, consisting of Horton's equation coupled with a drainage equation, equation (9),

$$d = f_c[1 - e^{(-kt)}] \tag{9}$$

in which d = drainage rate from the higher soil zone to a lower soil zone. With the addition of equation (9), infiltration can be modeled to account for the soil's ability to recover its infiltration capacity during dry times between storm events, which, in turn, demonstrates the importance of soil moisture and the dewatering process on infiltration (Aron, 1992).

Figure 26 illustrates Bauer's (1974) model for infiltration rate and drainage rate versus time. During dry conditions, before the start of the storm, the initial infiltration rate of the soil, f_o is at its peak and the potential for drainage is zero because there is no moisture to drain. As the storm continues and time approaches infinity, the soil becomes saturated and both the infiltration and drainage begin to approach the final infiltration rate f_c asymptotically (Aron, 1992).

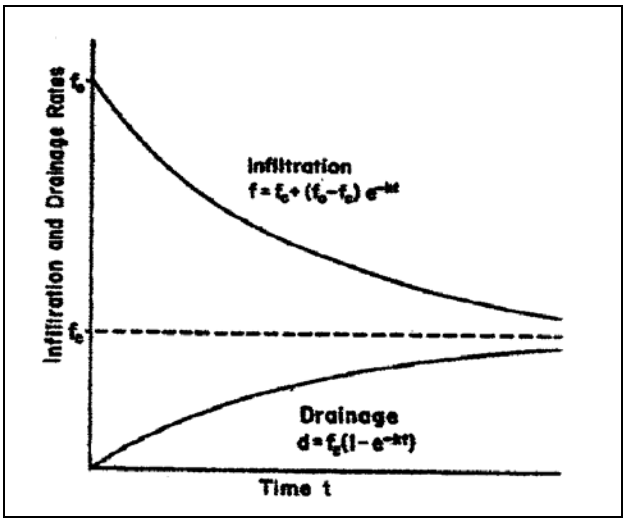

Figure 26. Bauer's concept of infiltration and drainage rates (Aron, 1992)

Bauer (1974) also derived a set of equations relating infiltration rate and drainage rate as functions of soil water storage, rather than time as in equations (8) and (9). The soil water in storage, S at any time is shown in equation (10).

$$S = \frac{f_o}{k}[1 - e^{(-kt)}] \tag{10}$$

Also, as shown in Figure 4, when time approaches infinity and the soil becomes saturated so is the maximum soil storage capacity, S_c achieved.

$$S_c = \frac{f_o}{k} \tag{11}$$

Combining equations (9) and (10), and equations (8), (10) and (11), the drainage rate, d can be expressed as a function of storage and a new term is expressed for potential infiltration rate f_p (Aron, 1992).

$$d = \frac{f_c}{f_o} kS \tag{12}$$

$$f_p = d + f_o - kS \tag{13}$$

Using Bauer's drainage equations, the Horton equation is modified to take into account the ability of the soil to recover its infiltration capacity between storm events, as well as to model the limiting effect that drainage has on infiltration rate when the interval between events is not long enough for the soil to completely recover.

2.3 Factors Affecting Infiltration

"The infiltration rate of a natural porous body depends on its sorptivity and saturated hydraulic conductivity, which in turn is a function of the intrinsic permeability of the medium and the fluidity of the penetrating liquid" (Lin et al., 2003). Initially, soil sorptivity is the primary factor affecting infiltration rate; but as infiltration time increases, the hydraulic conductivity becomes the controlling factor (Lin et al., 2003). Studies have been done to determine what causes alterations in infiltration rate. Seasonal temperature

change and basin design depth are two factors which have been shown to have a large affect on infiltration rate and are included in the following sections.

2.3.1 Temperature

Temperature effect on a soil's hydraulic conductivity and infiltration rate has been studied and preliminary results conclude that the infiltration rate into a soil will decrease as temperature of the system decreases, most likely due to the increased viscosity of the percolating water. Water viscosity changes by approximately 2% per degree Celsius in the relevant environmental temperature range of 15-35°C. This leads to an estimated 40% change of infiltration rate between the summer and winter months in arid regions (Lin et al., 2003). However, the majority of the previous studies on temperature effects were conducted under controlled conditions in the laboratory using small soil columns therefore, results may vary (Lin et al., 2003).

In experiments conducted by Lin et al. (2003), infiltration rate was studied for seasonal change over a 4 year period using a large-scale effluent recharge operation. The study took place at Shafdan wastewater treatment plant in Israel. As a final step to their treatment processes, effluent was pumped into fields of sub-surface infiltration basins used to recharge the Coastal Plain Aquifer. Each basin field consisted of a series of 4 to 5 leveled subbasins separated by earthen dams. The recharge cycle consisted of 1 to 2 days of flooding and 4 to 5 days of drainage and drying. During the course of the study, water and air temperatures, as well as the water level, were recorded for each of the underground basins on five minute increments (Lin et al., 2003). Through the water level readings, infiltration rate was calculated. The results for basin 103-4/5 of the study can be seen in Figure 27.

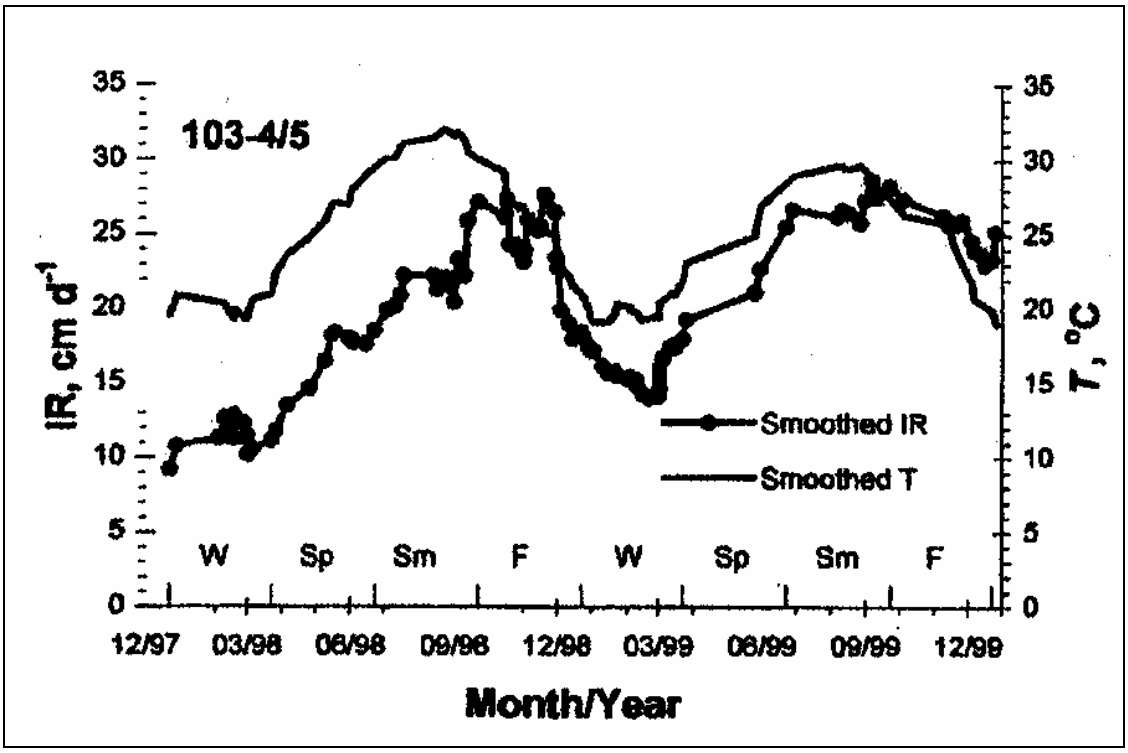

Figure 27. Infiltration and temperature results for Shafdan WWTP (Lin et al., 2003)

Results showed a repeating pattern of cyclical changes of infiltration rate as a function of temperature. As shown in Figure 27, the infiltration rate for basin 103-4/5 increased from approximately 10 cm/d in the winter of 1997-8 to 25 cm/d in summer of 1998 and again decreased to 15 cm/d in the winter 1998-9, increased to 30 cm/d in summer 1999 and finally decreased to 20 cm/d in December 1999 (Lin et al., 2003). A similar pattern was seen in all basins tested. Lin et al. (2003) found that the temperature effect tends to be larger by a factor of 1.5-2.5 times, than the change expected from effluent viscosity changes alone, suggesting the involvement of other factors.

The relationship of hydraulic conductivity to the soil and infiltrating water can be shown though the following equation:

$$K = kf \tag{14}$$

where K = hydraulic conductivity of the soil, k = intrinsic permeability of the soil and f = fluidity of water. Fluidity is inversely proportional to viscosity, thus as temperature increases, viscosity decreases, increasing fluidity and, overall, increasing the hydraulic conductivity (Lin et al., 2003).

The increase in hydraulic conductivity with increase in temperature is commonly attributed to the decrease in viscosity of the water. This effect was also reported in a number of laboratory studies; however, the magnitude of the change differed considerably among the reports and in some cases hydraulic conductivity changed by orders of magnitude more than predicted from viscosity change alone (Lin et al., 2003). Several possible causes for this increase in infiltration rate exist, due to the dependence of various water and soil properties on temperature. Some temperature dependent properties include: change in surface tension, greater temperature dependence of viscosity of soil water than of free water, change of diffuse double layer thickness, temperature induced structural changes, entrapped air volume decreases with increasing temperature, and/or temperature effects on infiltration rate by changing water viscosity and liquid conducting properties of the soil (Lin et al., 2003). It is also possible that changes of the viscosities of the two counterflowing fluids, water and air, jointly contribute and affect the change in infiltration rate with temperature (Lin et al., 2003).

2.3.2 Basin Water Depth

Achieving a maximum infiltration rate for recharge basins is essential, especially in urban settings where land is limited. The depth of water in recharge basins must be selected to achieve maximum infiltration rates. By increasing the depth of water stored in recharge basins small increases, significant increases, or even decreases in infiltration

rate can result. Although basin water depth is not usually considered in the design process, it can have a profound effect on the performance and management of the system (Bouwer, 1990). Specifically, water depth and infiltration rate are dependent on both the potential of the basin bottom to have a clogged layer and on the distance, or freeboard, available between the basin bottom and the groundwater table.

2.3.2.1 Clogged Basin Layer

Over time, the bottom of the infiltration basin can become clogged by a layer of inorganic and/or organic deposits creating a barrier between the basin and the wetted perimeter (Bouwer, 1990). As fine particles settle out and biological activity on the bottom continues, the thickness of the clogging layer can increase until infiltration rates eventually become so small that the function of the infiltration basin ends. If the groundwater table is well below the basin bottom, the vadose zone below the clogged basin is unsaturated, and the downward flow is at unit hydraulic gradient, or gravity flow. Therefore, infiltration rate is controlled by the hydraulic conductivity and the depth of the clogged layer. Using Darcy's Law:

$$f = K\frac{(H_w + L_c + S)}{L_c} \tag{15}$$

where f = infiltration rate, K = hydraulic conductivity of the soil, H_w = water depth in the basin, L_c = thickness of the clogged layer, and S = capillary suction head in the unsaturated zone below the clogged layer (Bouwer, 1990). Figure 28 illustrates the soil profile under a basin with a clogged layer.

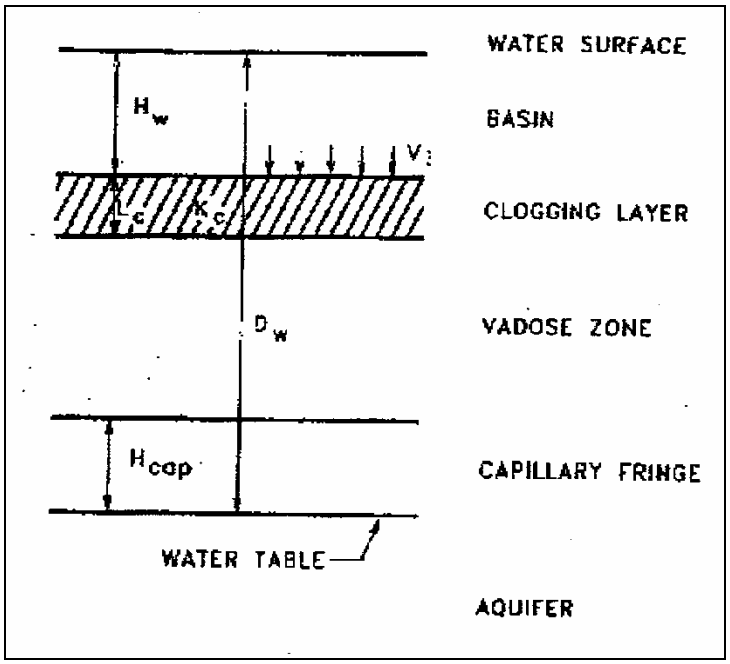

Figure 28. Schematic of infiltration basin with clogged layer (Bouwer, 1990)

Equation (15) shows a linear increase in infiltration rate with increasing water depth in the basin given the clogged layer and capillary suction remain low. However, if water depth is increased when a clogged layer is present, the depth of this layer will decrease slightly due to compaction, and the hydraulic conductivity will decrease significantly. This causes a "less linear" increase in infiltration rate with water depth, and even possibly a decrease (Bouwer, 1990). Therefore, increasing the water depth in infiltration basins with a clogged layer may, in fact, decrease the infiltration rate and increase the potential for the infiltration bed to fail during a rainstorm.

2.3.2.2 Groundwater Depth

The infiltration process for clean, unclogged basins is driven by the vertical difference, D_w between the water surface in the basin and the groundwater table. As D_w increases the curve begins to flatten out and asymptotically approach a maximum value

for infiltration that is reached when D_w is very (infinitely) large (Bouwer, 1990). At this point the groundwater table has no effect on the infiltration rate. Figures 29 and 30 illustrate the profile of the infiltration basin and the graphical relationship between infiltration rate and depth respectively.

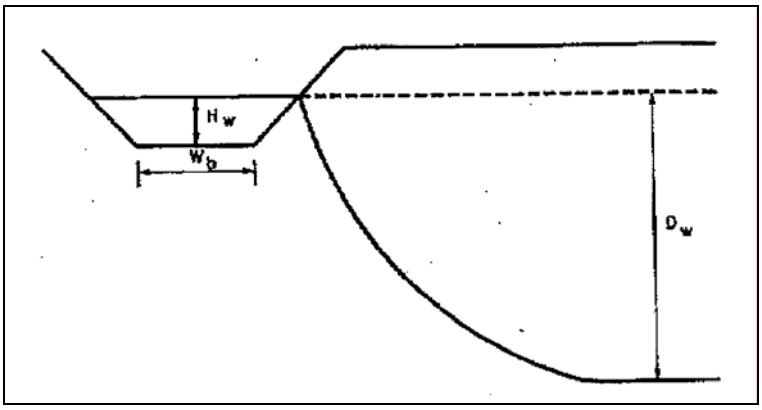

Figure 29. Geometry and symbols from clean recharge basin (Bouwer, 1990)

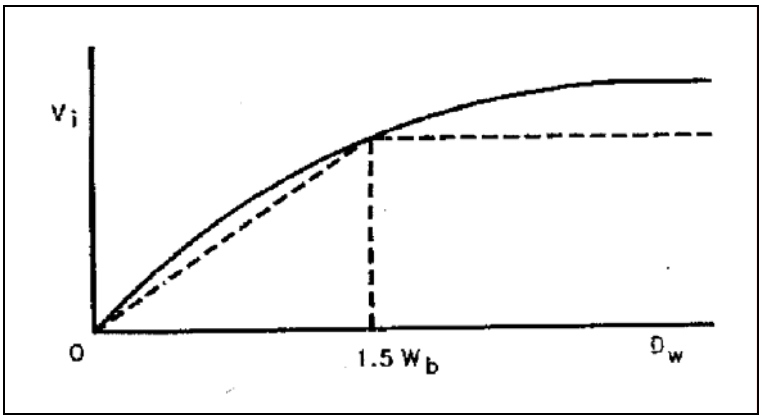

Figure 30. Infiltration rate vs. groundwater depth for a clean basin (Bouwer, 1990)

For the case of clogged infiltration basin, the groundwater table does not present a problem as long as the top of the capillary fringe above the groundwater table is below the bottom of the basin. In this case, infiltration rates are not significantly affected by the depth to groundwater. However, if the groundwater table rises from this depth, the infiltration rate will decrease linearly with decreasing D_w and reach zero when D_w has

become zero (Bouwer, 1990). Figure 31 illustrates the infiltration rate as a function of groundwater depth.

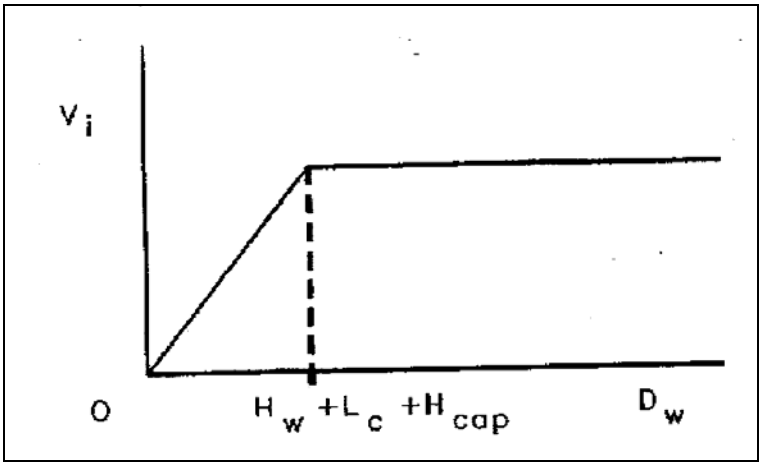

Figure 31. Infiltration rate vs. groundwater depth for a basin with clogging layer (Bouwer, 1990)

2.4 Infiltration Basin Design

The challenge presented in the design process for infiltration structures is to ensure that the basin size will capture the design storage volume and maintain its infiltration rate. Design parameters for an infiltration basin include stormwater storage volume, soil infiltration rate on the basin bottom, seepage rate through the soil medium underlying the basin, water mounding effects on the local groundwater table and overflow risk between storm events (Guo and Hughes, 2001). The following section evaluates a method of determining the storage control volume in conjunction with the need to assess overflow risk during the design process.

2.4.1 Control Volume

Infiltration structures are designed to store a "capture volume" of stormwater runoff for a period of "storage time," usually 72 hours. Design of these structures requires the calculation of a runoff hydrograph corresponding to a design storm (Akan,

2002). The computer program HEC-HMS, created by the Army Corps of Engineers is a hydrological model made to aid in this process of selecting a design storm and running the storm through a watershed, while separating the losses from rainfall and runoff calculations using different equations including the Green-Ampt, Kinematic Wave and SCS Curve Number Method, among others.

When sizing infiltration structures, most stormwater management regulations require post development peak discharge to equal pre-development levels for the design storm being used. Therefore, the control volume of the infiltration structure must capture all additional runoff occurring from the site's added impervious area after construction.

The next factor to consider is the time to fill the basin during a storm event. Many methods assume that infiltration occurs at a constant rate. Theoretically, the basin should begin to fill when the rate of runoff reaching the basin exceeds the rate of infiltration across the basin bottom, fA_f, and will continue to fill until the runoff rate falls to the pre-development discharge value (Akan, 2002).

Three general criteria control sizing infiltration structures: (i) the infiltration basin should drain completely within a specified storage time (usually 72 hours), (ii) the basin bottom should be a specified distance from the seasonal high groundwater table, (iii) the infiltration structure should have a control volume which has enough storage capacity to accommodate the capture volume, minus any infiltration occurring during the filling time (Akan, 2002). To ensure that criteria (i) and (ii) are satisfied there must be a specified maximum depth for the infiltration structure,

$$d_{\max} = \frac{fT_s}{n} \quad \text{and} \quad d_{\max} = GW - h_{req} \qquad (16), (17)$$

where T_s = storage time, n = porosity of aggregate material filling the infiltration structure (n = 1.0 if infiltration pond), GW = seasonal high groundwater table and h_{req} = minimum required distance between the bottom of the infiltration basin and GW. Lastly, equation (18) yields the width and length of a trapezoidal infiltration structure with side slopes z:1 (horizontal over vertical) to satisfy criterion (iii)

$$n[LWd + (L+W)zd^2 + \frac{4}{3}z^2d^3] = Vc + (L+2zd)(W+2zd)P - (L+zd)(W+zd)fT_f \quad (18)$$

where d = depth of the infiltration structure and P = rain falling directly over the structure (Akan, 2002).

2.4.2 Overflow Risk

Overflow risk is defined as the probability of having a rainfall event that produces a runoff volume more than the available storage capacity of the infiltration structure which is set to meet peak flow requirements (Guo, 2002). Selection of the basin size is a trade-off between costs and overflow risk.

From a stormwater control perspective, the larger the volume of the infiltration basin, the lower overflow risk. However, from the cost effective perspective, the smaller the basin, the lower the construction costs. Therefore, infiltration structures are usually designed for small drainage areas. Due to requirements of capturing the “first flush volume” or the “water quality capture volume” the control volume for an infiltration structure tends to be approximately 30% of a 2 yr 1-hr storm runoff depth or the volume associated with 1 inch of runoff from the structures contributing area (Guo and Hughes, 2001).

The emptying or drainage period for an infiltration basin can last as long as 2-3 days for large storms. During such a long and slow infiltration and draining process, the

chance for the basin to overflow due to the next rainfall event becomes a concern. During the draining process from an elapsed time, T, to the end of drainage time, T_d, the operational overflow risk during drainage time depends on two probabilities: (i) that the next event will come between T and T_d and (ii) that the rainfall depth of the next event will exceed the available storage volume in the basin (Guo and Hughes, 2001). Overflow risk then becomes the risk of overflow for the next event to occur during the waiting time or the time it takes the soil to drain. Therefore, for a cycle of basin operation, the total overflow risk is the sum of the overflow probabilities during the duration of the rainfall and the time it takes for the soils to drain and regain initial dry soil moisture content (Guo and Hughes, 2001).

Chapter 3: BMP Evaluation

3.1 Introduction

The focus of this research is to evaluate the infiltration characteristics of a Porous Concrete Infiltration Basin Best Management Practice (BMP) and to develop and assess the modeling techniques used in this evaluation. The site is a pedestrian area in the middle of Villanova University's campus. The BMP design includes three underground infiltration beds constructed in a cascading order and overlain with porous concrete, standard concrete, and paving stones. The rooftop gutter collection system is directly connected to the three beds through underground pipes. The infiltration beds were designed to capture and infiltrate the first 2 inches (5.1 cm) of all rainfall events. Excess runoff exceeding the capacity of the infiltration beds flows from the uppermost bed into the lowest bed and exits the site through the original storm sewer system.

The research in this report centers on the lower infiltration basin, as it is through this basin that all excess stormwater overflows from the site and is the location of all site instrumentation. Specifically, the model used will deal primarily with the recession limb of the outflow hydrograph, or the infiltration that occurs once the bed has filled to its peak, for each storm in question. Therefore, all rainfall inputs to the system have stopped and the only outflow is through infiltration. Before discussing the model it is necessary to review the BMP site characteristics, which include the infiltration bed design, instrumentation, and the underlying soil characteristics.

3.2 Infiltration Bed Characteristics

The size and storage capacity of the lower infiltration bed were determined for different elevations throughout the bed based on the AutoCAD drawings used for the

construction plans. The site plans illustrate the area of the bed bottom and bed top, as well as the slopes of the side walls. Figure 32 illustrates a cross section of a trapezoidal basin. The side wall ratio of the BMP is 2:1. The width, b is 28.2 ft (8.6 m) at one end and 14.7 ft (4.5m) at the other end, with a total length of 49.4 ft (15.1 m). The bed was separated into 40 slices, starting at the bottom of the bed and increasing 0.10 feet (0.03 m) until the top of the bed, y at 4.0 feet (1.2 m) was reached. By knowing the dimensions and areas of the top and bottom slices, a relationship was found which approximated the area of each slice as the elevation increased. A volume was calculated incrementally by comparing two slices. Once the volume-depth relationship of the bed was established, the volume of pore space available for storage was determined. This value is based on the fact that the AASHTO No. 2 stones provide a void space of 40%. Therefore, 40% of the total bed volume calculated accounts for the actual storage volume for the bed (Appendix A).

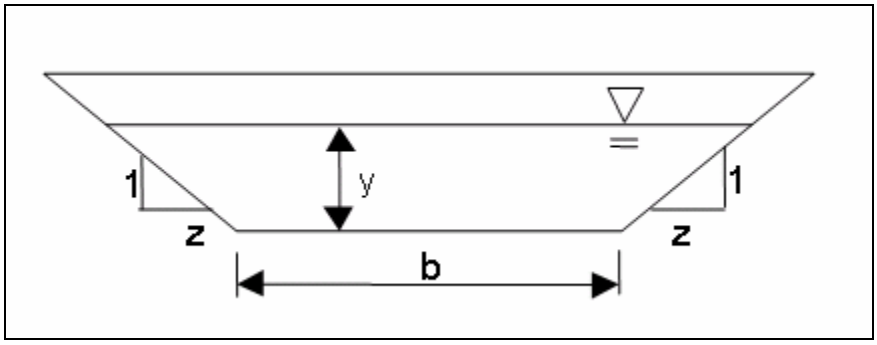

Figure 32. Trapezoidal basin cross section

Site overflow is comprised of the water that leaves the bed through the overflow pipe. This pipe is set at a height of 18 inches from the bed floor and leads to the catch basin where a V-Notch weir is located. Once the water surface in the bed reaches 18 inches overflow from the BMP will result. The modified weir flow equation, equation

(19), is used to measure the amount of water leaving the bed through the overflow pipe (Emerson, 2003). Until the water surface in the bed reaches this elevation, the only water leaving the bed is through infiltration.

$$Q = 3.6 * (0.785 * D) * H^{1.5} \quad (19)$$

Where: Q = Flow over the weir (cfs)

D = Diameter of the pipe (ft)

H = Height of water over the weir (ft)

The overflow from the pipe was calculated for every tenth of a foot increase in elevation within the bottom bed. Figure 33 shows a graph of this information for the lower infiltration bed. The overflow curve remains at zero until the water surface elevation in the bed reaches above 1.5 ft (0.46 m), which corresponds to the crest height of the weir.

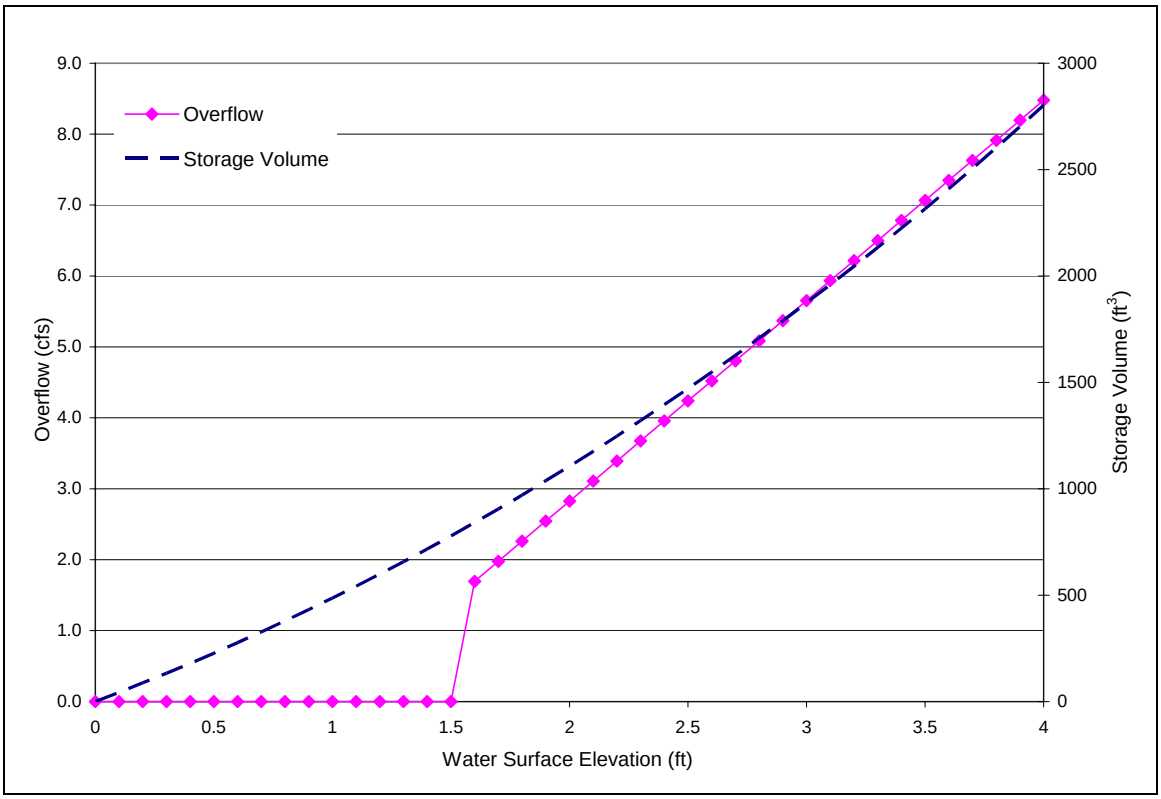

Figure 33. Elevation-Storage-Outflow Curve

When attempting to quantify infiltration, the side wall contribution is required. Since the infiltration bed in this study has sloped side walls, the wetted area of the bed increases with increased water surface elevation. Therefore, the area available for infiltration is higher during larger events that reach higher levels in the bed. Figure 34 illustrates the side wall contribution of the wetted area as a percent of the bed bottom area at different water surface elevations in the bed. A polynomial curve was then fit to the data, equation (20), and will later be used in the model discussed in Chapter 4.

$$y = 0.0001x^2 + 0.0255x \qquad (20)$$

Where: y = Increase in Area form Side Walls (%)

x = Bed Depth (in)

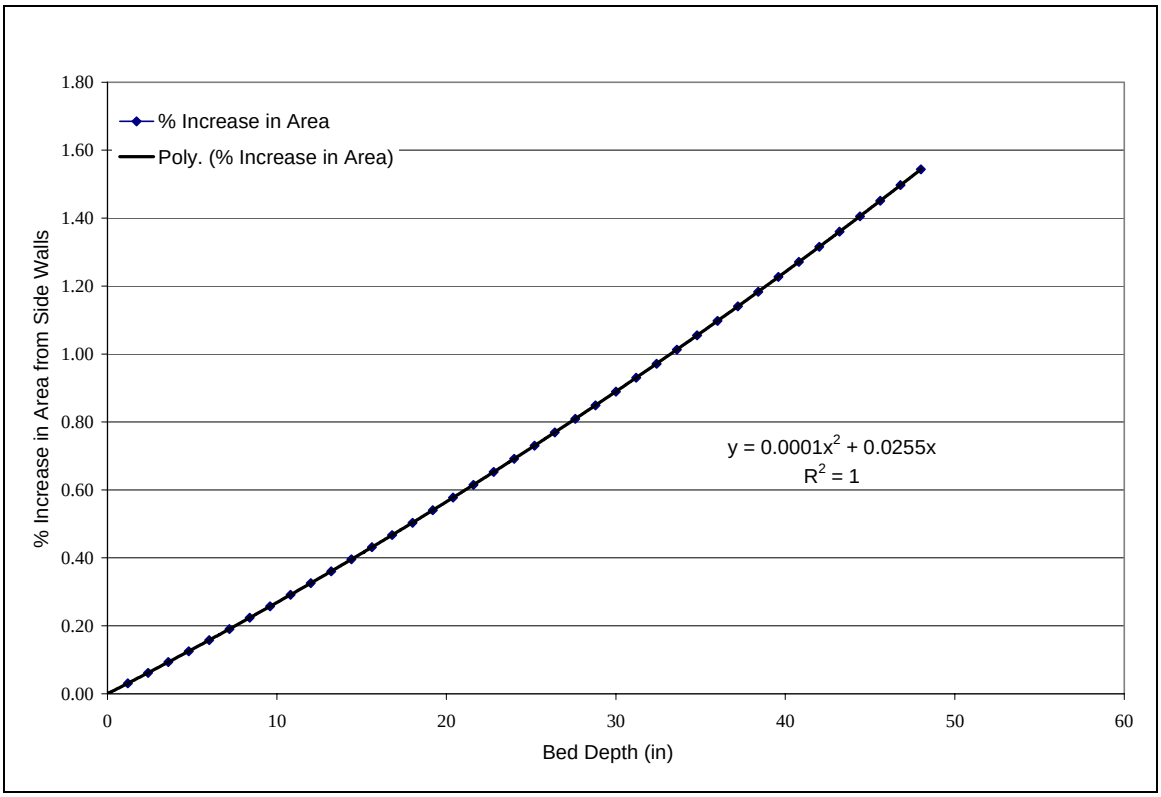

Figure 34. Area of side wall contribution

3.3 Site Instrumentation[2]

Water quantity instruments were installed to monitor the BMP's effectiveness during storm events and to support the development of models for the site. Due to the layout of the runoff collection system, there were many monitoring challenges present at the beginning of the project. The inflow pathways include a slot drain, a storm drain at the top of the site, fourteen downspout connections, and the porous concrete surface itself. Runoff exits the infiltration beds through both infiltration through the bed bottom and side walls, as well as through overflow over a V-Notch weir and into a storm sewer system, when a storm event is large enough to reach the weir crest elevation. Based on

[2] Portions of this section are taken from the Villanova Stormwater Porous Concrete Demonstration Site Quality Assurance Quality Control Project Plan (Traver et al. 2003).

experience and observations, only large storm events over two inches in depth or multiple storm events occurring successively will cause the water surface elevation to reach the 18 in (45.7 cm) height needed for discharge to occur over the weir (Ladd, 2004). Because of the multiple flow pathways entering the BMP, obtaining a directly measured inflow was not feasible. Ladd (2004) created a hydrologic computer model of the site, which approximates the amount of runoff entering and exiting the infiltration beds during a storm event. The model presented in this study will evaluate the infiltration occurring in the bed after the water elevation in the bed has reached its peak. To collect data for modeling, the study site was instrumented with a variety of measuring devices, located as shown in Figure 35.

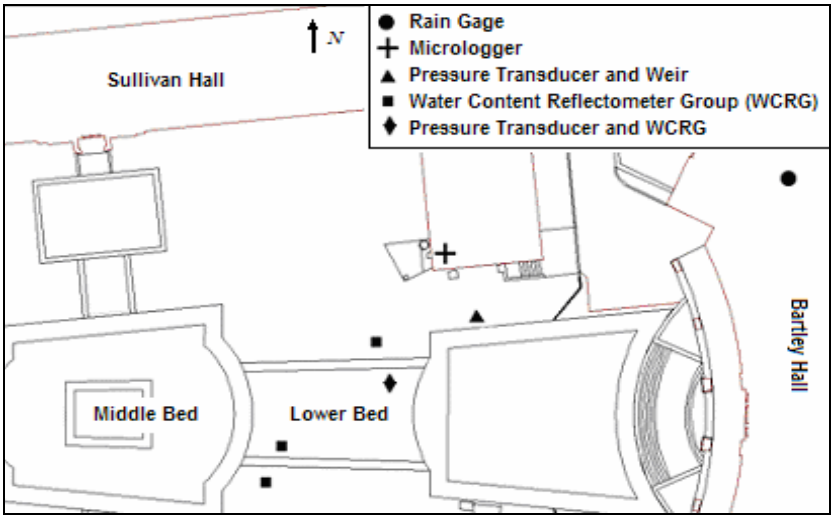

Figure 35. Site instrument locations

A spreadsheet of storm events was created to maintain a record of rainfall that took place on the site. Storm events are defined as periods of measurable rainfall with an inter-event time of 12 hours. The date and time of the beginning and end of the rainfall are recorded with the total amount of precipitation, the maximum one-hour precipitation, and the average intensity of the rainfall. Additional characteristics of each storm event

are also noted in the spreadsheet. These include the occurrence of flow over the weir, the amount of rain staying on site, and the maximum water surface elevation in the bed. The complete Storm List can be found in Appendix B.

A similar spreadsheet of BMP events was then created, based on the storm list, to maintain a record of events with an associated rise in bed water surface elevation. A BMP event begins by rainfall occurring over the site and extends to the time it takes for the water surface elevation in the bed to rise and subsequently empty out, which may or may not consist of more than one storm event. Similar characteristics to those for storm events are also noted for each BMP event. The complete BMP Event List can be found in Appendix C.

3.3.1 Rain Gage

A rain gage was installed on the roof of Bartley Hall. The rain gage used on site is a Scientific TE525WS Tipping Bucket Rain Gage, which features an eight-inch collector with tips of 0.01 inches per tip. The gage was set up such that measurements are taken and recorded in 5 minute increments. The rain gage was originally located on the roof of neighboring Sullivan Hall. However, after a few weeks of operation, it was discovered that the rain gage was not accurately reflecting the rainfall over the watershed. The results where compared to two other rain gages, located near the site on other research projects, for the same storm events. Based on those comparisons and a variety of tests and calibrations, it was determined that the location of the gage was creating the problem. It was theorized that because the gage was located on the outer side of the building, away from the study site, that prevailing wind currents caused inaccurate readings. To remedy this problem, a suitable location was found through experimenting

with portable rain gages in different locations over the course of a series of storms. The best location was then determined to be the roof of Bartley Hall where the gage was relocated and currently operates (Ladd, 2004).

Figure 36 graphically illustrates the data collected from the rain gage for a storm event in September 2004. The rain began on the 18th at 12:55 AM and continued until 3:05 PM the same day. The total precipitation for the 14.2 hour storm was 2.27 inches (5.77 cm). Each tip of the rain gage accounts for 0.01 inches (0.025 cm) of rainfall over the site. The strong intensity of the storm is illustrated by the discontinuity of the line created by the data points in Figure 36. The jumps in precipitation are an account of multiple rain gage tips occurring in a single five minute interval.

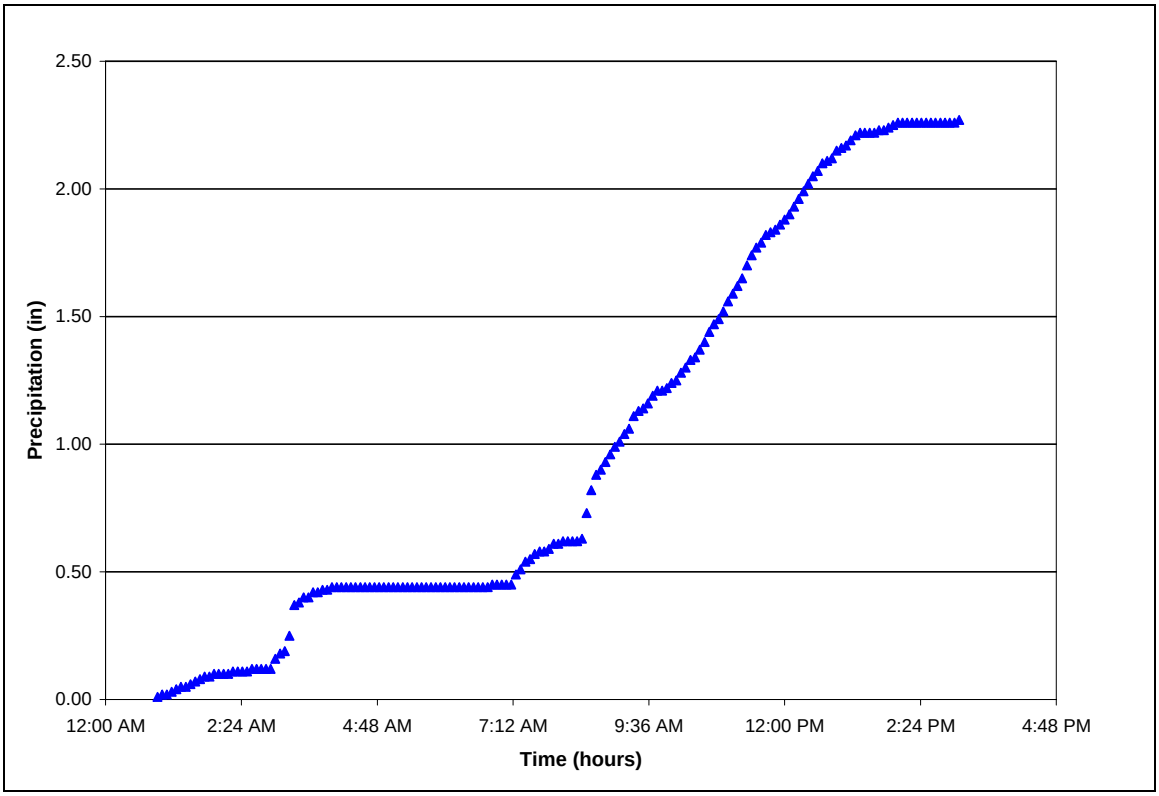

Figure 36. Rain gage mass curve for storm 9/18/04

3.3.2 Pressure Transducers

To monitor what was taking place in the infiltration beds, a pressure transducer probe was installed in the junction box located in the lower infiltration bed following reconstruction. The Instrumentation Northwest (INW) PS-9805 Pressure/Temperature Transducer measures the water surface elevation and water temperature in the bed. The probes were set up such that measurements were taken and recorded in 5 minute increments. By observing the drop in water surface elevation after the rainfall ceases, infiltration rates can be determined for each storm event. A second pressure transducer, in conjunction with the V-Notch weir, is located in the catch basin at the downstream end of the lower infiltration bed's overflow pipe. It measures the height of water in the catch basin chamber and, from that value, calculates the flow and volume of water passing over the weir and exiting the system. During some storm events, minimal flows were recorded flowing over the weir in the catch basin where the depth had not yet reached the overflow pipe. This minor flow was attributed to perforations or leaks in the pipe connecting the two structures and was deemed insignificant (Ladd, 2004).

Figure 37 is a plot of the data collected from the pressure transducer probe in the lower bed during the same rain storm recorded in Figure 36 occurring on September 18, 2004. The maximum depth reached in the bed was 17.1 inches (43.4 cm), only 0.9 inches (2.3 cm) lower than the depth at which overflow begins from the site. It took approximately 75.5 hours or 3.2 days for the bed to completely empty and infiltrate the 2.27 inch storm.

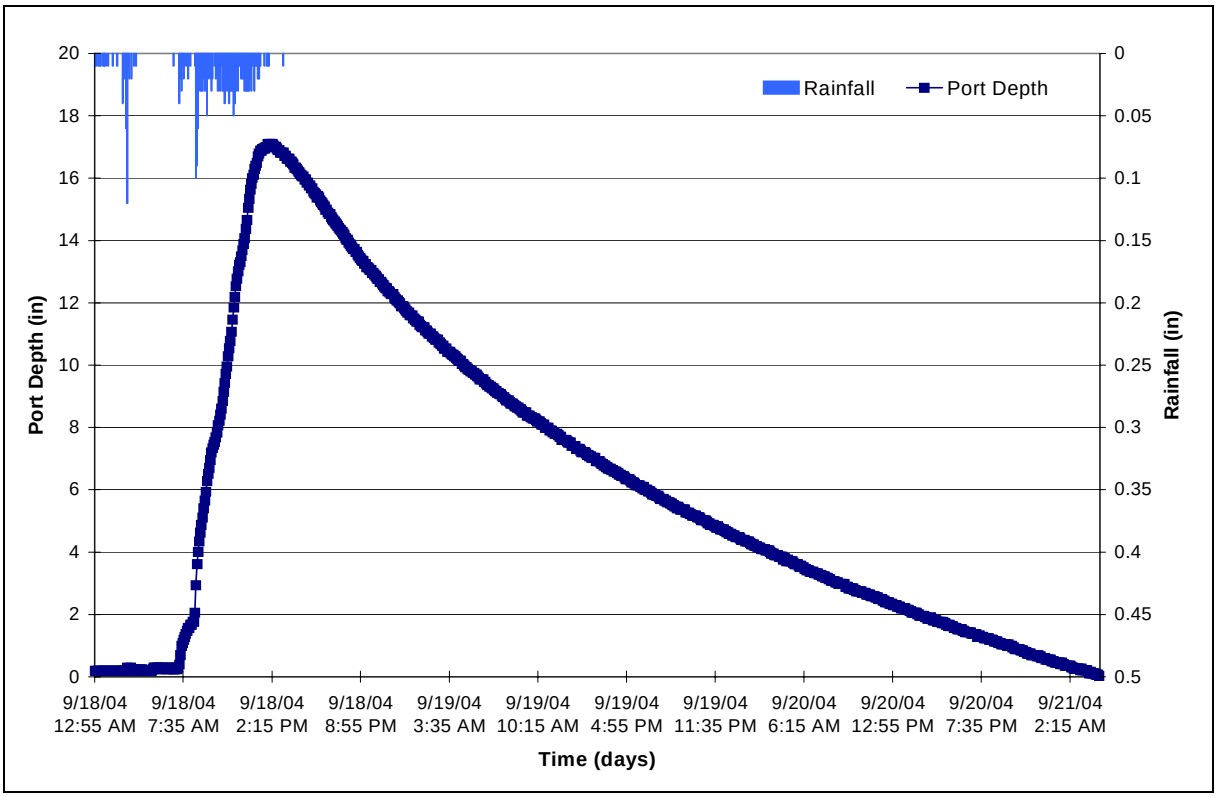

Figure 37. Pressure transducer probe data for event 9/18/04

3.3.3 Water Content Reflectometers

In-situ monitoring of the infiltration process is an important component of the soil study. Twelve Campbell Scientific CS616 Water Content Reflectometers were installed beneath and immediately outside the lower infiltration bed to monitor the passing moisture fronts as the infiltrating runoff changed the soil moisture content. The probes were set up to take measurements every 5 minutes and an average of this data was recorded in 15 minute increments (Kwiatkowski, 2004).

Figure 38 is a plot of the data collected for the month of September 2004 for the group of water content reflectometers located directly beneath the lower infiltration bed, in the southwest corner. The specific location can be seen in Figure 35. Three probes

labeled B11, B12, and B13, were placed at this location and staggered at 1.0 ft (0.3 m), 2.0 ft (0.6 m), and 4.0 ft (1.2 m) below the bed bottom, respectively. Three rainfall events are presented in this data subset. The second event relates to the September 18th storm.

The moisture fronts result from the infiltration of the stormwater collected in the infiltration bed. As the moisture front passes through the soil, the water content changes. Knowing the time for the moisture front to travel from one water content reflectometer to another helps create an estimate of the infiltration rate for the soil (Kwiatkowski, 2004). Complete technical information for the instruments used at the Porous Concrete Infiltration Basin BMP can be found in Appendix D.

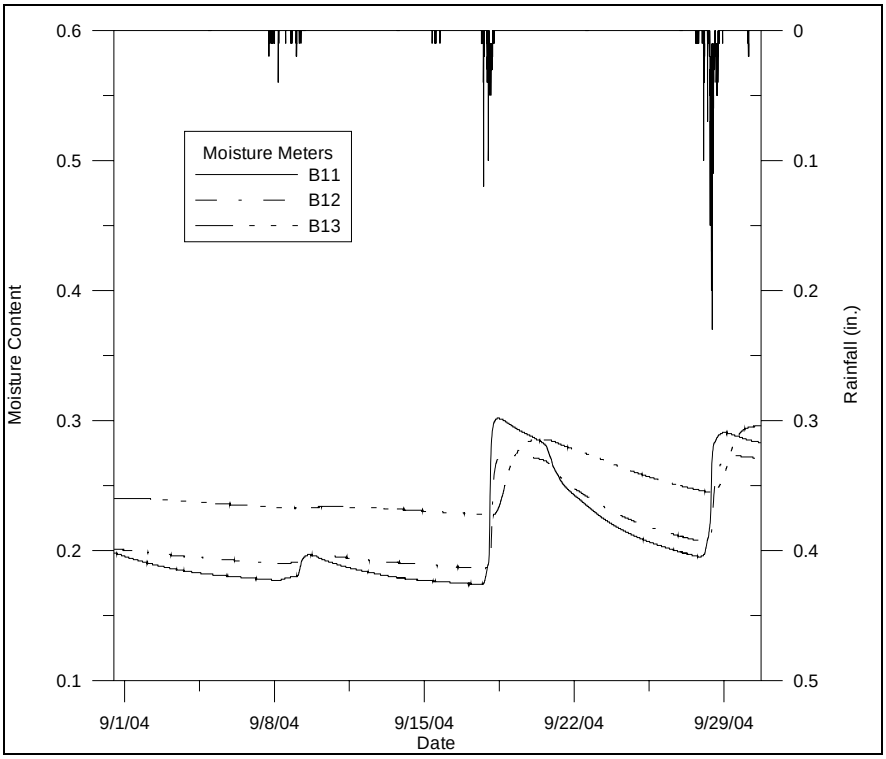

Figure 38. Water content reflectometer data for September 2004

3.4 Soil Analysis[3]

Identifying some of the basic site specific soil properties is essential for proper monitoring of a BMP. Consequently, a number of tests were performed to gather some necessary information on various soil properties. A soil sample was collected from the lower infiltration bed during the excavation stage of the construction process. A sieve analysis and hydrometer test were performed to classify the soil. The Atterberg limits were also determined. A flexible wall hydraulic conductivity test was performed. The procedures for test and setup, as well as the results of each of the soil tests mentioned, will be discussed briefly in the sections to follow.

[3] Portions of this section are taken from Chapter 3 & 4 of Water Quality Study of a Porous Concrete Infiltration Best Management Practice, Masters Thesis (Kwiatkowski, 2004).

3.4.1 Soil Classification

A soil sample was taken from the base of the lower infiltration bed during the excavation process and brought back to the lab for testing. The soil was classified according to the Unified Soil Classification System (USCS) (ASTM D-2487) by implementing grain-size analysis (ASTM D-422) and Atterberg limits (ASTM D-4318). All tests were conducted in accordance with American Society for Testing and Materials (ASTM) standards (Appendix E and F).

The results of the grain-size analysis utilizing sieve data, soil wash, and hydrometer data are shown in Figure 39. The Atterberg limits were utilized to identify the soil's liquid limit (LL) and plastic limit (PL), which were determined to be 42.9%, and 33.0%, respectively. The resulting plasticity index (PI) was 9.9%. Under the USCS the soil is classified as an inorganic silty sand (ML) of low plasticity.

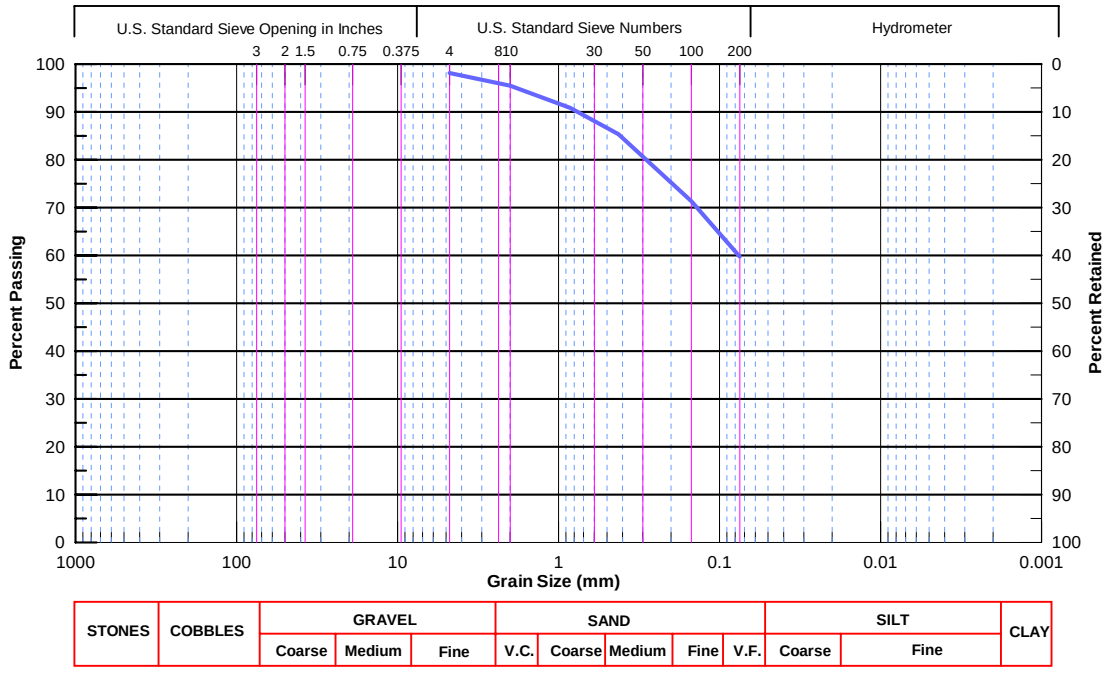

Figure 39. Grain-size distribution

3.4.2 Flexible Wall Hydraulic Conductivity

To determine the hydraulic conductivity of the soil beneath the infiltration beds, a flexible wall hydraulic conductivity test (ASTM D-5084) was performed. An undisturbed sample was used for the test. The sample was collected using a hollow tube sampler at the end of an extended auger shaft. Because the sample was collected after the infiltration beds had been constructed, there was no way to get an undisturbed sample from directly beneath the beds. Consequently, it was decided to auger down to the same approximate depth parallel to the lower infiltration bed and retrieve the sample. Once the hollowed tube was forced into the undisturbed soil, the apparatus was removed and disassembled such that the tube containing the sample could be capped and brought back to the lab to be extruded and tested.

The resulting saturated hydraulic conductivity was K = 0.24 in/hr (1.67×10^{-4} cm/sec). This value is based on the average of four measurements following the completion of the back saturation of the sample. The data can be found in Appendix F.

Chapter 4: Model Development and Analysis

4.1 Introduction

As of May 2005, the Porous Concrete Infiltration Basin BMP has recorded 115 storm events using a tipping bucket rain gage over a 20 month period (September 2003 - April 2005). From these 115 storm events, 48 BMP events have resulted. Fifteen of the BMP events were used to create and calibrate the infiltration model for the site. These events include all single peaking events in 2004 which have a clear distinct peak and smooth recession curve. Ten additional single peaking BMP events were used for model verification. The success of the calibration was based on how well the model reproduced the recession limb of the infiltration outflow hydrograph obtained from instrumentation located in the lower infiltration bed. An analysis was also completed on how well the model estimated the multiple recession limbs resulting from multi-peaking BMP events. Over the extent of the study, eight storm events overflowed from the site. In order to use these events, the model was run after overflow over the weir ceased, resulting in infiltration as the only outflow from the site. Aside from these eight events, the site was successfully able to store and infiltrate all storm events that occurred throughout the duration of this study.

It should be noted that two companion theses, Kwiatkowski (2004) and Ladd (2004), investigate and document the effectiveness of the Porous Concrete Infiltration Basin BMP from a water quality and water quantity perspective, respectively. Kwiatkowski (2004) obtained water samples from various locations and tested them for copper, nutrients, chloride, total and suspended solids, and conventional parameters including pH and conductivity. Composite samples collected from soil water samplers

buried beneath the lower infiltration bed were compared with samples taken from a soil water sampler outside of the lower infiltration bed, samples taken from combined runoff collected within the lower infiltration bed, as well as samples taken directly from rooftop downspouts. These tests were done to determine the effect of infiltration of stormwater on the soil and inevitably to the groundwater below the site. Specifically, the ability of the soil to retain and/or treat contaminants produced from the various impervious surfaces was examined (Kwiatkowski, 2004). These tests continue to be run for soil water samples and grab samples during storm events in addition to new first flush samples which were installed on site in the summer of 2004.

In the study done by Ladd (2004) a model of the site was created using the computer software program HEC-HMS Version 2.2.2. HEC-HMS, or Hydrologic Engineering Center – Hydrologic Modeling System, was developed by the U.S. Army Corps of Engineers to "simulate the precipitation-runoff processes of dendritic watershed systems" (HEC, 2001). The program allows users to enter the specific hydrologic characteristics of their watershed and analyze them under a variety of rainfall and flow conditions. Hydrologic site characteristics and a number of different size storm events were used to calibrate and verify the model. Included in the output are the water surface elevations for each infiltration bed. The model elevation of water in the lower bed was compared to the water surface depths recorded. It was through this method that the model was verified to ensure it accurately modeled the site (Ladd, 2004). In the current study, presented in this report, a new model was created to characterize the infiltration occurring in the underground basins.

4.2 Model Overview

The porous concrete site was designed to store and infiltrate runoff from the first 2.0 in (5.1 cm) of rainfall, which accounts for 80% of the annual rainfall events for this region. This study focuses on the recession limb of the outflow hydrograph consisting solely of "saturated" infiltration. The Green-Ampt formula was used to model the infiltration occurring in the lower infiltration bed once the water level in the bed had reached its maximum level.

Recall from Chapter 2, the original Green-Ampt equation, equation (1),

$$f_p = K_s \frac{(S - L)}{L} \tag{1}$$

where f_p = infiltration rate [L/T], K_s = saturated hydraulic conductivity [L/T], S = capillary suction at the wetting front [L] and L = distance from the ground surface to the wetting front [L]. The value for the distance to the wetting front L, an unmearsurable parameter, was then replaced by two measurable parameters, cumulative infiltrated water, F and initial and saturated soil moisture content, θ_i and θ_s. This equation was then derived and resulted in equation (4).

$$F - S(\theta_s - \theta_i)\ln(\frac{F + S(\theta_s - \theta_i)}{S(\theta_s - \theta_i)}) = K_s t \tag{4}$$

However, both equation (1) and equation (4) assume that the soil surface is covered by ponded water of negligible depth. In a study done by Al-Muttair and Al-Turbak (1991) a continuous system infiltration model, equation (5), was created to determine the cumulative infiltration at set time intervals. In this equation, the soil suction, moisture content, and a new parameter, H to account for a ponded depth, were grouped into one variable, the storage suction factor, S_f, equation (6). All variables in equations (5) and (6)

are measurable soil properties, which is why Green-Ampt formula is characterized as "physically approximative."

$$K_s(t_j - t_{j-1}) = F_j - F_{j-1} - S_{fj}\ln(\frac{S_{fj} + F_j}{S_{fj} + F_{j-1}}) \quad (5)$$

$$S_f = (S + H)(\theta_s - \theta_i) \quad (6)$$

There are three main assumptions for the use of this model. The first assumption is that the water is being infiltrated into a homogeneous soil. The second is that behind the wetting front, the soil is uniformly saturated with a constant hydraulic conductivity corresponding to that of natural saturation. The third and final assumption is that, at the wetting front, the soil suction pressure head remains constant

The infiltration model developed for this report utilizes the study done by Al-Muttair and Al-Turbak (1991), using equation (5) as its basis. However, the geometry of the basin in this study is slightly different. Instead of using an open surface infiltration basin with vertical side walls, the current study considers the infiltration bed, underlying the porous concrete site, which is filled with stone that provides a 40% void space and has 2H:1V sloped side walls. Also, instead of lining the walls of the basin to prevent lateral infiltration, the current study approximates the infiltration occurring from the side walls based on the ratio of wetted surface area of the side walls as it relates to the surface area of the bed bottom. Equation (20), formulated in Chapter 3, relates the elevation in the bed, x, to the % of bed bottom infiltration associated with the side walls, y.

$$y = 0.0001x^2 + 0.0255x \quad (20)$$

Since the model is based on a unit of bed bottom area, this equation bases the infiltration occurring through the side walls as a percent of the infiltration occurring from the bed

bottom. The total infiltration is thus the bed bottom area infiltration added to a percent of the bed bottom area described as side wall infiltration.

Lastly, this model is evaluated using actual rain data and bed elevation data collected and recorded at 5 minute intervals during storm events occurring over the site. This will give a better interpretation of the site performance since the analysis was done under actual field conditions. This model is ideal for infiltration bed analysis because it relies mainly on physical parameters, which can be evaluated from properties of the soils identified through simple field tests.

4.3 Model Input Parameters

During the infiltration process, it is assumed that water enters the soil uniformly to create a discrete "Wetting Front" a depth, L from the bed bottom, separating the saturated soil above from the unsaturated soil below. Figure 40 illustrates this for an underground infiltration bed with sloped side walls.

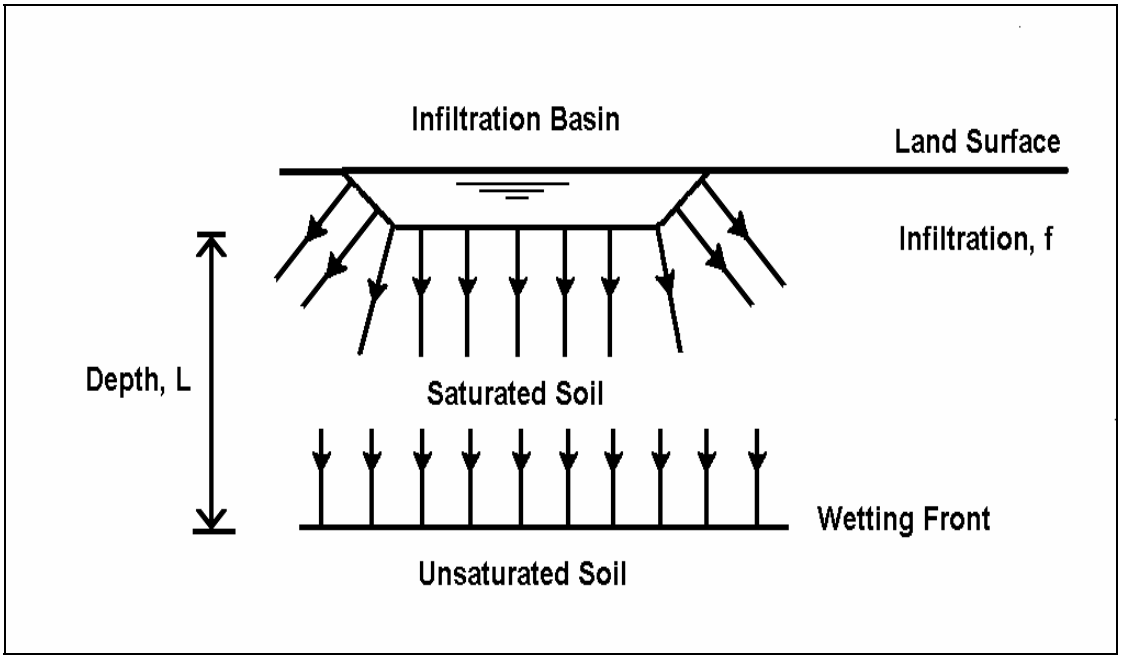

Figure 40. Infiltration basin wetting front

4.3.1 Storage Suction Factor

The storage suction factor is composed of the soil suction pressure head, the hydraulic pressure head, and the initial and saturated moisture content as seen below in equation (6) from Chapter 2.

$$S_f = (S + H)(\theta_s - \theta_i) \tag{6}$$

Using the Unified Soil Classification System (USCS), the soil at the porous concrete site was characterized as an inorganic silty sand (ML) of low plasticity. According to the United States Department of Agriculture (USDA) Soil Textures chart, an ML corresponds to a silt loam or a very fine sandy clay loam. With these characteristics and knowing the location of the site in Pennsylvania the soil was then classified a Silt Loam under Soil Class - B Type Soil (Rawls, Brakensiek, and Miller, 1983). The following model parameters will be based on this soil classification.

4.3.1.1 Soil Suction and Hydraulic Head

The soil suction head of a silt loam at the wetting front under Soil Class - B Type Soil is 6.57 in. (16.69 cm) (Rawls, Brakensiek, and Miller, 1983). A single standard deviation above and below this value results in 1.15 in (2.92 cm) and 37.56 in (95.40 cm) respectively. For the purpose of this study, 6.57 in (16.69 cm) was used in the model as an initial value.

The hydraulic head is taken from the data collected from the pressure transducer located in the lower infiltration bed. The maximum depth recorded in the bed is used as a starting point for the model. Using this value, the model is run and the next value for hydraulic head is calculated by subtracting the infiltration calculated during that time step from the initial maximum hydraulic head value.

4.3.1.2 Volumetric Moisture Content

In the study done by Al-Muttair and Al-Turbak (1991), soil samples were taken from different locations and depths in the basin before each test was run and an average initial moisture content was calculated and recorded. This process could not be done in the current study because the basin is under a developed site and is not accessible. However, water content reflectometers, or moisture meters (labeled B11, B12, and B13), are located below the bed bottom of the lower infiltration bed. These meters record volumetric moisture content at depths of 1.0 ft (0.31 m), 2.0 ft (0.61 m), and 4.0 ft (1.22 m) below the bed bottom, respectively, as described in Chapter 3. By plotting bed depth with the volumetric moisture content across time, the initial volumetric moisture content for the three moisture meters was found for each storm. These values were then averaged to obtain composite initial moisture content. Figure 41 displays this graph for the months of April through May 2004. All graphs for 2004 and data for each moisture meter can be found in Appendix H and Appendix I.

The initial moisture content, the lowest value before the water level in the bed began to rise and the volumetric moisture content began to increase, varied widely in range from approximately 0.17 to 0.25. It was noticed that antecedent dry time had an effect on these values. Figure 42 illustrates the moisture content for B11, B12, B13 and the Composite Initial value for all events versus the antecedent dry time. In this analysis, the antecedent dry time was based on the time between when the bed level in the port fell to zero and the time of the next rain storm. For graphical purposes the last three data points were omitted from Figure 42, due to their extended antecedent dry time (between 450 and 1000 hrs). However these points were used in the computational analysis.

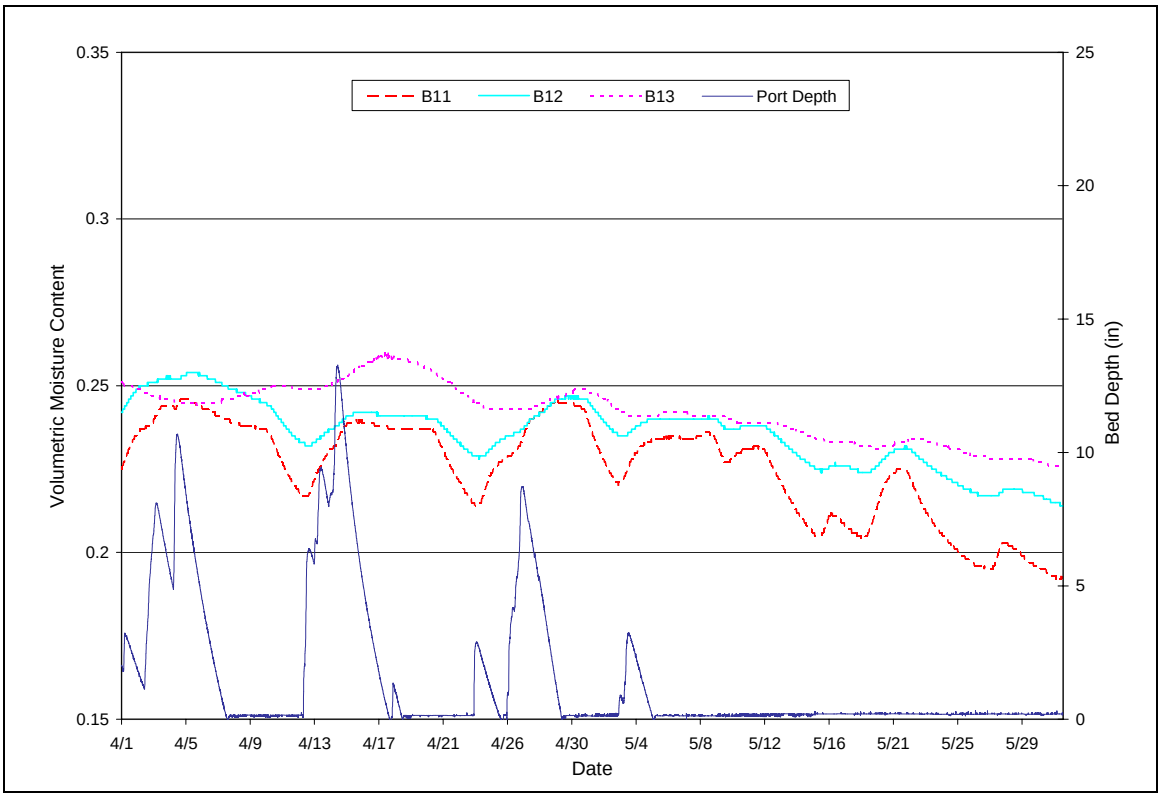

Figure 41. Moisture content and bed depth (April - May 2004)

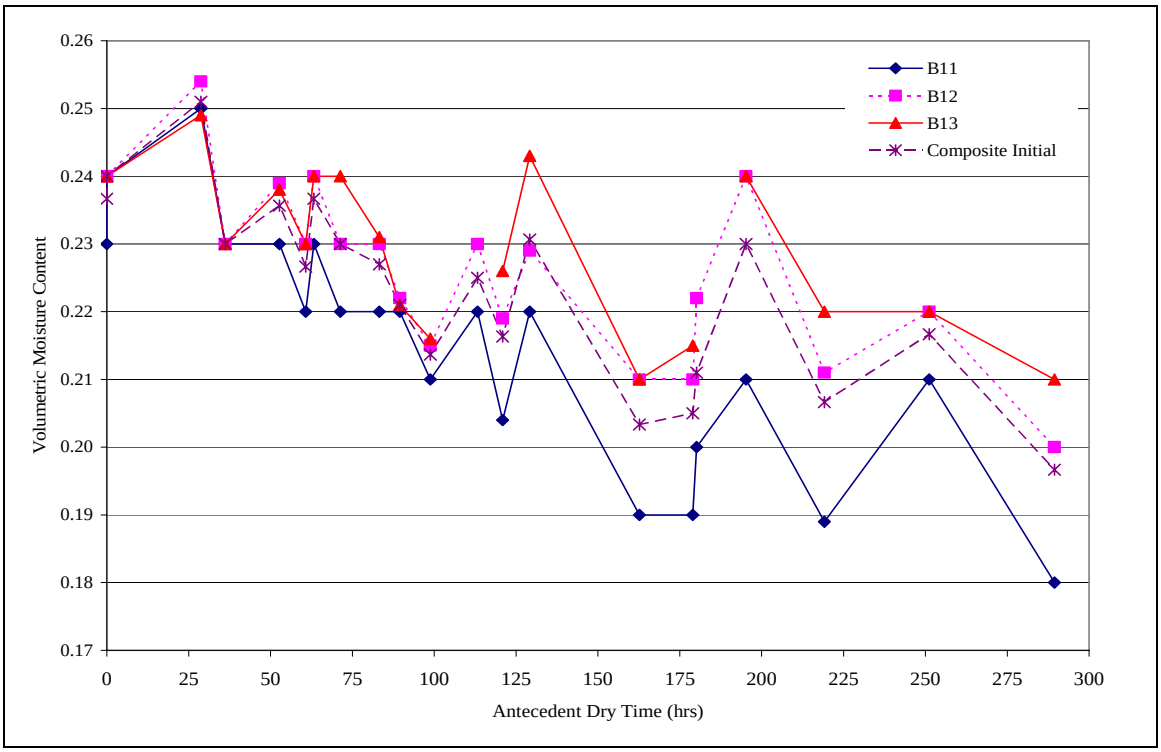

Figure 42. Antecedent dry time vs. initial moisture content (April - December 2004)

Figure 42 illustrates that as antecedent dry time increases the soil is drying out and the volumetric moisture content is decreasing. Therefore, in the model, the value for initial moisture content will instead be based on the antecedent dry time. The saturated moisture content was also found for each event in a similar manner, and the final values for both initial and saturated moisture content by antecedent dry time are displayed in Table 3.

Table 3. Moisture content by antecedent dry time (April - December 2004)

Antecedent Dry Time		Initial MC	Saturated MC
0-2 days	0-48 hrs	0.24	0.25
2-3 days	48-72 hrs	0.23	0.25
3-5 days	72-120 hrs	0.22	0.24
5+ days	120+ days	0.21	0.24

Since the moisture content at saturation should remain constant throughout the soil, one value should be used for all BMP events. In this case, the value chosen for the model was 0.245, which is based on the average of the saturated moisture content values in Table 3. This value is a good fit for the data as shown in Figure 43 which illustrates the saturated moisture content data in addition to error bars of one standard deviation in each direction, placing 0.245 at approximately the center of this deviation.

The moisture content data evaluated thus far has consisted of the months of April 2004 through December of 2004. However, as shown in Figure 44, this data does not fit events occurring in December of 2003 through March of 2004. Therefore, a different set of moisture content values was necessary for the model evaluation.

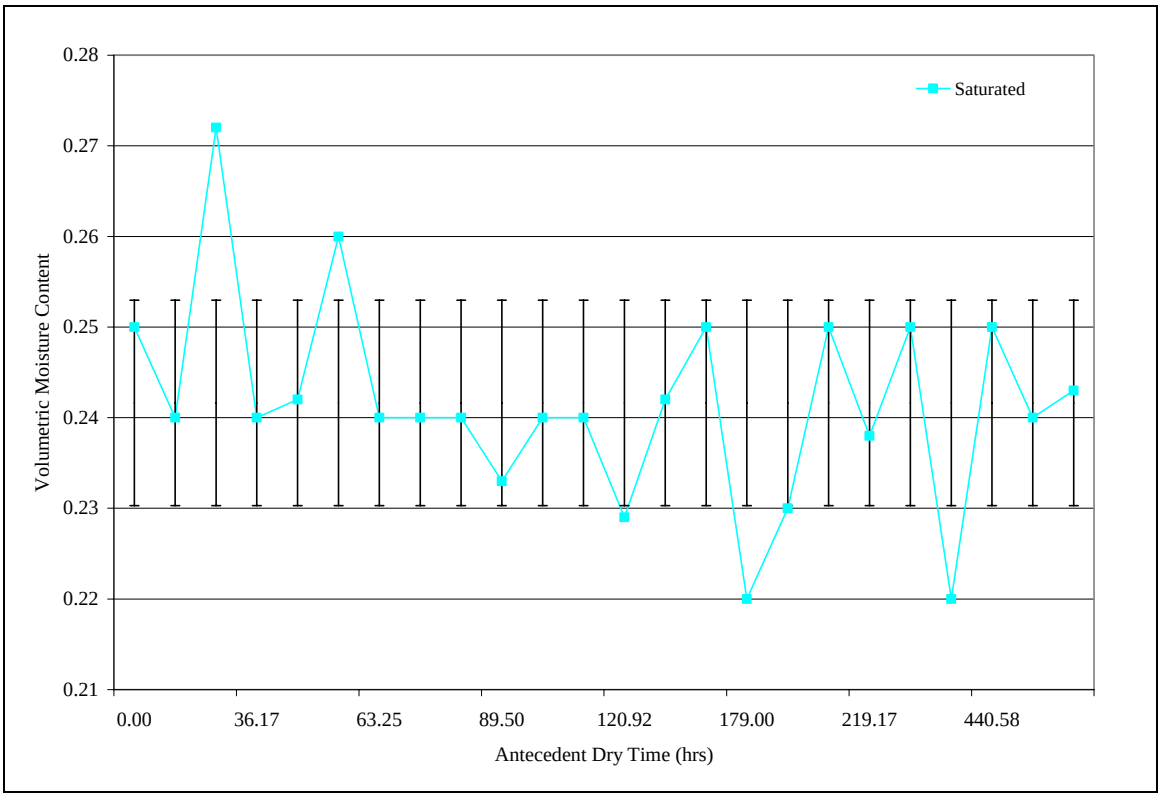

Figure 43. Antecedent dry time vs. saturated moisture content (April - December 2004)

During the winter months, when the temperature is lower, the soil response is drastically different from summer. The water infiltrating through the bed bottom creates a wetting front that is slower moving, meaning that the time between moisture content peaks for B11, B12 and B13 is longer. Additionally, the saturation peaks are much higher than for summer data. This response could be due to different soil and water interactions that occur during colder temperatures. A statistical analysis was completed on the winter data. For the months of January through March a new data set for moisture content will be used, rather than those previously supplied in Table 3. A value of 0.25 will be used for initial moisture content and 0.36 will be used for saturated moisture content. The data for this analysis can be reviewed in Appendix I.

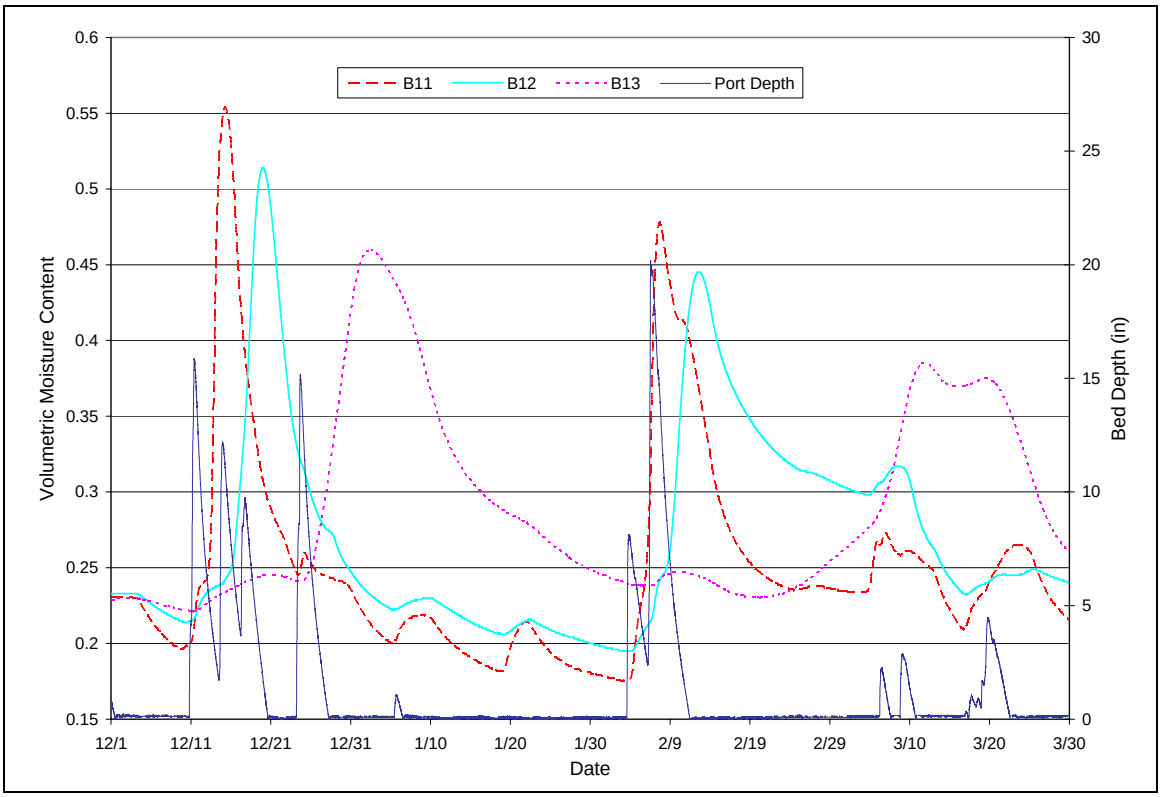

Figure 44. Moisture content and bed depth (December 2003 - March 2004)

4.3.2 Initial Infiltrated Depth

The value for initial infiltrated depth was chosen by evaluating all single peaking BMP events in 2004. For each event, the initial infiltrated depth was recorded from the peak bed level to the next recorded value five minutes later. A statistical analysis was then done and the mean of these values was recoded as 0.050 in. (0.127 cm). This value was then set as a constant for all storms as a starting point for the model to begin calculating infiltration using the previously supplied equation (5).

4.3.3 Saturated Hydraulic Conductivity

The hydraulic conductivity of a silt loam at the wetting front, saturated conditions, under Soil Class - B Type Soil is 0.268 in/hr (0.68 cm/hr) (Rawls, Brakensiek, and Miller, 1983). The saturated hydraulic conductivity resulting from the flexible wall

hydraulic conductivity test done on the soil sample on site was 0.24 in/hr (0.61 cm/hr), based on the average of four measurements. For the purpose of this study 0.24 in/hr will be used as a starting value for saturated hydraulic conductivity since it is the result of actual field data from the site. A summary of all model input parameters is listed in Table 4.

Table 4. Model parameter summary

Parameter:	Soil Suction Head	Hydraulic Head	Moisture Content		Initial Infiltrated Depth	Saturated Hydraulic Conductivity
			Initial	Saturated		
U. S.	6.57 in	based on bed depth	based on antecedent dry time (0.25 Jan-Mar)	0.245 (0.36 Jan-Mar)	0.05 in	0.24 in/hr
Metric	16.69 cm				0.13 cm	0.61 cm/hr

Once the parameters are determined they are put into an Excel worksheet (Appendix J) and the model is run utilizing code in Visual Basic (Appendix K) which performs the trial and error manipulation of equation (5). Figure 45 illustrates the excel worksheet input parameters needed to run the model for event 9/18/2004.

Green-Ampt Analysis:	Storm	09/18/2004		
			End Row	759
Parameters				
Hydraulic Conduct., K_s	0.24	in/hr		
Antecedent Dry Time	1085.33	hrs		
Moisture Content, θ_i	0.21	(MMs)	Accuracy = 0.001	
Moisture Content, θ_s	0.245	(MMs)		
Suction Head, S	6.57	in (book)		
Initial Port Depth	17.10	in (data)		
Initial Infiltrated Depth	0.05	in (data)		

Figure 45. Event 09/18/2004 model input worksheet

4.4 Model Calibration

Once the model run is complete, the results are plotted for comparison to the observed data. Figure 46 shows the results of the recession limb of the preliminary run for event 08/01/04. The solid line is the actual data, as recorded from the pressure transducer in the lower bed, and the dashed line is the result from the model.

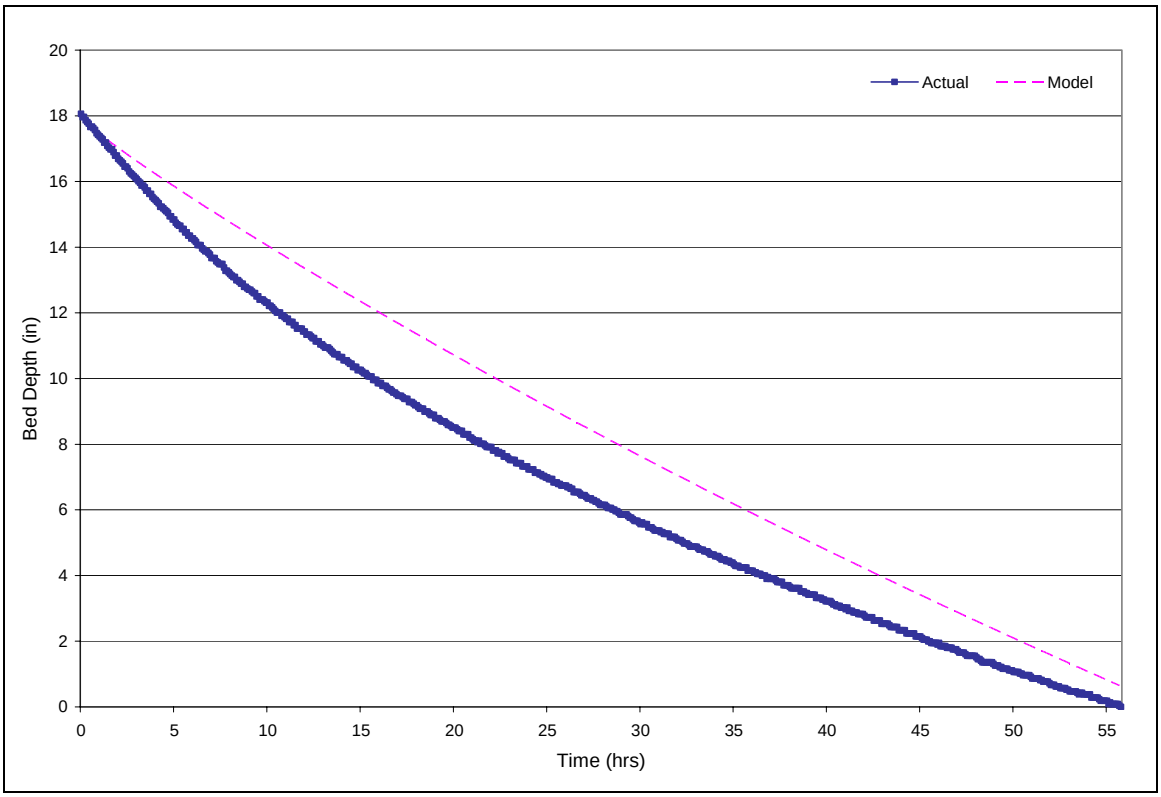

Figure 46. Recession limb for event 08/01/04

The model results in a very close estimate of the event. However, the model does not show as much curvature as the actual data and it underestimates the total infiltrated depth. This can be seen more clearly in Figure 47.

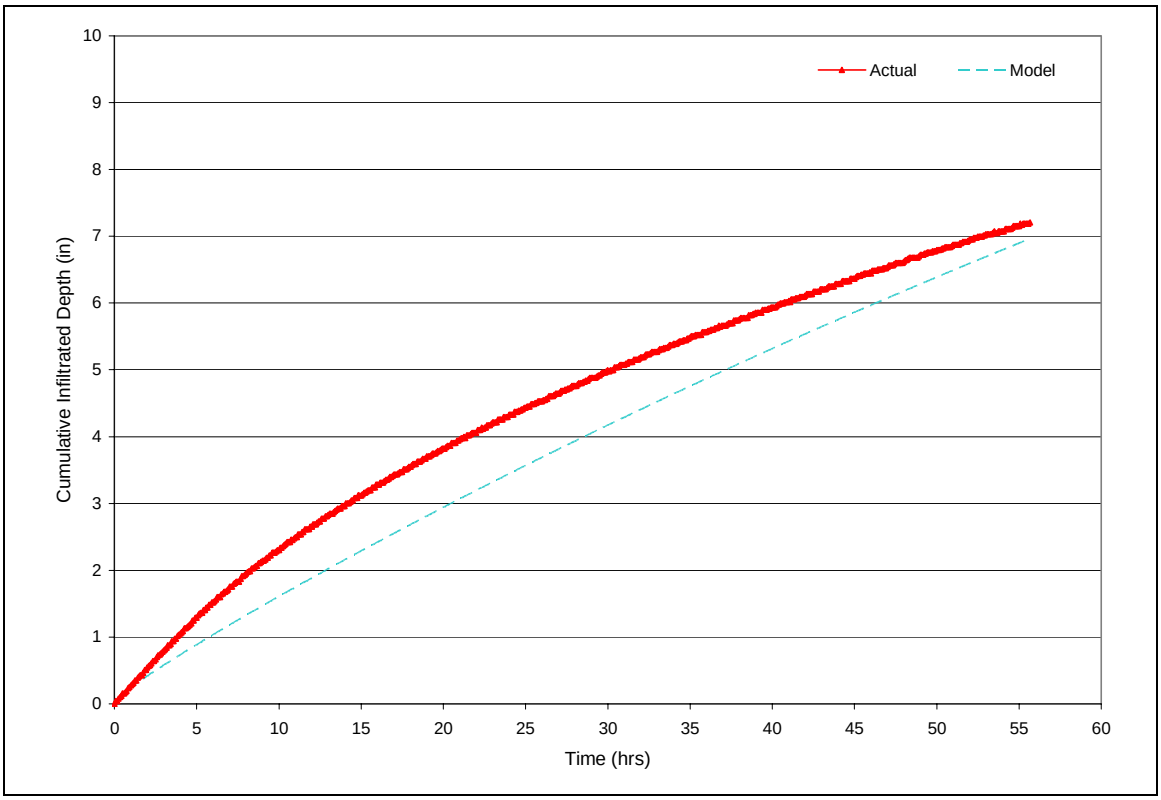

Figure 47. Cumulative infiltrated depth for event 08/01/04

Figure 47 shows the cumulative infiltrated depth of water across the duration of the event. These values are approximately 40% of those shown in Figure 46. Figure 46 illustrates the recession limb of the outflow hydrograph, or what is actually occurring in the infiltration bed during a BMP event. The bed depth decreases over time as water is infiltrating into the soil below. However, the amount of water that is actually infiltrating from the bed into the subsurface soil is only a fraction of the change in bed depth. A limited amount of void space is provided by the AASHTO #2 stone which resides in the bed. Therefore, the actual depth of infiltrated water is only 40% of the change in bed depth.

The results for event 03/07/04 are shown in Figure 48 and Figure 49. In this case, the model results are poor.

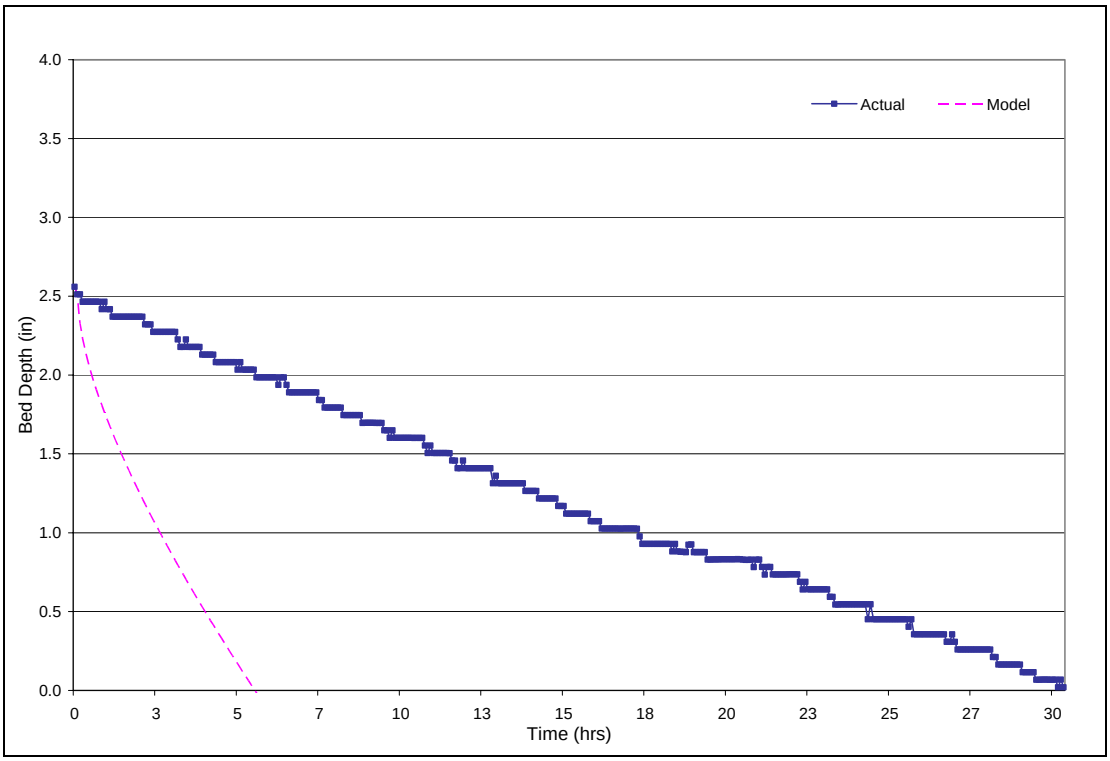

Figure 48. Recession limb for event 03/07/04

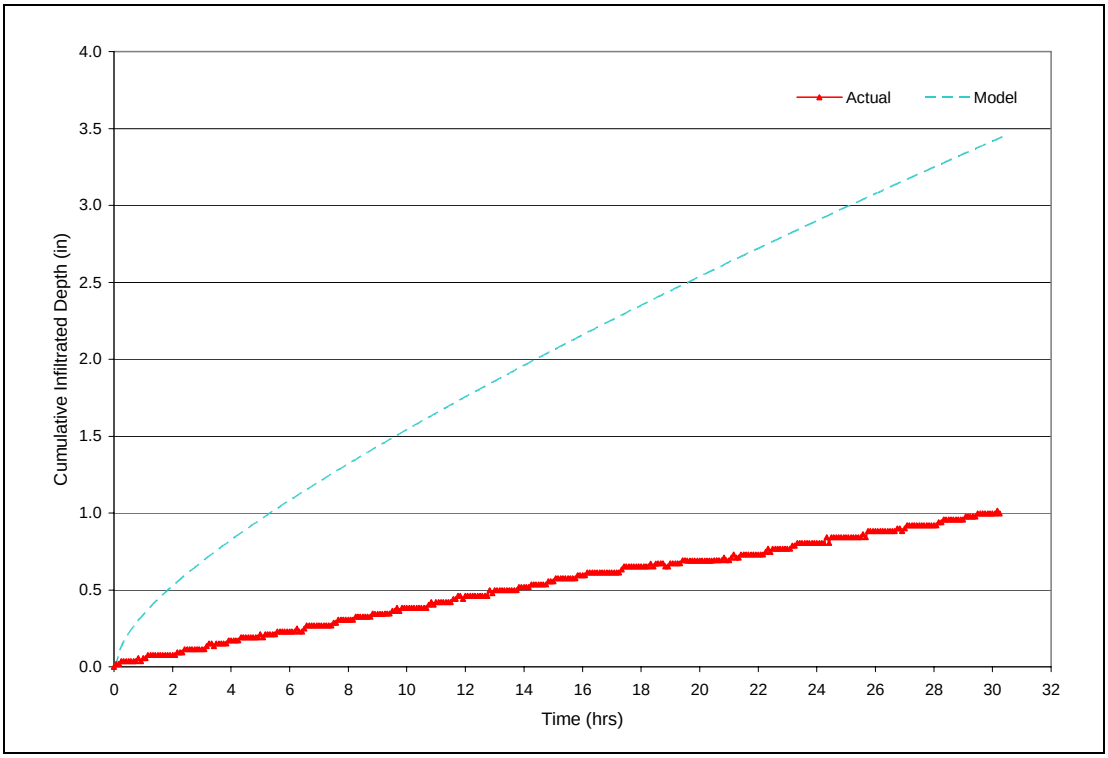

Figure 49. Cumulative infiltrated depth for event 03/07/04

The model highly overestimates the infiltration capacity of the BMP, resulting in an empty bed nearly 24 hours earlier than the actual event as shown in Figure 48, or over triple the infiltrated stormwater as shown in Figure 49. This trend was seen in most events modeled necessitating an evaluation of the error present between the actual and the model values and further investigation of the sensitivity of the input parameters. Results for all events modeled for the preliminary analysis can be seen in Appendix L and M.

4.4.1 Statistical Analysis

In order to determine how well the model portrays the actual observed data for each event a numerical representation is required. The Mean Square Error (MSE) was chosen to accomplish this. The MSE is an old, proven measure of control and quantity and equals the mean of the squares of the deviations from the target value as shown in equation (21).

$$MSE = \frac{1}{m}\sum_{i=1}^{m}(x_i - T)^2 \tag{21}$$

Where: x_i = ith value of a group of m values (model value),

T = target or intended value for the product variable of interest (actual value) (Battaglia, 1996).

The MSE was then calculated for the data sets for each event modeled and the results are shown in Table 5. The closer the error is to zero, the better the model fit to the actual data, with a zero error being an exact fit. The MSE for the Cumulative Infiltration is 40% squared the MSE for the Recession Limb, as is expected due to the void space. Knowing the current error a sensitivity analysis was completed to evaluate the effect that each parameter had on the overall MSE for each event data set.

Table 5. Preliminary results: Mean Square Error

Event	Mean Square Error	
	Preliminary Run	
	Recession Limb	Cumulative Infiltration
01/04/04	8.98	1.44
03/06/04	13.18	2.08
03/07/04	15.91	2.55
04/23/04	15.10	2.41
06/16/04	4.61	0.74
06/22/04	4.08	0.55
07/18/04	7.23	1.16
07/23/04	6.30	1.01
08/01/04	2.78	0.44
09/18/04	1.50	0.25
10/30/04	8.90	1.42
11/04/04	54.78	8.77
11/12/04	76.26	12.18
12/07/04	16.28	2.60
12/23/04	23.96	3.83

4.4.2 Sensitivity Analysis

A sensitivity analysis was completed for three input parameters to the model, the soil suction pressure head, the volumetric moisture content, and the saturated hydraulic conductivity. By quantifying how each parameter changes the resulting MSE between the actual and the model data sets, the calibration process can be accomplished more accurately by changing only the parameters which result in the greatest decrease in overall error for the data sets.

The soil suction pressure head, S was the first parameter altered. Since it was noted previously that the input value of 6.57 in (16.69 cm) had a single standard deviation above and below resulting in 1.15 in (2.92 cm) and 37.56 in (95.40 cm) respectively, it was these values that were chosen to evaluate the sensitivity of this parameter. The resulting MSE for each event is recorded in Table 6.

Table 6. MSE evaluation for soil suction pressure head

Event	Mean Square Error: Soil Suction Pressure Head					
	S (-1 STD)			S (+1 STD)		
	Recession Limb	Cumulative Infiltration	% Change from Preliminary	Recession Limb	Cumulative Infiltration	% Change from Preliminary
01/04/04	5.23	0.84	-41.78	25.28	4.05	181.54
03/06/04	8.35	1.31	-36.67	35.15	5.58	166.60
03/07/04	10.44	1.67	-34.41	40.74	6.52	156.02
04/23/04	12.93	2.06	-14.37	24.66	3.94	63.30
06/16/04	3.31	0.53	-28.29	10.87	1.74	135.64
06/22/04	3.15	0.42	-22.89	8.29	1.18	103.18
07/18/04	6.24	1.00	-13.71	11.79	1.89	63.11
07/23/04	5.01	0.80	-20.47	12.34	1.97	95.76
08/01/04	3.10	0.50	11.38	1.51	0.24	-45.67
09/18/04	1.03	0.17	-31.33	6.80	1.11	353.33
10/30/04	6.92	1.10	-22.19	16.70	2.67	87.76
11/04/04	50.60	8.10	-7.64	74.86	11.98	36.64
11/12/04	71.32	11.39	-6.48	99.78	15.94	30.84
12/07/04	14.73	2.36	-9.47	22.95	3.67	41.00
12/23/04	20.45	3.27	-14.62	39.92	6.39	66.62

The MSE decreased with decreasing soil suction pressure head in every event, with the exception of event 08/01/04 which was the only event that was initially overestimated by the model. Correspondingly, with increasing soil suction pressure head, MSE increased as well, again with the exception of event 08/01/04. Therefore, a potential way to decrease the overall error in the model and create a better fit between the model and the actual data would be to decrease the soil suction pressure head input value. However, the percent change from the preliminary data run for each event ranges from approximately as little as 6% to as large as 40%. This leaves a large discrepancy between values, and although changing the value for S would help some events, the amount of reduced error is unequal between events.

The second variable that was altered was the volumetric moisture content. The initial and saturated volumetric moisture content for the soil are both inputs to the model. Yet the difference between these values, or the initial moisture deficit (IMD) is what is actually used within the equation for the model. To simplify the analysis, an evaluation was done to see how important the volumetric moisture content is to the model. Therefore, instead of separating the moisture content by antecedent dry time, the total

average values were used and the results were recorded. Therefore, values of 0.21 and 0.24 were used for initial and saturated volumetric moisture content, respectively. Since the average moisture contents were already used for the months of January through March, the analysis will not include events in these months. The results for this analysis can be seen in Table 7.

Table 7. MSE evaluation for volumetric moisture content

Event	Antecedant Dry Time (hrs)	Mean Square Error		
		Average Vol. MC Values		
		Recession Limb	Cumulative Infiltration	% Change from Preliminary
01/04/04	180.17	-	-	-
03/06/04	566.42	-	-	-
03/07/04	6.00	-	-	-
04/23/04	129.17	15.62	2.49	3.46
06/16/04	1009.00	4.36	0.70	-5.59
06/22/04	120.92	4.31	0.59	5.63
07/18/04	52.75	8.49	1.36	17.40
07/23/04	83.25	6.65	1.06	5.48
08/01/04	28.75	0.32	0.05	-88.32
09/18/04	1085.33	0.97	0.16	-35.07
10/30/04	179.00	8.58	1.37	-3.56
11/04/04	98.83	56.36	9.02	2.88
11/12/04	89.50	78.06	12.47	2.36
12/07/04	63.25	17.91	2.87	10.05
12/23/04	219.17	23.25	3.72	-2.97

Changing the moisture content to the average values had mixed effects on the MSE of the data sets. The events with the greater antecedent dry times (>150 hrs) had errors that decreased whereas most other values increased slightly, with the highest increases occurring with the lowest antecedent dry time. This result is expected because it is the events with the shortest antecedent dry time that received the greatest increase in initial moisture deficit. Again, event 08/01/04 was an exception with the highest decrease in error and the lowest antecedent dry time. This is because the initial error for this event was so small that even the slightest decrease in error would have a large effect on the percent change from the preliminary run. However, as with the soil suction

pressure head, the changes in moisture content only altered the error slightly and the results were varied between events. Therefore, the original moisture contents would remain in the model and the moisture content would continue to be based on antecedent dry time, as this is the most accurate representation of the actual data.

The parameter that showed the most influence on the model was the hydraulic conductivity, which in this model is assumed to be saturated. It was shown in the preliminary runs that the initial value of 0.24 in/hr (0.61 cm/hr) was too high in nearly every event. As a result, this value was decreased by 20-percent and the results were recorded in Table 8.

Table 8. MSE evaluation for saturated hydraulic conductivity

Event	Mean Square Error		
	Sat. Hydraulic Conductivity, K (-20%)		
	Recession Limb	Cumulative Infiltration	% Change from Preliminary
01/04/04	6.04	0.97	-32.74
03/06/04	8.36	1.31	-36.57
03/07/04	10.01	1.60	-37.11
04/23/04	8.62	1.37	-42.90
06/16/04	2.34	0.37	-49.36
06/22/04	2.31	0.30	-43.39
07/18/04	3.58	0.57	-50.43
07/23/04	3.15	0.50	-50.02
08/01/04	11.14	1.78	300.68
09/18/04	1.36	0.21	-9.47
10/30/04	5.30	0.85	-40.39
11/04/04	28.19	4.51	-48.55
11/12/04	41.38	6.61	-45.74
12/07/04	9.72	1.56	-40.26
12/23/04	13.16	2.11	-45.06

In all cases, less one, the MSE decreased with decreasing saturated hydraulic conductivity. This decrease in error was in the range of approximately 30 to 50-percent decrease with a 20-percent decrease in saturated hydraulic conductivity. Event 08/01/04 was the only event to result in an increased error due to the fact that the initial run underestimated the infiltrated water and by decreasing the saturated hydraulic

conductivity, it further underestimates the actual data. The infiltration rate for all other events was overestimated and by decreasing the hydraulic conductivity, the error was decreased significantly.

4.4.3 Calibration Results

After evaluating the results of the sensitivity analysis, it was decided that the calibration process would consist of changing the value for saturated hydraulic conductivity for each event, while holding all other variables constant, until the error was decreased to as close to zero as possible. During the calibration process it was observed that for larger events, events that showed a less linear relationship with decreasing bed depth, when altering the saturated hydraulic conductivity the model's curve was not matching the actual curve. It was then noted, that by increasing the side wall contribution the magnitude of the curve also increased creating a better match to actual data. Therefore, the side wall infiltration contribution for all storms was increased by 40-percent, which can be seen in the new equation for side wall contribution, equation (22), which replaced the previous equation (20).

$$y = 0.0002x^2 + 0.0357x \tag{22}$$

Similar to equation (20), this equation bases the infiltration occurring through the side walls as a percent of the infiltration occurring from the bed bottom. However, equation (22) is 40-percent greater than equation (20). This increase in side wall contribution is justified by the fact that the actual constructed geometry of the infiltration bed may not correspond exactly to the plans from which the initial side wall infiltration equation was based. The bed's side walls may have been constructed in a more parabolic or curved shape rather than the intended trapezoidal shape, or the constructed slope of the

side walls could be gentler than intended, thus increasing the surface area of the side walls. In addition, the infiltration through the side walls may be greater than the infiltration through the bed bottom due to some clogging of the bed bottom that may have occurred through both of its reconstruction periods. Therefore, all events were modeled with this new side wall infiltration equation. The resulting MSE and storm specific saturated hydraulic conductivities for all events are recorded in Table 9 and Table 10.

Table 9. Final MSE for small storm events

Event	Hydraulic Conductivity (in/hr)	Max Bed Depth (in.)	Mean Square Error			
			Preliminary Run		Final Run	
			Recession Limb	Cumulative Infiltration	Recession Limb	Cumulative Infiltration
01/04/04	0.02	1.079	8.98	1.44	0.010	0.002
03/06/04	0.04	2.271	13.18	2.08	0.049	0.006
03/07/04	0.04	2.897	15.91	2.55	0.021	0.003
04/23/04	0.06	2.890	15.10	2.41	0.025	0.004
06/16/04	0.08	2.829	4.61	0.74	0.019	0.003
06/22/04	0.08	2.097	4.08	0.55	0.098	0.003
07/18/04	0.08	3.219	7.23	1.16	0.013	0.002
07/23/04	0.08	3.071	6.30	1.01	0.015	0.002
10/30/04	0.04	1.731	8.90	1.42	0.009	0.001
12/07/04	0.04	2.562	16.28	2.60	0.008	0.001

Table 10. Final MSE for large storm events

Event	Hydraulic Conductivity (in/hr)	Max Bed Depth (in.)	Mean Square Error			
			Preliminary Run		Final Run	
			Recession Limb	Cumulative Infiltration	Recession Limb	Cumulative Infiltration
08/01/04	0.26	21.710	2.78	0.44	0.580	0.093
09/18/04	0.18	17.010	1.50	0.25	0.836	0.127
11/04/04	0.08	9.390	54.78	8.77	0.036	0.006
11/12/04	0.07	9.650	76.26	12.18	0.098	0.016
12/23/04	0.07	4.523	23.96	3.83	0.023	0.004

The model results were separated in two tables based on the maximum bed depth. All events below 4 in (10.16 cm) were labeled “small storm events”, whereas the events with a higher bed depth were labeled “large storm events”. The mean square error for each event in both Table 9 and Table 10 dropped drastically to well below 1.0. However, the hydraulic conductivity is different for nearly every event. To gain a better

understanding of how the hydraulic conductivity was changing, the results for all 2004 events were plotted in Figure 50 and Figure 51.

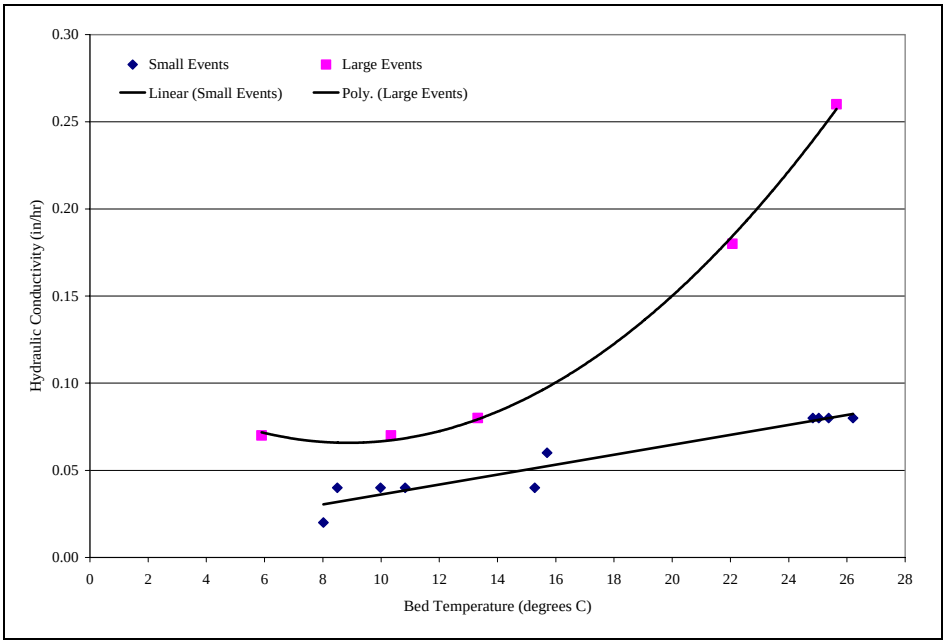

Figure 50. Hydraulic conductivity vs. bed temperature for 2004 events

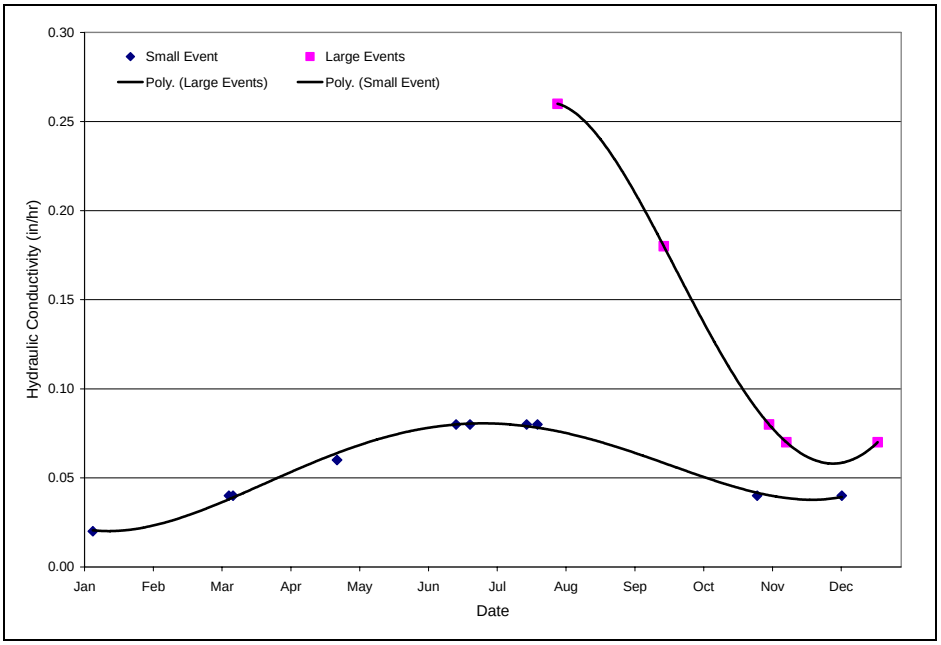

Figure 51. Monthly hydraulic conductivity for 2004 events

Figure 50 shows a relationship between hydraulic conductivity and temperature for both the small and large events. A linear trend line and a polynomial trend line were fit to the small and large event data, respectively, which further illustrates this relationship.

Figure 51 shows the hydraulic conductivity plotted versus the date for each event. As shown in the figure, the small event data has a relatively even spread from January to December of 2004, but the data for the larger events dates from only August to December of 2004. Therefore, three more events in early 2005 were added to the calibration analysis to formulate the beginning of the curve in order to determine if the larger events followed a pattern similar to that for the smaller events. The three additional storms and their associated MSE, hydraulic conductivity, and bed depth are listed in Table 11. Graphical results for these events can be found in Appendix P. Figures 52 and 53 illustrate the updated figures with the addition of the 2005 events.

Table 11. MSE for additional calibrated 2005 events

Event	Hydraulic Conductivity (in/hr)	Max Bed Depth (in.)	Mean Square Error	
			Final Run	
			Recession Limb	Cumulative Infiltration
01/13/05	0.17	15.980	0.747	0.119
03/27/05	0.10	13.690	0.319	0.051
04/01/05	0.25	21.660	0.259	0.041

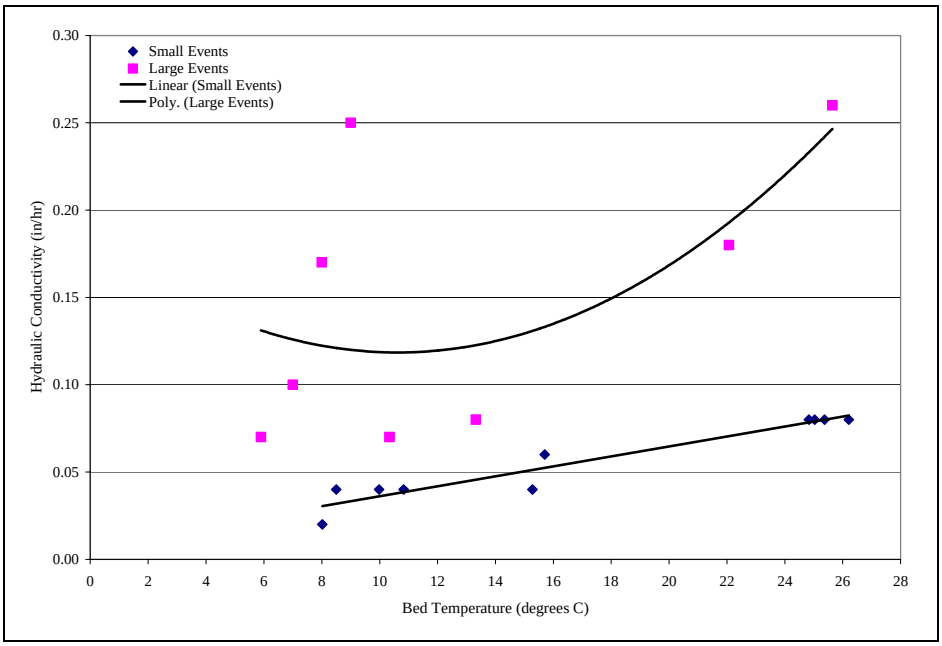

Figure 52. Updated hydraulic conductivity vs. bed temperature for 2004 and additional 2005 events

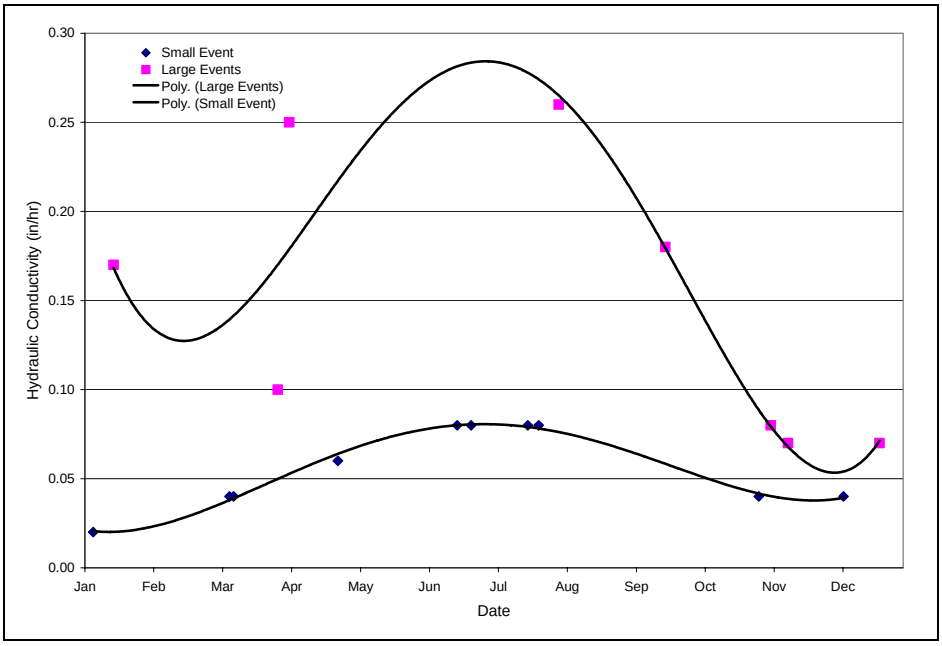

Figure 53. Updated monthly hydraulic conductivity for 2004 and additional 2005 events with third order trend lines

It can be seen in Figure 52 and 53 that the same trends noticed for the small events are not present to the same degree for the larger events. The smaller events are all between the bed depths of approximately 1 in (1.54 cm) and 4 in (10.16 cm). The larger events vary widely between 4 in (10.16 cm) and 22 in (55.88 cm). Therefore, the discrepancy may be due to volume of water infiltrating into the system and thus the maximum depth in the bed for each storm should be analyzed. The bed depth data for both small and large events is plotted in Figure 54.

Figure 54 shows a strong relationship between bed depth and hydraulic conductivity. The polynomial trend line shows that the hydraulic conductivity is a function of bed depth or the maximum water surface elevation reached in the bed during a storm event. It can be assumed that smaller storms do not provide enough volume of stormwater in the bed to fully saturate the soil and the true saturated hydraulic conductivity results only from the largest of storms. The saturated hydraulic conductivity based on Figure 54 is 0.26 in/hr, which is the value estimated by the specified soil type at the site, a Silty Loam, and is also further verified by the field test. Therefore, the model is operating with an unsaturated hydraulic conductivity for all events lower than approximately 22 in (55.88 cm) in bed depth.

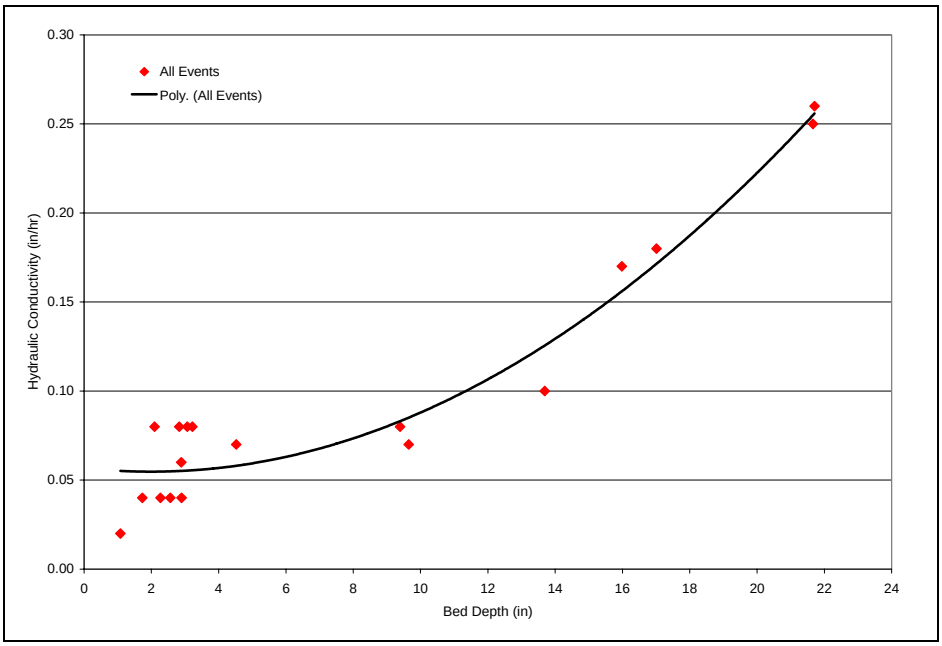

Figure 54. Hydraulic conductivity vs. bed depth

To select a hydraulic conductivity to verify the model, the characteristics of both the 2004 and 2005 events used for calibration were evaluated in Table 12.

Table 12. Event data by hydraulic conductivity

Event	Hydraulic Conductivity (in/hr)	Max Bed Depth (in.)	Mean Temperature (°C)	
			Bed	Ambiant
Small Events				
07/18/04	0.08	3.22	25	22
07/23/04	0.08	3.07	26	23
06/16/04	0.08	2.83	25	25
06/22/04	0.08	2.10	25	24
04/23/04	0.06	2.89	16	13
03/07/04	0.04	2.90	10	3
03/06/04	0.04	2.27	11	11
12/07/04	0.04	2.56	9	7
10/30/04	0.04	1.73	15	16
01/04/04	0.02	1.08	8	6
Large Events				
08/01/04	0.26	21.71	26	26
04/01/05	0.25	21.66	9	9
09/18/04	0.18	17.01	22	17
01/13/05	0.17	15.98	8	3
03/27/05	0.10	13.69	7	8
11/04/04	0.08	9.39	13	9
11/12/04	0.07	9.65	10	5
12/23/04	0.07	4.52	6	2

Since all the data for the small events have relatively the same bed depth, the main parameter causing the changes in hydraulic conductivity is temperature. Therefore, the hydraulic conductivity for all small storm events (< 4" in bed depth) will be chosen based on the temperature in the bed and the trend line formulated in Figure 55.

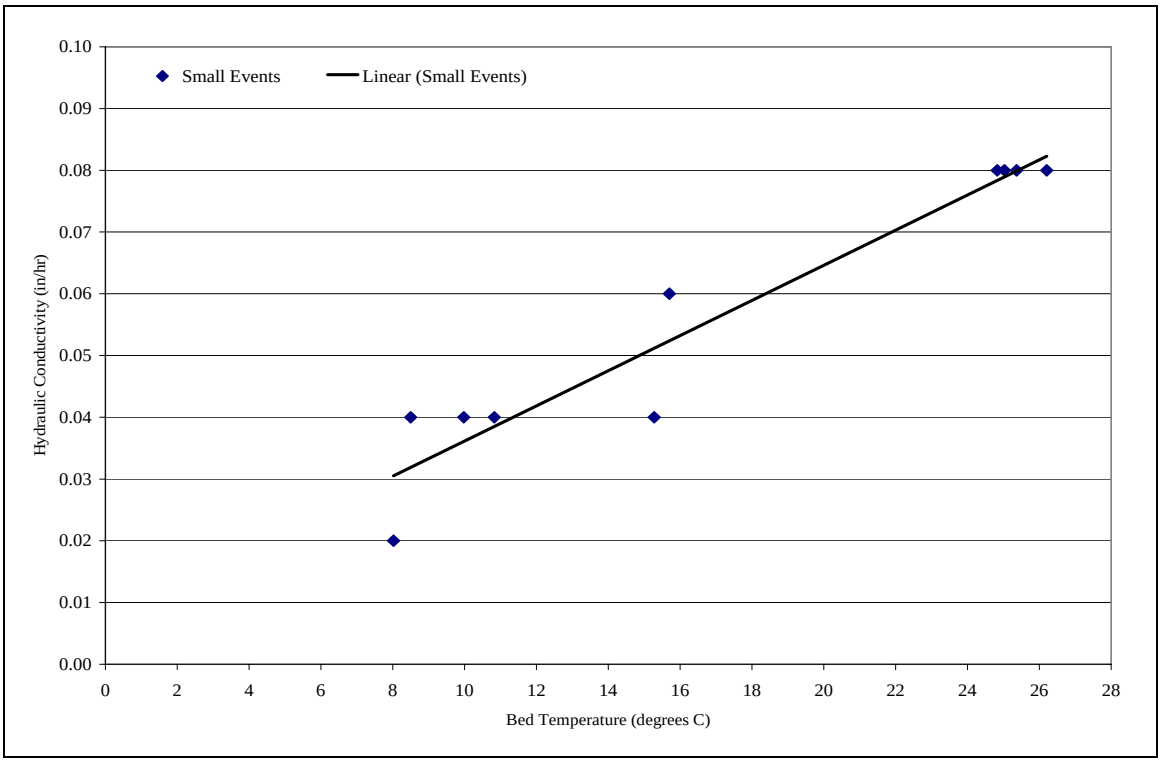

Figure 55. Calibration trend line for hydraulic conductivity of small storm events

Since the ambient temperature varies only slightly from the bed temperature, with slightly lower values in the winter and slightly higher values in the summer, these values could have been used for the verification process. However, the bed temperature gave the most accurate representation of actual conditions and was used for the analysis.

Contrarily, the variability in the hydraulic conductivity for large storm events resulted from the maximum depth of water in the infiltration bed. Therefore, the values

for the verification process for hydraulic conductivity were chosen from the trend line in Figure 56, where the results are based on bed depth.

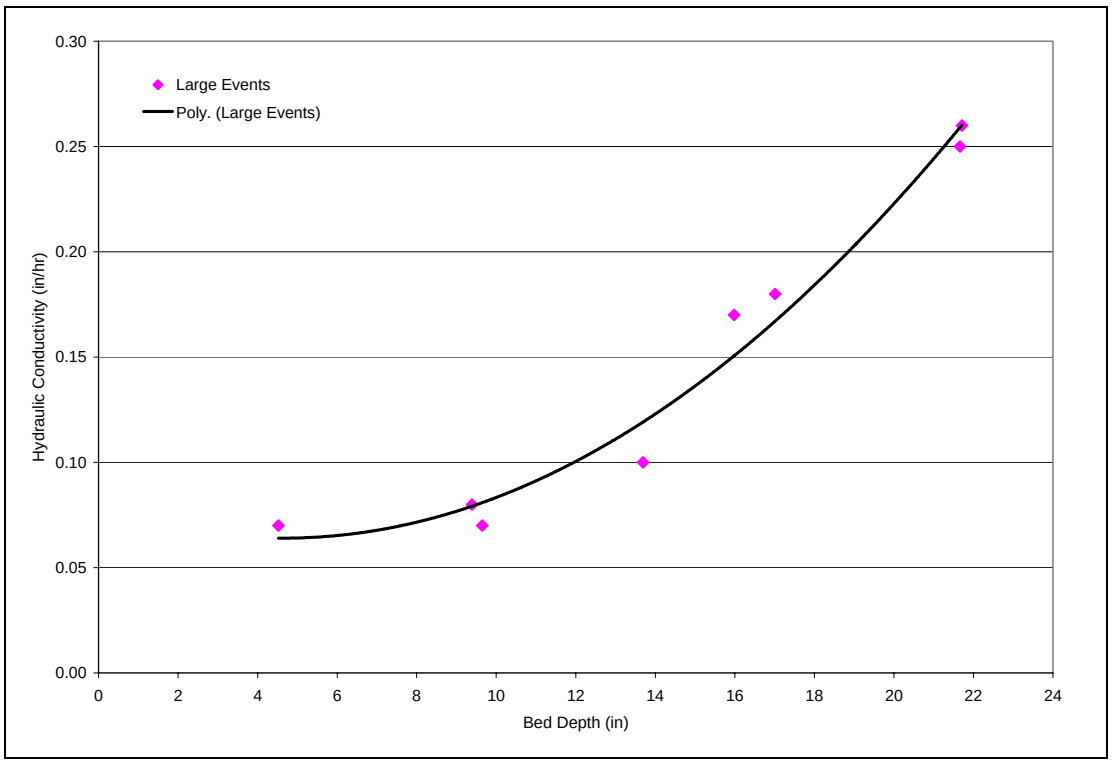

Figure 56. Calibration trend line for hydraulic conductivity of large storm events

4.5 Model Verification

Ten events were used to verify the model, five small events and five large events. The tabular results for these events are shown in Table 13 through Table 16 with complete graphical results in Appendix Q and R.

The model hydraulic conductivity for the small events was determined from the calibration trend line in Figure 55, which based the hydraulic conductivity on the temperature in the infiltration bed. To check the accuracy of this value, the event specific hydraulic conductivity, which provided the least MSE and the best match to actual data, was determined. The results for are shown in Table 13 and Table 14.

Table 13. Model vs. event specific hydraulic conductivity for small events

Event	Max Bed Depth (in.)	Mean Bed Temp.* (°C)	Model Hydraulic Conductivity (in/hr)	Event Specific Hydraulic Conductivity (in/hr)	Percent Difference from Event Specific
01/11/05	1.707	6	0.025	0.030	-16.7
04/07/05	1.590	13	0.045	0.055	-18.2
09/27/03	2.831	**22**	0.070	0.070	0.0
10/17/03	1.917	18	0.060	0.070	-14.3
11/04/03	1.968	17	0.055	0.050	10.0

*Bolded Mean Bed Temp. were estimated due to missing data between 09/16/03 and 09/29/03.

Table 14. MSE for verified small storm events

Event	Mean Square Error			
	Model		Event Specific	
	Recession Limb	Cumulative Infiltration	Recession Limb	Cumulative Infiltration
01/11/05	0.023	0.004	0.018	0.003
04/07/05	0.035	0.006	0.002	0.000
09/27/03	0.020	0.003	0.020	0.003
10/17/03	0.034	0.005	0.007	0.001
11/04/03	0.026	0.004	0.012	0.002

For all small storm events, the difference between the model and the event specific hydraulic conductivity was less than 20-percent. In every case, the calculated difference was between, 0.005 in/hr (0.0127 cm/hr) or 0.010 in/hr (0.0254 cm/hr), proving the reliability of the model for smaller events. Additionally, Table 14 shows the resulting MSE for both the model and the event specific data, as they compare to actual data. In every event the error is well below 1.0. The event specific hydraulic conductivity only improved the error from the model for cumulative infiltration by between 0.001 and 0.006 units, making the model extremely accurate at estimating the infiltration for the smaller storms. Figure 57 through 60 illustrate the graphical results for the greatest and least MSE events respectively.

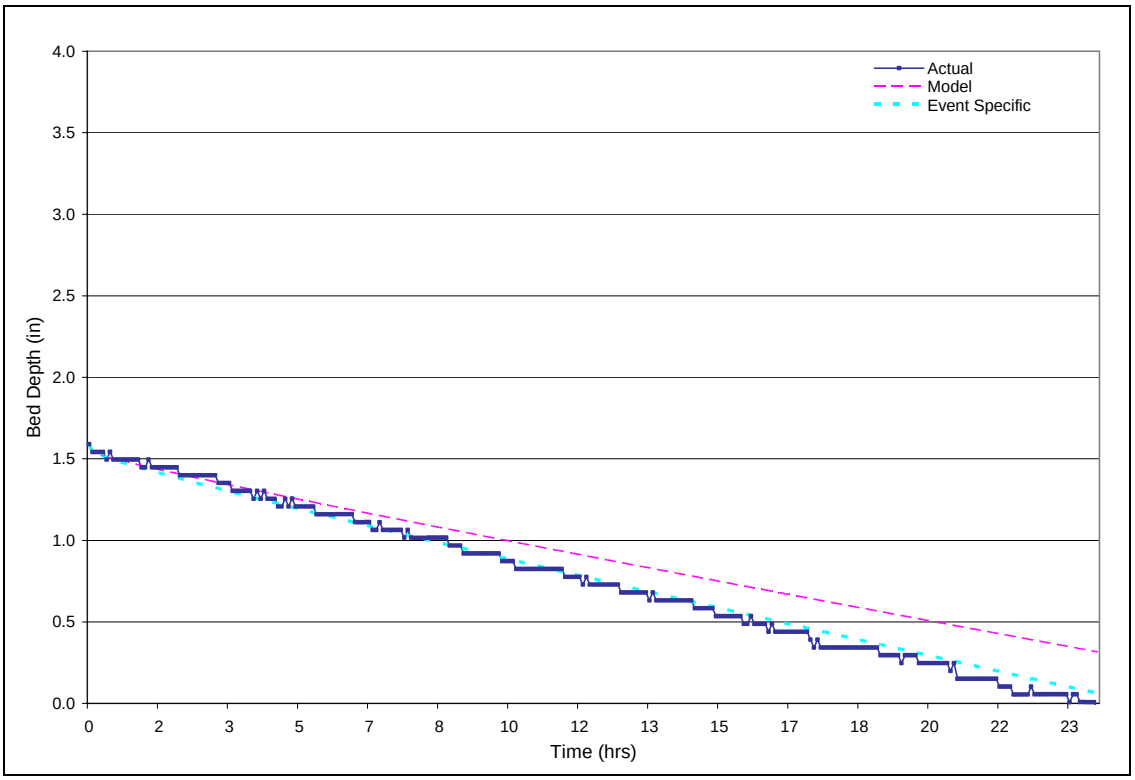

Figure 57. Recession limb model results for event 04/07/2005

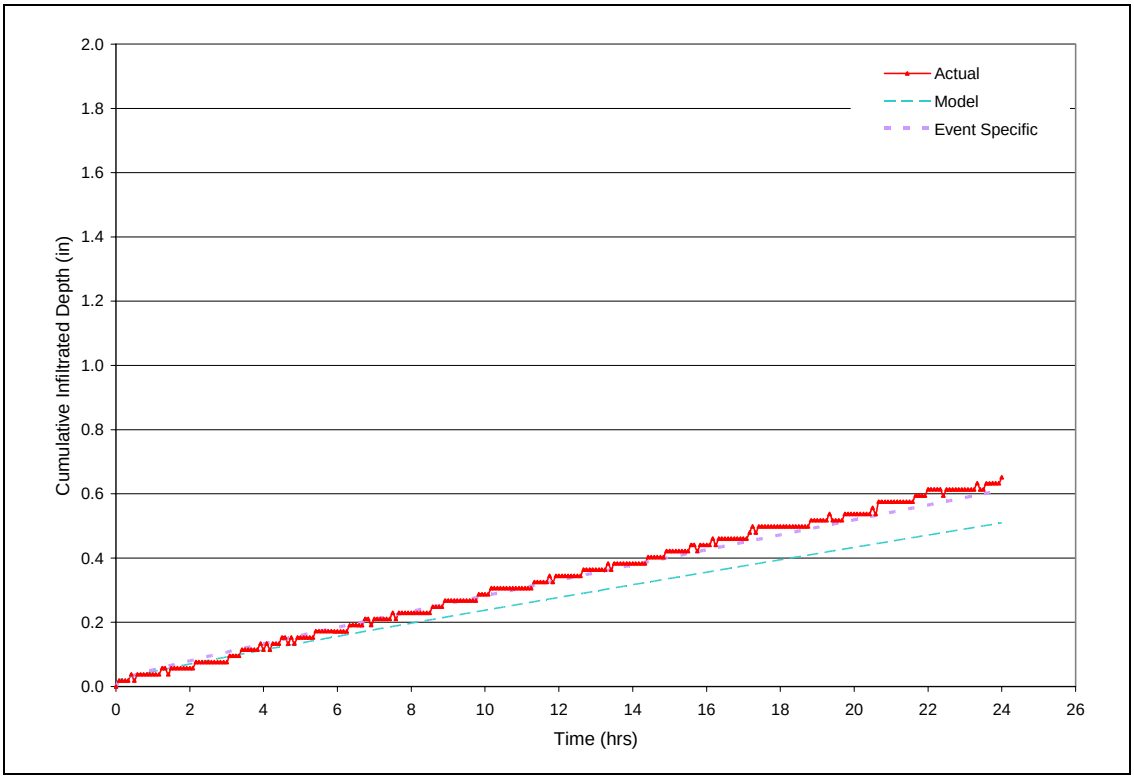

Figure 58. Cumulative infiltration model results for event 04/07/2005

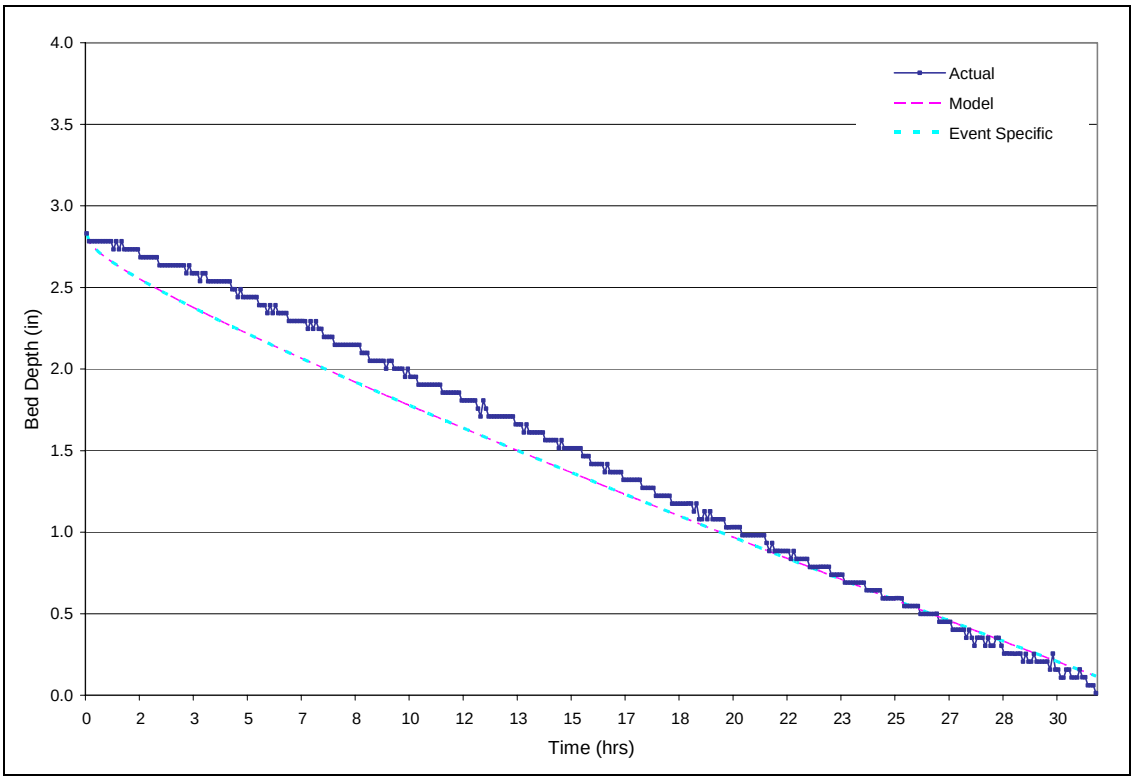

Figure 59. Recession limb model results for event 09/27/2003

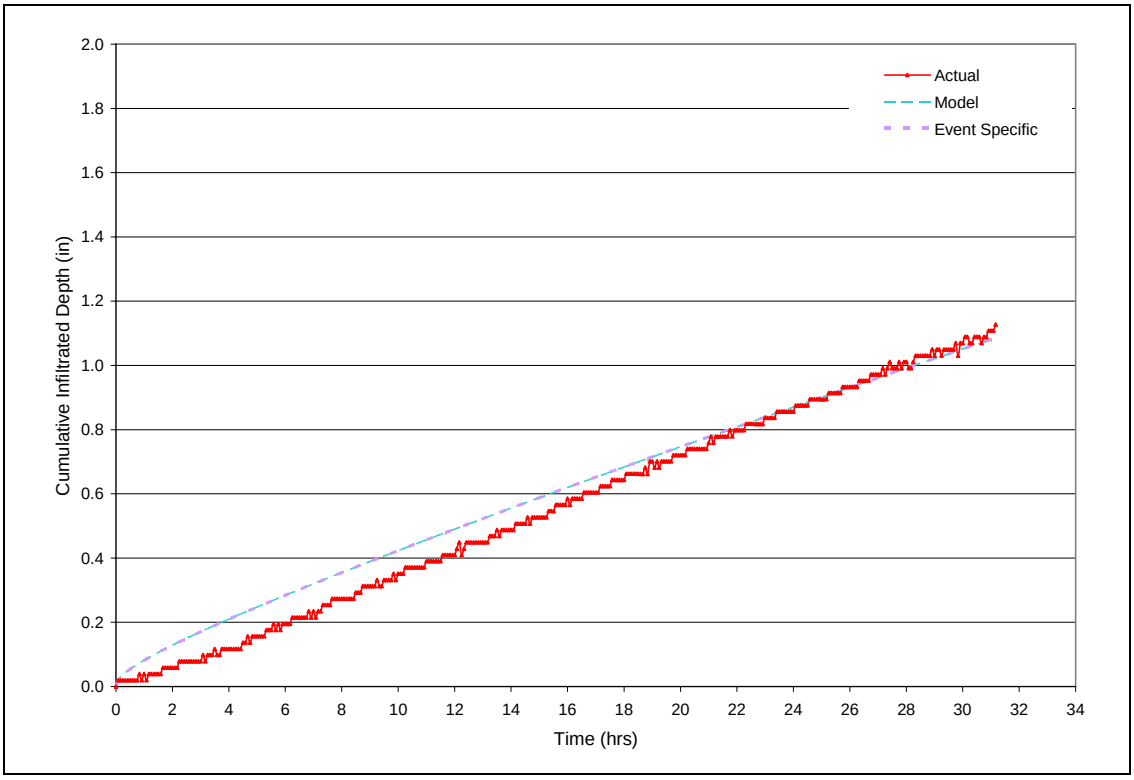

Figure 60. Cumulative infiltration model results for event 09/27/2003

The model hydraulic conductivity for the large events was determined from the calibration trend line in Figure 56, which based the hydraulic conductivity on the water surface elevation in the infiltration bed. To check the accuracy of this value, the event specific hydraulic conductivity, which provided the least MSE and the best match to actual data, was determined. The model results are shown in Table 15 and Table 16.

Table 15. Model vs. event specific hydraulic conductivity for large events

Event	Max Bed Depth (in.)	Mean Bed Temp.* (°C)	Model Hydraulic Conductivity (in/hr)	Event Specific Hydraulic Conductivity (in/hr)	Percent Difference from Event Specific
09/18/03	11.885	**23**	0.100	0.185	-45.9
09/22/03	5.800	**22**	0.065	0.100	-35.0
10/14/03	8.210	19	0.075	0.090	-16.7
11/19/03	11.980	14	0.100	0.110	-9.1
12/24/03	15.170	7	0.135	0.130	3.8

*Bolded Mean Bed Temp. were estimated due to missing data between 09/16/03 and 09/29/03.

Unlike the small events, where the difference between the model and the event specific hydraulic conductivities was less than 20-percent, the difference for the large events ranges from approximately 4 to 46-percent. Further evaluation was therefore needed to understand the discrepancy in the values for hydraulic conductivity.

Referring to Table 12, under “Large Events”, it can be seen that event pair 08/01/04 and 04/01/05, and event pair 09/18/04 and 1/13/05 have depths of approximately 22 in (55.88 cm) and 16 in (40.64 cm) respectively. One event at each depth has a high temperature value, of approximately 24°C, and a low temperature value, of approximately 8°C. Conversely, for the events in Table 12 with depths below approximately 16 in (40.64 cm) the temperature varies from 6-13°C, with no higher temperature event values for hydraulic conductivity used for calibration. This presents an issue for verification purposes since there were three events used in the verification

process, events 09/18/03, 09/22/03, and 10/14/03 (Table 15), which were below 16 in (40.64 cm) in bed depth, but had bed temperatures in the high range between 19-23°C. For these events, the hydraulic conductivities chosen from the trend line in Figure 46 were highly underestimated, whereas the other two events, events 11/19/03 and 12/24/03, with lower bed temperature had less than a 10-percent error in hydraulic conductivity. This further illustrates the dependency of the hydraulic conductivity on temperature, in addition to bed depth for larger events.

Table 16. MSE for verified large storm events

Event	Mean Square Error			
	Model		Event Specific	
	Recession Limb	Cumulative Infiltration	Recession Limb	Cumulative Infiltration
09/18/03	17.708	2.833	0.054	0.009
09/22/03	1.169	0.187	0.013	0.002
10/14/03	0.457	0.073	0.068	0.011
11/19/03	0.312	0.050	0.078	0.012
12/24/03	0.251	0.040	0.226	0.036

The results in Table 16 show the resulting MSE for both the model and the event specific data, as compared to the actual data. In every event, less one, the error is below 1.0. The error for event 09/18/03 is the highest due to this event having the highest temperature, with no similar temperature events used in the calibration process, as described previously. In all other events, the event specific hydraulic conductivity improved the error from the model for the cumulative infiltration by between 0.004 and 0.185 units. Therefore, the model remains suitable at estimating the infiltration processes of larger events, however a more accurate representation of actual data could have been provided had there been a greater number of storms to calibrate the model with over a larger range of temperatures and depths. Figure 61 through 64 illustrate the results for the greatest and least error events respectively.

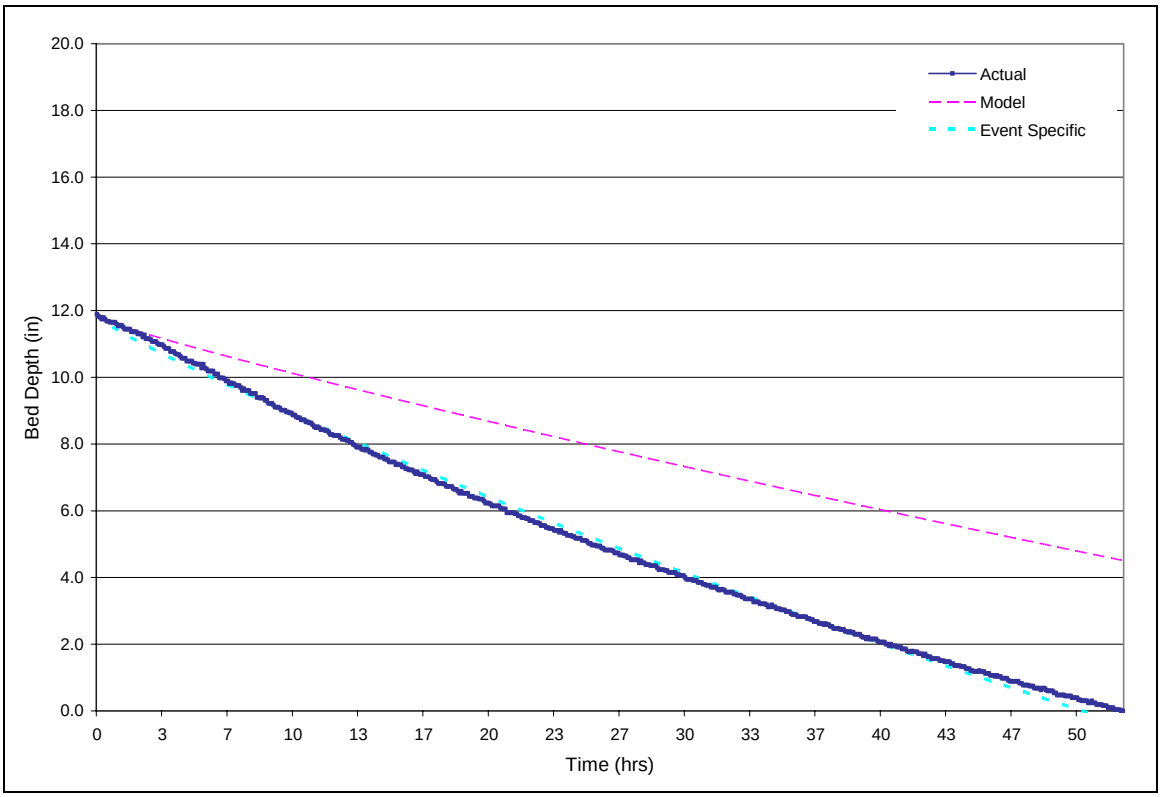

Figure 61. Recession limb model results for event 09/18/2003

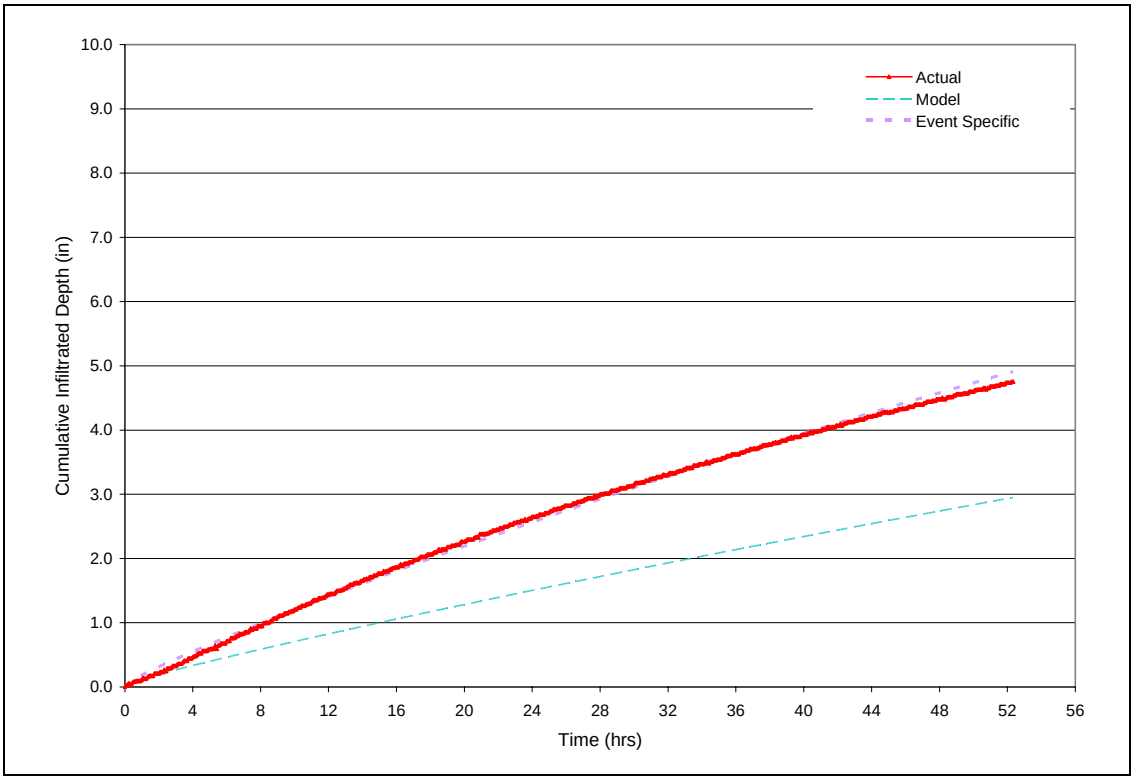

Figure 62. Cumulative infiltration results for event 09/18/2003

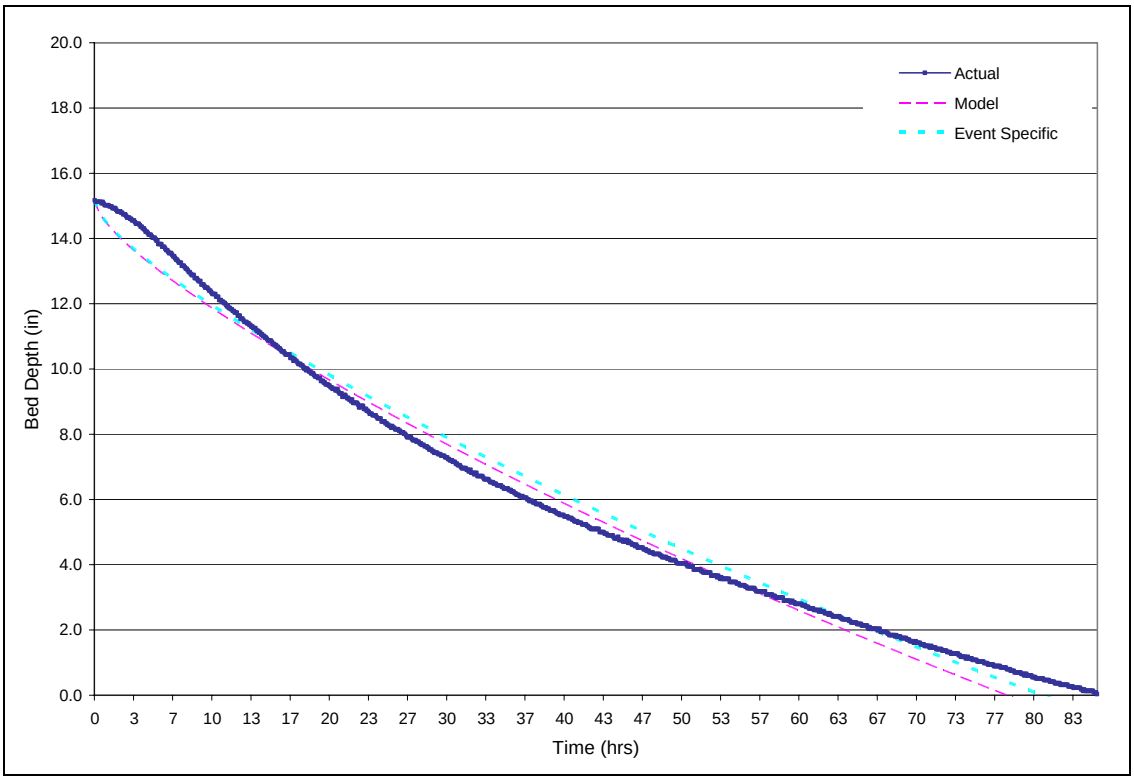

Figure 63. Recession limb model results for event 12/23/2003

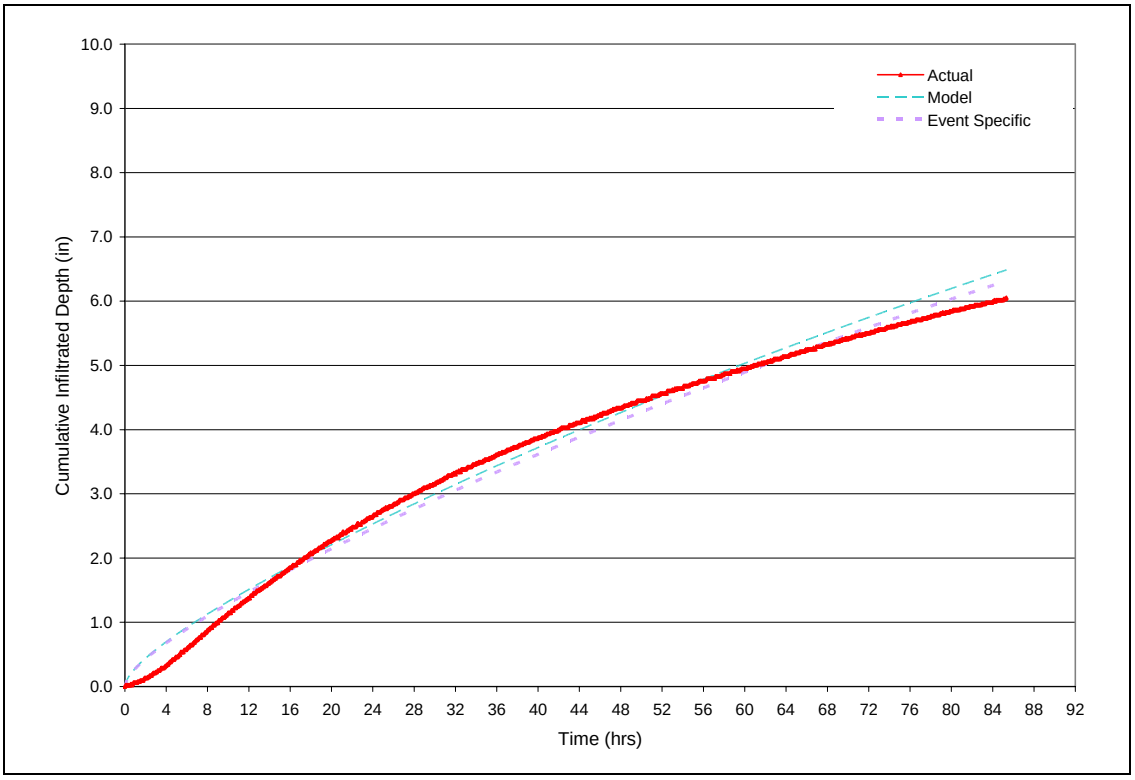

Figure 64. Cumulative infiltration model results for event 12/23/2003

4.5.1 Multi-peaking Event Comparison

An analysis was also completed to evaluate the model's accuracy at replicating the multiple recession limbs generated from a multi-peaking storm event. In this case, a separate model run was completed for each recession limb. The hydraulic conductivity for each recession limb was based on whether the recession limb followed the characteristics of a small or a large event. The results were then plotted on the event hydrograph to illustrate how well the model estimated the actual data.

To check the accuracy of the model, the event specific hydraulic conductivity, which provided the least MSE and the best match to actual data, was determined for each recession limb. Both the model and event specific values for hydraulic conductivity are shown in Table 17, with the resulting MSE shown in Table 18.

Table 17. Calibrated vs. event specific hydraulic conductivity for event 03/30/04

Event 03/30/2004	Max Bed Depth (in.)	Mean Bed Temp. (°C)	Model Hydraulic Conductivity (in/hr)	Event Specific Hydraulic Conductivity (in/hr)	Percent Difference from Event Specific K
Recession 1	3.33	10	0.035	0.025	40.0
Recession 2	3.23	11	0.040	0.030	33.3
Recession 3	8.11	10	0.070	0.040	75.0
Recession 4	10.69	9	0.090	0.075	20.0

Table 18. MSE for multi-peaking event 03/30/04

Event 03/30/2004	Mean Square Error			
	Model		Event Specific	
	Recession Limb	Cumulative Infiltration	Recession Limb	Cumulative Infiltration
Recession 1	0.121	0.019	0.018	0.003
Recession 2	0.162	0.026	0.033	0.005
Recession 3	0.898	0.144	0.080	0.013
Recession 4	0.969	0.155	0.368	0.059

Table 17 shows that the model hydraulic conductivity overestimated the event specific values for each recession limb. Also, for both the model and the event specific, the hydraulic conductivities increased as the event proceeded. However, the model MSE was well under 1.0 for each recession limb, which provides a good representation of the actual data. It is interesting to note that both the model and the event specific MSE increased from Recession 1 to Recession 4. Therefore, as the storm event proceeds and level in the bed increases, the soil is becoming more saturated, and the model becomes less accurate at representing actual conditions.

The outflow hydrograph for event 03/30/2004 with the resulting model and event specific recession limb data are shown in Figures 65 and 66. The model data (Figure 65) has a much steeper slope at the beginning of each recession limb curve, which corresponds to a higher infiltration rate than the actual data. However, as the storm continues, the model curve becomes parallel to the actual data, corresponding to nearly identical infiltration rates. In Figure 66, although the actual and event specific curves are ending at approximately the same point, the event specific recession curve has a steeper slope at the beginning of the storm, overestimating the infiltration rate, and a gentler slope at the end of the event, underestimating the infiltration rate, which results in the event specific recession limb crossing over the actual bed depth curve.

Both the model and the event specific curves are useful at determining different infiltration characteristics in the infiltration bed. The model curve is an extremely accurate representation of the infiltration rate as the bed is emptying out, with only a short portion of the recession curve initially overestimated. The event specific curve does not present an accurate representation of the infiltration rate, but instead gives a good

measurement for the time it takes for the bed to empty, or in this case reach a minimum bed depth value, from its peak.

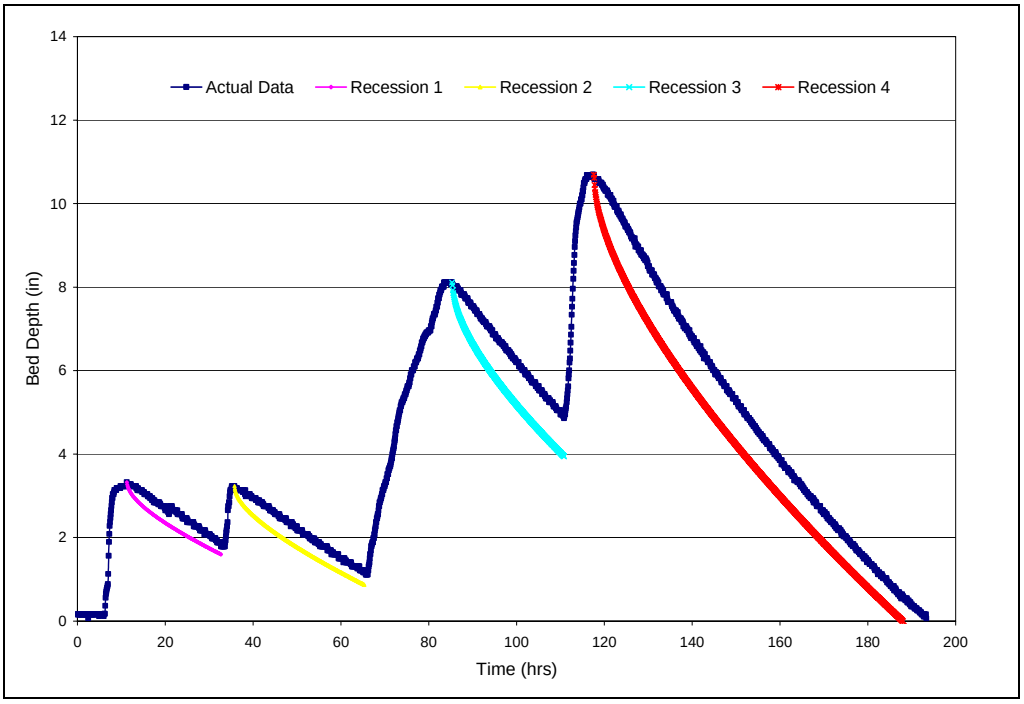

Figure 65. Outflow hydrograph using model K values for event 03/30/2004

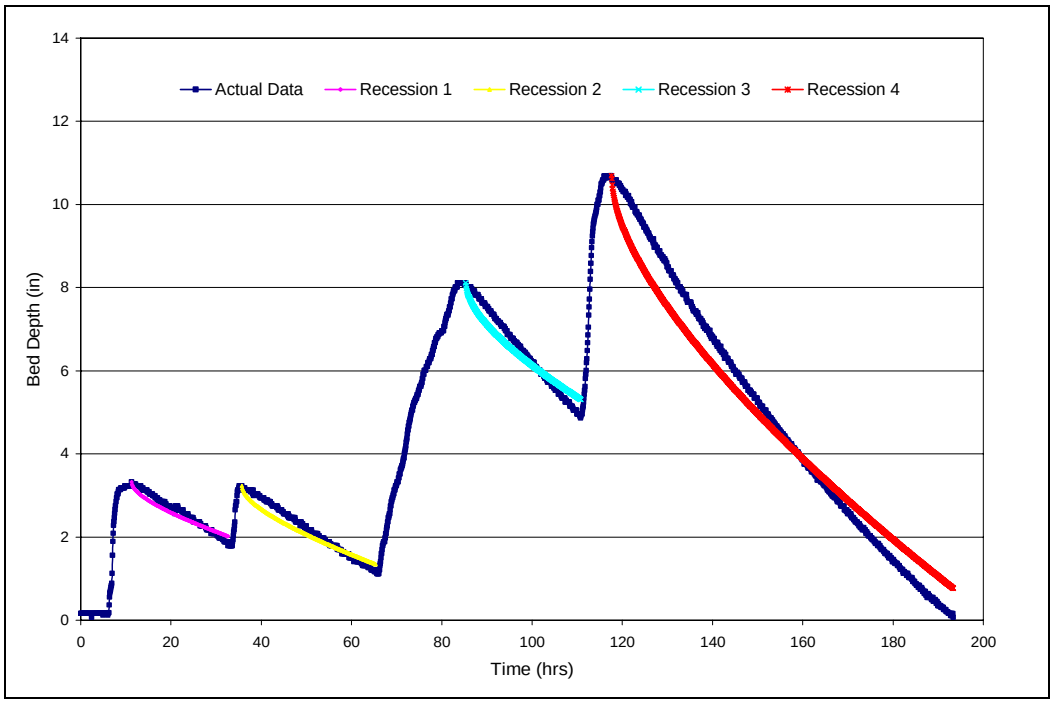

Figure 66. Outflow hydrograph using event specific K values for event 03/30/2004

Chapter 5: Discussion

5.1 Infiltration Rate Analysis

After calibrating and verifying the model it is important to evaluate the results as they relate to infiltration. The infiltration rate for each event was determined from the results of each event's cumulative infiltrated depth versus time curve. The results for this analysis for small and large storms events are discussed in the following sections.

5.2 Small Storm Events

The infiltration rate for the smaller storm events was determined by fitting a linear trend line to the data from the cumulative infiltrated depth graphs for each event. The infiltration rate is the slope of the linear trend line in inches per hour. This was done for both the actual and the model cumulative infiltrated depth curves, despite the model having a slightly stronger curve at the beginning of the event than the actual data. In all cases, the R^2 values were between 0.996 and 0.999 proving how well the linear trend line matched the data. The model and actual infiltration rates for the five events used for verification are shown in Table 19.

Table 19. Infiltration rates: small events

Event	Max Bed Depth (in.)	Mean Bed Temp.* (°C)	Infiltration Rate (in/hr)		Percent Difference from Actual
			Model	Actual	
01/11/05	1.707	6	0.018	0.025	-28.5
04/07/05	1.590	13	0.020	0.026	-23.6
09/27/03	2.831	**22**	0.033	0.037	-10.1
10/17/03	1.917	18	0.027	0.036	-25.8
11/04/03	1.968	17	0.027	0.029	-6.2

*Bolded Mean Bed Temp. were estimated due to missing data between 09/16/03 and 09/29/03.

The actual infiltration rate varies between 0.025 (0.064) and 0.037 in/hr (0.094 cm/hr). The model results have a similar range, but underestimate the actual infiltration rate in each event with values between 0.018 (0.046) and 0.033 in/hr (0.084 cm/hr). To

evaluate why this occurs, the infiltration rate was plotted against time for both the actual and the model data sets for event 09/27/03 (Figure 67).

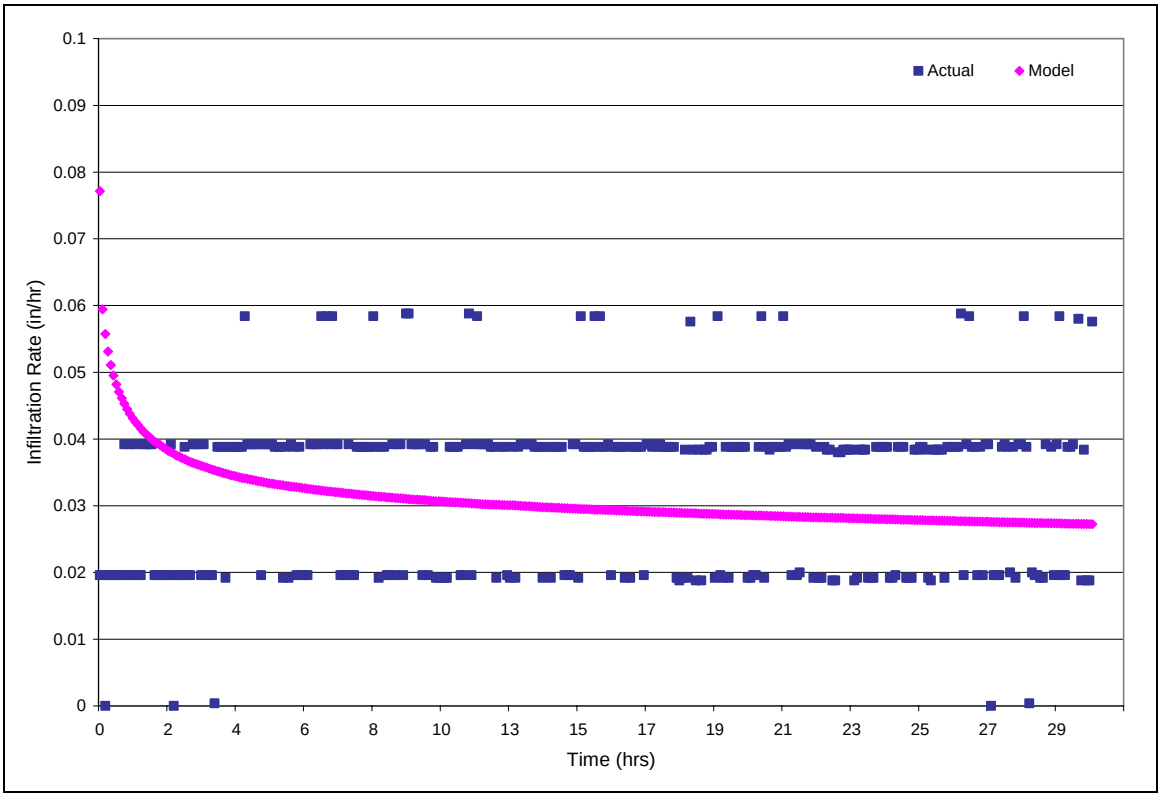

Figure 67. Infiltration rate vs. time for small event 09/27/03

The model event data begins with a high infiltration rate of approximately 0.08 in/hr (0.203 cm/hr) and within the first 6 hours, the rate drops by nearly 0.05 in/hr (0.127 cm/hr). At this point, the change in infiltration rate slows and ends with a final rate of 0.028 in/hr (0.071 cm/hr). Therefore, the model's infiltration rate varies over time, beginning at a maximum point and decreasing asymptotically. The actual data behaves quite differently. Figure 67 illustrates the actual infiltration rate as iterating from approximately 0.02 (0.051) to 0.04 (0.102) to 0.06 in/hr (0.0152 cm/hr), across the duration of the event. Although it is illustrated as such, in truth, the infiltration rate is constant and the noise associated with the electrical instrument, in this case the pressure

transducer, displays the irregular readings. Since the model data in Table 19 is a smoothed, constant representation of the infiltration rate, this could account for the model underestimating the actual infiltration rate in all events. Both the actual and the model data behave similarly in all small events. All infiltration graphs for small events are found in Appendix S.

Figures 68 and 69 illustrate the actual and the modeled recession limb results for all small events used for verification. In Figure 68, the slopes of the recession curves for all events, or the infiltration rates, are relatively the same, with two event pairs, 09/27/03 and 10/17/03, as well as 01/11/05 and 04/07/05 having nearly the same infiltration rates. In Figure 69, the modeled events 10/17/03 and 11/04/03 are nearly identical. The differences between the actual and the model infiltration rate for each event are results of the actual and the model data's varying dependency on temperature. The model was calibrated by fitting a trend line to the data from 10 events, therefore setting a different hydraulic conductivity to each event based on temperature. This resulted in a higher hydraulic conductivity and thus a higher infiltration rate with warmer temperatures. In actuality this trend is followed, but not to such a sharp degree as is shown through the data in Figures 68 and 69. Other factors besides temperature, including soil suction pressure head, antecedent dry time, and the overall conditions of the soil, may also have some effect on the event's infiltration rate. Nevertheless, it remains true that infiltration rate, like hydraulic conductivity, is greatly affected by temperature, as is further proved in Figure 70, which plots all actual infiltration rate and temperature data for all events used for model calibration and verification between September of 2003 to April of 2005.

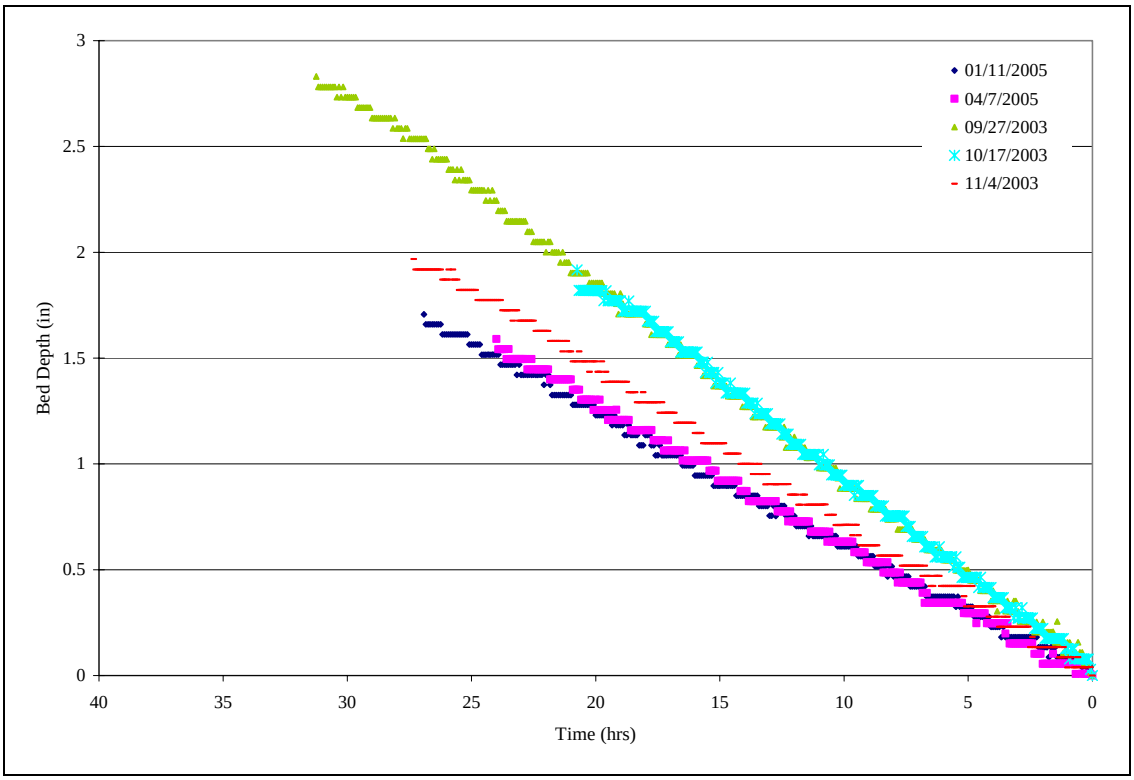

Figure 68. Small event recession limb analysis: actual events

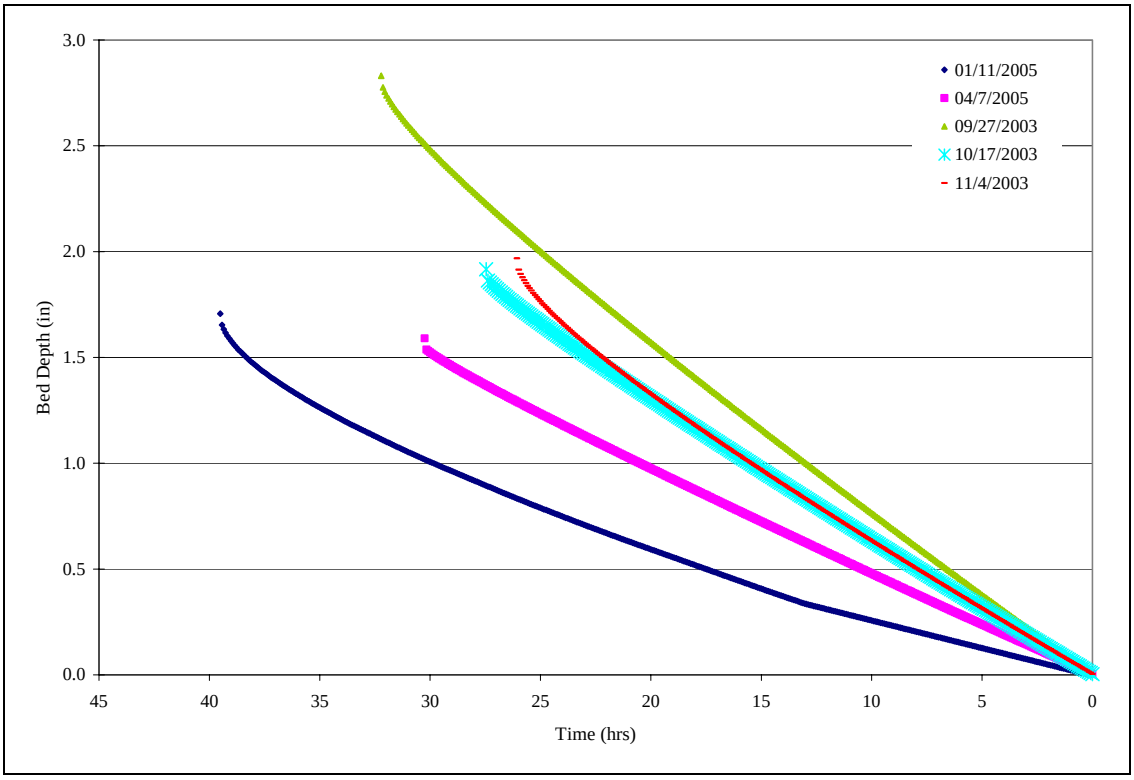

Figure 69. Small event recession limb analysis: model events

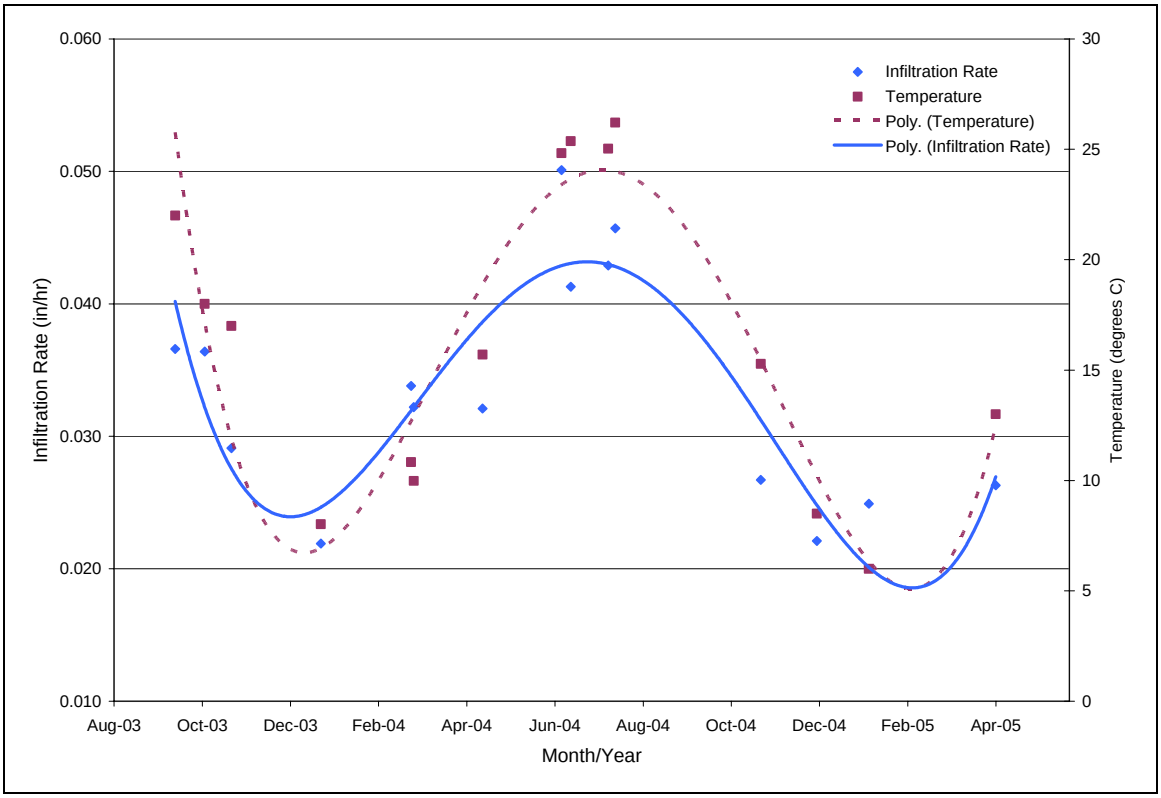

Figure 70. Infiltration rate and temperature data for small events in 2003-2005

If we refer to Chapter 2, in a study done by Lin et al. (2003) the results showed a repeating pattern of cyclical changes of infiltration rate as a function temperature (Figure 27). The same trend is seen in Figure 70. It was discussed in Lin's study that the viscosity of water changes by approximately 2-percent per degree Celsius between the temperature range of 15-35°C, and this change is suggested to lead to an estimated 40% change of infiltration rate between the summer and winter months (Lin et al., 2003). The data in the current study shows a change from 0.050 in/hr (0.127 cm/hr) in 06/16/04 to 0.022 in/hr (0.056 cm/hr) in 01/04/04, a change of 56%. Lin et al. (2003) also found that the temperature effects on infiltration rate tend to be larger by a factor of 1.5-2.5 times than the change expected from effluent viscosity changes alone. Therefore, other factors

specific to the soil may also be affected by temperature thus increasing the infiltration rate with increasing temperature. As shown in the model, hydraulic conductivity is one of these factors.

To determine the repeatability of the data in Figure 70 on a monthly basis, a polynomial was fit to all events in 2004. This data was then plotted with the five additional events in 2003 and 2005 as a separate series, as illustrated in Figure 71. The infiltration rate data points for the events in 2003 and 2005 do not fall directly on the trend line, but they do present a good fit to the 2004 data. This demonstrates how the infiltration rate not only follows a cyclical high and low pattern during the duration of a few years, but also shows the repeatability and accuracy of the data over a seasonal or monthly period.

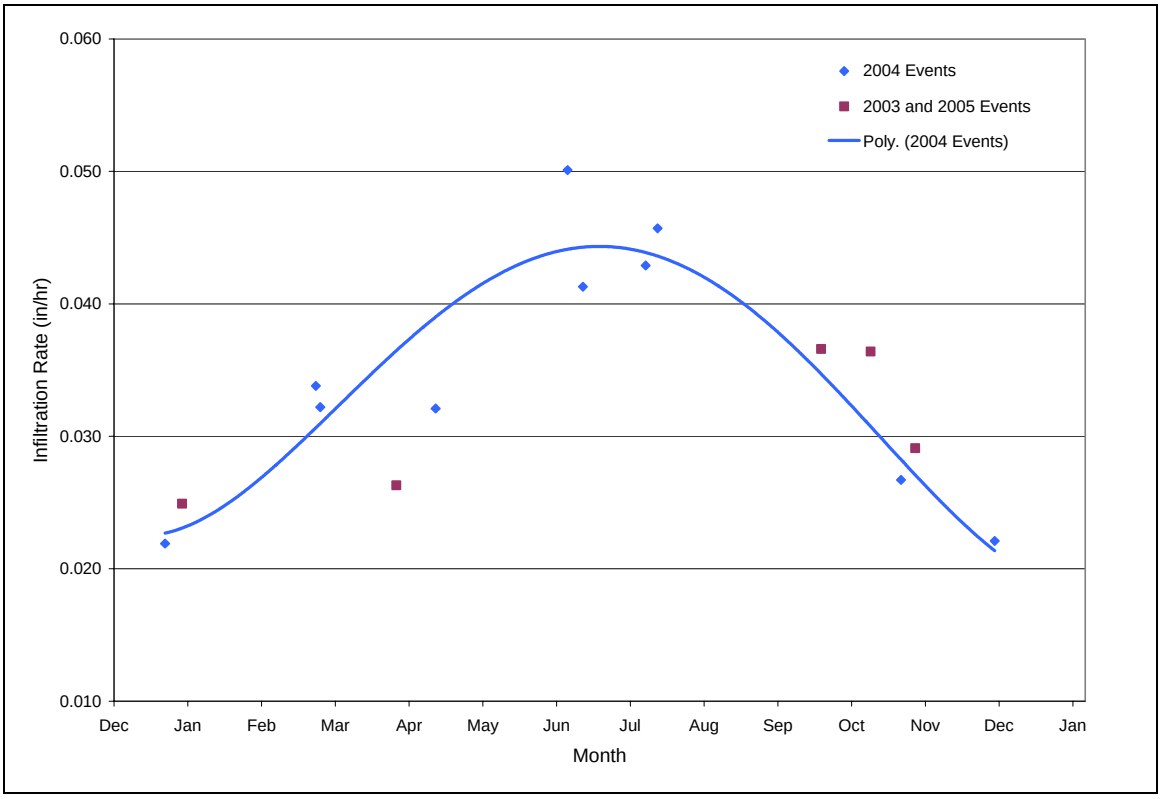

Figure 71. Seasonal comparison of infiltration rates for small events

5.3 Large Storm Events

The infiltration rate for the large events was determined by using the cumulative infiltrated depth curve. However, since the curves for the larger events were more polynomial in shape, a series of linear trend lines were applied to the curve. The actual data for each event is broken into three linear trend lines based on the depth of the water in the bed. The trend lines range from a bed depth greater than 8 in (20.32 cm), 8 in (20.32 cm) to 4 in (10.16 cm), and below 4 in (10.16 cm). Therefore, a different infiltration rate is determined for each series. The model trend lines follow a similar pattern, but have an additional linear trend line which accounts for the first inch of infiltration in all events, due to the extremely steep slope of this segment of the curve. The slopes of each linear trend line account for the infiltration rate through the bed during that period of time. The results are displayed in Table 20 and Table 21.

Table 20. Actual infiltration rates: large events

Event	Max Bed Depth (in.)	Mean Bed Temp.* (°C)	Infiltration Rate (in/hr)		
			Actual		
			Series 1 (H>8")	Series 2 (8">H>4")	Series 3 (4">H>0)
09/18/03	11.885	**23**	0.121	0.094	0.072
09/22/03	5.800	**22**	n/a	0.052	0.047
10/14/03	8.210	19	n/a	0.063	0.042
11/19/03	11.980	14	0.096	0.063	0.044
12/24/03	15.170	7	0.115	0.066	0.045

*Bolded Mean Bed Temp. were estimated due to missing data between 09/16/03 and 09/29/03.

Table 21. Model infiltration rates: large events

Event	Max Bed Depth (in.)	Mean Bed Temp.* (°C)	Infiltration Rate (in/hr)			
			Model			
			First Inch	Series 1 (H>8")	Series 2 (8">H>4")	Series 3 (4">H>0)
09/18/03	11.885	**23**	0.073	0.058	0.051	0.055
09/22/03	5.800	**22**	0.036	n/a	n/a	0.030
10/14/03	8.210	19	0.080	n/a	0.044	0.036
11/19/03	11.980	14	0.149	0.072	0.054	0.046
12/24/03	15.170	7	0.213	0.090	0.070	0.059

*Bolded Mean Bed Temp. were estimated due to missing data between 09/16/03 and 09/29/03.

The R^2 values ranged from 0.996 to 1.000 for Series 1, 2, and 3 for both the actual and model data trend lines. The R^2 values for the first inch of the model were slightly higher and ranged from 0.968 to 0.997. When evaluating the actual data in Table 20, all events seem to have generally the same infiltration rates for each series, with the exception of event 09/18/03. Contrarily, the model results have a much larger scatter than is present in the actual results. This is seen more clearly in Figure 72.

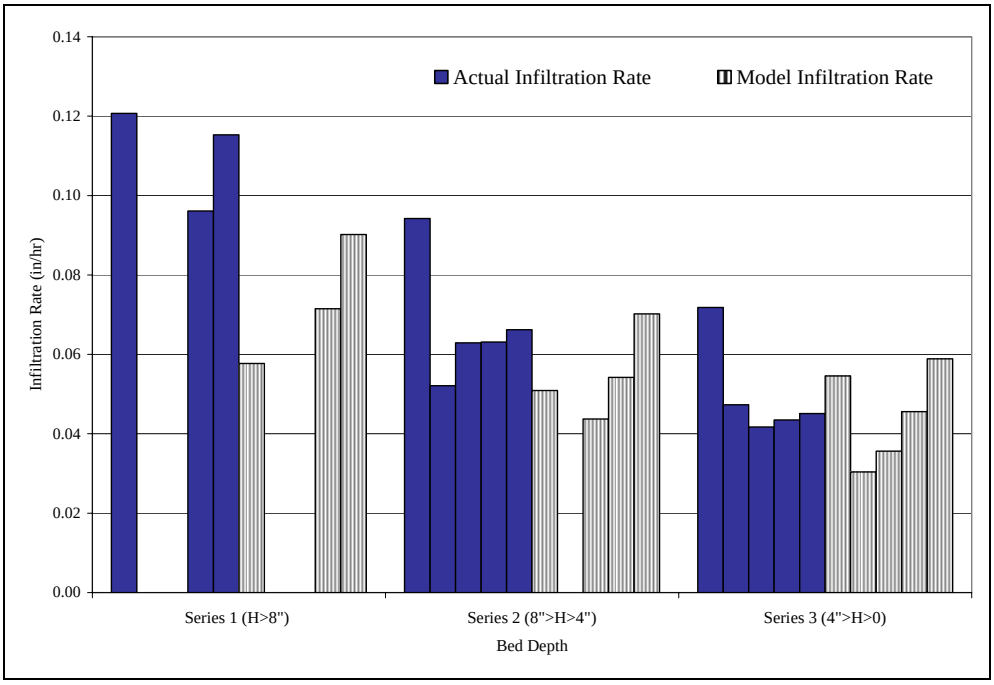

Figure 72. Actual and model infiltration rate vs. bed depth for large events (Table 20)

The actual data is indicated by the solid bars, which are generally the same height in each series, with the exception of the first bar in each series which corresponds to event 9/18/03. Although there is more variation in the model data, which is indicated by the striped bars, and the infiltration rate tends to be lower than the actual data, the model data still follows the same pattern that is seen in the actual data between each event.

Figure 73 illustrates the infiltration rate across time in inches per hour for both the model and the actual results for event 12/24/03. The model data follows the identical trend seen previously for the small events, as expected. The model event data begins with a high infiltration rate and within the first few hours of the event, the change in infiltration rate begins to slowly level off asymptotically. Contrarily, the actual data for the large events follow a much different curve than was previously seen for both the model and the small events. The infiltration rate begins at a slower rate and increases to a peak infiltration rate at approximately 8 hours into the event. The infiltration rate then follows a similar pattern as the model and begins to level off asymptotically.

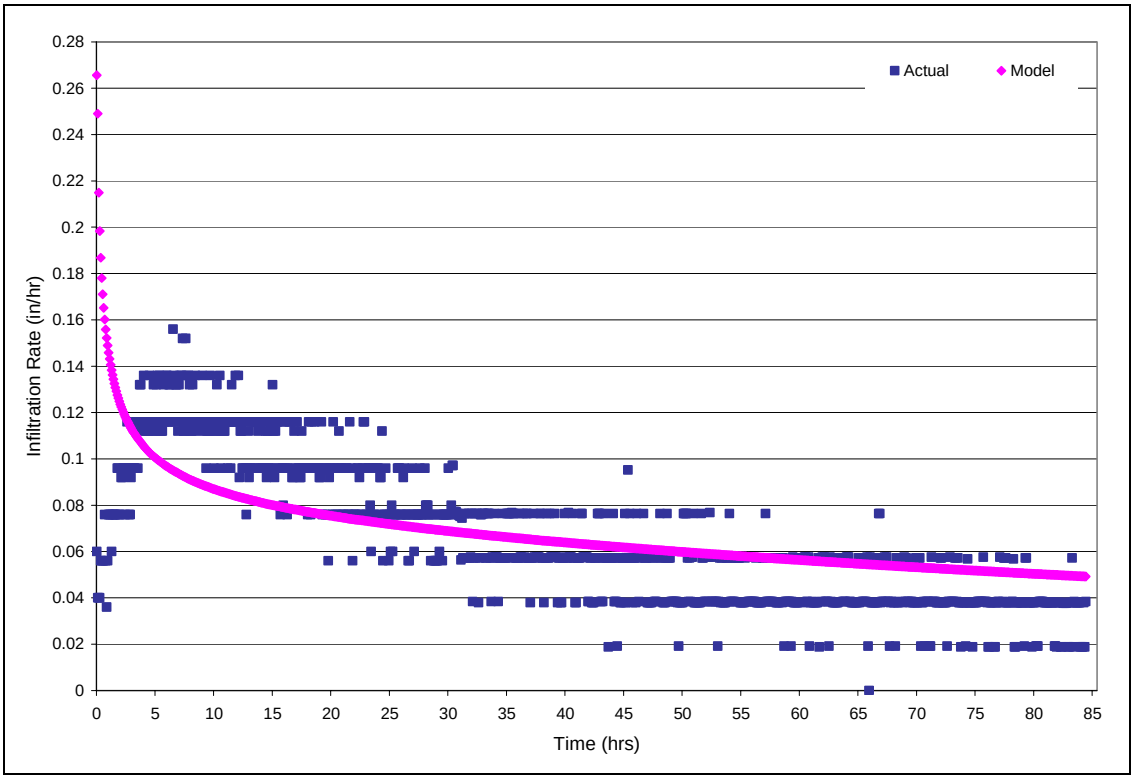

Figure 73. Infiltration rate vs. time for large event 12/24/03

The actual infiltration rate pattern shown in Figure 73 could be due to the fact that initially, before the event begins, the soil is relatively dry, and as the water begins to

infiltrate the soil is increasingly saturated. The peak in infiltration rate may be in response to the soil achieving the maximum level of saturation exhibited for the amount of water in the bed and the resulting pressure applied to the soil profile below. However, this is not true saturation because this only occurs for very large storms with a bed depth of approximately 22 inches. Then, as the bed level decreases, so does the infiltration rate as the percolation process brings the infiltrated water and thus the wetting front further from the bed bottom.

The peak in the infiltration rate does not correspond to the peak level in the infiltration bed when the greatest surface area is available for infiltration, which in this study is presented as time zero. This delayed peak in infiltration rate may be a result of the "initial soil moisture gulp". Since infiltration is limited by the rate of percolation and percolation is faster or nearly instantaneous at the beginning of the event when the soil is dry, which is termed the "initial soil moisture gulp", the soil remains unsaturated until this time period elapses. Subsequently, as the event continues and rate of percolation decreases, the soil directly below the infiltration bed becomes increasingly saturated with the infiltration rate reaching a peak when the soil reaches the peak saturation level for the event. This same trend is seen in all large events for both the actual and the model data. This trend does not occur in the small events due to the fact that the pressure head and the volume of water in the infiltration bed is much less and saturation is not approached. All infiltration graphs for the large events are found in Appendix T.

Figures 74 and 75 illustrate the actual and the model recession limb results for all large events used for verification.

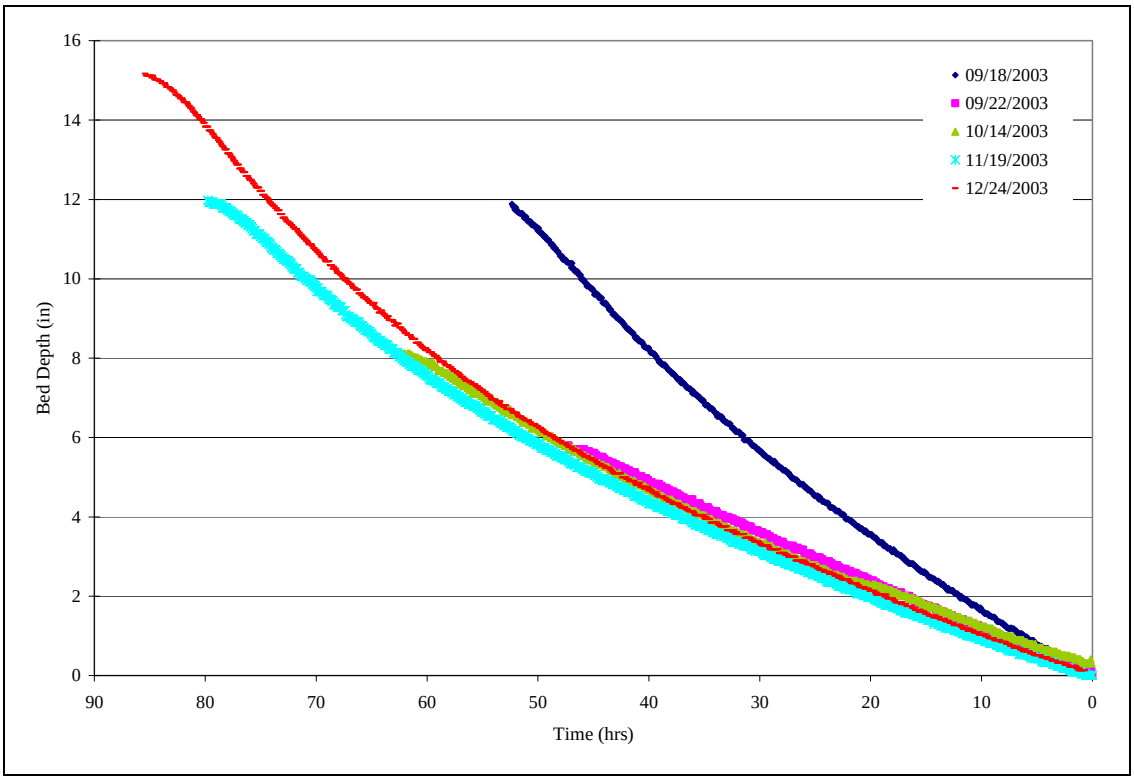

Figure 74. Large event recession limb analysis: actual events

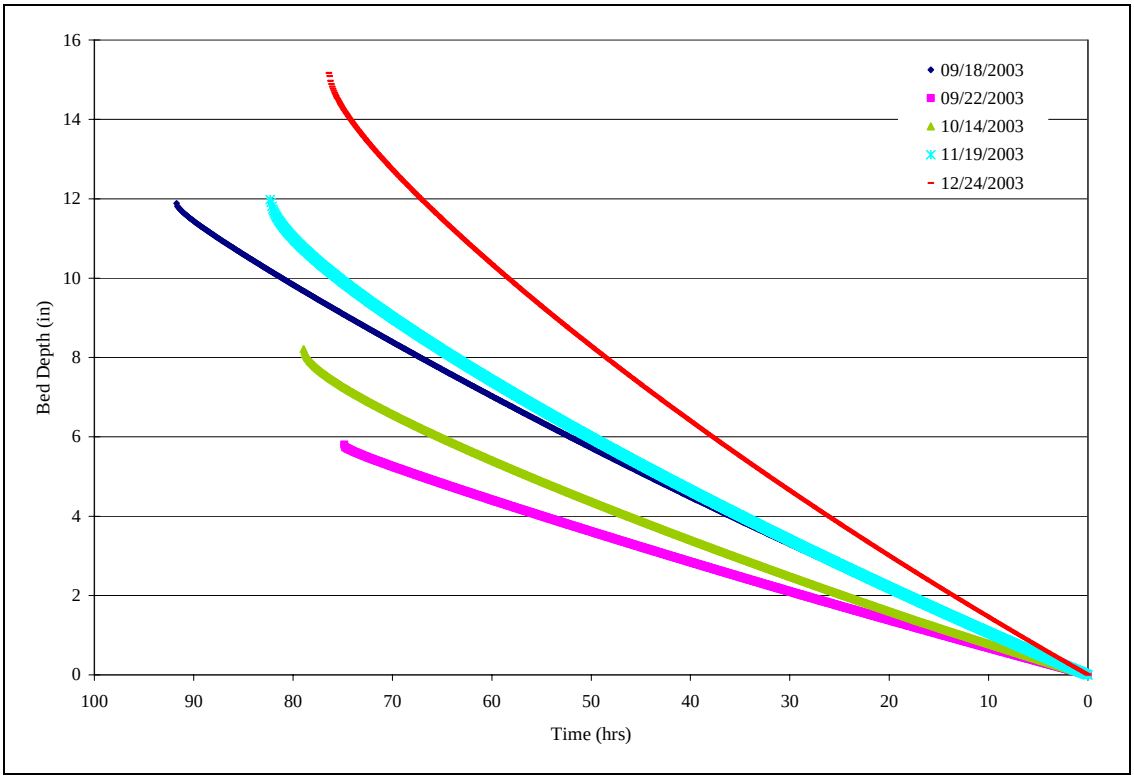

Figure 75. Large event recession limb analysis: modeled events

In Figure 74, the slope of the recession curve for each event, or the infiltration rate, are relatively the same at the same depths, with the exception of event 09/18/03. Event 09/18/03 was evaluated earlier and it was determined that based on the fact that it is an event with a high temperature, it stands out from the other events with a much higher infiltration rate. In Figure 75, each storm has a different infiltration rate and thus recession limb curve, with the highest occurring for the event with the highest bed depth.

The model hydraulic conductivity was chosen based on the maximum water surface elevation in the infiltration bed. Although hydraulic conductivity is a function of the bed depth, it is clear that hydraulic conductivity changes with changing depth, similar to the infiltration rate. The actual data shows four events with nearly identical infiltration rates and as the depth in the bed increases the slope of the curves increase. However, the model data shows a different curve and thus infiltration rate for each event with no correlation to bed depth, which was the original determinant in the calibration process. A better representation of the actual data would have been accomplished by applying hydraulic conductivity as a function of bed depth, rather than assigning a set hydraulic conductivity for an entire event. This also could have improved the fact that the model curves appear much more linear than the actual data. Changing the hydraulic conductivity at certain depths could have accomplished this. In addition, increasing the wetted area of side wall contribution could have a similar effect.

Another potential reason for the curve in the recession limb being less linear could be due to clogging of the bed bottom. Over time, the bed bottom of the infiltration basin could have become clogged creating a barrier between the basin and the wetted perimeter.

In a study done by Bouwer (1990), discussed previously in Chapter 2, infiltration rate was expressed in a linear relationship as shown in equation (15),

$$f = K\frac{(H_w + L_c + S)}{L_c} \tag{15}$$

where f = infiltration rate, K = hydraulic conductivity of the soil, H_w = water depth in the basin, L_c = thickness of the clogged layer, and S = capillary suction head in the unsaturated zone below the clogged layer (Bouwer, 1990). Equation (15) shows a linear increase in infiltration rate with increasing water depth in the basin given the clogged layer and capillary suction remain low. However, if water depth is increased when a clogged layer is present, the depth of this layer will decrease slightly due to compaction, and the hydraulic conductivity will decrease significantly. This causes a "less linear" increase in infiltration rate with water depth, and even possibly a decrease (Bouwer, 1990). To determine whether clogging has occurred in the infiltration bed, three event pairs in different years, which occurred during the same month, with similar temperatures and bed depths were plotted and infiltration rate evaluated. The results are shown in Figures 76 and Figure 77.

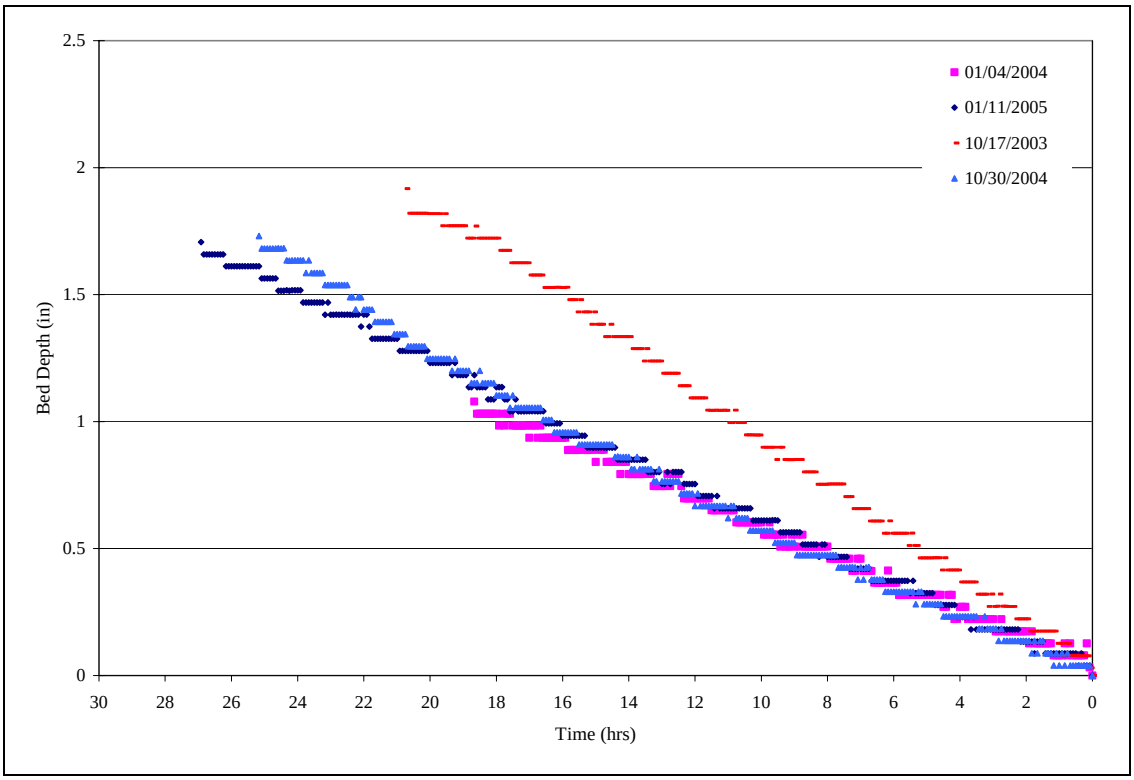

Figure 76. Clogging evaluation: small events

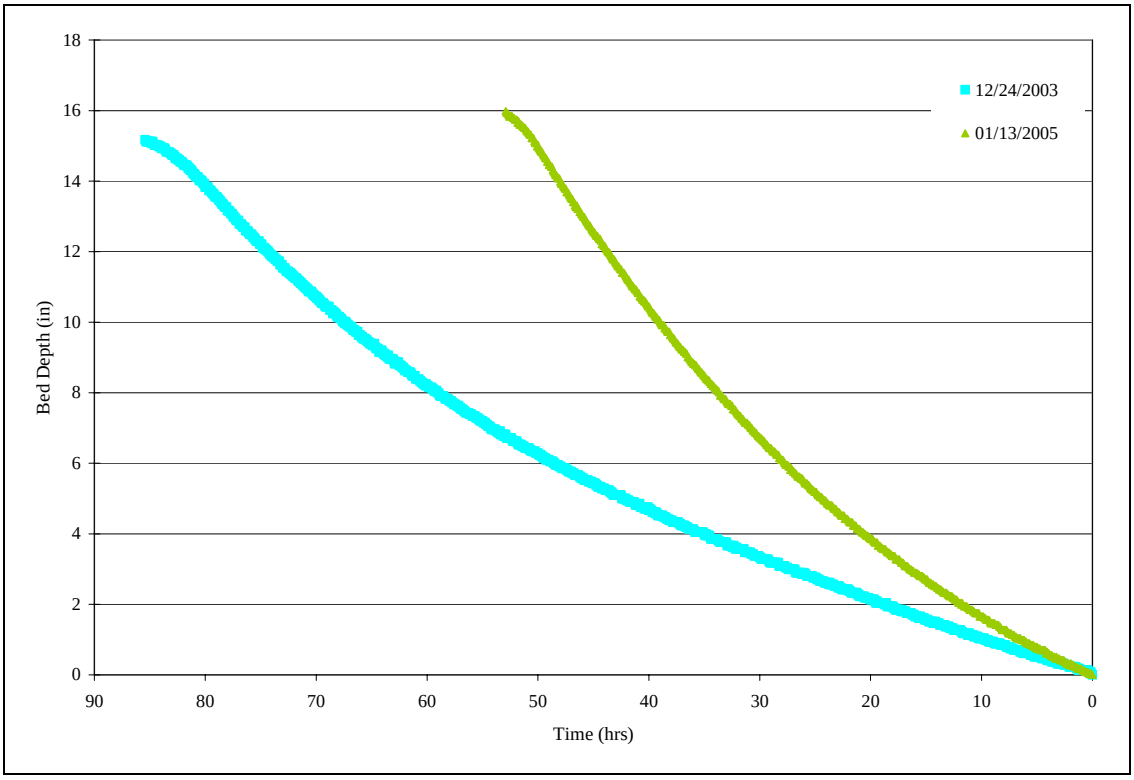

Figure 77. Clogging evaluation: large events

Figure 76 illustrates the recession limbs for event pair 01/04/04 and 01/11/05 and event pair 10/17/03 and 10/30/04. When assessing the January storm events for 2004 and 2005, the data sets are nearly identical. However, the events in October of 2003 and 2004 are much different. The October 2003 event has a much steeper sloped line and thus a higher infiltration rate than the October 2004 data set, which seems to be a closer match to the January events. At first glance this would seem to suggest that the bed is clogging. However, after considering Figure 77, where the large event in January of 2005 has a much higher infiltration rate than that of the December 2003 event, this does not hold true. After further investigation it was determined that both event 10/17/03 and event 01/13/05 had antecedent dry times of approximately 0 and 18 hours, respectively. Therefore, the higher infiltration rates of these events could be due to the fact that before each of the events had occurred a previous event had just emptied from the bed, which means that the soil would not have had a chance to dry out before the new event. Thus, the hydraulic conductivity for each of the new events would have been close to saturated which translates to a higher infiltration rate.

Chapter 6: Conclusions and Recommendations

A model was created to characterize the infiltration occurring in underground infiltration beds with decreasing ponded depth using the Green-Ampt formula. Through an evaluation of the soil parameters that affect infiltration including, soil suction pressure head, volumetric soil moisture content and hydraulic conductivity it was determined that hydraulic conductivity plays the most influential role in characterizing infiltration. Therefore, the hydraulic conductivity that would characterize the storm event best, needed to be determined. The results of the model calibration process revealed that two separate methods for determining hydraulic conductivity were needed, one for small storm events and one for large storm events. The events were then modeled using a calibration curve for determining the hydraulic conductivity. The calibration curve for the small events was based on the temperature in the bed, while the calibration curve for the large events was based on the water surface elevation in the bed.

The model results for both the small and the large events proved to be an accurate representation of the actual results. The model provided a good representation of the recession limb of the outflow hydrograph which corresponds to the activity in the infiltration bed, starting with a full bed and modeling how the bed slowly empties, in addition to modeling how that decrease in depth in the infiltration bed relates to what is actually infiltrating through the bed bottom. However, the results for the large events had a higher MSE than the small events. It is hypothesized that temperature, as well as bed depth, influences the infiltration rate of the large events. Research on this was limited due to the limited availability of a variety of events with wide range of temperature and bed depth.

After evaluating the results, the infiltration rate occurring through the bottom of the infiltration bed was discussed. There is a strong relationship between infiltration rate and temperature, with a cyclical pattern of higher and lower infiltration rates occurring across the year concurrently with higher and lower temperatures in the infiltration bed. Also, for larger events it was determined that a more accurate model representation could be provided by making hydraulic conductivity a function of water surface elevation in the bed, with higher infiltration rates at higher depths and lower infiltration rates at lower depths. Currently, the model sets the hydraulic conductivity as a constant over the duration of the event.

Lastly the potential of the infiltration bed to have a clogged layer was evaluated and disproved. However, by doing so the importance of antecedent dry time on infiltration rate was analyzed. As antecedent dry time decreases, the infiltration rate in the bed increases due to the soil being more saturated below the bed, thus relating to a higher hydraulic conductivity closer to that of saturation.

Based on the limited information provided by field tests and instrumentation on site, in addition to a number of assumptions, fairly accurate results were obtained for the model and a viable discussion was made concerning factors affecting infiltration rate. It was shown that the when the bed depth is shallow (under 4 inches) the governing factor affecting hydraulic conductivity and infiltration rate is temperature, with higher rates during warmer temperatures. For events with higher bed depths, the governing factor is the maximum bed depth, although it is proposed that temperature also plays an important role in hydraulic conductivity and infiltration rate. It was also shown during shorter antecedent dry time when the soil has not drained completely between events, the

infiltration rates tend to be higher than otherwise expected. It is hoped that the research in this thesis will provide researchers and engineers with a better understanding of infiltration processes in underground infiltration beds and the varying dependency of infiltration rate on temperature, soil saturation, and bed depth.

Achieving a maximum infiltration rate for recharge basins is essential. Therefore, if infiltration beds are designed taking this research into consideration, the maximum depth of these structures could be decreased. Predicting the hydraulic conductivity is the major weakness of the model. However, with more research on the affects of bed temperature and bed depth on the infiltration rate, calibration curves for different soil types under a range of bed depths and temperature could be developed, optimizing the accuracy of the model. By choosing a hydraulic conductivity based on specific site conditions and running a continuous simulation model it could be seen that the majority of storm events occur when temperatures and thus infiltration rates are higher. It is hoped that the work in this study will help provide some answers and raise new questions on how to effectively and more efficiently design and implement these systems as a standard best management practice.

- Recommendations

    1. More comprehensive monitoring is needed. Pressure transducer probes or another type of water depth measuring device should be installed in the upper and middle infiltration beds. This would help understand what infiltration is occurring in these beds and if it corresponds well to the research done on lower infiltration bed.

2. A double ring infiltrometer or another type of infiltration measuring devise should be installed at the site and used to compare to the infiltration rate and hydraulic conductivity results in this study.
3. This study identified the significance of temperature and water surface elevation on the infiltration rate within infiltration beds. That impact should be further examined.
    - More storm events over a variety of depths and temperatures should continue to be collected to further evaluated the strength of the dependency of these parameters to infiltration.
    - The results from the infiltration analysis presented in this report should be combined with the hydrologic model created by Ladd (2004) to create a composite model that would better represent the site.
    - The effect of time between storm events on the site and more specifically the effects of soil saturation should be further investigated. This would determine the extent of which antecedent dry time and soil moisture content has on the performance of the infiltration beds.
    - The infiltration capacity of underground infiltration beds should be evaluated and compared to other structural infiltration BMP's like infiltration trenches or bioinfiltration gardens. This would aid in the making the process of choosing a BMP based on site specific criteria rather than purely aesthetics.

References

American Society for Testing Materials (2000). “Standard Test Method for Measurement of Hydraulic Conductivity of Saturated Porous Materials Using a Flexible Wall Permeameter (ASTM D 5084-90),” *Annual Book of ASTM Standards*, Section Four, Construction, Volume 4.08.

American Society for Testing Materials (2001), "Standard Test Method for Open Channel Flow Measurement of Water with This-Plate Weirs (D 5242-92)," ASTM International.

Akan, A. Osman (2002). “Modified Rational Method for Sizing Infiltration Structures.” *Canadian Journal of Civil Engineering*, 29(4), 539-542.

Al-Muttair, Fouad F. and Al-Turbak, Abdulaziz S. (1991). “Modeling of Infiltration from an Artificial Recharge Basin with a Decreasing Ponded Depth.” *Journal of King Saud University – Engineering Sciences*, 3(1), 89-99.

Aron, Gert (1992). “Adaptation of Horton and SCS Infiltration Equations to Complex Storms.” *Journal of Irrigation and Drainage Engineering*, 118(2), 275-284.

Barbosa, A. E.; Hvitved-Jacobsen, T. (2001). “Infiltration Pond Design for Highway Runoff Treatment in Semiarid Climates.” *Journal of Environmental Engineering*, 127(11), 1014-1022.

Battaglia, Glen J. (1996). “Mean Square Error.” *AMP Journal of Technology*, 5(1), 31-36.

Bauer, S.W. (1974). “A Modified Horton Equation During Intermittent Rainfall.” Hydrol. Sci. Bull., 19(2/6), 219-229.

Bouwer, Herman M. (1990). “Effect of Water Depth and Groundwater Table on Infiltration from Recharge Basins.” *Irrig Drain Proc 1990 Natl Conf*, 377-384.

Cahill Associates, Environmental Consultants (2003). http://www.thcahill.com

Campbell Scientific (2003). “CR200 Datalogger Operator’s Manual.” Campbell Scientific, Logan, UT.

Campbell Scientific (2000). “CR23X Micrologger Operator’s Manual.” Campbell Scientific, Logan, UT.

Campbell Scientific (2002). “CS616 Water Content Reflectometer Instruction Manual.” Campbell Scientific, Logan, UT.

Campbell Scientific (2002). “LoggerNet User Manual Version 2.0.” Campbell Scientific, Logan, UT.

Campbell Scientific (2003). “NL100/105 Network Link Interface Instruction Manual.” Campbell Scientific, Logan, UT.

Campbell Scientific (2003). “TE525 Tipping Bucket Rain Gage.” Campbell Scientific, Logan, UT.

Eco-Creto of Texas, Inc. (2004). http://www.ecocreto.com

Emerson, C. (2003). “Evaluation of the Additive Effects of Stormwater Detention Basins at the Watershed Scale.” *Masters Thesis*. Drexel University, Philadelphia, PA.

Guo, James C. Y. (2002). “Overflow Risk Analysis for Stormwater Quality Control Basins.” Journal of Hydrologic Engineering, 7(6), 428-434.

Guo, James C. Y. and Hughes, William (2001). “Storage Volume and Overflow Risk for Infiltration Basin Design.” *Journal of Irrigation and Drainage Engineering*, 127(3), 170-175.

Hsu, Shaohua M.; Ni, Chuen-Fa; Hung, Pi-Fang (2002). “Assessment of Three Infiltration Formulas based on Model Fitting on Richards Equation.” Journal of Hydrologic Engineering, 7(5), 373-379.

Instrumentation Northwest (2002). “PS-9805 Submersible Pressure/Temp. Transducer Instruction Manual.” Instrumentation Northwest, Kirkland, WA.

Instrumentation Northwest (2002). “Submersible Pressure Transmitter PS9800 Instruction Manual.” Instrumentation Northwest, Kirkland, WA.

Kwiatkowski, M. (2004). “A Water Quantity Study of a Porous Concrete Infiltration Best Management Practice.” *Masters Thesis*. Villanova University, Villanova, PA.

Ladd, T. (2004). “A Water Quantity Study of a Porous Concrete Infiltration Best Management Practice.” *Masters Thesis.* Villanova University, Villanova, PA.

Lin, C.; Greenwald, D.; Banin, A. (2003). “Temperature Dependence of Infiltration Rate During Large Scale Water Recharge into Soil.” *Soil Science Society American Journal*, 67, 487-493.

Mikkelsen, P.S.; Jacobsen, P.; Fujita, S. (1996). “Infiltration Practice for Control of Urban Stormwater.” *Journal of Hydraulic Research*, 34(6), 827-840.

Prokop, M. (2003). "Determining the Effectiveness of the Villanova Bio-Infiltration Traffic Island in Infiltrating Annual Runoff." *Masters Thesis.* Villanova University, Villanova, PA.

Rawls, W. J.; Brakensiek, D. L.; and Miller N. (1983). "Green-Ampt Infiltration Parameters from Soils Data." *J. Hydraulic Div., ASCE,* 109(1), 62-70.

Risse, L. M.; Nearing, M. A.; Savabi, M. R. (1994). "Determining the Green-Ampt Effective Hydraulic Conductivity from Rainfall-Runoff Data for the WEPP Model." *American Society of Agricultural Engineers,* 37(2), 411-418.

U.S. EPA (1999). "Storm Water Technology Fact Sheet: Porous Pavement." U.S. Environmental Protection Agency. <http://www.epa.gov/owm/mtb/porouspa.pdf>

Traver, R. and Welker A. (2003). "Quality Assurance – Quality Control Project Plan" Villanova Stormwater Porous Concrete Demonstration Site – A Retrofit.

Traver, R.; Welker, A.; Emerson, C.; Kwiatkowski, M.; Ladd, T.; Kob, L. (2003). "Lessons Learned – Porous Concrete Demonstration Site." *Stormwater* 5(6).

Traver, R.; Welker, A.; Horst, M.; Braga, A.; Vanacore, M.; Kob, L. (2005). "Lessons Learned II– Porous Concrete Demonstration Site." *Stormwater* (In Press).

U.S. Army Corps of Engineers Hydrologic Engineering Center (2001). "Hydrologic Modeling System HEC-HMS User's Manual; Version 2.1." U.S. Army Corps of Engineers Hydrologic Engineering Center, Davis, CA.

U.S. Environmental Protection Agency (USEPA) (2002). "National Management Measures to Control Nonpoint Source Pollution from Urban Areas".

Viessman Jr., Warren and Lewis, Gary L. (2003). Introduction to Hydrology. Pearson Education, Inc., 5 ed. Upper Saddle River, NJ.

The Weather Underground (2005). <http://www.wunderground.coml>

Appendix A – Elevation Storage Outflow Table

Lower Infiltration Bed Volume Calculations						
Depth (ft)	Surface Area (ft^2)	Wetted Area (ft^2)	Wetted Area of Side Walls (ft^2)	Volume (ft^3)	Volume of Pore Space (ft^3)	Outflow (cfs)
0	1060.83	1060.83	0.00	0.00	0.00	0
0.1	1090.81	1093.48	32.64	107.58	43.03	0
0.2	1121.14	1126.55	65.71	218.18	87.27	0
0.3	1151.82	1160.04	99.21	331.83	132.73	0
0.4	1182.86	1193.96	133.13	448.56	179.42	0
0.5	1214.25	1228.31	167.48	568.42	227.37	0
0.6	1246.00	1263.08	202.25	691.43	276.57	0
0.7	1278.10	1298.28	237.44	817.63	327.05	0
0.8	1310.56	1333.90	273.06	947.07	378.83	0
0.9	1343.37	1369.94	309.11	1079.76	431.91	0
1	1376.54	1406.41	345.58	1215.76	486.30	0
1.1	1410.06	1443.31	382.48	1355.09	542.04	0
1.2	1443.93	1480.63	419.80	1497.79	599.12	0
1.3	1478.16	1518.37	457.54	1643.89	657.56	0
1.4	1512.75	1556.54	495.71	1793.44	717.38	0
1.5	1547.69	1595.14	534.31	1946.46	778.58	0
1.6	1582.98	1634.16	573.33	2102.99	841.20	1.6956
1.7	1618.63	1673.60	612.77	2263.07	905.23	1.9782
1.8	1654.64	1713.47	652.64	2426.74	970.70	2.2608
1.9	1691.00	1753.77	692.94	2594.02	1037.61	2.5434
2	1727.71	1794.49	733.66	2764.95	1105.98	2.826
2.1	1764.78	1835.63	774.80	2939.58	1175.83	3.1086
2.2	1802.20	1877.20	816.37	3117.93	1247.17	3.3912
2.3	1839.98	1919.20	858.37	3300.04	1320.01	3.6738
2.4	1878.11	1961.62	900.79	3485.94	1394.38	3.9564
2.5	1916.60	2004.46	943.63	3675.68	1470.27	4.239
2.6	1955.44	2047.73	986.90	3869.28	1547.71	4.5216
2.7	1994.63	2091.43	1030.59	4066.78	1626.71	4.8042
2.8	2034.18	2135.55	1074.71	4268.22	1707.29	5.0868
2.9	2074.09	2180.09	1119.26	4473.64	1789.45	5.3694
3	2114.35	2225.06	1164.23	4683.06	1873.22	5.652
3.1	2154.96	2270.45	1209.62	4896.52	1958.61	5.9346
3.2	2195.93	2316.27	1255.44	5114.07	2045.63	6.2172
3.3	2237.26	2362.52	1301.68	5335.73	2134.29	6.4998
3.4	2278.94	2409.19	1348.35	5561.54	2224.62	6.7824
3.5	2320.97	2456.28	1395.45	5791.53	2316.61	7.065
3.6	2363.36	2503.80	1442.97	6025.75	2410.30	7.3476
3.7	2406.10	2551.74	1490.91	6264.22	2505.69	7.6302
3.8	2449.20	2600.11	1539.28	6506.99	2602.80	7.9128
3.9	2492.65	2648.90	1588.07	6754.08	2701.63	8.1954
4	2536.46	2698.12	1637.29	7005.54	2802.21	8.478

Appendix B – Storm List

Table B-1. 2003 Storm List

Rainfall Start	Rainfall End	Rainfall Duration (hrs)	Max 1 Hour precip (in.)	Flow Start	Flow End	Rainfall (in.)	Rain Gauge	Intensity (in./hr)	Outflow Volume (ft^3)
9/12/03 11:10 PM	9/15/03 6:45 PM	67.58	0.52	9/13/03 8:45 AM	9/15/03 5:50 PM	2.3	WL	0.03	4.644
9/18/03 2:25 PM	9/19/03 2:55 AM	12.50	0.40	9/18/03 9:15 PM	9/19/03 3:15 AM	1.27	PC	0.10	12.571
9/22/03 8:35 PM	9/23/03 12:00 PM	15.42	0.52	9/23/03 6:20 AM	9/23/03 9:55 AM	0.93	PC	0.06	7.367
9/27/03 2:15 PM	9/28/03 6:55 AM	16.67	0.54	9/28/03 12:35 AM	9/28/03 1:35 AM	0.7	PC	0.04	2.391
10/4/03 8:45 AM	10/4/03 5:35 PM	8.83	0.06	-	-	0.11	PC	0.01	0.000
10/14/03 8:10 PM	10/15/03 4:25 AM	8.25	0.62	10/14/03 9:00 PM	10/15/03 3:25 AM	1.35	PC	0.16	24.920
10/16/03 7:55 PM	10/16/03 10:20 PM	2.42	0.02	-	-	0.05	PC	0.02	-
10/17/03 5:30 PM	10/18/03 3:25 AM	9.92	0.08	10/17/03 8:35 PM	10/18/03 1:05 AM	0.27	PC	0.03	0.790
10/22/03 7:25 AM	10/22/03 11:35 AM	4.17	0.07	-	-	0.1	PC	0.02	-
10/26/03 9:05 PM	10/27/03 7:50 PM	22.75	0.86	10/26/03 11:20 PM	10/27/03 9:25 PM	2.73	PC	0.12	161.053
10/28/03 7:40 PM	10/29/03 2:30 PM	18.83	0.21	10/28/03 8:55 PM	10/29/03 12:05 PM	1.36	PC	0.07	82.383
11/4/03 9:00 PM	11/6/03 10:20 PM	49.33	0.16	11/5/03 5:30 PM	11/6/03 11:25 PM	0.78	PC	0.02	4.963
11/12/03 12:20 AM	11/12/03 7:10 AM	6.83	0.12	11/12/03 1:55 AM	11/12/03 8:20 AM	0.44	PC	0.06	1.600
11/19/03 5:05 AM	11/20/03 3:40 AM	22.58	0.68	11/19/03 4:05 PM	11/20/03 4:25 AM	1.64	PC	0.07	50.545
11/24/03 7:55 PM	11/25/03 12:10 AM	4.25	0.09	11/24/03 9:25 PM	11/25/03 12:30 AM	0.21	PC	0.05	0.318
11/28/03 7:50 AM	11/29/03 2:00 AM	18.17	0.32	11/28/03 6:15 PM	11/29/03 12:35 AM	0.84	PC	0.05	19.506
12/9/03 2:50 PM	12/11/03 1:15 PM	46.42	0.26	12/9/03 2:50 PM	12/11/03 4:05 PM	1.56	PC	0.03	215.016
12/14/03 12:30 PM	12/14/03 10:35 PM	10.08	0.26	12/14/03 2:45 PM	12/15/03 4:10 AM	1.06	PC	0.11	92.219
12/17/03 6:05 AM	12/17/03 4:25 PM	10.33	0.29	12/17/03 6:45 AM	12/17/03 9:40 PM	0.75	PC	0.07	30.203
12/24/03 1:55 AM	12/24/03 3:50 PM	13.92	0.53	12/24/03 3:40 AM	12/24/03 9:15 PM	1.81	PC	0.13	137.219

Table B-2. 2003 Storm List (cont.)

Rainfall Start	Flow (in./area)	Staying on site (in./area)	Max Port Depth (in.)	Time to Port = 0	Entered into BMP Database	Storms with Quality Data	Modeled Storms	Notes
9/12/03 11:10 PM	0.00	1.89	9.806	9/17/03 8:00 PM	x	x	x	bartely gage and port pt up
9/18/03 2:25 PM	0.00	1.04	11.885	9/21/03 8:00 AM	x	x	x	
9/22/03 8:35 PM	0.00	0.76	5.800	9/25/03 11:00 AM	x	x	x	
9/27/03 2:15 PM	0.00	0.57	2.831	9/29/03 11:45 AM	x		x	
10/4/03 8:45 AM	0.00	0.09	0.273	non peaking	x	x	x	
10/14/03 8:10 PM	0.01	1.11	8.210	bed not empty	x			
10/16/03 7:55 PM	-	0.04	2.446	bed not empty				
10/17/03 5:30 PM	0.00	0.22	1.917	10/18/03 9:55 PM				
10/22/03 7:25 AM	-	0.08	0.227	non peaking	x	x	x	
10/26/03 9:05 PM	0.03	2.24	19.710	bed not empty	x	x	x	
10/28/03 7:40 PM	0.02	1.12	19.190	11/1/03 9:05 AM	x	x	x	
11/4/03 9:00 PM	0.00	0.64	1.968	11/8/03 3:50 AM	x	x	x	
11/12/03 12:20 AM	0.00	0.36	0.917	11/13/03 2:20 AM				
11/19/03 5:05 AM	0.01	1.34	11.980	11/23/03 10:30 AM	x	x	x	
11/24/03 7:55 PM	0.00	0.17	0.241	non peaking				
11/28/03 7:50 AM	0.00	0.69	4.526	12/1/03 12:25 PM	x			
12/9/03 2:50 PM	0.04	1.28	15.860	bed not empty	x	x	x	
12/14/03 12:30 PM	0.02	0.87	12.200	bed not empty	x			
12/17/03 6:05 AM	0.01	0.62	9.730	12/20/03 3:50 PM	x			
12/24/03 1:55 AM	0.03	1.48	15.170	12/28/03 6:10 AM	x			

Table B-3. 2004 Storm List

Rainfall Start	Rainfall End	Rainfall Duration (hrs)	Max 1 Hour precip (in.)	Flow Start	Flow End	Rainfall (in.)	Rain Gauge	Intensity (in./hr)	Outflow Volume (ft^3)
1/4/04 6:20 PM	1/5/04 11:00 PM	28.67	0.12	1/5/04 3:45 AM	1/5/04 7:00 PM	0.55	PC	0.02	10.967
2/3/04 10:50 AM	2/3/04 6:20 PM	7.50	0.22			0.68	PC	0.09	
2/6/04 6:25 AM	2/7/04 8:50 AM	26.42	0.31	2/6/04 7:00 AM	2/7/04 4:50 PM	1.85	PC	0.07	499.250
3/4/04 4:10 AM	3/4/04 12:05 PM	7.92	0.10	3/4/04 6:45 AM	3/4/04 9:35 AM	0.22	PC	0.03	1.110
3/6/04 1:50 AM	3/6/04 12:05 PM	10.25	0.16	3/6/04 4:00 AM	3/6/04 3:25 PM	0.55	PC	0.05	21.594
3/7/04 9:30 PM	3/10/04 8:05 AM	58.58	0.08	3/8/04 5:25 PM	3/9/04 1:10 PM	0.68	PC	0.01	28.047
3/17/04 10:45 AM	3/17/04 5:20 PM	6.58	0.01	3/16/04 10:10 AM	3/18/04 5:40 AM	0.06	PC	0.01	39.676
3/18/04 9:05 AM	3/19/04 2:05 PM	29.00	0.28	3/18/04 11:55 PM	3/19/04 10:35 PM	1.33	PC	0.05	32.973
3/30/04 5:40 PM	3/31/04 2:00 AM	8.33	0.20	3/30/04 9:25 PM	3/31/04 8:10 AM	0.67	PC	0.08	37.200
4/1/04 3:10 AM	4/1/04 4:45 AM	1.58	0.16	4/1/04 3:50 AM	4/1/04 9:15 AM	0.2	PC	0.13	5.920
4/2/04 11:40 AM	4/3/04 5:35 AM	17.92	0.11	4/2/04 12:25 PM	4/3/04 1:20 PM	0.84	PC	0.05	60.390
4/4/04 5:35 AM	4/4/04 1:05 PM	7.50	0.30	4/4/04 9:00 AM	4/4/04 9:10 PM	0.71	PC	0.09	59.660
4/8/04 12:55 PM	4/8/04 11:45 PM	10.83	0.06	-	-	0.12	PC	0.01	-
4/11/04 9:50 AM	4/11/04 3:45 PM	5.92	0.03	-	-	0.06	PC	0.01	-
4/12/04 12:15 PM	4/15/04 2:25 AM	62.17	0.23	4/12/04 4:05 PM	4/15/04 7:15 AM	2.1	PC	0.03	157.111
4/23/04 6:10 PM	4/23/04 11:15 PM	5.08	0.44	4/23/02 6:40 PM	4/24/02 12:55 AM	0.77	PC	0.15	24.309
4/25/04 12:00 PM	4/26/04 9:35 PM	33.58	0.24	4/25/02 11:25 PM	4/27/02 3:20 AM	1.34	PC	0.04	71.363
4/27/04 5:45 PM	4/28/04 7:30 AM	13.75	0.06	-	-	0.12	PC	0.01	-
5/2/04 11:35 AM	5/3/04 10:05 PM	34.50	0.28	5/2/04 10:55 PM	5/3/04 11:05 PM	0.95	PC	0.03	22.325
5/7/04 2:10 PM	5/7/04 2:50 PM	0.67	0.37	5/7/04 2:25 PM	5/7/04 3:10 PM	0.37	PC	0.56	2.158
5/9/04 7:40 PM	5/10/04 3:10 AM	7.50	0.19	5/10/04 12:15 AM	5/10/04 5:00 AM	0.4	PC	0.05	4.733
5/15/04 8:10 PM	5/16/04 9:35 AM	13.42	0.12	-	-	0.2	PC	0.01	-
5/18/04 4:40 PM	5/19/04 3:00 PM	22.33	0.22	5/18/04 9:35 PM	5/19/04 3:30 PM	0.55	PC	0.02	2.095
5/25/04 7:50 PM	5/26/04 8:10 AM	12.33	0.08	-	-	0.11	PC	0.01	-
5/27/04 2:15 AM	5/27/04 2:25 AM	0.17	0.14	-	-	0.14	PC	0.84	-
5/31/04 11:40 AM	6/1/04 2:35 PM	26.92	0.14	5/31/04 2:20 PM	6/1/04 2:50 PM	0.42	PC	0.02	0.411
6/3/04 2:25 AM	6/3/04 4:30 AM	2.08	0.08	-	-	0.11	PC	0.05	-
6/5/04 4:10 AM	6/6/04 3:25 AM	23.25	0.07	6/5/04 8:40 AM	6/5/04 10:40 PM	0.5	PC	0.02	0.986
6/10/04 5:45 PM	6/11/04 2:40 PM	20.92	0.12	6/11/04 8:35 AM	6/11/04 8:45 AM	0.31	PC	0.01	0.027
6/14/04 6:30 PM	6/15/04 4:55 PM	22.42	0.32	6/15/04 4:25 PM	6/15/04 5:25 PM	0.59	PC	0.03	2.021
6/16/04 11:25 AM	6/16/04 7:40 PM	8.25	0.53	6/16/04 6:40 PM	6/16/04 8:30 PM	0.56	PC	0.07	5.943
6/17/04 4:40 PM	6/17/04 8:05 PM	3.42	0.06	6/17/04 7:40 PM	6/17/04 8:30 PM	0.55	PC	0.16	0.394
6/22/04 5:35 PM	6/22/04 6:05 PM	0.50	0.59	6/22/04 5:50 PM	6/22/04 6:55 PM	0.59	PC	1.18	4.771
6/25/04 5:10 PM	6/25/04 7:35 PM	2.42	0.04	-	-	0.05	PC	0.02	-
6/29/04 12:10 AM	6/29/04 12:30 AM	0.33	0.22	6/29/04 12:25 AM	6/29/04 12:45 AM	0.22	PC	0.66	0.899
7/7/04 4:50 PM	7/7/04 7:40 PM	2.83	0.22	7/7/04 5:40 PM	7/7/04 6:05 PM	0.33	PC	0.12	0.024
7/12/04 2:00 AM	7/13/04 2:20 AM	24.33	0.70	7/12/04 6:30 AM	7/12/04 8:05 PM	3.58	PC	0.15	641.508
7/14/04 4:20 PM	7/14/04 8:50 PM	4.50	0.35	7/14/04 7:50 PM	7/14/04 8:10 PM	0.43	PC	0.10	0.472
7/18/04 4:55 AM	7/18/04 9:30 PM	16.58	0.15	7/18/04 9:20 AM	7/18/04 6:30 PM	0.74	PC	0.04	4.106
7/23/04 1:50 PM	7/23/04 4:45 PM	2.92	0.73	7/23/04 2:30 PM	7/23/04 4:50 PM	0.85	PC	0.29	5.224
7/27/04 10:40 AM	7/28/04 3:55 AM	17.25	1.13	7/27/04 12:50 PM	7/28/04 1:15 AM	2.73	PC	0.16	250.614
7/28/04 7:40 PM	7/28/04 8:30 PM	0.83	0.40	7/28/04 7:55 PM	7/28/04 9:00 PM	0.4	PC	0.48	2.307
7/30/04 5:35 AM	7/30/04 5:45 PM	12.17	0.09	-	-	0.13	PC	0.01	-
8/1/04 4:20 AM	8/1/04 9:00 AM	4.67	0.97	8/1/04 5:10 AM	8/1/04 10:20 AM	2.08	PC	0.45	277.479
8/4/04 7:15 PM	8/4/04 7:45 PM	0.50	0.13	-	-	0.13	PC	0.26	-
8/12/04 8:25 PM	8/13/04 4:00 AM	7.58	0.07	-	-	0.09	PC	0.01	-
8/14/04 6:20 PM	8/14/04 11:40 PM	5.33	0.10	8/14/04 10:30 PM	8/14/04 11:45 PM	0.21	PC	0.04	0.194
8/16/04 5:15 AM	8/16/04 5:50 AM	0.58	0.04	-	-	0.04	PC	0.07	-
8/21/04 12:40 PM	8/21/04 2:45 PM	2.08	0.29	8/21/04 1:35 PM	8/21/04 2:45 PM	0.36	PC	0.17	1.519
8/30/04 6:00 PM	8/31/04 5:50 AM	11.83	0.25	8/30/04 6:05 PM	8/30/04 6:15 PM	0.31	PC	0.03	0.488
9/8/04 4:30 AM	9/9/04 4:10 PM	35.67	0.09	9/9/04 11:35 AM	9/9/04 11:40 AM	0.33	PC	0.01	0.015
9/15/04 6:05 PM	9/16/04 2:50 AM	8.75	0.02	-	-	0.05	PC	0.01	-
9/18/04 12:55 AM	9/18/04 3:05 PM	14.17	0.51	9/18/04 3:10 AM	9/18/04 4:10 PM	2.27	PC	0.16	119.361
9/27/04 11:05 PM	9/29/04 5:10 AM	30.08	1.38	9/28/04 8:00 AM	9/29/04 3:35 AM	5.91	PC	0.20	2708.668
9/30/04 9:20 AM	9/30/04 10:25 AM	1.08	0.13	9/30/04 10:20 AM	9/30/04 10:45 AM	0.14	PC	0.13	0.307
10/14/04 3:35 AM	10/14/04 10:40 AM	7.08	0.29	10/14/04 4:20 AM	10/14/04 12:15 PM	0.91	PC	0.13	63.737
10/15/04 2:10 PM	10/15/04 7:50 PM	5.67	0.13	10/15/04 6:40 PM	10/15/04 7:20 PM	0.21	PC	0.04	0.825
10/18/04 11:10 PM	10/19/04 5:10 PM	18.00	0.26	10/19/04 1:05 AM	10/19/04 12:35 PM	0.77	PC	0.04	13.950
10/20/04 11:05 PM	10/21/04 1:10 AM	2.08	0.10	10/21/04 12:10 AM	10/21/04 1:35 AM	0.15	PC	0.07	0.532
10/21/04 7:45 PM	10/21/04 10:05 PM	2.33	0.08	-	-	0.09	PC	0.04	-
10/30/04 1:55 AM	10/30/04 4:55 AM	3.00	0.47	10/30/04 2:15 AM	10/30/04 5:35AM	0.57	PC	0.19	8.860
11/4/04 10:45 AM	11/4/04 8:10 PM	9.42	0.44	11/4/04 12:10 PM	11/4/04 10:45 PM	1.33	PC	0.14	88.504
11/12/04 6:30 AM	11/13/04 3:25 AM	20.92	0.13	11/12/04 8:45 AM	11/13/04 5:05 AM	1.36	PC	0.07	31.476
11/20/04 6:05 AM	11/20/04 9:40 PM	15.58	0.11	11/20/04 8:30 PM	11/20/04 9:05 PM	0.17	PC	0.01	0.355
11/24/04 5:40 AM	11/25/04 11:50 AM	30.17	0.16	11/24/04 1:50 PM	11/25/04 11:00 AM	0.42	PC	0.01	1.379
11/27/04 8:15 PM	11/28/04 11:00 AM	14.75	0.52	11/27/04 11:50 PM	11/28/04 1:15 PM	2.09	PC	0.14	249.147
11/30/04 9:55 PM	12/1/04 11:35 AM	13.67	0.19	12/1/04 3:05 AM	12/1/04 2:15 PM	0.92	PC	0.07	48.647
12/7/04 4:55 AM	12/8/04 4:35 AM	23.67	0.04	12/7/04 9:30 AM	12/8/04 1:20 AM	0.63	PC	0.03	6.691
12/9/04 3:25 PM	12/11/04 1:10 PM	45.75	0.04	12/9/04 4:30 PM	12/8/04 1:25 AM	0.98	PC	0.02	15.755
12/19/04 2:45 PM	12/19/04 6:40 PM	3.92	0.04	-	-	0.07	PC	0.02	-
12/23/04 9:30 AM	12/23/04 6:40 PM	9.17	0.01	12/23/04 12:40 PM	12/23/04 7:35 PM	1.11	PC	0.12	25.902

Table B-4. 2004 Storm List (cont.)

Rainfall Start	Flow (in./area)	Staying on site (in./area)	Max Port Depth (in.)	Time to Port = 0	Entered into BMP Database	Storms with Quality Data	Modeled Storms	Notes
1/4/04 6:20 PM	0.00	0.45	1.079	1/6/04 1:25 PM	x		x	
2/3/04 10:50 AM	0.00	0.56	8.130	bed not empty				
2/6/04 6:25 AM	0.10	1.52	20.180	2/11/04 11:25 AM	x	x	x	includes snow melt
3/4/04 4:10 AM	0.00	0.18	0.169	non peaking				may include snow melt
3/6/04 1:50 AM	0.00	0.45	2.271	3/7/04 3:30 PM	x			may include snow melt
3/7/04 9:30 PM	0.01	0.56	2.897	3/10/04 6:00 PM	x		x	may include snow melt
3/17/04 10:45 AM	0.01	0.05	1.074	bed not empty	x	x		may include snow melt
3/18/04 9:05 AM	0.01	1.09	4.473	3/22/04 2:25 PM				may include snow melt
3/30/04 5:40 PM	0.01	0.55	3.327	bed not empty	x	x	x	may include snow melt
4/1/04 3:10 AM	0.00	0.16	3.231	bed not empty	x			
4/2/04 11:40 AM	0.01	0.69	8.110	bed not empty	x		x	
4/4/04 5:35 AM	0.01	0.58	10.690	4/7/04 7:00 PM	x		x	
4/8/04 12:55 PM	0.00	0.10	0.160	non peaking				
4/11/04 9:50 AM	0.00	0.05	0.157	non peaking				
4/12/04 12:15 PM	0.03	1.72	13.280	4/18/04 9:00 AM	x	x	x	
4/23/04 6:10 PM	0.01	0.63	2.890	4/25/04 12:00 PM	x		x	
4/25/04 12:00 PM	0.01	1.10	8.720	bed not empty	x		x	
4/27/04 5:45 PM	0.00	0.10	6.218	4/29/04 12:15 PM				
5/2/04 11:35 AM	0.00	0.78	3.226	5/5/04 10:25 AM	x		x	
5/7/04 2:10 PM	0.00	0.30	0.222	non peaking				
5/9/04 7:40 PM	0.00	0.33	0.219	non peaking	x		x	
5/15/04 8:10 PM	-	0.16	0.295	non peaking				
5/18/04 4:40 PM	0.00	0.45	0.290	non peaking	x		x	
5/25/04 7:50 PM	-	0.09	0.333	non peaking				
5/27/04 2:15 AM	-	0.11	0.196	non peaking				
5/31/04 11:40 AM	0.00	0.34	0.309	non peaking				
6/3/04 2:25 AM	-	0.09	0.250	non peaking				
6/5/04 4:10 AM	0.00	0.41	0.294	non peaking	x	x	x	
6/10/04 5:45 PM	0.00	0.25	0.288	non peaking				
6/14/04 6:30 PM	0.00	0.48	0.443	non peaking	x	x	x	
6/16/04 11:25 AM	0.00	0.46	2.829	bed not empty	x		x	
6/17/04 4:40 PM	0.00	0.45	0.431	6/18/04 12:40 AM				
6/22/04 5:35 PM	0.00	0.48	2.097	6/23/04 5:25 PM	x		x	
6/25/04 5:10 PM	-	0.04	0.237	non peaking				
6/29/04 12:10 AM	0.00	0.18	0.312	non peaking				
7/7/04 4:50 PM	0.00	0.27	0.291	non peaking	x	x	x	
7/12/04 2:00 AM	0.13	2.94	21.370	bed not empty	x	x	x	
7/14/04 4:20 PM	0.00	0.35	4.146	7/16/04 12:10 AM	x		x	
7/18/04 4:55 AM	0.00	0.61	3.219	7/20/04 2:35 AM	x	x	x	
7/23/04 1:50 PM	0.00	0.70	3.071	7/24/04 9:55 PM	x		x	
7/27/04 10:40 AM	0.05	2.24	21.040	bed not empty	x	x	x	
7/28/04 7:40 PM	0.00	0.33	11.900	bed not empty	x		x	
7/30/04 5:35 AM	-	0.11	1.650	7/30/04 11:35 PM				
8/1/04 4:20 AM	0.06	1.71	21.710	8/3/04 7:35 PM	x		x	
8/4/04 7:15 PM	-	0.11	0.283	non peaking				
8/12/04 8:25 PM	-	0.07	0.286	non peaking				
8/14/04 6:20 PM	0.00	0.17	0.288	non peaking				
8/16/04 5:15 AM	-	0.03	0.287	non peaking				
8/21/04 12:40 PM	0.00	0.30	0.296	non peaking				8/27/04 FF System and Silt Bag in Inlet
8/30/04 6:00 PM	0.00	0.25	0.280	non peaking				
9/8/04 4:30 AM	0.00	0.27	0.294	non peaking	x	x	x	
9/15/04 6:05 PM	-	0.04	0.237	non peaking				
9/18/04 12:55 AM	0.02	1.86	17.100	9/21/04 4:25 AM	x		x	
9/27/04 11:05 PM	0.56	4.85	23.020	bed not empty	x	x	x	
9/30/04 9:20 AM	0.00	0.11	6.816	10/2/04 2:10 AM	x		x	
10/14/04 3:35 AM	0.01	0.75	5.206	bed not empty	x		x	
10/15/04 2:10 PM	0.00	0.17	5.014	10/17/04 11:00 AM			x	PC Construction
10/18/04 11:10 PM	0.00	0.63	5.542	bed not empty	x	x	x	
10/20/04 11:05 PM	0.00	0.12	2.744	bed not empty				
10/21/04 7:45 PM	-	0.07	1.394	10/22/04 2:55 PM				
10/30/04 1:55 AM	0.00	0.47	1.731	10/31/04 7:55AM	x		x	
11/4/04 10:45 AM	0.02	1.09	9.390	11/8/04 1:00 PM	x		x	
11/12/04 6:30 AM	0.01	1.12	9.650	11/17/04 9:05 AM	x	x	x	
11/20/04 6:05 AM	0.00	0.14	0.340	non peaking				
11/24/04 5:40 AM	0.00	0.34	0.251	11/25/04 11:50 AM				
11/27/04 8:15 PM	0.05	1.71	17.490	bed not empty	x		x	
11/30/04 9:55 PM	0.01	0.75	9.460	12/4/04 1:40 PM	x	x	x	
12/7/04 4:55 AM	0.00	0.52	2.562	bed not empty	x	x	x	
12/9/04 3:25 PM	0.00	0.80	7.200	12/14/04 6:20 AM	x		x	
12/19/04 2:45 PM	-	0.06	0.195	non peaking				SNOW/SLEET EVENT
12/23/04 9:30 AM	0.01	0.91	4.523	12/25/04 9:35 PM	x		x	

Table B-5. 2005 Storm List

Rainfall Start	Rainfall End	Rainfall Duration (hrs)	Max 1 Hour precip (in.)	Flow Start	Flow End	Rainfall (in.)	Rain Gauge	Intensity (in./hr)	Outflow Volume (ft^3)
1/3/05 3:30 PM	1/4/05 6:25 AM	14.92	0.01	-	-	0.09	PC	0.01	-
1/5/05 2:10 AM	1/7/05 2:15 AM	48.08	0.02	1/5/05 3:05 AM	1/6/05 6:15 PM	0.99	PC	0.02	13.430
1/7/05 9:30 PM	1/8/05 12:20 PM	14.83	0.04	1/8/05 10:10 AM	1/8/05 2:05 PM	0.43	PC	0.03	6.046
1/11/05 3:00 PM	1/11/05 11:50 PM	8.83	0.02	1/11/05 8:00 PM	1/11/05 11:10 PM	0.35	PC	0.04	2.099
1/13/05 10:50 PM	1/14/05 11:35 AM	12.75	0.12	1/13/05 11:15 PM	1/14/05 2:25 PM	1.68	PC	0.13	229.677
1/25/05 12:40 PM	1/25/05 4:35 PM	3.92	0.01	-	-	0.08	PC	0.02	-
1/26/05 8:45 AM	1/26/05 5:15 PM	8.50	0.01	-	-	0.2	PC	0.02	-
1/30/05 11:10 AM	1/30/05 2:25 PM	3.25	0.01	-	-	0.04	PC	0.01	-
2/10/05 3:00 AM	2/10/05 6:00 AM	3.00	0.01	2/10/05 4:10 AM	2/10/05 7:05 AM	0.12	PC	0.04	0.405
2/14/05 9:35 AM	2/14/05 10:55 PM	13.33	0.07	2/14/05 1:05 PM	2/15/05 1:10 AM	1.15	PC	0.09	27.831
2/16/05 2:00 PM	2/16/05 4:00 PM	2.00	0.02	-	-	0.24	PC	0.12	-
2/21/05 10:50 AM	2/23/05 9:55 AM	47.08	0.18	2/21/05 10:05 AM	2/22/05 12:25 AM	0.57	PC	0.01	0.554
2/25/05 10:30 AM	2/25/05 11:25 AM	0.92	0.08	2/25/05 11:25 AM	2/25/05 1:10 PM	0.08	PC	0.09	0.083
3/1/05 10:30 AM	3/1/05 12:15 PM	1.75	0.24	3/1/05 11:20 AM	3/1/05 5:15 PM	0.26	PC	0.15	6.170
3/8/05 5:10 AM	3/8/05 9:45 AM	4.58	0.01	3/8/05 6:40 AM	3/8/05 6:25 PM	0.24	PC	0.05	12.695
3/11/05 8:55 PM	3/12/05 9:50 AM	12.92	0.02	3/12/05 12:30 AM	3/12/05 1:25 AM	0.08	PC	0.01	0.369
3/20/05 3:10 AM	3/20/05 8:25 PM	17.25	0.01	?	3/20/05 9:25 PM	0.25	PC	0.01	0.794
3/23/05 4:55 AM	3/23/05 10:30 PM	17.58	0.03	?	?	1.11	PC	0.06	?
3/27/05 6:00 PM	3/29/05 1:25 AM	31.42	0.05	3/28/05 12:10 PM	3/29/05 2:30 AM	1.64	PC	0.05	154.185
4/1/05 10:05 PM	4/3/05 6:15 PM	44.17	0.16	4/2/05 1:20 AM	4/3/05 8:25 AM	3.77	PC	0.09	1036.832
4/7/05 8:40 PM	4/8/05 5:50 AM	9.17	0.02	4/8/05 9:55 AM	4/8/05 7:20 PM	0.59	PC	0.06	26.688
4/23/05 5:15 AM	4/23/05 11:40 PM	18.42	0.10	4/23/05 1:55 PM	4/23/05 10:30 PM	0.66	PC	0.04	14.297
4/27/05 12:35 AM	4/27/05 3:50 AM	3.25	0.03	4/23/05 2:00 PM	4/23/05 10:35 PM	0.25	PC	0.08	5.103
4/30/05 2:55 AM	5/1/05 6:55 AM	28.00	0.04	4/23/05 2:05 PM	4/23/05 10:40 PM	0.66	PC	0.02	23.981

Table B-6. 2005 Storm List (cont.)

Rainfall Start	Flow (in./area)	Staying on site (in./area)	Max Port Depth (in.)	Time to Port = 0	Entered into BMP Database	Storms with Quality Data	Modeled Storms	Notes
1/3/05 3:30 PM	-	0.07	0.226	non peaking				
1/5/05 2:10 AM	0.00	0.81	2.755	bed not empty	x		x	
1/7/05 9:30 PM	0.00	0.35	3.948	1/10/05 6:20 PM	x		x	
1/11/05 3:00 PM	0.00	0.29	1.707	1/13/05 4:50 AM	x		x	
1/13/05 10:50 PM	0.05	1.38	15.980	1/16/04 5:30 PM	x		x	
1/25/05 12:40 PM	-	0.07	0.111	non peaking				
1/26/05 8:45 AM	-	0.16	0.151	non peaking				
1/30/05 11:10 AM	-	0.03	0.109	non peaking				
2/10/05 3:00 AM	0.00	0.10	0.186	non peaking				
2/14/05 9:35 AM	0.01	0.94	8.950	bed not empty	x	x	x	
2/16/05 2:00 PM	-	0.20	4.808	2/18/05 1:35 PM	x		x	
2/21/05 10:50 AM	0.00	0.47	0.229	non peaking				
2/25/05 10:30 AM	0.00	0.07	0.151	non peaking				
3/1/05 10:30 AM	0.00	0.21	0.149	non peaking				
3/8/05 5:10 AM	0.00	0.20	0.228	non peaking				
3/11/05 8:55 PM	0.00	0.07	0.236	non peaking				
3/20/05 3:10 AM	0.00	0.21	0.273	non peaking				
3/23/05 4:55 AM	?	0.91	?	?		x		Data missing from 3/22/05 to 3/28/05
3/27/05 6:00 PM	0.03	1.34	13.690	4/1/05 2:25 AM		x	x	lost a week of data/ got end of storm data only
4/1/05 10:05 PM	0.22	3.09	21.660	4/5/05 9:55 AM	x		x	4/3/04 Daylight Savings Time - Now clock is behind 1 hou
4/7/05 8:40 PM	0.01	0.48	1.590	4/9/05 7:55 PM			x	
4/23/05 5:15 AM	0.00	0.54	0.427	non peaking				
4/27/05 12:35 AM	0.00	0.21		non peaking				
4/30/05 2:55 AM	0.00	0.54	0.861	5/1/05 3:55 PM				

Appendix C – BMP Event List

Table C-1. Single Peaking BMP Events

Event Start (Rain Start)	Event End (Port Depth =0)	Event Duration (hrs)	Rainfall (in.) Storm 1	Outflow Volume (ft^3)	Max Port Depth (in.)	Antecedant Dry Time (hrs)	Event Type
9/18/03 2:25 PM	9/21/03 8:00 AM	65.58	1.27	12.571	11.885	18.417	SP
9/22/03 8:35 PM	9/25/03 11:00 AM	62.42	0.93	7.367	5.800	36.583	SP
9/27/03 2:15 PM	9/29/03 11:45 AM	45.50	0.7	2.391	2.831	51.250	SP
10/14/03 8:10 PM	10/17/03 5:30 PM	69.33	1.35	24.920	8.210	368.417	SP
10/17/03 5:30 PM	10/18/03 9:55 PM	28.42	0.27	0.790	1.917	0.000	SP
11/4/03 9:00 PM	11/8/03 3:50 AM	78.83	0.78	4.963	1.968	83.917	SP
11/12/03 12:20 AM	11/13/03 2:20 AM	26.00	0.44	1.600	0.917	92.500	SP
11/19/03 5:05 AM	11/23/03 10:30 AM	101.42	1.64	50.545	11.980	146.750	SP
11/28/03 7:50 AM	12/1/03 12:25 PM	76.58	0.84	19.506	4.526	117.333	SP
12/24/03 1:55 AM	12/28/03 6:10 AM	100.25	1.81	137.219	15.170	82.083	SP
1/4/04 6:20 PM	1/6/04 1:25 PM	43.08	0.55	10.967	1.079	180.167	SP
3/6/04 1:50 AM	3/7/04 3:30 PM	37.67	0.55	21.594	2.271	566.417	SP
3/7/04 9:30 PM	3/10/04 6:00 PM	68.50	0.68	28.047	2.897	6.000	SP
4/23/04 6:10 PM	4/25/04 12:00 PM	41.83	0.77	24.309	2.890	129.167	SP
6/16/04 11:25 AM	6/17/04 4:40 PM	29.25	0.56	5.943	2.829	1009.000	SP
6/22/04 5:35 PM	6/23/04 5:25 PM	23.83	0.59	4.771	2.097	120.917	SP
7/18/04 4:55 AM	7/20/04 2:35 AM	45.67	0.74	4.106	3.219	52.750	SP
7/23/04 1:50 PM	7/24/04 9:55 PM	32.08	0.85	5.224	3.071	83.250	SP
8/1/04 4:20 AM	8/3/04 7:35 PM	63.25	2.08	277.479	21.710	28.750	SP
9/18/04 12:55 AM	9/21/04 4:25 AM	75.50	2.27	119.361	17.100	1085.333	SP
10/30/04 1:55 AM	10/31/04 7:55 AM	30.00	0.57	8.860	1.731	179.000	SP
11/4/04 10:45 AM	11/8/04 1:00 PM	98.25	1.33	88.504	9.390	98.833	SP
11/12/04 6:30 AM	11/17/04 9:05 AM	122.58	1.36	31.476	9.650	89.500	SP
12/7/04 4:55 AM	12/9/04 2:50 PM	57.92	0.63	22.446	2.562	63.250	SP
12/23/04 9:30 AM	12/25/04 9:35 PM	60.08	1.11	25.902	4.523	219.167	SP
1/11/05 3:00 PM	1/13/05 4:50 AM	37.83	0.35	2.099	1.707	20.667	SP
1/13/05 10:50 PM	1/16/05 5:30 PM	66.67	1.68	229.677	15.980	18.000	SP
3/27/05 6:00 PM	4/1/05 2:25 AM	104.42	1.64	154.185	13.690	892.417	SP
4/1/05 10:05 PM	4/5/05 9:55 AM	83.83	3.77	1036.832	21.660	19.667	SP
4/7/05 8:40 PM	4/9/05 7:55 PM	47.25	0.59	14.297	1.590	6.760	SP

Table C-2. Multi-Peaking BMP Events

Event Start (Rain Start)	Event End (Port Depth =0)	Event Duration (hrs)	Rainfall (in.)				Outflow Volume (ft^3)	Max Port Depth (in.)	Antecedant Dry Time (hrs)	Event Type
			Storm 1	Storm 2	Storm 3	Storm 4				
9/12/03 11:10 PM	9/17/03 8:00 PM	116.83	2.3				4.644	9.806		MP
10/26/03 9:05 PM	11/1/03 9:05 AM	132.00	2.73	1.36			243.436	19.710	191.167	MP
12/9/03 2:50 PM	12/20/03 3:50 PM	265.00	1.56	1.06	0.75		337.438	15.860	917.750	MP
2/3/04 10:50 AM	2/11/04 11:25 AM	192.58	0.68	1.85			499.250	20.180	669.417	MP
3/17/04 10:45 AM	3/22/04 2:25 PM	123.67	0.06	1.33			72.649	4.473	160.750	MP
3/30/04 5:40 PM	4/7/04 7:00 PM	193.33	0.67	0.2	0.84	0.71	163.170	10.690	195.250	MP
4/12/04 12:15 PM	4/18/04 9:00 AM	140.75	2.1				157.111	13.280	113.250	MP
4/25/04 12:00 PM	4/29/04 12:15 PM	96.25	1.34	0.12			71.363	8.720	0.000	MP
5/2/04 11:35 AM	5/5/04 10:25 AM	70.83	0.95				22.325	3.226	71.333	MP
7/12/04 2:00 AM	7/16/04 12:10 AM	94.17	3.58	0.43			641.980	21.370	440.583	MP
7/27/04 10:40 AM	7/30/04 11:35 PM	84.92	2.73	0.4	0.13		252.921	21.040	60.750	MP
9/27/04 11:05 PM	10/2/04 2:10 AM	99.08	5.91	0.14			2708.975	23.020	162.667	MP
10/14/04 3:35 AM	10/17/04 11:00 AM	79.42	0.91	0.21			64.562	5.206	289.417	MP
10/18/04 11:10 PM	10/22/04 2:55 PM	87.75	0.77	0.15	0.09		14.482	5.542	36.167	MP
11/27/04 8:15 PM	12/4/04 1:40 PM	161.42	2.09	0.92			297.794	17.490	251.167	MP
12/9/04 2:50 PM	12/14/04 6:20 AM	111.50	0.98				15.755	7.200	0.000	MP
1/5/05 2:10 AM	1/10/05 6:20 PM	136.17	0.99	0.43			19.476	3.948	244.583	MP
2/14/05 9:35 AM	2/18/05 1:35 PM	100.00	1.15	0.24			27.831	8.950	688.083	MP

Appendix D – Instrumentation

(Ladd, 2004)

The first component of the water quantity balance is precipitation. For rainfall measurements a Campbell Scientific (CS) Tipping Bucket TE525WS Rain Gage (Campbell, 2003c) was installed. In conjunction with the rain gage, accurate outflow measurements are necessary to properly assess the effectiveness of the BMP for infiltrating runoff. The infiltration storage beds are interconnected and drain to the lower bed as mentioned in previous sections. The lower storage bed is equipped with an Instrumentation Northwest (INW) PS-9805 Pressure/Temperature Transducer which measures the water surface elevation and water temperature in the bed. The probe is located in the junction box in the lower corner of the infiltration bed as discussed previously. An INW PS-9800 Pressure/Temperature Transducer and V-notch weir were installed in the catch basin at the downstream end of the overflow pipe. The transducer, in conjunction with the weir, gives an accurate flow rate measurement of water leaving the site. In order to also account for the outflow leaving the site through infiltration a total of twelve CS616 Water Content Reflectometers were installed beneath, and immediately outside, the lower infiltration bed to monitor the constant fluctuations in the moisture content of the soil. The reflectometers measure the volumetric water content of the surrounding soil, which changes as stormwater infiltrates through the lower bed and the moisture front passes through the soil profile. A CS CR23X Micrologger (Campbell, 2000) is used to power the instruments and collect and store data. A CS CR200 Datalogger (Campbell, 2003a) is used to collect and store data from the Tipping Bucket

Rain Gage. Two CS NL100 Network Link Interfaces (Campbell, 2003b) connect the Loggers to the Villanova computer network.

Configuration

The CS CR23X Micrologger is the primary data acquisition device for the majority of the instruments. The CS CR200 is the primary acquisition device for the CS Tipping Bucket Rain Gage. Both Loggers are connected to the Network Link Interfaces (NLI) using standard 9 pin communications cables. The NLIs are in turn connected to the University's 10 Base-T port using twisted pair cables with male RJ-45 plug connectors. The Campbell Scientific TE525WS Tipping Bucket Rain Gage is connected to the Datalogger using the P_SW Pulse Channel Input and two Ground Terminals. The INW 9805 Pressure/Temperature Transducer is connected to the Micrologger using two Voltage Excitation Channels, two full Differential Channels, one Single Ended Analog Channel, and three Ground Terminals. The INW 9800 Pressure/Temperature Transducer is connected using one 12 Volt Output Channel, one Single Ended Analog Channel, and one Ground Terminal. The twelve CS616 Water Content Reflectometers MM are connected using one 12 Volt Output Channel, one Single Ended Analog Channel, and two Ground Terminals.

LoggerNet software Version 2.1c (Campbell, 2002b) is used in conjunction with both Loggers. The software allows users to set up, configure, and retrieve data from the Loggers remotely through the University's network. The Edlog program is used for the creation, editing, and documenting of programs for the CR23X Micrologger. The "Short Cut for Windows" program is used for the creation, editing, and documenting of the

program for the CR200 Datalogger. Edlog uses a programming language designed specifically for Campbell Scientific Dataloggers. Short Cut uses a programming language similar in structure to the BASIC programming language. Each instrument requires unique instruction commands to function. These instructions are discussed more in the following sections. The time intervals, data format, and storage locations are also set in the program editors. The Loggers' Battery voltages are monitored to prevent any lost of data due to low battery voltage. Table D-1 shows the various measurements, the units in which they are recorded, and the recording time intervals.

Measurement	Units	Time Increment
Battery Voltages	Volts	1 hour
Rainfall	Inches	5 minutes
Port Water Depth	Inches	5 minutes
Port Temperature	^{o}C	5 minutes
Weir Water Depth	Inches	5 minutes
Soil Moisture Content	Fraction	15 minutes

Table D-1. Measurement units and time increments

The Campbell Scientific TE525WS Tipping Bucket Rain Gage features an eight-inch collector with tips of 0.01 inches per tip. The rain gage has a 6.25 inch overall diameter, a height of 9.5 inches and weighs two and a half pounds. The funnel is a gold anodized spun aluminum knife-edge collector ring and funnel assembly. The funnel collector diameter is 8 inches. The rain gage features a side bracket with clamps for pole mounting. The gage was mounted on the North side of Bartley Hall to a pole on the roof.

The rain gage connector cable is a two-conductor shielded cable. The signal output is a momentary switch closure that is activated by the tipping bucket mechanism. See Table D-2 for the rain gage wiring summary. In the CR200 Datalogger program created by Short Cut, the rain gage functions are programmed using the "PulseCount"

command for rainfall measurement. The Pulse Channel, Configuration, and counting method are all set in this command. The multiplier used in the command determines the units in which the rainfall is reported. In this case, the units have been kept in inches using a multiplier of 0.01 inches per tip. The program is set to run one repetition every five minutes thereby recording the number of tips in the previous five minutes. The program then stores the values in the Rainfall table on the Datalogger. The rain gage has a resolution of one tip. It can function properly in temperatures between 0^{o} and $+50^{o}$C and humidity between 0 and 100%.

Color	Function	Connection
Black	Signal	Pulse Ch. P_SW
White	Signal Return	Ground
Clear	Ground at logger	Ground

Table D-2. Wiring summary for the rain gage

The INW PS-9805 Pressure Transducer is connected to the CR23X Micrologger by a nine conductor vented cable. The cable is run through the wall of the catch basin in a 1.5" diameter electrical conduit directly to the basement of Sullivan Hall where the Micrologger is located. The wiring summary is shown in Table D-3.

Color	Function	Micrologger Connection
White	V(+) excitation (800 mV)	Excitation Ch. EX1
Green	Analog Ground	Ground
Blue	Vr (+)	Differential Ch. 7H
Red	Vr (-)	Differential Ch. 7L
Yellow	Vo (+)	Differential Ch. 8H
Purple	Vo (-)	Differential Ch. 8L
Shield	Ground at logger	Ground
Orange	(T1) temperature excitation	Excitation Ch. EX2
Brown	(T2) temperature out	Single Ended Ch. 18
Black	Temperature analog ground	Ground

Table D-3. Wiring summary for the 9805 Pressure Transducer

In addition to the nine conductors and shield there is also a vent tube in the cable. This vent tube enables the pressure transducer to reference atmospheric pressure as detailed in the Analytical Methods section below. The pressure transducer is programmed using "Instruction 8" in Edlog. "Instruction 8" is an Input/Output Instruction that applies an excitation voltage, delays for a specified amount of time, and then makes a differential voltage measurement (Campbell, 2002b). The transducer is excited and records a port water depth and port temperature every five minutes. The Micrologger stores this data in arrays 103 and 104 respectively.

The INW PS-9800 Pressure Transducer is also connected to the CR23X Micrologger by a nine conductor vented cable. Of the nine conductors, three are in use. A 100-ohm resistor is also used connecting the Single Ended Channel and the Ground Terminal to complete the voltage loop. The cable is run into Sullivan Hall in the same manner as the INW PS-9805. The wiring summary for this Pressure Transducer is shown below in Table D-4.

Color	Function	Micrologger Connection
Blue	Pressure signal return	Single Ended Ch. 24
White	V (+) pressure	12 Volt Output Channel
Shield	Ground at logger	Ground

Table D-4. Wiring summary for the 9800 Pressure Transducer

As with the INW PS-9805, the PS-9800 also has a vent tube in the cable that enables atmospheric pressure to be referenced. The PS-9800 Pressure Transducer is programmed using "Instruction 1" in Edlog. "Instruction 1" is an Input/Output Instruction that measures the input voltage with respect to ground with the output is measured in millivolts (Edlog On-Line Help). The PS-9800 Transducer is excited and

records the water surface elevation behind the weir every five minutes. The Micrologger stores this data in array 105.

The CS616 Water Content Reflectometer is comprised of two, 30 cm (11.8 in.) long, stainless steel rods attached to a printed circuit board. The circuit board is encased in epoxy and connected to a shielded four-conductor cable. The cable is run through a 3.8 cm (1.5 in) diameter electrical conduit into the basement of Sullivan Hall. The cable is connected to the Micrologger using the wiring scheme in Table D-5.

Color	Function	Micrologger Connection
Red	Power (+12 V)	12 V
Green	Output	Single ended analog channel
Black	Output Ground	Ground
Orange	Enable	Control Port
Clear	Shield/Power Ground	Ground

Table D-5. Wiring summary for the CS616

The printed circuit board is designed to function as a bi-stable multi-vibrator. The output signal created by the vibrator is directed down the probe rods which act as a guide. The time it takes the signal to travel down the rods depends on the dielectric permittivity of the material surrounding them. Water is the only soil constituent that has both a high value for dielectric permittivity and is the only component other than air that changes in concentration. Therefore the CS616's sensitivity to the dielectric permittivity can be used to measure soil volumetric water content. The Campbell Scientific CS616 Water Content Reflectometer Instruction Manual details the specifics of the CS616 operation as follows.

> Electromagnetic pulses will propagate along a transmission line (the probe rod) at a velocity dependent on the dielectric constant of the material surrounding the line. As dielectric constant increases the propagation velocity decreases. The travel time of the applied signal determines the output period of the CS616. The CS616 circuit generates a high-speed

> pulse that is applied to the probe rods. This electromagnetic pulse travels the length of the rods and is reflected back to the source. A part of the circuit detects the reflection and triggers the next pulse. Subsequently, this pulse travels the rod length and returns to trigger another pulse. The frequency of the applied pulse is monitored by a scaling circuit which reduces the frequency to the response range of a datalogger. The final output of the probe is a square wave with amplitude ± 0.7 volts and frequency dependent on dielectric constant, or water content (Campbell Scientific, 2002a).

"Instruction 138" is a special Micrologger instruction that was developed specifically for the CS616. Instruction 138 measures the output period of the CS616 in microseconds. The output period is then converted into volumetric water content. The Edlog program enables the probes every 5 minutes and the Micrologger takes a reading. Every 15 minutes the Micrologger is programmed to average the last three readings and record the averaged value. The Micrologger then stores the values.

Analytical Methods

The INW PS-9805 Pressure Transducer indirectly measures both the absolute pressure and the atmospheric pressure. The difference between these pressures is the hydrostatic pressure created by the depth of ponded water. The depth of water is directly related to the hydrostatic pressure exerted by the water. This relation is shown below:

$$P = \gamma * h \qquad \text{(D-1)}$$

Where: P = pressure in lb/in^2 (psi)

γ = specific weight of water in lb/ft^3

h = height of water in ft

The transducer sends a voltage signal representing each pressure measurement. The CR23X then calculates a ratio (L) of the signals as follows:

$$L = 100 * \frac{V_0}{V_r} \quad \text{(D-2)}$$

Where: V_o = voltage corresponding to the absolute pressure at the depth of the transducer (mV)

V_r = voltage corresponding to the atmospheric pressure (mV)

The ratio is then converted to a pressure by the following formula:

$$P = m * L + b \quad \text{(D-3)}$$

Where: P = pressure (psi)

m = calibration constant

b = calibration constant (psi)

The calibration procedure is outlined below in the Instrument Calibration and Frequency section. The pressure is then converted to a depth of water by means of the following equation:

$$h = [P * 2.31 ft \frac{H_2 0}{psi}] * 12 \frac{in}{ft} \quad \text{(D-4)}$$

Where: h = depth of water (in)

The PS-9800 Pressure Transducer also indirectly measures absolute pressure and atmospheric pressure. Zero pressure, the pressure exerted when the probe is above the surface of the liquid, is converted to a current flow of 4 mA. The increase in current is linear with the increase in liquid depth until a maximum value of 20 mA is reached. From this linear plot, “m” and “b” values can be obtained for the slope and y-intercept of the line. I think these constants take into account unit conversion to inches.

$$h = (m * V) + b \quad \text{(D-5)}$$

Where: h = depth of water (in)

m = calibration constant

b = calibration constant

V = mA draw

The geometry of the V-notch weir makes it ideal for accurately measuring both low and high flows. The weir was machined from a ¼" 6061 Aluminum plate. This alloy is both easily machined and is resistant to weathering. The weir plate was securely mounted and sealed to a cedar frame. The frame was lug-bolted and caulked into the concrete catch basin. A ½" clear Plexiglas cover was installed over the area of the catch basin upstream of the weir. This cover prevents off-site run-off from being included in outflow measurements. The design, construction, and discharge coefficient of the weir are based on the guidelines set in the ASTM Standard Test for Open-Channel Flow Measurement of Water with Thin-Plate Weirs (ASTM, 2001). The weir is 15" high and 18" wide with an angle of approximately 62 degrees. The INW 9800 Pressure Transducer is securely fastened to the upstream face of the weir. The crest of the weir is 14.82 in above the transducer. Therefore the head on the weir is equal to the depth of water minus 14.82 in. This calculation and the corresponding flow rate calculation are

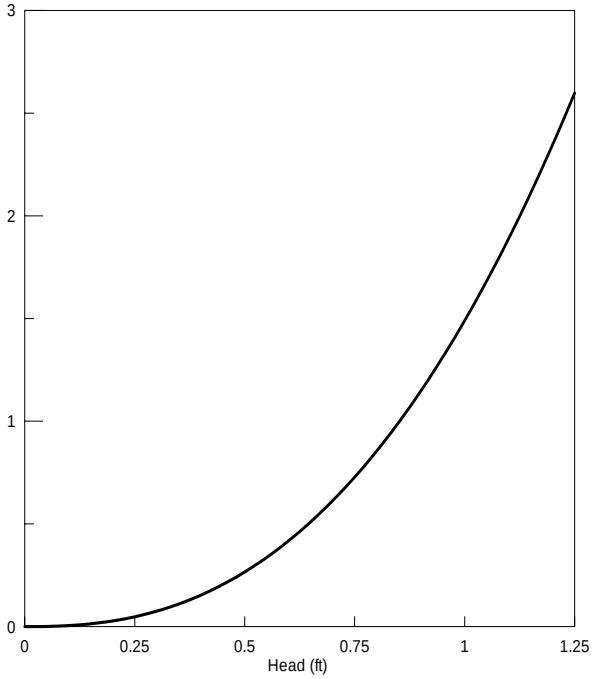

Figure D-1. Weir rating curve

done manually and results are kept in the main data spreadsheet. See the Data Management section below for more information on the data spreadsheets. With a maximum head of 15 inches, the weir can measure flows from 0 to 2.6 cfs as shown in the rating curve in Figure D-1. The equation used to relate depth of water to flow rate for this weir is below.

$$Q = (\frac{8}{15})(2 * g)^{\frac{1}{2}} C_{et} \tan(\frac{\theta}{2})(H + \delta_{Ht})^{\frac{5}{2}} \quad \text{(D-6)}$$

Where: g = gravity (ft/s^2)

C_{et} = is the coefficient of discharge, 0.575

θ = angle of V-notch (radians), 1.08

H = head on weir (ft)

δ_{Ht} = head correction, 0.004 ft

The CS616 Water Content Reflectometer period was converted to a volumetric water content measurement by “Instruction 55”. The instruction uses a quadratic equation to relate the CS616 period to the volumetric water content. The resolution of the CS616 is 0.10% of the volumetric water content. This is the minimum change that can reliably be detected.

Campbell Scientific supplies three sets of coefficients for different soil characteristics. The standard set of coefficients apply to soils with a bulk electrical conductivity of less than 0.5 dS/m, a bulk density of less than 1.55 g/cm^3, and a clay content less than 30%. The other two sets of coefficients are for sandy clay loams with bulk densities of 1.6 g/cm^3 and the specified bulk electrical conductivities. These coefficients are summarized in Table . Figure D-2 illustrates the difference between the three sets of coefficients.

Condition	C_0	C_1	C_2
Standard	-0.0663	-0.0063	0.0007
0.4 dS/m	0.095	-0.0211	0.001
0.75 dS/m	-0.018	-0.007	0.0006

Table D-6. Quadratic fit coefficients

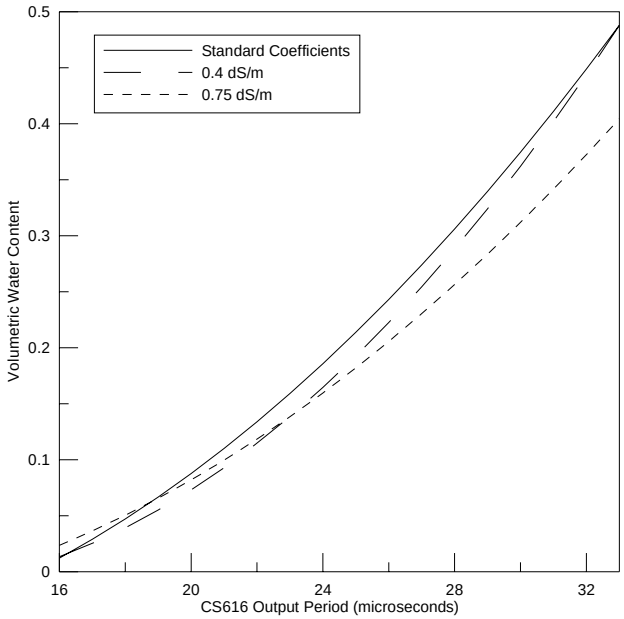

Figure D-2. CS616 quadratic fit coefficients

Alternatively, the coefficients for the equation can be determined through a calibration procedure using soil samples collected from the site.

Quality Control

The data is downloaded and reviewed on a weekly basis. A quality control review is conducted to check the data for erroneous values.

Instrument Testing, Inspection, and Maintenance

The Campbell Scientific CR23X Micrologger is mounted and locked inside a 16" by 18" Campbell Scientific enclosure along with the NL 100 Network Link Interface. The enclosure is mounted to a concrete wall in a closet in the basement of Sullivan Hall, the dormitory building adjacent to the site. The enclosure contains packets of desiccant to protect the equipment from moisture. There is a humidity indicator on the inside panel of the enclosure that is checked on a monthly basis to insure that the desiccant is still effective. The Ground Lug on the Micrologger is connected to a lug on the enclosure, which is in turn connected to the building's ground in an electrical outlet using 12 American Wire Gage (AWG) copper wire as per the manufacturer's instructions. The CS CR200 Datalogger and NL 100 are mounted in a similar fashion inside a 10" by 12" Campbell Scientific enclosure. The enclosure is securely mounted to a metal beam on the roof of Bartley Hall, the neighboring Commerce and Finance building. Desiccant packets and a humidity indicator are also contained in the enclosure. The Ground Lug on the Datalogger is connected to a lug on the enclosure, which is in turn connected to a metal support beam using 12 AWG copper wire.

The Campbell Scientific Tipping Bucket TE525WS Rain Gage requires minimal maintenance. There is a bubble level inside the gage to insure the gage is properly leveled. The rain gage debris filter, funnel, and the bucket reservoirs should be kept clean. Common causes of inaccurate rainfall measurements are birds and other wildlife. To prevent birds and other wildlife from tampering with the gage, a ring of Nixalite Model S bird control wire was installed around the funnel of the rain gage. The bird wire consists of a series of stainless steel needles set at various angles. "The deliberate pattern

creates a barrier that keeps birds and other climbing animals off of surfaces and structures" according to the company's website. To this date, the bird wire has been successful and no problems with birds or other animals have been encountered.

The accuracy of the gage varies depending on the rainfall rate. With a rainfall rate of up to one inch per hour, the gage is accurate to within ± 1%. For a rainfall rate between one to two inches per hour, the accuracy of the gage is between 0 and -2.5%. For rainfalls over two inches per hour, the accuracy is between 0 and -3.5%. The Rain Gage is located in close proximity to the site as recommended by the EPA manual Urban Stormwater BMP Performance Monitoring. There are two other data logging rain gages located within a quarter-mile used to verify the rainfall data collected at the site.

The INW pressure transducers and V-notch weir are inspected on a monthly basis. Visual observations are compared to recorded data for quality control purposes. The pressure transducers' vent tubes have desiccant tubes that are located on the Micrologger end of the cables. The desiccant is checked at least once every two months as per the manufacturer's specifications. The desiccant should be bright blue, as moisture is absorbed the desiccant becomes lighter in color and will need to be replaced. If viable desiccant is not maintained permanent damage may occur to the transducers.

Instrument Calibration and Frequency

The Campbell Scientific TE525WS Tipping Bucket Rain Gage is calibrated in the factory and should not require field calibration. However, Campbell Scientific includes a calibration check in the TE525WS Tipping Bucket Rain Gage Instruction Manual. They recommend this check, which is described below, every 12 months.

> Secure a metal can with a capacity of at least one quart of water. Punch a very small hole in the bottom of the can. Place the can in the top funnel and pour 16 fluid ounces of water into the can. If it takes less than forty-five minutes for the water to run out, the hole in the can is too large. For the TE525WS Rain Gage, 57 ± 2 tips should occur. If adjustment is required, adjusting screws are located on the bottom of the gage adjacent to the large center drain hole. Adjust both screws the same number of turns. Rotation in the clockwise direction increases the number of tips while counterclockwise rotation decreases the number of tips. One half turn of both screws causes a 2-3% change. After adjustment, check and re-level the rain gage lid. If factory recalibration is required, contact Campbell Scientific.

The calibration constants for the pressure transducers are determined by a simple calibration procedure. For the PS-9805 Pressure Transducer, the probe is first left unsubmerged and Voltage readings are taken. The probe is then submerged under known depths of water with calculated hydrostatic pressures and corresponding readings are taken. L is plotted versus P as illustrated in Figure D-2 below. The slope of the line is the ‘m’ calibration constant and the y-intercept is the ‘b’ constant. For the 9805 Pressure Transducer, SN#2233005, the ‘m’ and ‘b’ constants are 0.263 and 0.139 psi respectively. For the 9800 Pressure Transducer, the procedure is the same with readings taken in mA instead of Volts. For the probe, SN#2206014, the “m” and “b” constants are 0.00868 and -36.026 respectively. These values are based on a calibration curve of mA plotted against water height in inches. The pressure transducers were factory calibrated at the time of shipment. As per the manufacturer’s recommendations, the transducers are recalibrated every six months.

The weir calibration will be verified every 12 months by a manual flow rate measurement taken with a graduated cylinder and stopwatch.

The calibration of the CS616 Water Content Reflectometer consists of calibrating the probes in the identical soil in which they were installed is extremely important and difficult. The soil sample was collected from the lower infiltration bed for calibration, as this was the location in which the probes were installed.

Calibration of the probes involved determining the period associated with various predetermined volumetric water contents. The soils were compacted to a target dry density of 1.60 g/cm^3 (100 pcf) for each of the tests. The resulting period for each of the volumetric water contents was plotted. This plot was fit with a quadratic equation to describe volumetric water content as a function of CS616 period. The calibration coefficients were taken from this equation. The resulting calibration coefficients were -0.358, 0.0173 and 0.000156 for C_0, C_1, and C_2, respectively. The calibration curve is presented in Figure D-3.

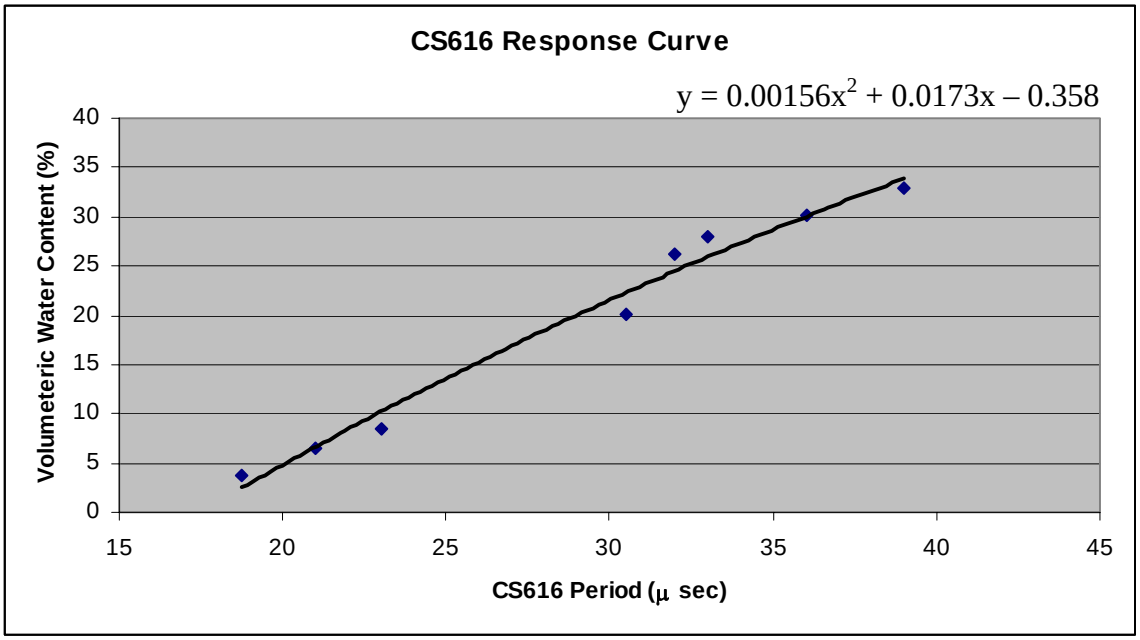

Figure D-3. C616 water content reflectometer calibration curve

Data Management

The data management goals for both the water quantity and quality aspect of this project are based on the guidelines set in the EPA manual Urban Stormwater BMP Performance Monitoring. The database should be one that is easy to "…store, retrieve, and transfer data…" (USEPA, 2002)

Data is downloaded from the CR23X Micrologger and CR200 Datalogger once a week or more often as needed to a computer located in the laboratory. The files obtained from the loggers are *.dat data files. The file name of the data file is the date range for which the data applies to followed by the letters "pc" to denote that the data file is for the porous concrete site. For example a data file from December 10th 2002 to January 3rd 2003 would be labeled as "12-10-02 to 01-03-03pc.dat". Rainfall data files follow the same labeling scheme, with the word "rainfall" added after the "pc." For the CR23X Micrologger, each data file is associated with an *.fsl file. The *.fsl is a final storage label file that is created when the program is compiled in Edlog. It contains all of the column headings for each of the arrays. In each array the following column headings are found: array number and individual columns for year, day, hour, minute, and second that the measurement represents. Since a single program is used, the *.fsl file for all data files is the same. The data files are then opened in Excel and converted into *.xls spreadsheets. The readings from the different sensors are stored in the arrays as prescribed in the Edlog program as seen in Table D-7 below. When converted, the arrays are all located in a single worksheet. Creating an individual worksheet for each array within the Excel file then separates the data. Copies of both the original data files and the

Excel spreadsheets are kept locally on the laboratory computer and backed-up on a weekly basis to the University's network.

Array Number	Instrument	Measurement
101	Micrologger	Battery Voltage
102	C616 Water Content Reflectometer	Volumetric Moisture Content
103	9805 Pressure Transducer	Port Water Depth
104	9805 Pressure Transducer	Port Water Temperature
105	9800 Pressure Transducer	Weir Water Depth
Table 1	Rain Gage	Rainfall

Table D-7. Array / Measurement Table

The pressure transducer measurements for weir water depth are stored in array 105. Additional columns are added to the Excel spreadsheets, which convert the height of the water in the chamber to head on the weir. That head is then converted to a flow rate using the weir equation for flow over a triangular weir as discussed previously.

Edlog Program for CR23X Micrologger and Attached Instruments

```
;{CR23X}
;
;Tells the CR23X to run the program in Table 1 every five minutes.
*Table 1 Program
  01: 300       Execution Interval (seconds)

;Instruction that reads the Battery Voltage of the CR23X.
;"Loc 1" Temporarily store the voltage reading in Loc 1.
1:  Batt Voltage (P10)
 1: 1       Loc [ BattVolt  ]

;Do the following set of instructions.
2:  Do (P86)
 1: 41      Set Port 1 High

;Instruction 138 measures the period of the CS616 Water Content Reflectometer.
;There are 4 of these instructions. Each one operates 3 of the CS616s.
;Note: This instruction does not output the Moisture content (see Polynomial p55)
;"3 Reps" Run this instruction 3 times. 4 instructions * 3 reps = 12 CS616s
```

;"1 SE Channel" SE port 1 on the CR23X (Green wire) the instruction will iterate SE ports.
;"1 C1 ...Control Port" This port enables the CS616s, all 3 CS616s will be attached here (Orange wires)
;"1.0 Mult" No multiplier.
;"0.0 Offset" No offset.

```
   3:  CS616 Water Content Reflectometer (P138)
    1: 3        Reps
    2: 1        SE Channel
    3: 11       All reps use C1
    4: 3        Loc [ A11Period ]
    5: 1.0      Mult
    6: 0.0      Offset

   4:  CS616 Water Content Reflectometer (P138)
    1: 3        Reps
    2: 4        SE Channel
    3: 12       All reps use C2
    4: 6        Loc [ A21Period ]
    5: 1.0      Mult
    6: 0.0      Offset

   5:  CS616 Water Content Reflectometer (P138)
    1: 3        Reps
    2: 7        SE Channel
    3: 13       All reps use C3
    4: 9        Loc [ B11Period ]
    5: 1.0      Mult
    6: 0.0      Offset

   6:  CS616 Water Content Reflectometer (P138)
    1: 3        Reps
    2: 10       SE Channel
    3: 14       All reps use C4
    4: 12       Loc [ B21Period ]
    5: 1.0      Mult
    6: 0.0      Offset
```

;This instruction converts the period from P138 to a Moisture Content.
;"12 Reps" Instruction must convert 12 readings.
;"3 X Loc [MM1Period]" This is the first stored period reading. Iterate from location 3 - 14.
;"15 F(X) Loc [MM1_VWC]" This is the first stored converted value. Iterate from loc. 15 - 26.
;The following coefficients are listed in the CS616 Manual; C0 through C5.

```
   7:  Polynomial (P55)
```

```
   1: 12       Reps
   2: 3        X Loc [ A11Period ]
   3: 15       F(X) Loc [ A11_VWC    ]
   4: -0.358   C0
   5: 0.0173   C1
   6: 0.000156 C2
   7: 0.0      C3
   8: 0.0      C4
   9: 0.0      C5

;This instruction turns the probes off.
   8:  Do (P86)
   1: 51       Set Port 1 Low

;This is the section of code that we're having trouble with.  There are 2 sections, 1 for
;each pressure transducer.  Both are connected following the wiring diagram in the book.
;The first is hooked to Diff channels 7 and 8 (SE 13-16) for the voltages and SE channel
17
;for the temp.
;The white and orange excitation are hooked to EX 1 and 2 respectively.  We decided not
to
;store the L value, the D is depth in inches.
;The second is in Diff channels 10 and 11 and SE channel 23.
;The white and orange for these are in EX 3 and 4.
;Lines 26-43 deal with storing the data.  I'm sure we have some extra lines but it gets us
the
;data the way that we want it.  We put an instruction 71(average), for the differential
;voltages and then instruction 70(sample) for the temps.  Is this right?  We just used what
we
;had for our moisture meters since there were no storage examples in the PS9805 book.
;When we download the data, we're getting -6999 for both Vr's and for both temps.

;Serial #:2233005
;m=0.263, b=0.139

   9:  Ex-Del-Diff (P8)
   1: 2        Reps
   2: 22       50 mV, 60 Hz Reject, Slow Range
   3: 7        DIFF Channel
   4: 1        Excite all reps w/Exchan 1
   5: 1        Delay (0.01 sec units)
   6: 800      mV Excitation
   7: 27       Loc [ Vr1       ]
   8: 1.0      Mult
   9: 0.0      Offset
```

```
L1=100*(Vo1/Vr1)

P1=0.263*L1+0.139

PortDepth=(P1*2.31)*12

    10:  Temp (107) (P11)
     1: 1        Reps
     2: 17       SE Channel
     3: 2        Excite all reps w/E2
     4: 34       Loc [ PortTemp  ]
     5: 1.0      Mult
     6: 0.0      Offset

;Serial #: 2206014
;m=0.0868, b=-36.026

    11:  Volt (SE) (P1)
     1: 1        Reps
     2: 24       1000 mV, 60 Hz Reject, Slow Range
     3: 24       SE Channel
     4: 32       Loc [ Voltage   ]
     5: 1.0      Mult
     6: 0.0      Offset
WeirDepth=((0.0868*Voltage)-36.026)

;These 4 instructions (10 - 13) actually write the battery voltage each hour.
;Instruction (P80) Place the written data in the final storage area 1 in array 101.
;Instruction (P77) Time stamp.
;Instruction (P71) AVERAGE the voltage readings from each program interval.

    12:  If time is (P92)
     1: 0000     Minutes (Seconds --) into a
     2: 60       Interval (same units as above)
     3: 10       Set Output Flag High (Flag 0)

    13:  Set Active Storage Area (P80)
     1: 1        Final Storage Area 1
     2: 101      Array ID

    14:  Real Time (P77)
     1: 1221     Year,Day,Hour/Minute,Seconds (midnight = 2400)

    15:  Average (P71)
     1: 1        Reps
     2: 1        Loc [ BattVolt  ]
```

```
;These 4 instructions (18 - 21) actually write the moisture meter data every 30 minutes.
;Instruction (P80) Write data in the final storage area 1 in array 103.
;Instruction (P77) Time stamp.
;Instruction (P71) Average moisture content over the given program interval.

   16:  If time is (P92)
    1: 0000     Minutes (Seconds --) into a
    2: 15       Interval (same units as above)
    3: 10       Set Output Flag High (Flag 0)

   17:  Set Active Storage Area (P80)
    1: 1        Final Storage Area 1
    2: 102      Array ID

   18:  Real Time (P77)
    1: 1221     Year,Day,Hour/Minute,Seconds (midnight = 2400)

   19:  Average (P71)
    1: 12       Reps
    2: 15       Loc [ A11_VWC   ]

   20:  If time is (P92)
    1: 0000     Minutes (Seconds --) into a
    2: 5        Interval (same units as above)
    3: 10       Set Output Flag High (Flag 0)

   21:  Set Active Storage Area (P80)
    1: 1        Final Storage Area 1
    2: 103      Array ID

   22:  Real Time (P77)
    1: 1221     Year,Day,Hour/Minute,Seconds (midnight = 2400)

   23:  Average (P71)
    1: 2        Reps
    2: 27       Loc [ Vr1       ]

   24:  Sample (P70)
    1: 2        Reps
    2: 30       Loc [ P1        ]

   25:  If time is (P92)
    1: 0000     Minutes (Seconds --) into a
    2: 5        Interval (same units as above)
    3: 10       Set Output Flag High (Flag 0)
```

```
   26:  Set Active Storage Area (P80)
    1: 1        Final Storage Area 1
    2: 104      Array ID
   27:  Real Time (P77)
    1: 1221     Year,Day,Hour/Minute,Seconds (midnight = 2400)

   28:  Average (P71)
    1: 1        Reps
    2: 34       Loc [ PortTemp  ]

   29:  If time is (P92)
    1: 0000     Minutes (Seconds --) into a
    2: 5        Interval (same units as above)
    3: 10       Set Output Flag High (Flag 0)

   30:  Set Active Storage Area (P80)
    1: 1        Final Storage Area 1
    2: 105      Array ID

   31:  Real Time (P77)
    1: 1221     Year,Day,Hour/Minute,Seconds (midnight = 2400)

   32:  Average (P71)
    1: 2        Reps
    2: 32       Loc [ Voltage   ]

End Program

Input Locations

1     [ BattVolt  ]  RW--   1       1      ----- ------ ---
2     [ _________ ]  ----   0       0      ----- ------ ---
3     [ A11Period ]  RW--   1       1      Start ------ ---
4     [ A12Period ]  RW--   1       1      ----- Member ---
5     [ A13Period ]  RW--   1       1      ----- ------ End
6     [ A21Period ]  RW--   1       1      Start ------ ---
7     [ A22Period ]  RW--   1       1      ----- Member ---
8     [ A23Period ]  RW--   1       1      ----- ------ End
9     [ B11Period ]  RW--   1       1      Start ------ ---
10    [ B12Period ]  RW--   1       1      ----- Member ---
11    [ B13Period ]  RW--   1       1      ----- ------ End
12    [ B21Period ]  RW--   1       1      Start ------ ---
13    [ B22Period ]  RW--   1       1      ----- Member ---
14    [ B23Period ]  RW--   1       1      ----- ------ End
15    [ A11_VWC   ]  RW--   1       1      Start ------ ---
```

```
16    [ A12_VWC   ] RW--   1      1      ----- Member ---
17    [ A13_VWC   ] RW--   1      1      ----- Member ---
18    [ A21_VWC   ] RW--   1      1      ----- Member ---
19    [ A22_VWC   ] RW--   1      1      ----- Member ---
20    [ A23_VWC   ] RW--   1      1      ----- Member ---
21    [ B11_VWC   ] RW--   1      1      ----- Member ---
22    [ B12_VWC   ] RW--   1      1      ----- Member ---
23    [ B13_VWC   ] RW--   1      1      ----- Member ---
24    [ B21_VWC   ] RW--   1      1      ----- Member ---
25    [ B22_VWC   ] RW--   1      1      ----- Member ---
26    [ B23_VWC   ] RW--   1      1      ----- ------ End
27    [ Vr1       ] RW--   1      1      Start ------ ---
28    [ Vo1       ] RW--   1      1      ----- ------ End
29    [ L1        ] ----   0      0      ----- ------ ---
30    [ P1        ] R---   1      0      ----- ------ ---
31    [ PortDepth ] R---   1      0      ----- ------ ---
32    [ Voltage   ] RW--   1      1      ----- ------ ---
33    [ WeirDepth ] R---   1      0      ----- ------ ---
34    [ PortTemp  ] RW--   1      1      ----- ------ ---
```

Short Cut Program for CR200 Datalogger and TE525 Rain Gage

```
'CR200 Series
'Created by SCWIN (Version 2.0 (Beta))
Public Flag(8)
Public Batt_Volt
Public Rain_in
DataTable(Rainfall,True,-1)
  DataInterval(0,5,Min)
  Totalize(1,Rain_in,0)
EndTable
DataTable(Table2,True,-1)
  DataInterval(0,1440,Min)
  Minimum(1,Batt_Volt,0,0)
EndTable
BeginProg
Scan(5,Min)
' Code for datalogger Battery Voltage measurement, Batt_Volt:
  Battery(Batt_Volt)
' Code for Rain measurement, Rain_in:
  PulseCount(Rain_in,P_SW,2,0,0.01,0)
CallTable(Rainfall)
CallTable(Table2)
NextScan
EndProg
```

Appendix E – Sieve Analysis

The following data represent the sieve analysis used to classify the soil at the Porous Concrete Infiltration Basin BMP.

Mass in grams of:

Pan	325.64
Pan & soil	853.2
Soil (before wash - moist)	527.56
Soil (before wash - dry)	**405.063**
Pan & soil (after wash - dry)	487.23
Soil (after wash - dry), W	161.59
Soil washed out	243.473

Description of Soil: Brown silty sand **Date:** 6/18/2002

Sieve No.	Sieve Opening (mm)	Cumm. Mass of soil retained on each sieve (g)	Mass of soil retained on each sieve, Wn	Percent of mass retained on each sieve, Rn	Cumulative percent retained, Rn	Percent Finer
4	4.75	7.49	7.49	1.85	1.85	98.15
10	2.00	18.30	10.81	2.67	4.52	95.48
20	0.85	36.95	18.65	4.60	9.12	90.88
40	0.43	59.23	22.28	5.50	14.62	85.38
100	0.15	115.95	56.72	14.00	28.63	71.37
200	0.08	163.02	47.07	11.62	40.25	59.75
Pan	----	163.76	0.74	0.18	40.43	59.57
			♦ **163.76**	= W_1		

Mass loss during sieve analysis = (W - W_1)/W x 100 = -1.34 ← ***GOOD***

Moisture Content of soil before wash - dry

Can No.	Mass of can (g)	Mass of can + moist sample (g)	Mass of can + oven dry sample (g)	Moisture Content (%)
A (53)	16.01	37.522	32.527	30.2

Appendix F – Atterburg Limits

Liquid Limit Test

Description of Soil: (A) Brown silty sand **Sample No.:** A

Location: Pit #1 (Closest to Bartley)

Date: 6/18/2002

Test No.	1	2	3	4	5
Can No.	78	36	53	104	65
Mass of can, W_1 (g)	16.051	15.745	16.011	15.207	16.057
Mass of can + moist soil, W_2 (g)	24.046	23.947	22.998	21.999	24.313
Mass of can + dry soil, W_3 (g)	21.675	21.432	20.897	19.991	21.802
Moisture content, w (%) = (W2 - W3)/(W3 - W1) x 100	42.16	44.22	43.00	41.97	43.71
Number of blows, N	35	14	21	33	20

Liguid Limit = **42.9**

$LL = w_N (\%) (N/25)^{0.121}$ where w_N (%) = moisture content, in percent, for 1/2 in. (12.7 mm) groove closure in the liquid limit device at N number of blows

Plastic Limit Test

Description of Soil: (A) Brown silty sand **Sample No.:** A

Location: Pit #1 (Closest to Bartley)

Michael Kwiatkowski and Tyler Ladd **Date:** 6/18/2002

Test No.	1	2	3
Can No.	26	30	30
Mass of can, W_1 (g)	15.913	16.16	16.159
Mass of can + moist soil, W_2 (g)	18.478	19.638	22.735
Mass of can + dry soil, W_3 (g)	17.741	18.637	21.102
Plastic Limit (PL) = $(W_2 - W_3)/(W_3 - W_1)$ x 100	40.32	40.41	**33.04**

→ 40.36

Average of 1&2

LL (prior test) = 42.9

PI = LL - PL = **9.86**

Activity (A) = PI/(% of clay - size fraction, by weight)

Typical values of PI of several clay minerals…

Clay Minerals	PI
Kaolinite	20 - 40
Illite	35 - 50
Montmorillonite	50 -100

Appendix G – Flexible Wall Hydraulic Conductivity Test

(Kwiatkowski, 2004)

$$k = \frac{a_{in} a_{out} L}{At(a_{in} + a_{out})} \ln(h_1 / h_2)$$

The following data represent the four runs, or time increments, used to determine the saturated hydraulic conductivity of the soil sample. The start time and finish time for each of the runs are represented by T_1 and T_2 respectively. The readings on the burettes are represented by bottom and top for the head water and tail water levels, respectively.

Time: 11:19 AM - 11:26 AM

	T_1:		T_2:	
Bottom:	18.1	Bottom:	29.2	
Top:	17.9	Top:	7.1	

Where:

a_{in} =	1	0.0001	Cross-sectional area of the reservoir containing the influent liquid, cm^2...m^2
a_{out} =	1	0.0001	Cross-sectional area of the reservoir containing the effluent liquid, cm2...m^2
L =	8.2	0.082	Length of the specimen, cm...m
A =	1.54	0.000994	Cross-sectional area of the specimen, in^2...m^2
t =	0.116667	420	Elapsed time between determination of h_1 and h_2, hr...s
h_1 =	1.408		Head loss across the specimen at time t_1, m
h_2 =	1.189		Head loss across the specimen at time t_2, m

k = 1.66E-04 cm/s

Time: 1:22 PM - 1:33 PM

	T_1:		T_2:	
Bottom:	1.8	Bottom:	23.75	
Top:	34.7	Top:	13.5	

Where:

a_{in} =	1	0.0001	Cross-sectional area of the reservoir containing the influent liquid, cm^2...m^2
a_{out} =	1	0.0001	Cross-sectional area of the reservoir containing the effluent liquid, cm2...m^2
L =	8.2	0.082	Length of the specimen, cm...m
A =	1.54	0.000994	Cross-sectional area of the specimen, in^2...m^2
t =	0.183333	660	Elapsed time between determination of h_1 and h_2, hr...s
h_1 =	1.739		Head loss across the specimen at time t_1, m
h_2 =	1.3075		Head loss across the specimen at time t_2, m

k = 1.78E-04 cm/s

Time: 1:41 PM - 1:47 PM

	T_1:		T_2:	
Bottom:	23.75	Bottom:	33.2
Top:	13.5	Top:	4

Where:

a_{in} =	1	0.0001	Cross-sectional area of the reservoir containing the influent liquid, cm^2...m^2
a_{out} =	1	0.0001	Cross-sectional area of the reservoir containing the effluent liquid, cm2...m^2
L =	8.2	0.082	Length of the specimen, cm...m
A =	1.54	0.000994	Cross-sectional area of the specimen, in^2...m^2
t =	0.1	360	Elapsed time between determination of h_1 and h_2, hr...s
h_1 =	1.3075		Head loss across the specimen at time t_1, m
h_2 =	1.118		Head loss across the specimen at time t_2, m

k = 1.79E-04 cm/s

Time: 1:47 PM - 1:55 PM

	T_1:		T_2:	
Bottom:	6.2	Bottom:	19.65
Top:	35.7	Top:	23.1

Where:

a_{in} =	1	0.0001	Cross-sectional area of the reservoir containing the influent liquid, cm^2...m^2
a_{out} =	1	0.0001	Cross-sectional area of the reservoir containing the effluent liquid, cm2...m^2
L =	8.2	0.082	Length of the specimen, cm...m
A =	1.54	0.000994	Cross-sectional area of the specimen, in^2...m^2
t =	0.133	480	Elapsed time between determination of h_1 and h_2, hr...s
h_1 =	1.705		Head loss across the specimen at time t_1, m
h_2 =	1.4445		Head loss across the specimen at time t_2, m

k = 1.43E-04 cm/s

AVERAGE K = 1.67E-04

Appendix H – Moisture Content and Bed Depth Graphs

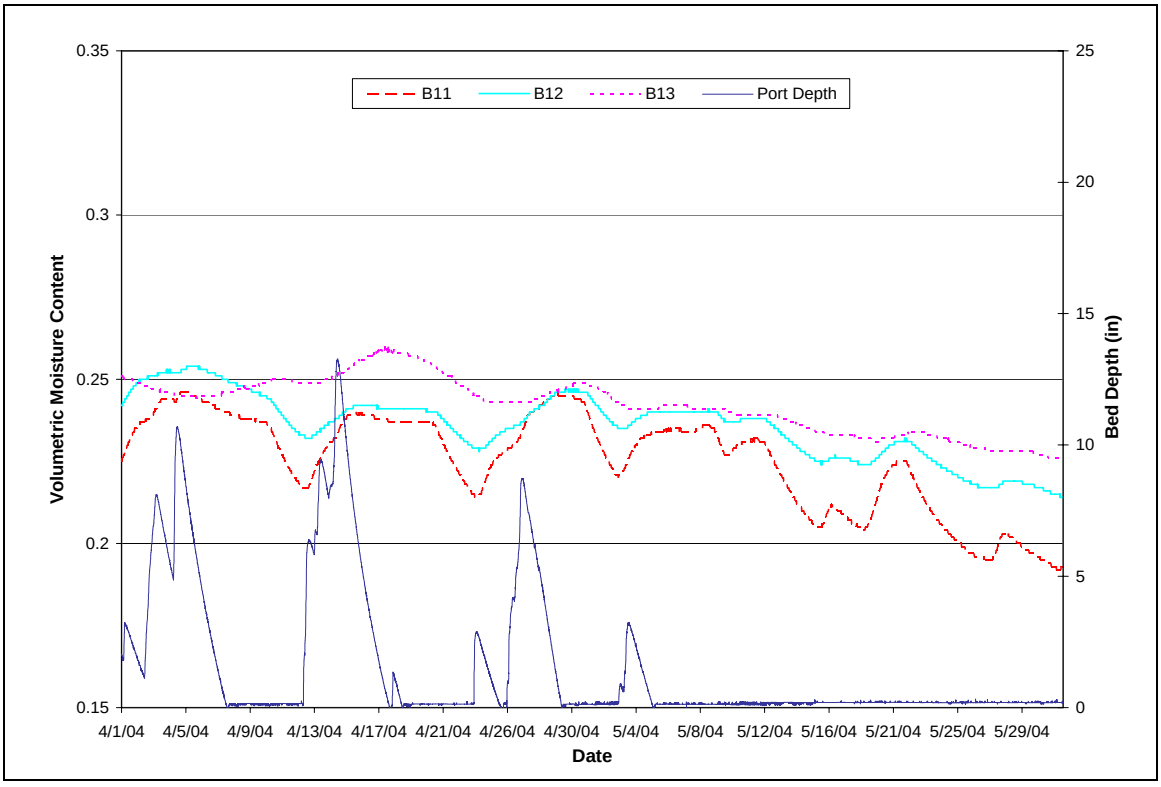

Figure H-1. Moisture Content and Bed Depth (April - May 2004)

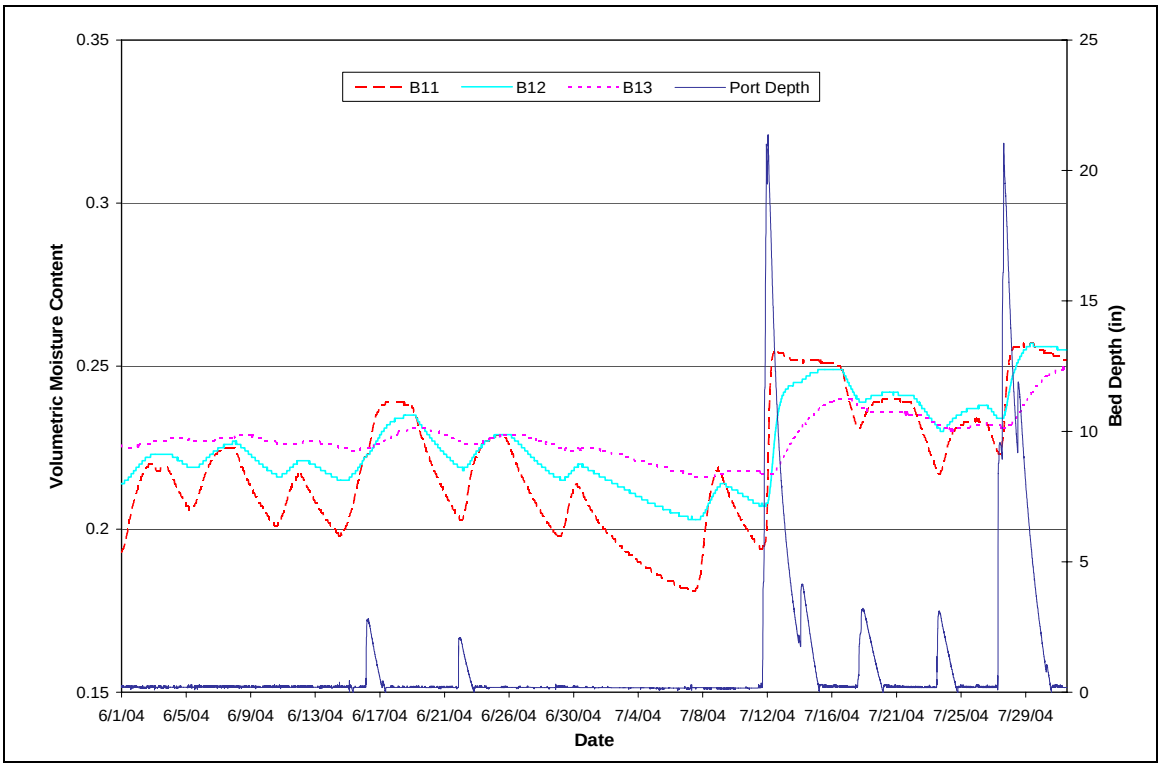

Figure H-2. Moisture Content and Bed Depth (June - July 2004)

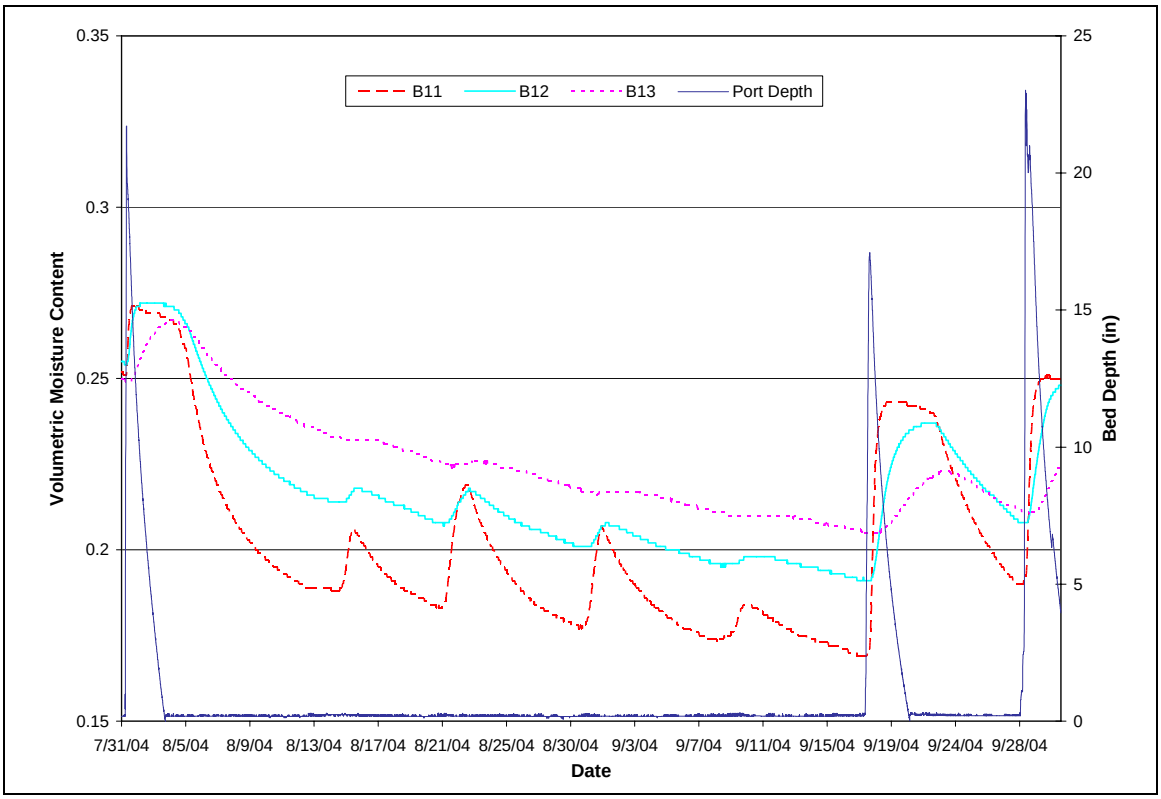

Figure H-3. Moisture Content and Bed Depth (August – September 2004)

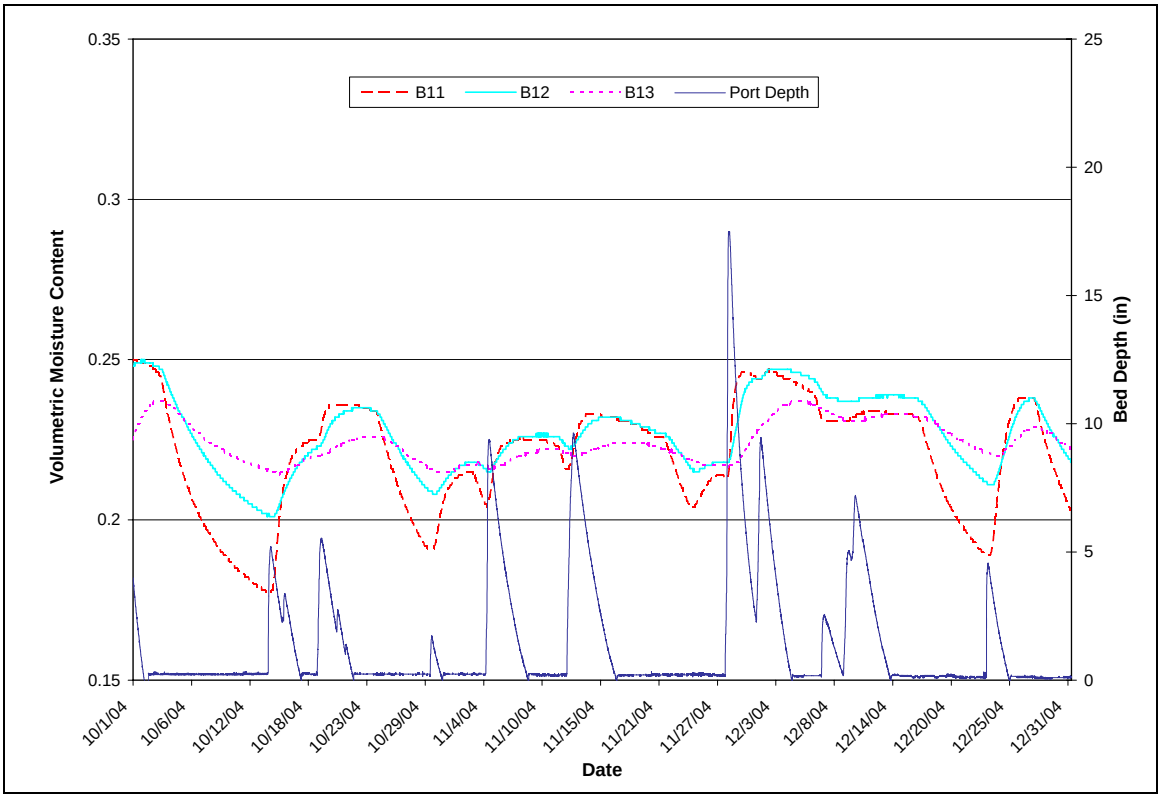

Figure H-4. Moisture Content and Bed Depth (October – December 2004)

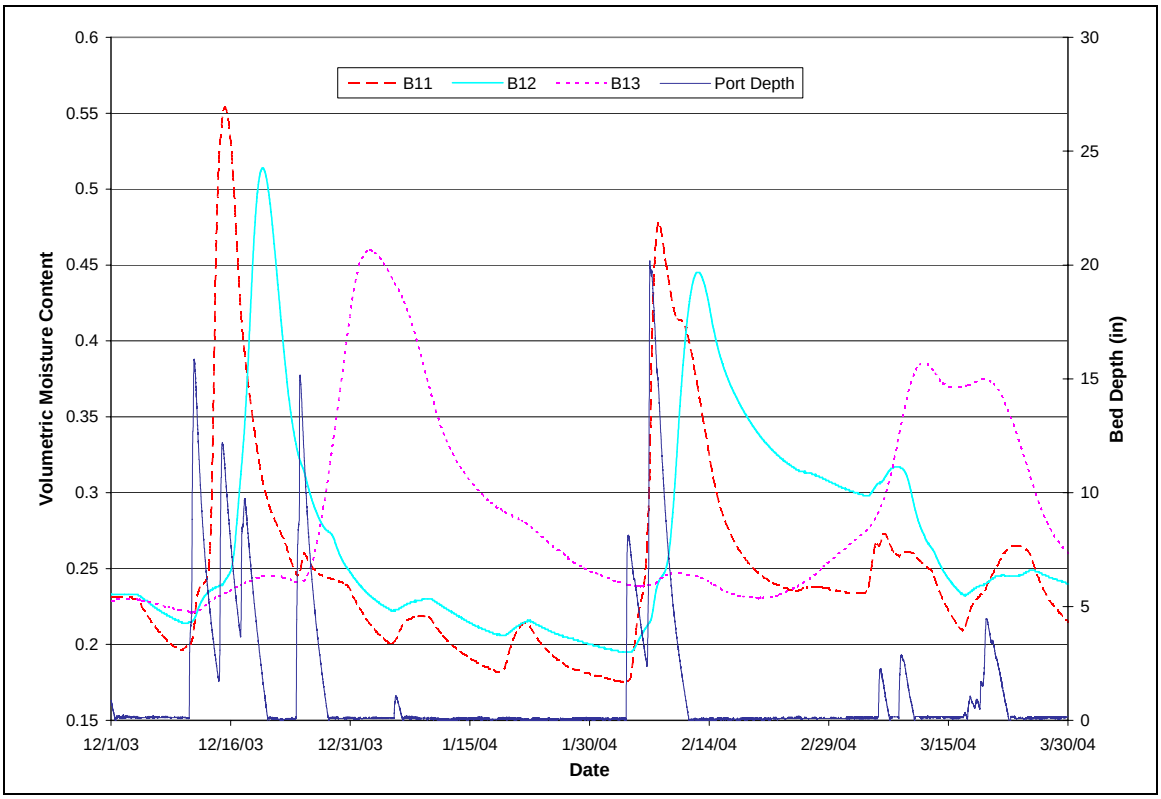

Figure H-5. Moisture Content and Bed Depth (December 2003 - March 2004)

Appendix I – Moisture Content Data

Table I-1. Moisture Content by Antecedent Dry Time (April – December 2004)

Event Start (Rain Start)	Antecedant Dry Time (hrs)	Initial WC				Saturated WC
		b11	b12	b13	Composite	
0-2 days	0-48 hrs					
4/25/04 12:00 PM	0.000	0.23	0.24	0.24	0.237	0.25
12/9/04 2:50 PM	0.000	0.24	0.24	0.24	0.240	0.24
8/1/04 4:20 AM	28.750	0.25	0.25	0.25	0.251	0.27
10/18/04 11:10 PM	36.167	0.23	0.23	0.23	0.230	0.24
2-3 days	48-72 hrs					
7/18/04 4:55 AM	52.750	0.23	0.24	0.24	0.236	0.24
7/27/04 10:40 AM	60.750	0.22	0.23	0.23	0.227	0.26
12/7/04 4:55 AM	63.250	0.23	0.24	0.24	0.237	0.24
5/2/04 11:35 AM	71.333	0.22	0.23	0.24	0.230	0.24
3-5 days	72-120 hrs					
7/23/04 1:50 PM	83.250	0.22	0.23	0.23	0.227	0.24
11/12/04 6:30 AM	89.500	0.22	0.22	0.22	0.221	0.23
11/4/04 10:45 AM	98.833	0.21	0.22	0.22	0.214	0.24
4/12/04 12:15 PM	113.250	0.22	0.23		0.225	0.24
5+ days	120+ hrs					
6/22/04 5:35 PM	120.917	0.20	0.22	0.23	0.216	0.23
4/23/04 6:10 PM	129.167	0.22	0.23	0.24	0.231	0.24
9/27/04 11:05 PM	162.667	0.19	0.21	0.21	0.203	0.25
10/30/04 1:55 AM	179.000	0.19	0.21	0.22	0.205	0.22
3/30/04 5:40 PM	195.250	0.21	0.24	0.24	0.230	0.25
12/23/04 9:30 AM	219.167	0.19	0.21	0.22	0.207	0.24
11/27/04 8:15 PM	251.167	0.21	0.22	0.22	0.217	0.25
10/14/04 3:35 AM	289.417	0.18	0.20	0.21	0.197	0.22
7/12/04 2:00 AM	440.583	0.19	0.21	0.22	0.207	0.25
6/16/04 11:25 AM	1009.000	0.20	0.22	0.22	0.213	0.24
9/18/04 12:55 AM	1085.333	0.17	0.19	0.21	0.189	0.24
Overall:	**Min**	0.17	0.19	0.205	0.19	0.22
	Max	0.25	0.25	0.249	0.25	0.27
	Ave	0.21	0.22	0.227	0.22	0.24
	Median	0.22	0.23	0.228	0.23	0.24

Table I-2. Statistics by Antecedent Dry Time (April – December 2004)

	Initial WC				Saturated WC
	b11	b12	b13	Composite	
0-2 days 0-48 hrs					
Min	0.23	0.23	0.230	0.23	0.24
Max	0.25	0.25	0.249	0.25	0.27
Ave	0.24	0.24	0.240	0.24	0.25
Median	0.24	0.24	0.240	0.24	0.25
2-3 days 48-72 hrs					
Min	0.22	0.23	0.230	0.23	0.24
Max	0.23	0.24	0.240	0.24	0.26
Ave	0.23	0.23	0.237	0.23	0.25
Median	0.23	0.23	0.239	0.23	0.24
3-5 days 72-120 hrs					
Min	0.21	0.22	0.216	0.21	0.23
Max	0.22	0.23	0.231	0.23	0.24
Ave	0.22	0.22	0.223	0.22	0.24
Median	0.22	0.23	0.221	0.22	0.24
5+ days 120+ hrs					
Min	0.17	0.19	0.205	0.19	0.22
Max	0.22	0.24	0.243	0.23	0.25
Ave	0.20	0.21	0.221	0.21	0.24
Median	0.19	0.21	0.220	0.21	0.24

Table I-3. Moisture Content and Statistics (December 2003 – March 2004)

Event Start (Rain Start)	Antecedant Dry Time (hrs)	Initial WC				Saturated WC
		b11	b12	b13	Composite	
3/7/04 9:30 PM	6.000	0.26	0.31	0.38	0.317	0.34
12/24/03 1:55 AM	82.083	0.25	0.32	0.25	0.25	
3/17/04 10:45 AM	160.750	0.21	0.23	0.36	0.267	0.26
1/4/04 6:20 PM	180.167	0.20	0.22		0.211	0.25
12/9/03 2:50 PM	194.417	0.20	0.22	0.23	0.217	0.50
3/6/04 1:50 AM	566.417	0.23	0.30	0.27	0.267	0.33
2/3/04 10:50 AM	669.417	0.17	0.20	0.23	0.200	0.45
Overall:	**Min**	0.17	0.20	0.23	0.200	0.250
	Max	0.26	0.32	0.38	0.317	0.500
	Ave	0.22	0.26	0.29	0.247	0.355
	Median	0.21	0.23	0.26	0.250	0.335

Appendix J – Sample Model Input Worksheet

Green-Ampt Analysis: Storm 09/18/2004

End Row 756

Parameters

Hydraulic Conduct., K_s	0.24	in/hr	
Antecedent Dry Time	1085.33	hrs	
Moisture Content, θ_i	0.21	(MMs)	Accuracy = 0.001
Moisture Content, θ_s	0.245	(MMs)	
Suction Head, S	6.57	in (book)	
Initial Port Depth	17.01	in (data)	
Initial Infiltrated Depth	0.05	in (data)	

Date	Time (hrs)	Storage-Suction Factor, S_j (in)	Cumulative Infiltration		Side Wall Infiltration, F_j (in)	Cumulative Infiltration, ΣF_j (in)
			F_j (in)	F_{j-1} (in)		
9/18/04 2:30 PM	0.00			0	0	0.000
9/18/04 2:35 PM	0.08	0.825		0.0500	0.023	0.073
9/18/04 2:40 PM	0.17	0.823	0.200	0.2005	0.092	0.293
9/18/04 2:45 PM	0.25	0.815	0.286	0.2864	0.131	0.418
9/18/04 2:50 PM	0.33	0.811	0.356	0.3560	0.163	0.519
9/18/04 2:55 PM	0.42	0.807	0.417	0.4170	0.190	0.607
9/18/04 3:00 PM	0.50	0.804	0.473	0.4728	0.215	0.688
9/18/04 3:05 PM	0.58	0.801	0.524	0.5245	0.238	0.762
9/18/04 3:10 PM	0.67	0.799	0.573	0.5733	0.259	0.833
9/18/04 3:15 PM	0.75	0.796	0.619	0.6199	0.280	0.900
9/18/04 3:20 PM	0.83	0.794	0.664	0.6644	0.299	0.964
9/18/04 3:25 PM	0.92	0.792	0.707	0.7074	0.318	1.025
9/18/04 3:30 PM	1.00	0.789	0.748	0.7489	0.336	1.085
9/18/04 3:35 PM	1.08	0.787	0.789	0.7893	0.353	1.143
9/18/04 3:40 PM	1.17	0.785	0.828	0.8288	0.370	1.199
9/18/04 3:45 PM	1.25	0.783	0.867	0.8673	0.387	1.254
9/18/04 3:50 PM	1.33	0.781	0.904	0.9049	0.403	1.308
9/18/04 3:55 PM	1.42	0.780	0.941	0.9418	0.419	1.360
9/18/04 4:00 PM	1.50	0.778	0.977	0.9780	0.434	1.412
9/18/04 4:05 PM	1.58	0.776	1.013	1.0137	0.449	1.463
9/18/04 4:10 PM	1.67	0.774	1.048	1.0488	0.464	1.513
9/18/04 4:15 PM	1.75	0.772	1.083	1.0834	0.478	1.562
9/18/04 4:20 PM	1.83	0.771	1.117	1.1174	0.492	1.610
9/18/04 4:25 PM	1.92	0.769	1.150	1.1510	0.506	1.657
9/18/04 4:30 PM	2.00	0.767	1.184	1.1843	0.520	1.705
9/18/04 4:35 PM	2.08	0.766	1.217	1.2172	0.534	1.751
9/18/04 4:40 PM	2.17	0.764	1.249	1.2498	0.547	1.797
9/18/04 4:45 PM	2.25	0.762	1.281	1.2819	0.561	1.842
9/18/04 4:50 PM	2.33	0.761	1.313	1.3138	0.574	1.887
9/18/04 4:55 PM	2.42	0.759	1.345	1.3454	0.586	1.932
9/18/04 5:00 PM	2.50	0.758	1.376	1.3767	0.599	1.976
9/18/04 5:05 PM	2.58	0.756	1.407	1.4078	0.612	2.020
9/18/04 5:10 PM	2.67	0.755	1.438	1.4385	0.624	2.063
9/18/04 5:15 PM	2.75	0.753	1.468	1.4690	0.637	2.106
9/18/04 5:20 PM	2.83	0.752	1.499	1.4993	0.649	2.148
9/18/04 5:25 PM	2.92	0.750	1.529	1.5294	0.661	2.190
9/18/04 5:30 PM	3.00	0.749	1.559	1.5593	0.673	2.232

Appendix K – Model Visual Basic Code

```
Sub green()
Dim wj(25000)
k = Cells(4, 2).Value
dt = 0.085
wj(1) = Cells(10, 2).Value
x = 2
guess = 0.0005
finish = Cells(2, 5).Value
For i = 15 To finish
Do
answer = (k * dt) + wj(x - 1) + (Cells(i, 3).Value * (Log((Cells(i, 3).Value + guess) /
(Cells(i, 3).Value + wj(x - 1)))))
difference = Abs(answer - guess)
guess = guess + 0.0005
Loop Until difference < 0.001
wj(x) = answer
x = x + 1
Cells(i, 4).Value = guess
Cells(i, 5).Value = answer
Next i
```

Appendix L – Preliminary Model Results: Recession Limb

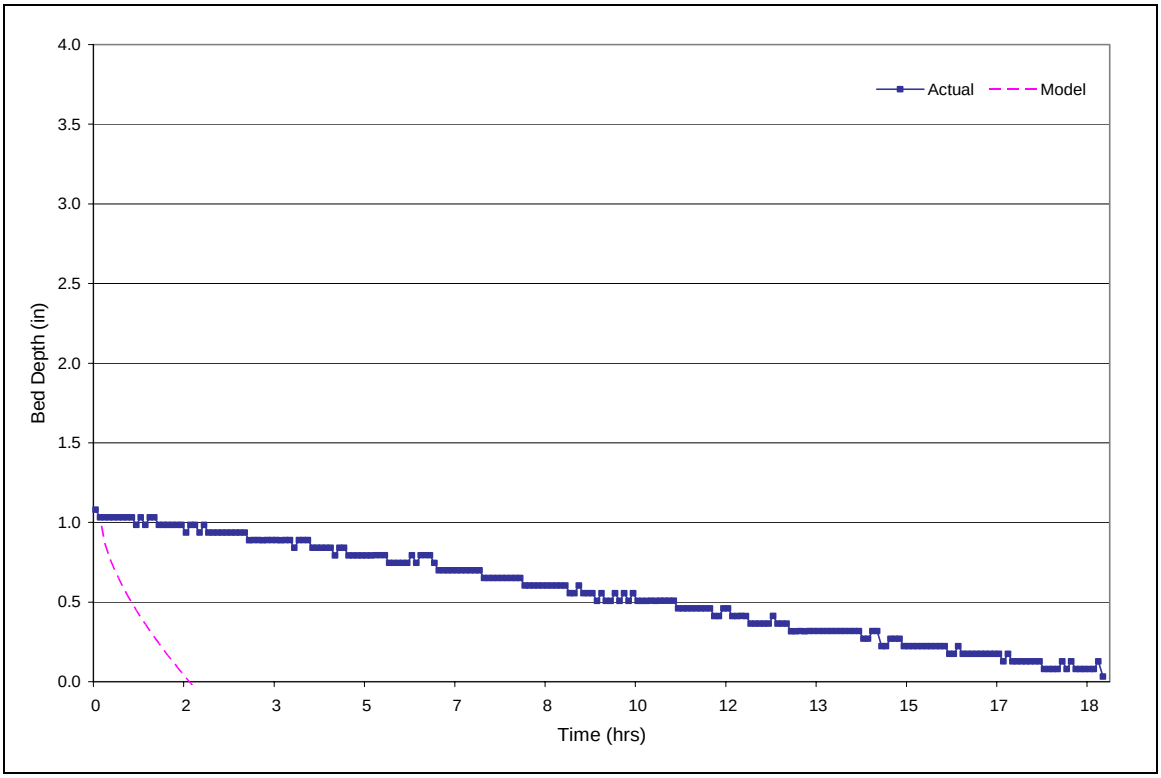

Figure L-1. Event 1/04/2004

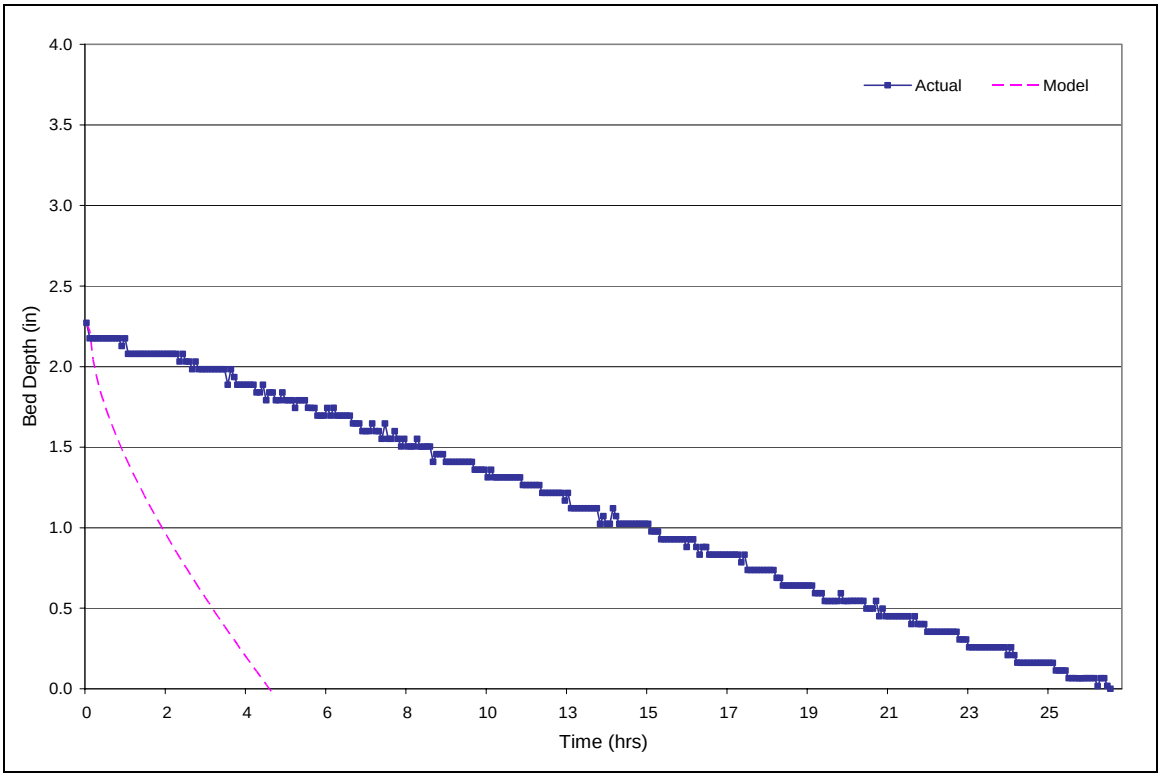

Figure L-2. Event 3/06/2004

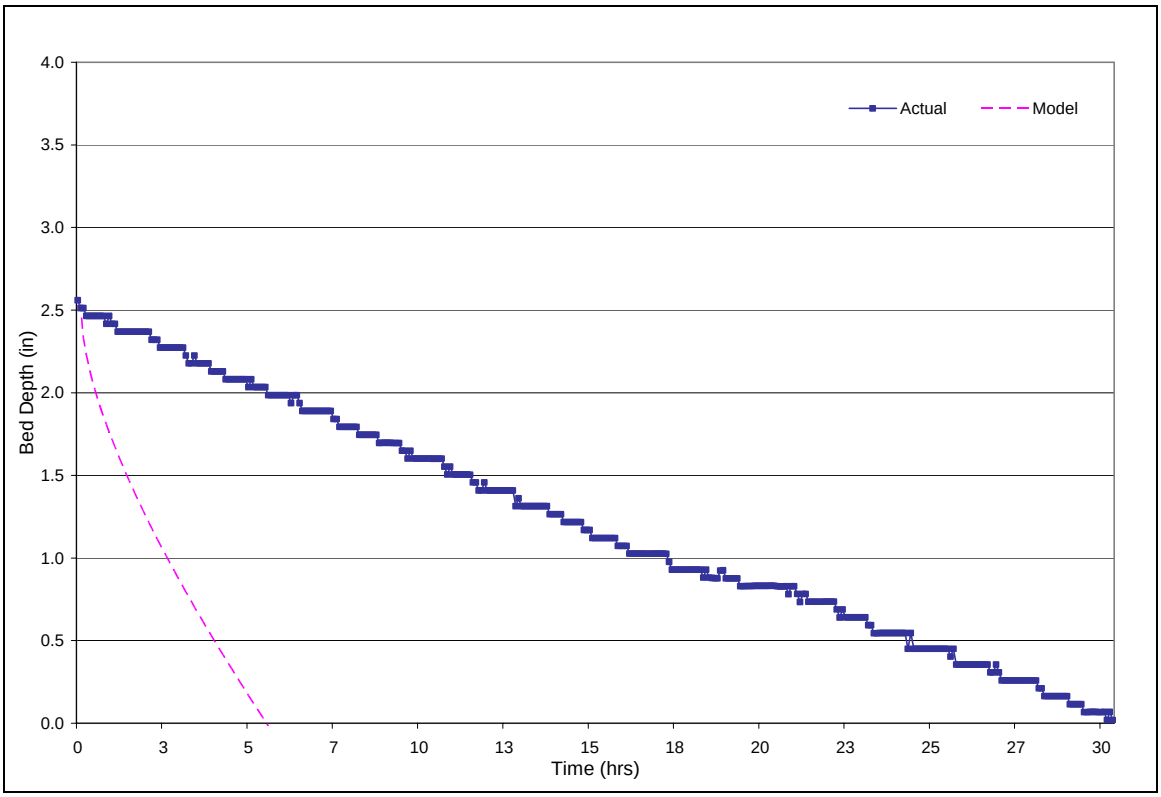

Figure L-3. Event 3/07/2004

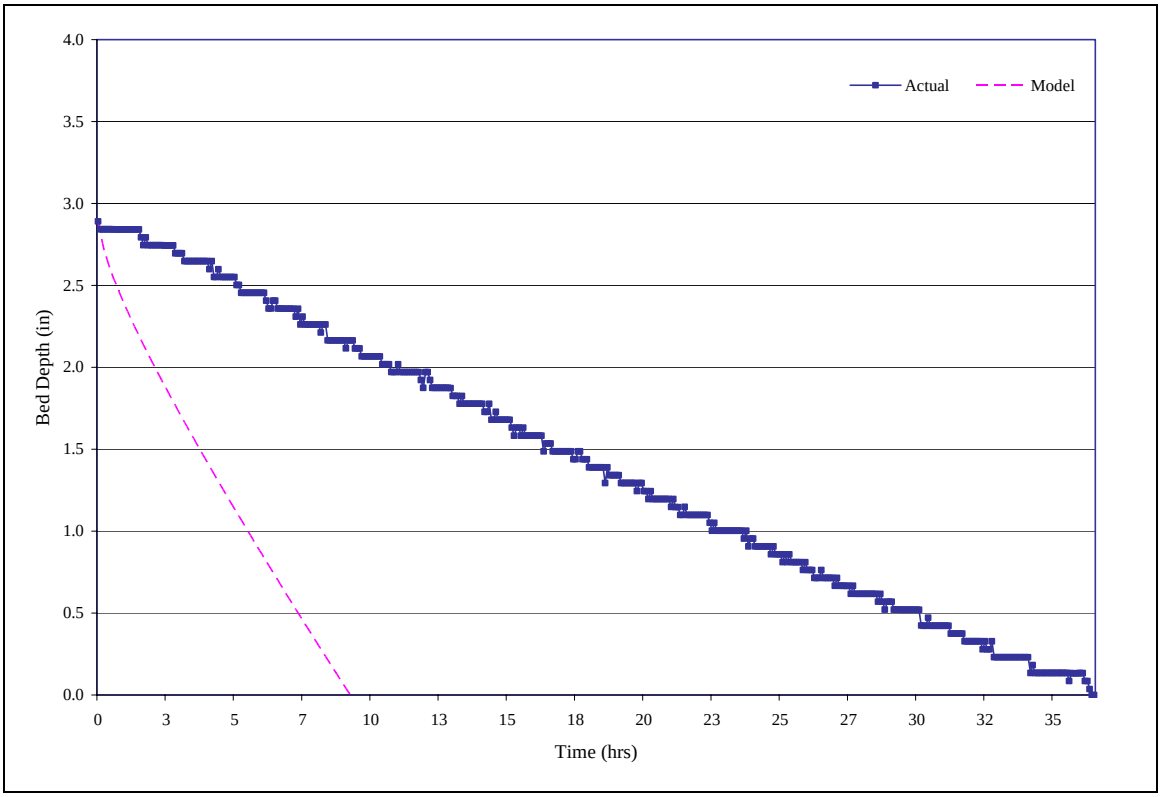

Figure L-4. Event 4/23/2004

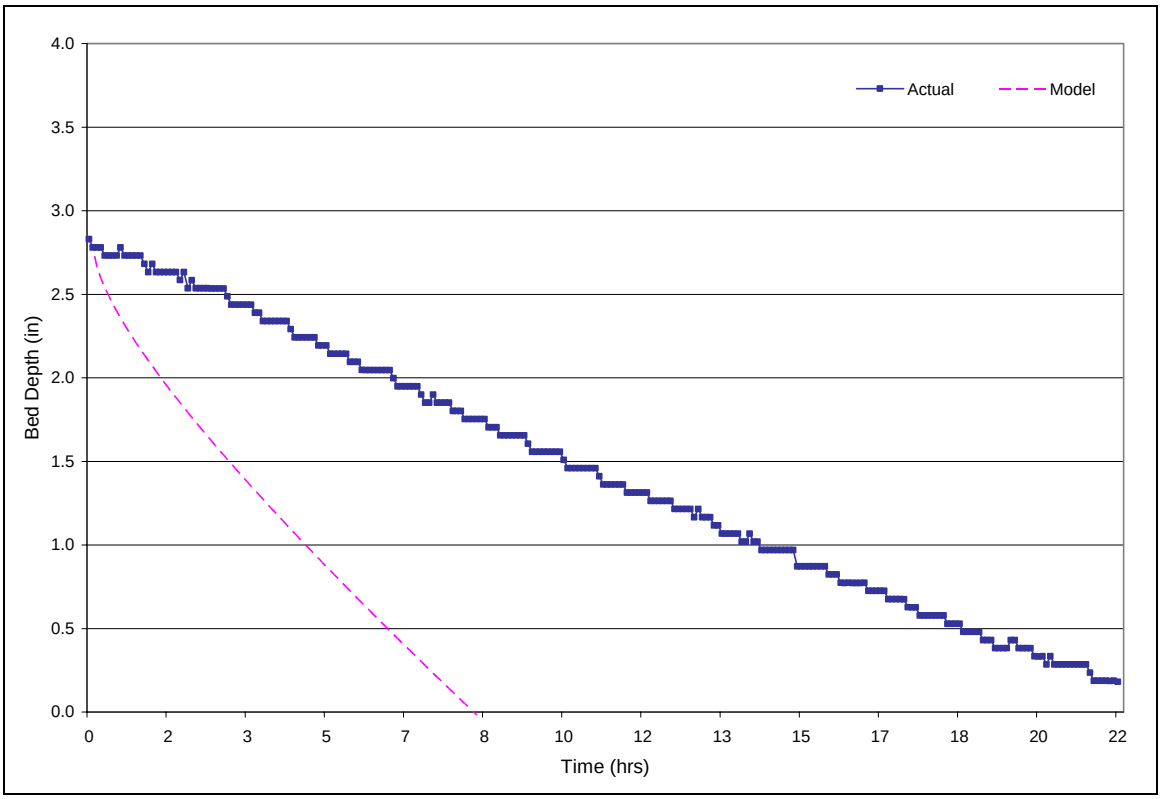

Figure L-5. Event 6/16/2004

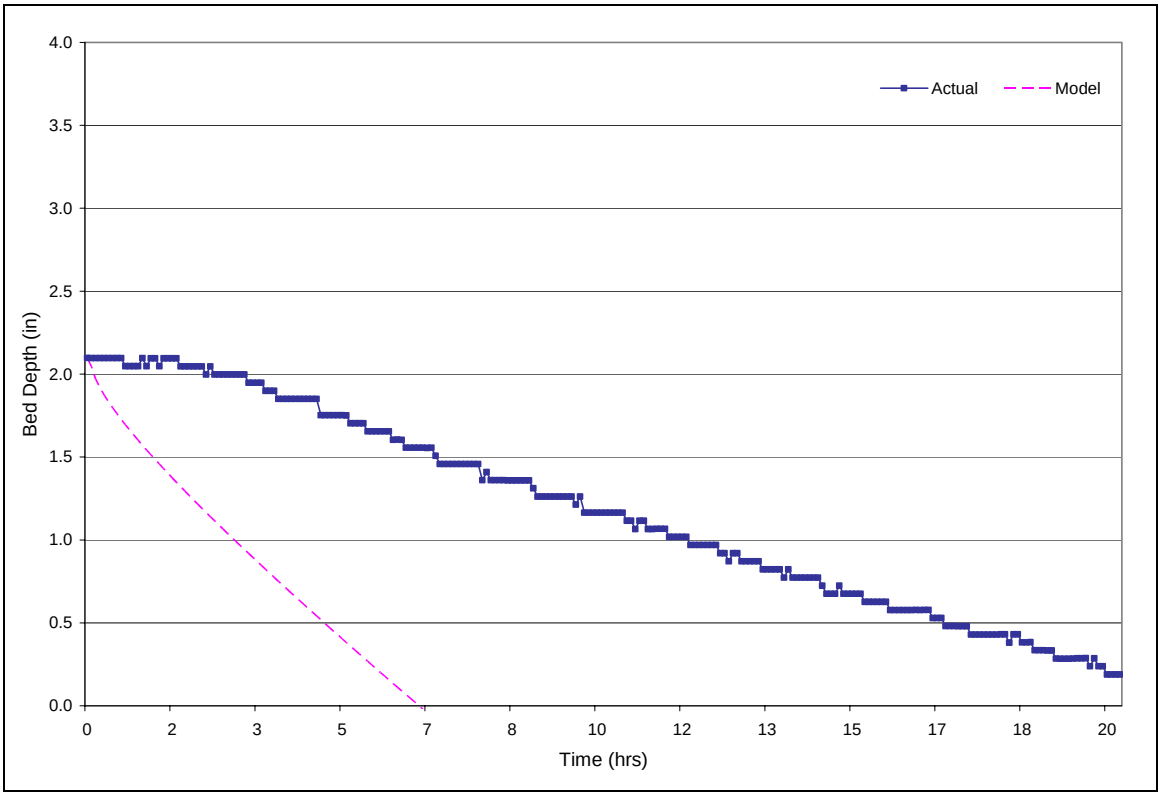

Figure L-6. Event 6/22/2004

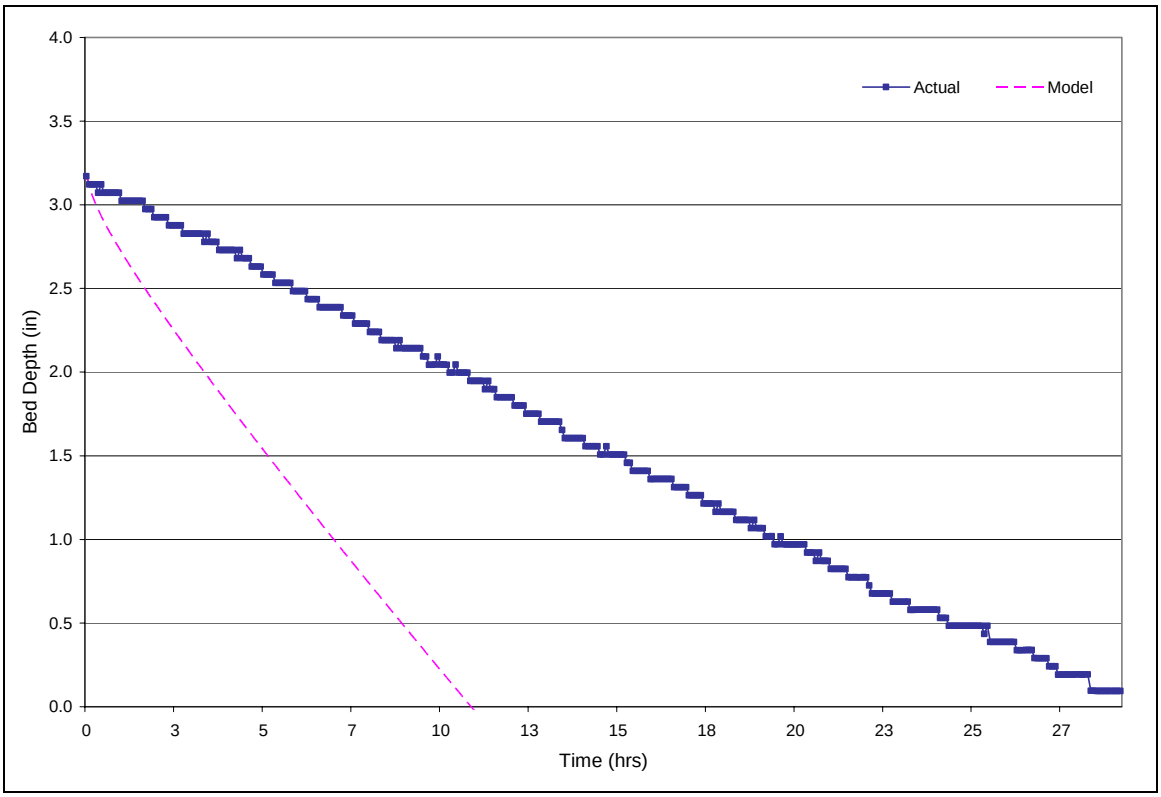

Figure L-7. Event 7/18/2004

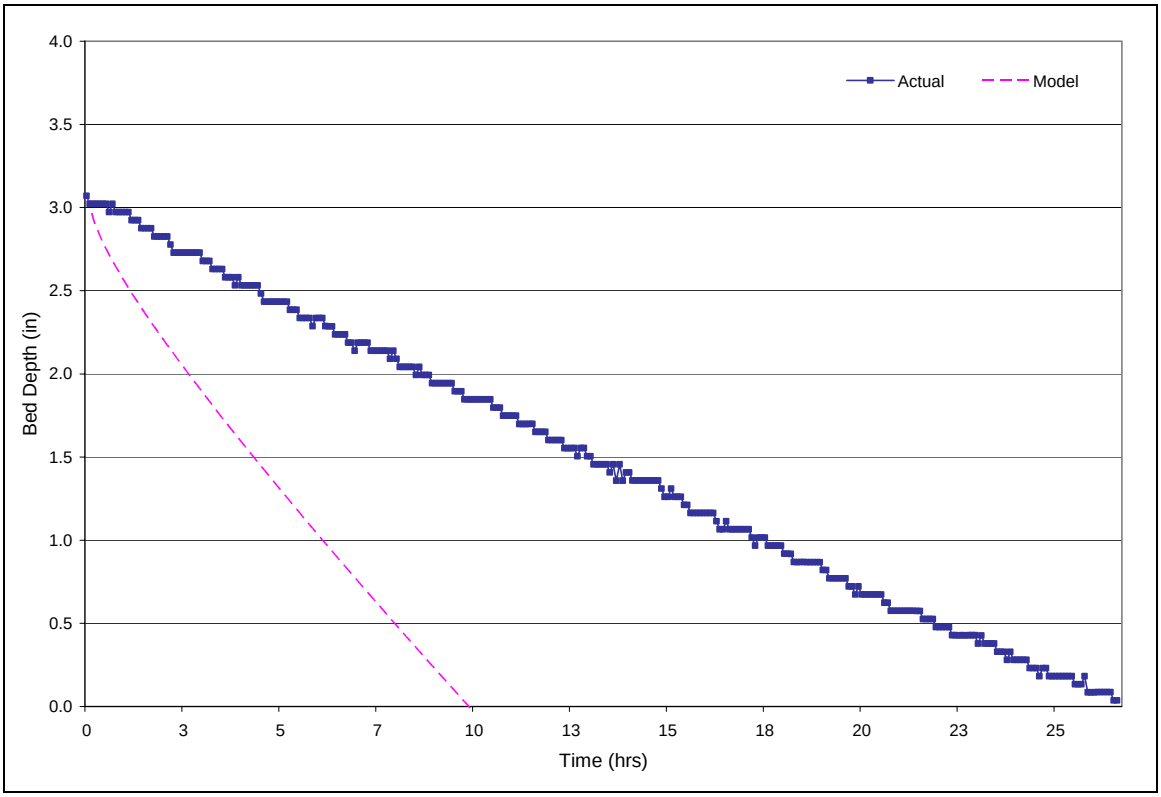

Figure L-8. Event 7/23/2004

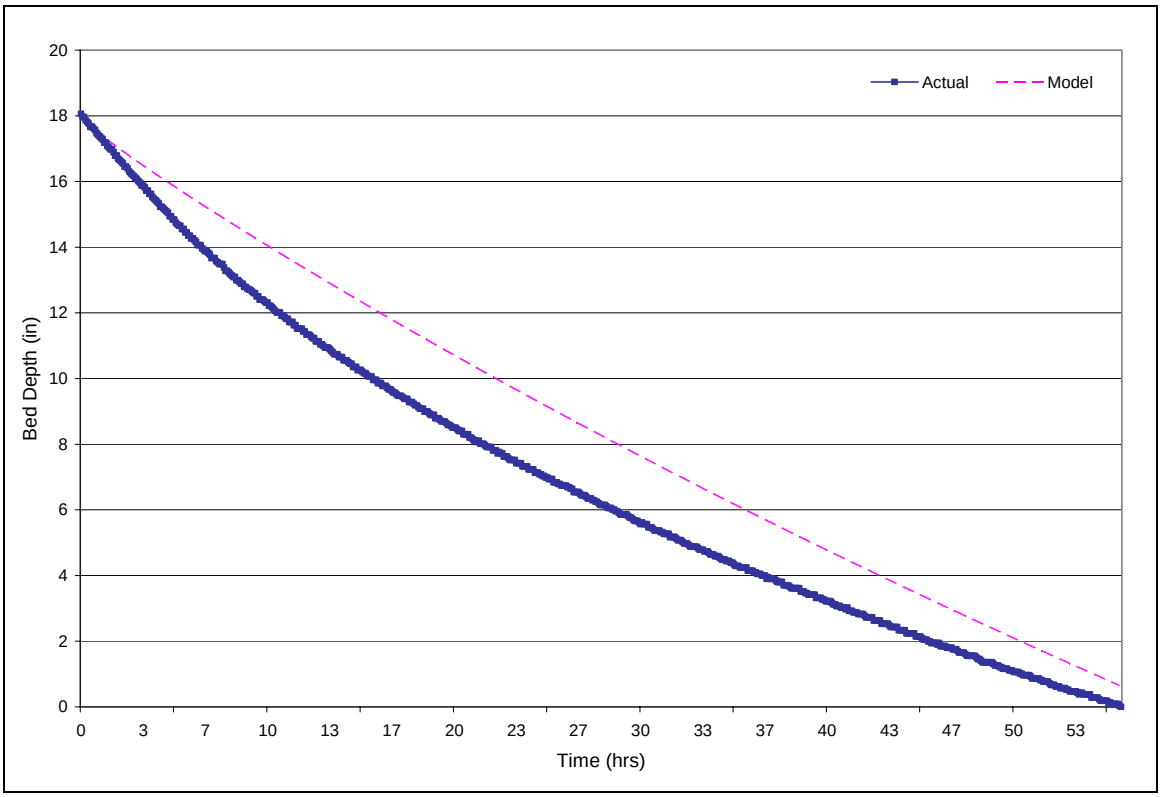

Figure L-9. Event 8/01/2004

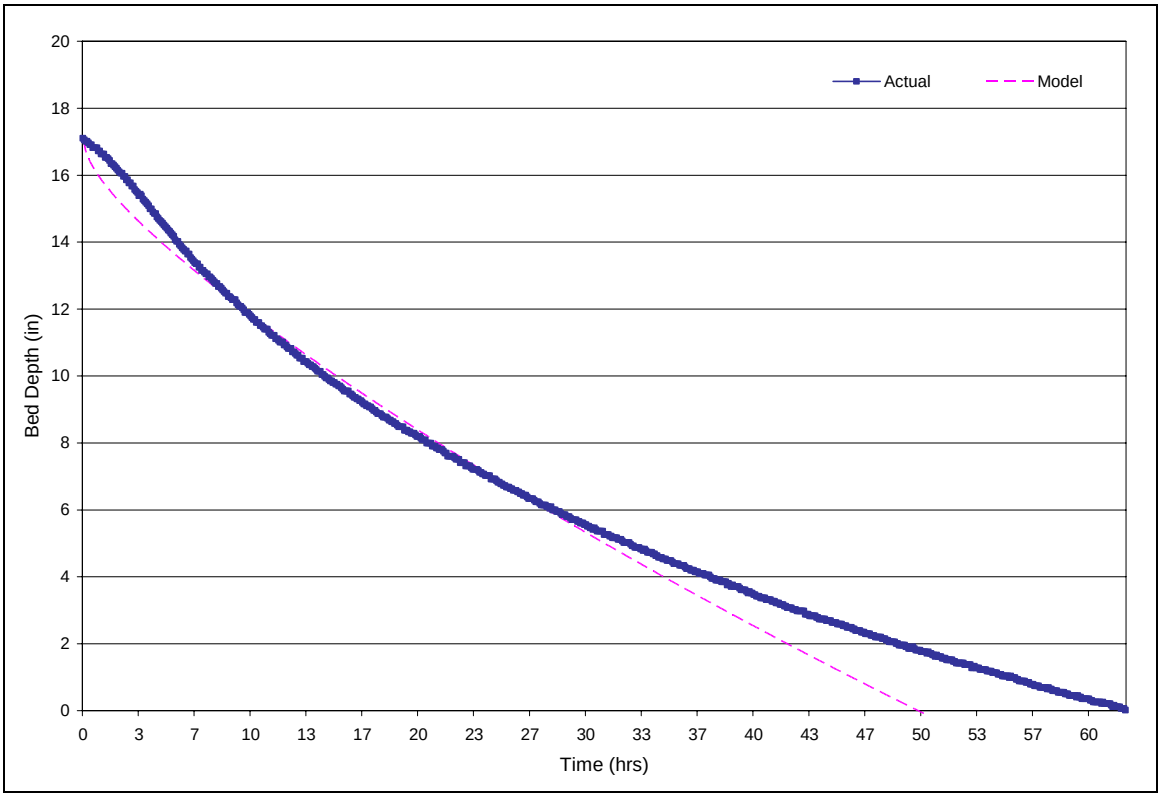

Figure L-10. Event 9/18/2004

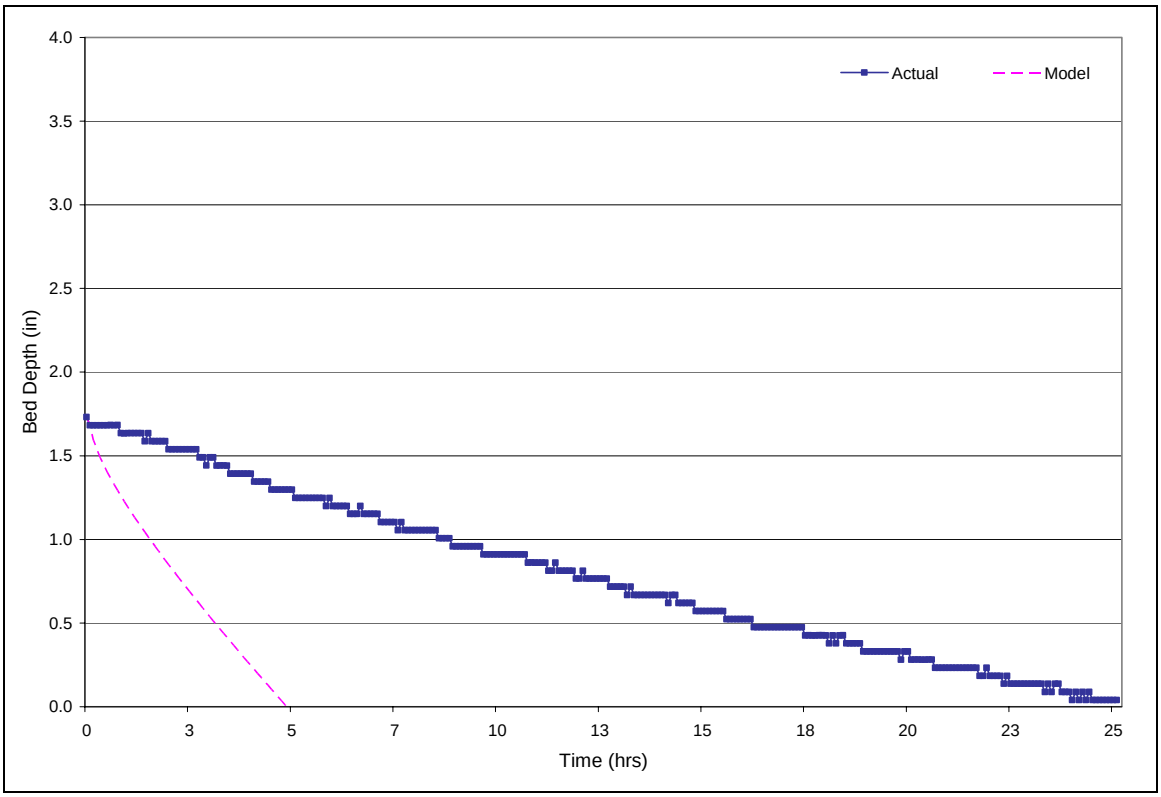

Figure L-11. Event 10/30/2004

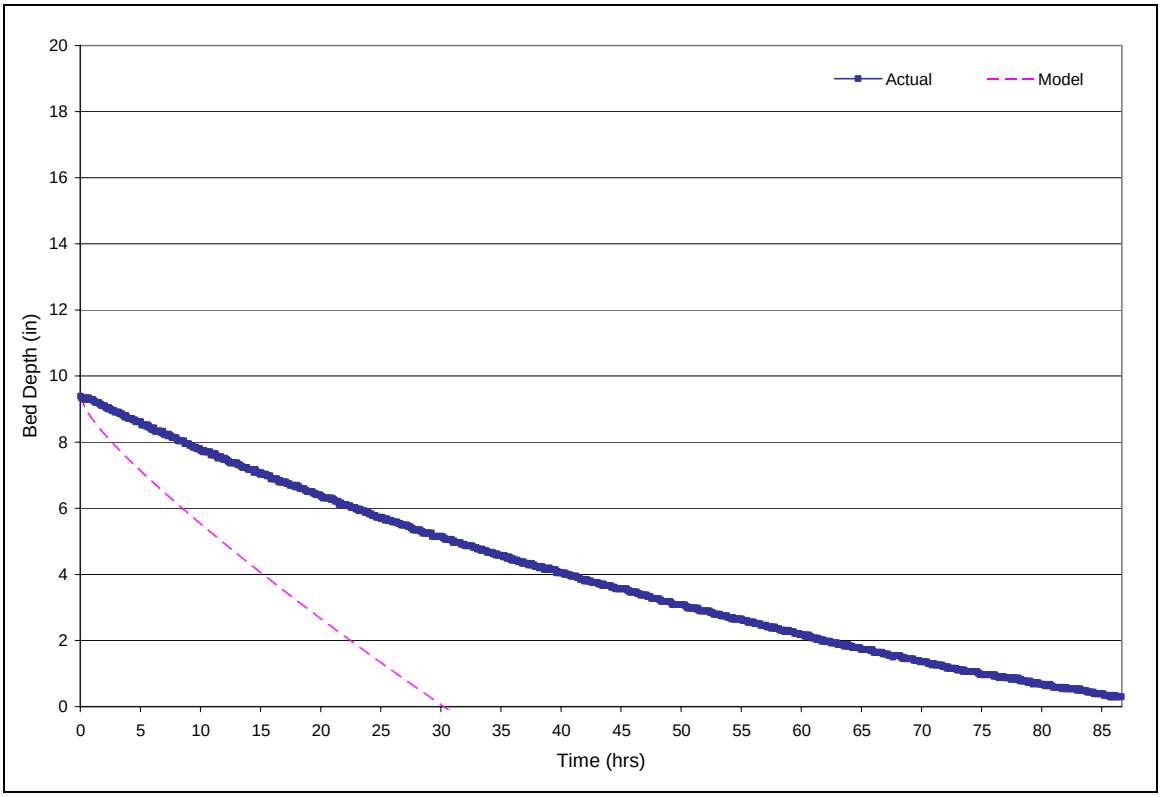

Figure L-12. Event 11/04/2004

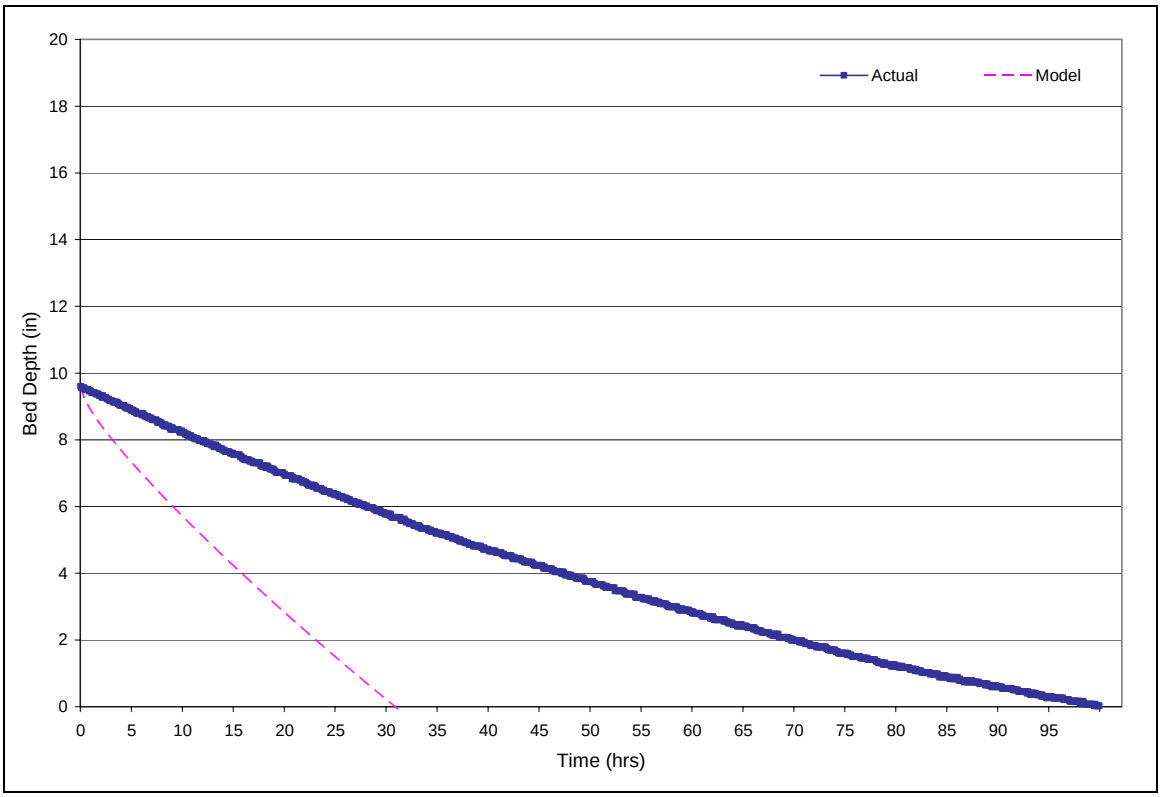

Figure L-13. Event 11/12/2004

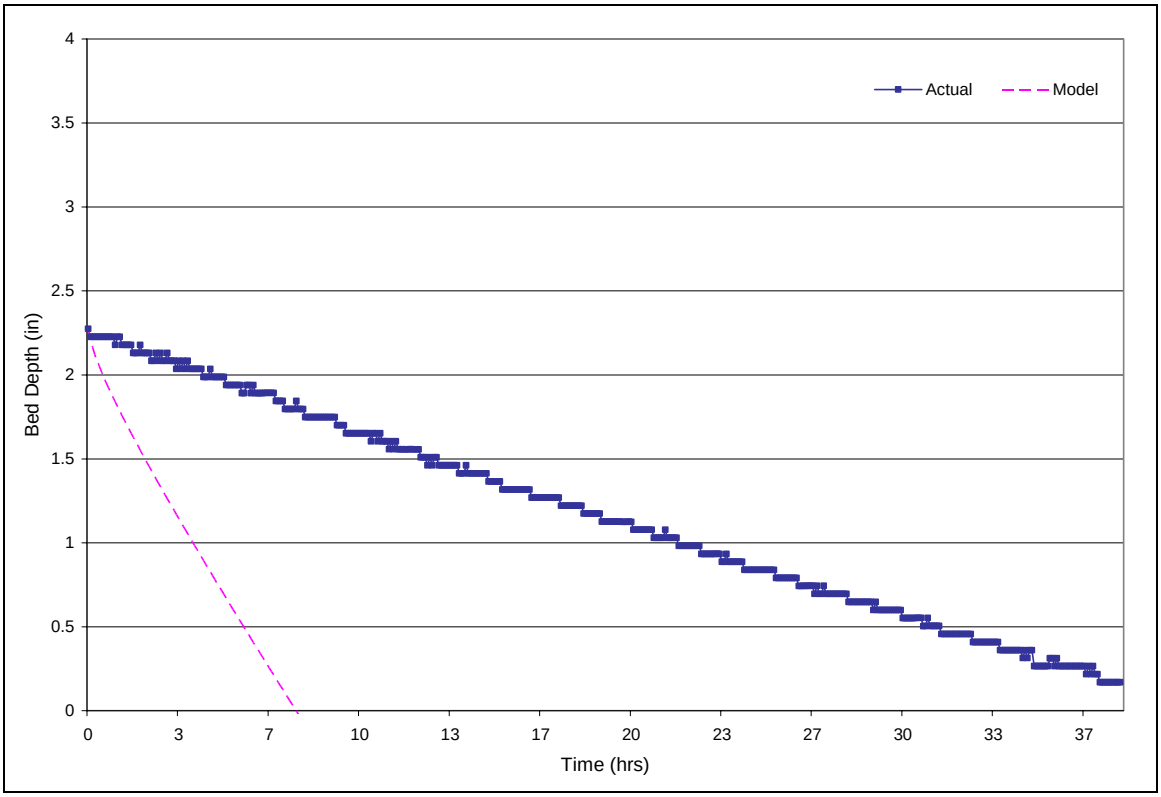

Figure L-14. Event 12/07/2004

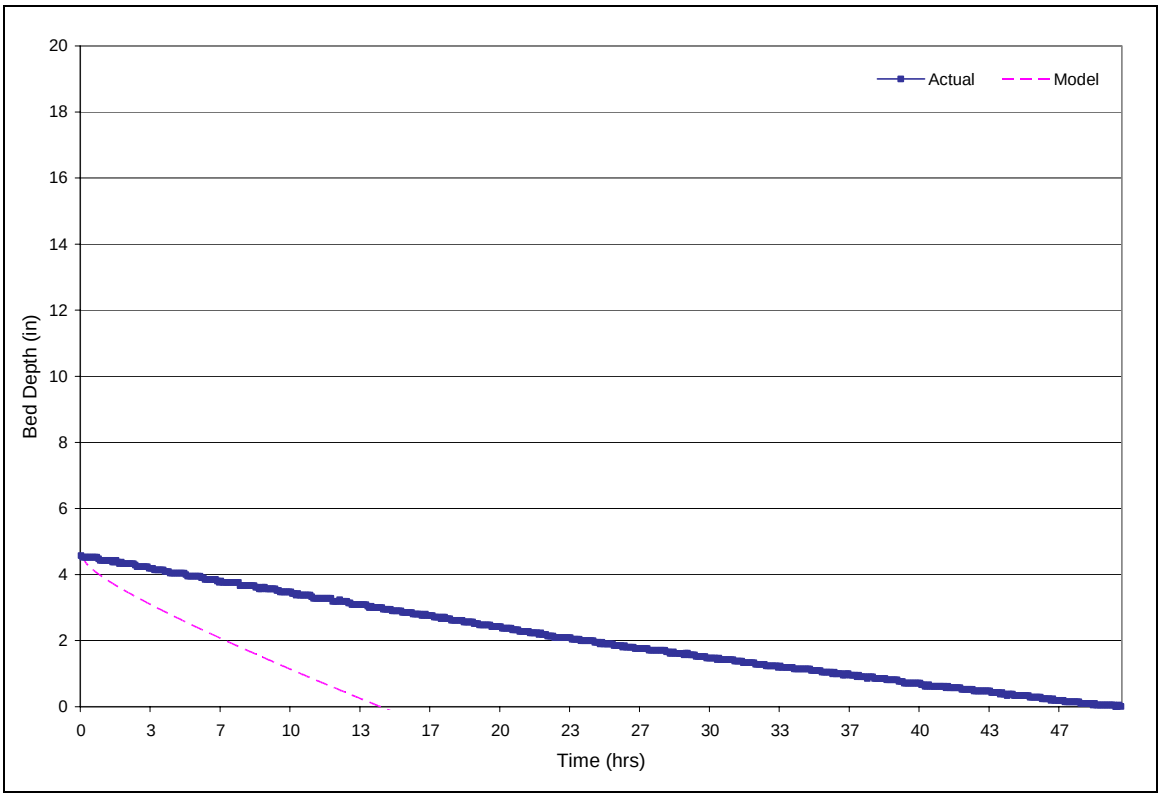

Figure L-15. Event 12/23/2004

Appendix M – Preliminary Model Results: Cumulative Infiltrated Depth

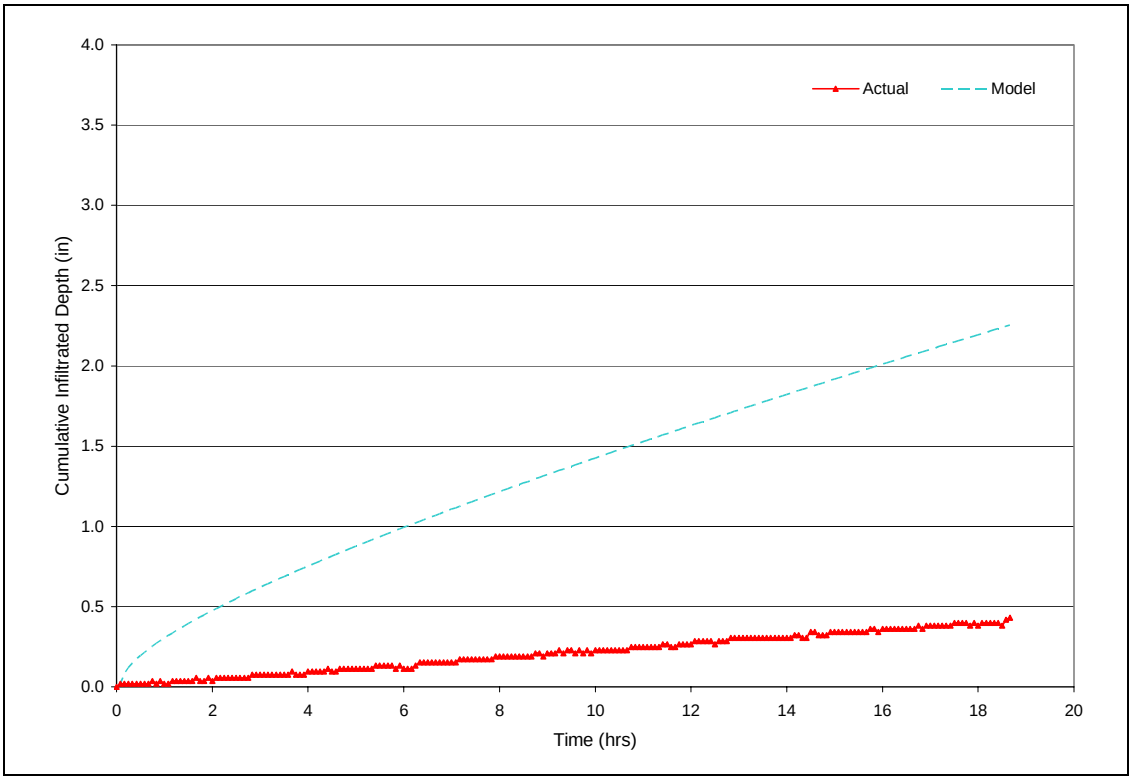

Figure M-1. Event 1/04/2004

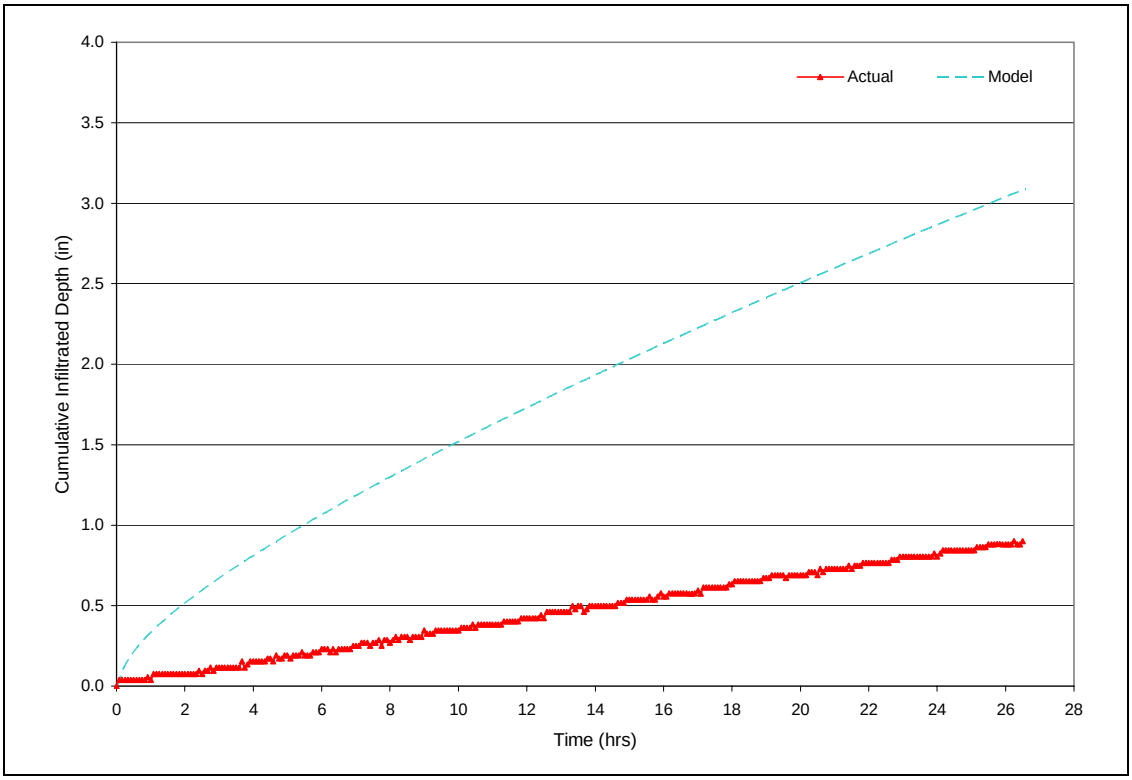

Figure M-2. Event 3/06/2004

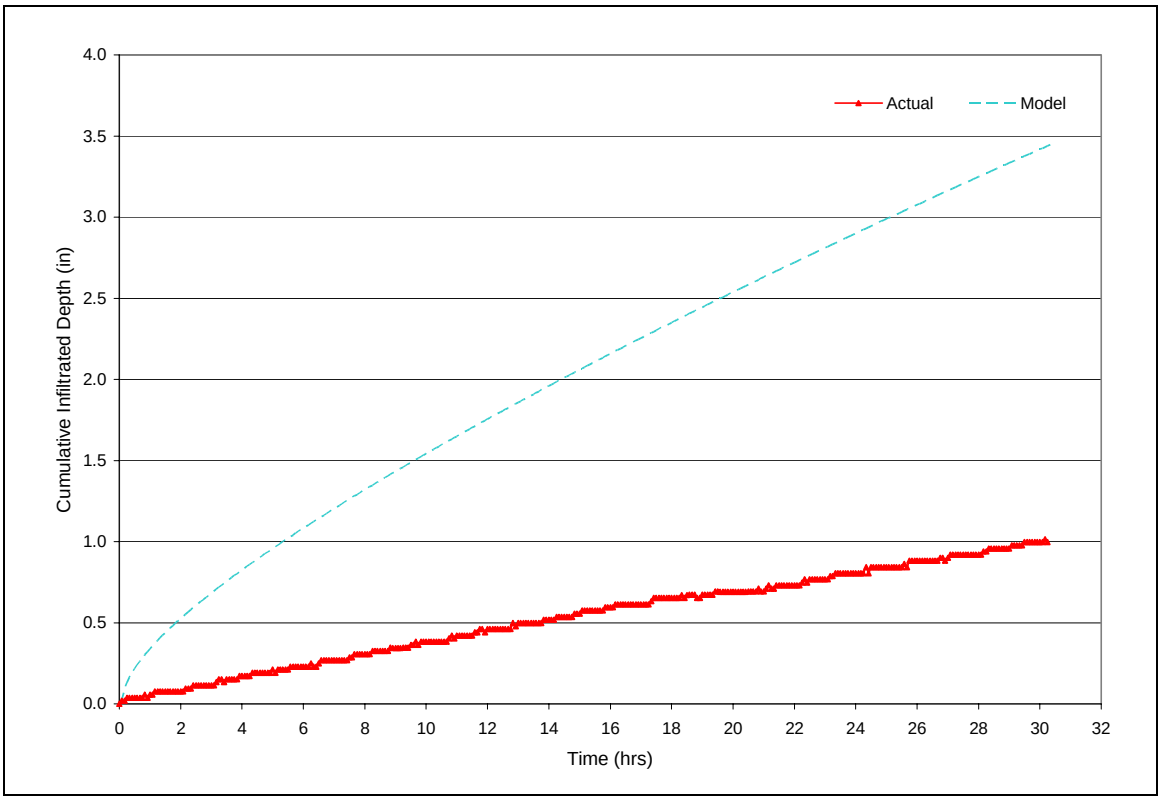

Figure M-3. Event 3/07/2004

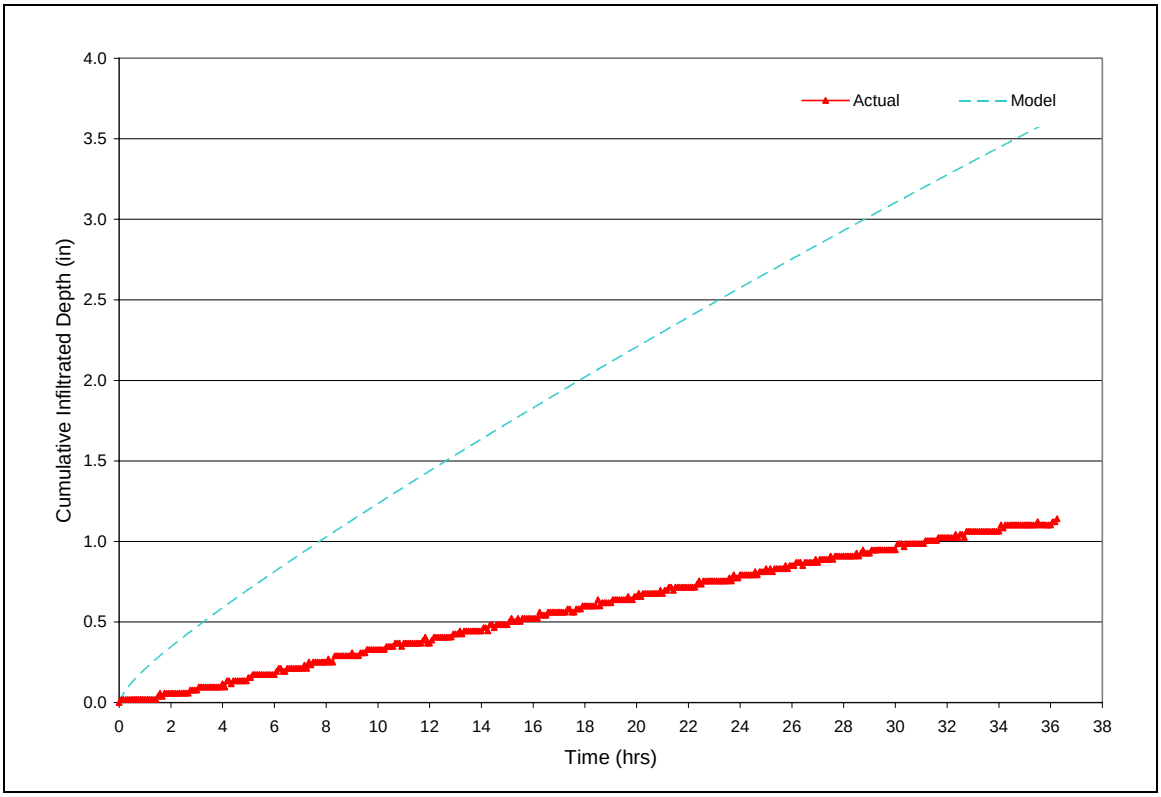

Figure M-4. Event 4/23/2004

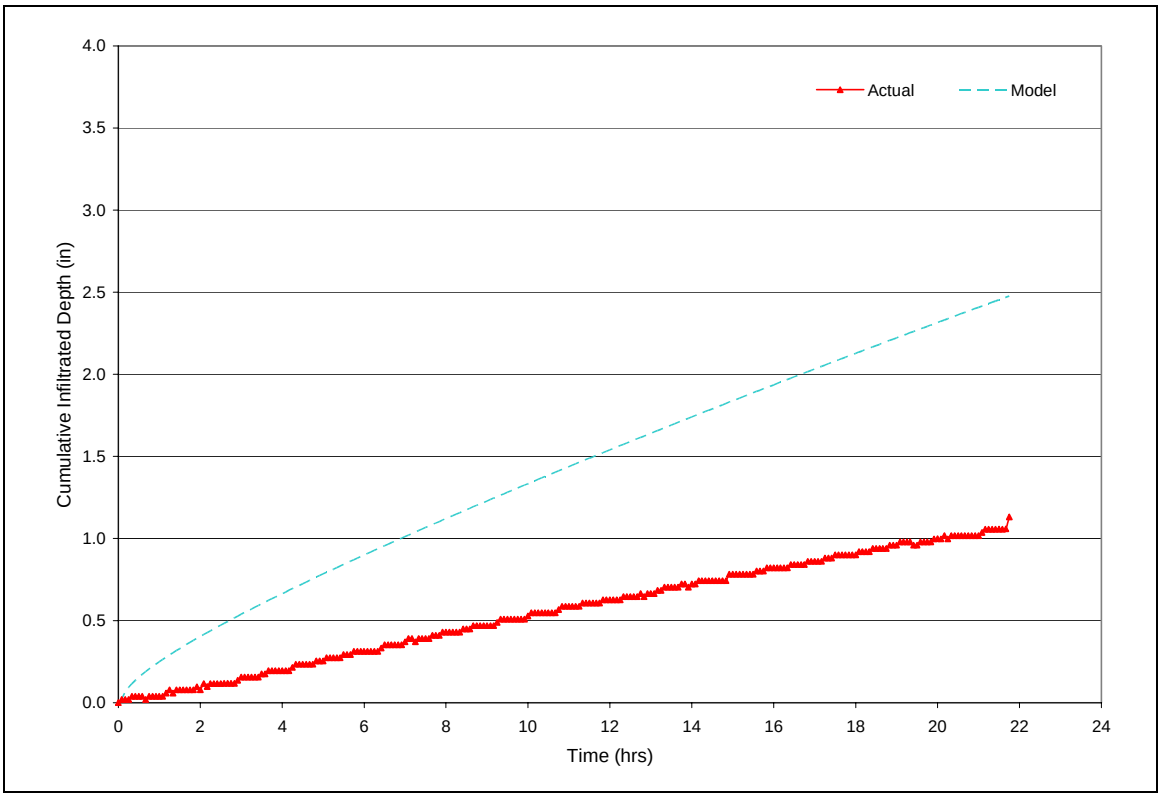

Figure M-5. Event 6/16/2004

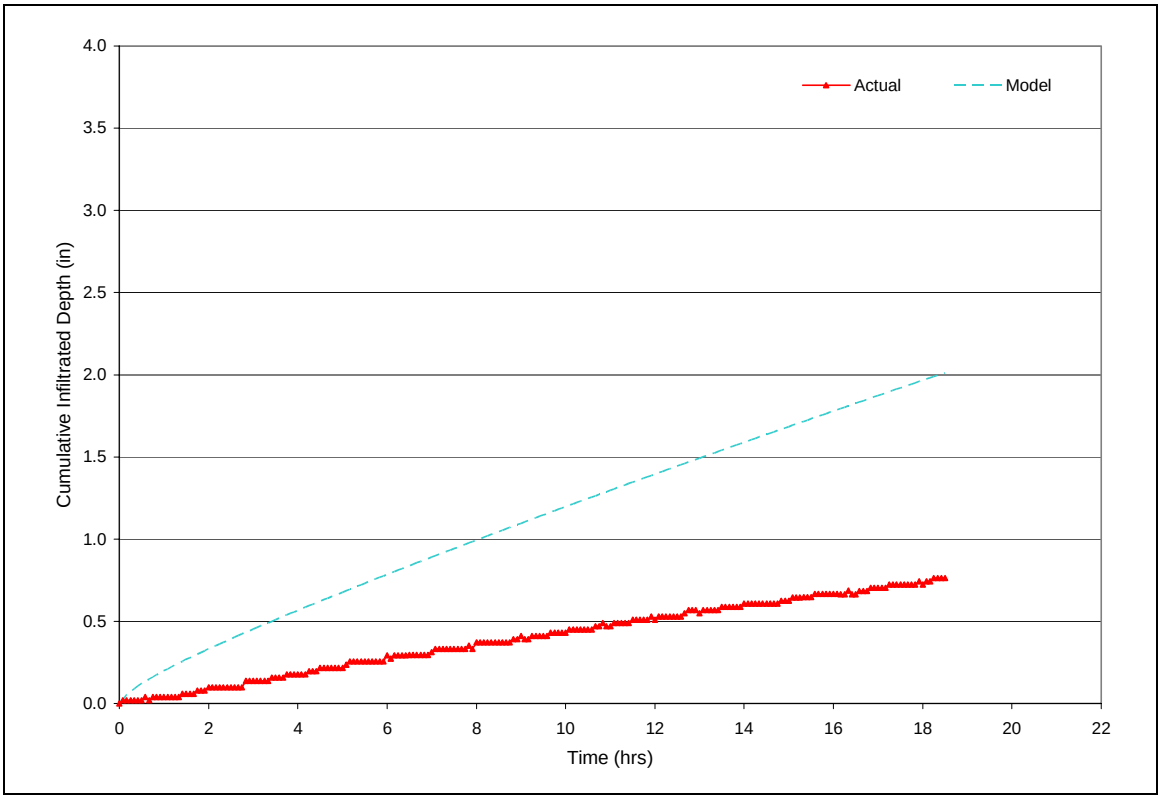

Figure M-6. Event 6/22/2004

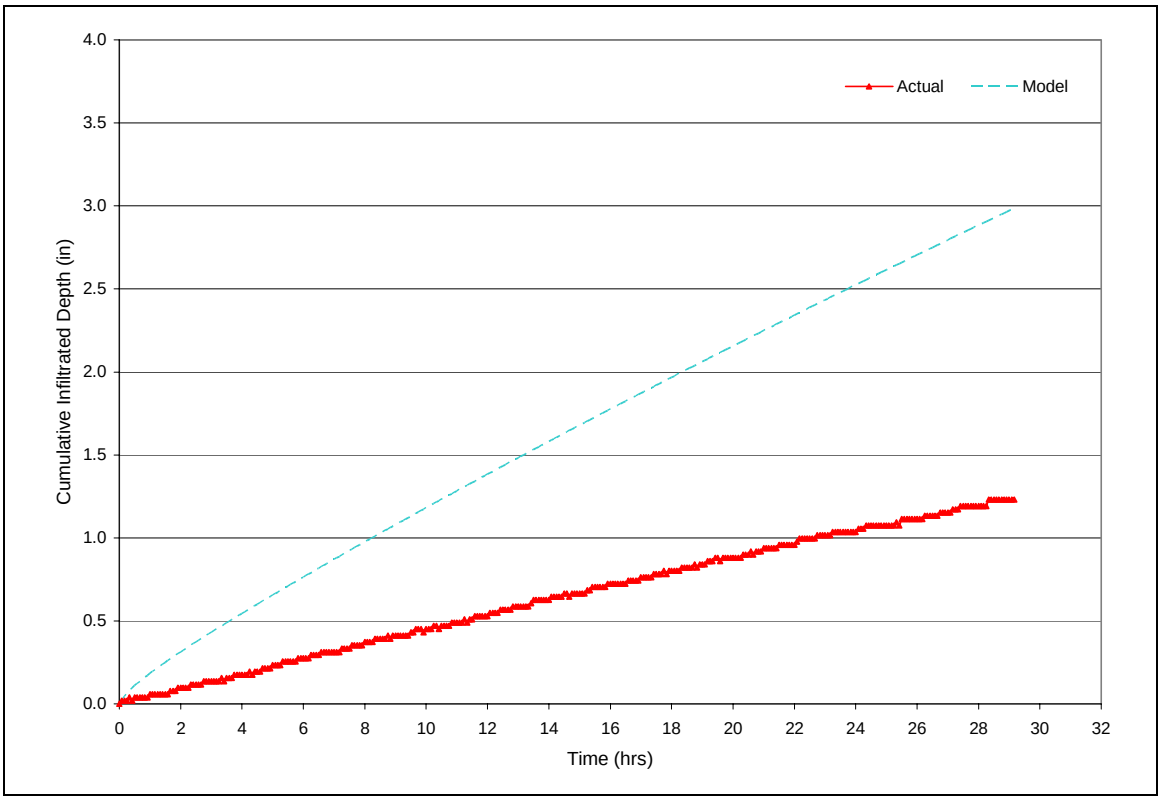

Figure M-7. Event 7/18/2004

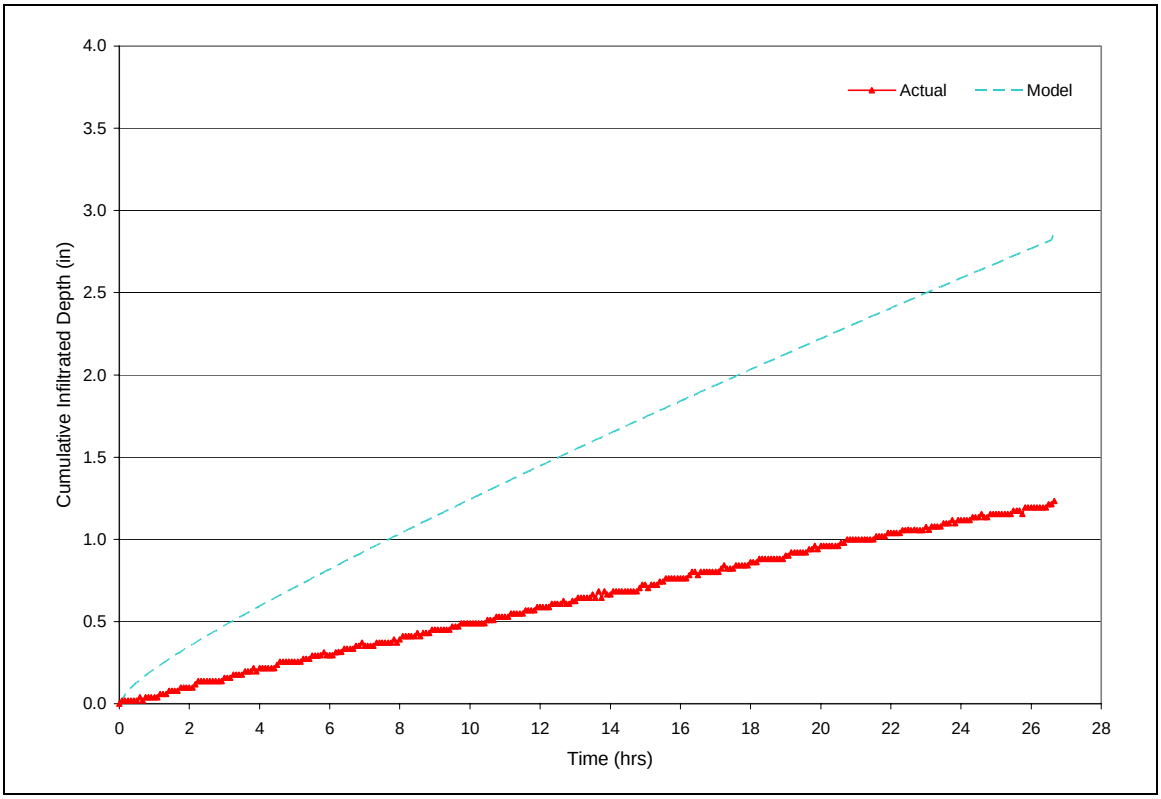

Figure M-8. Event 7/23/2004

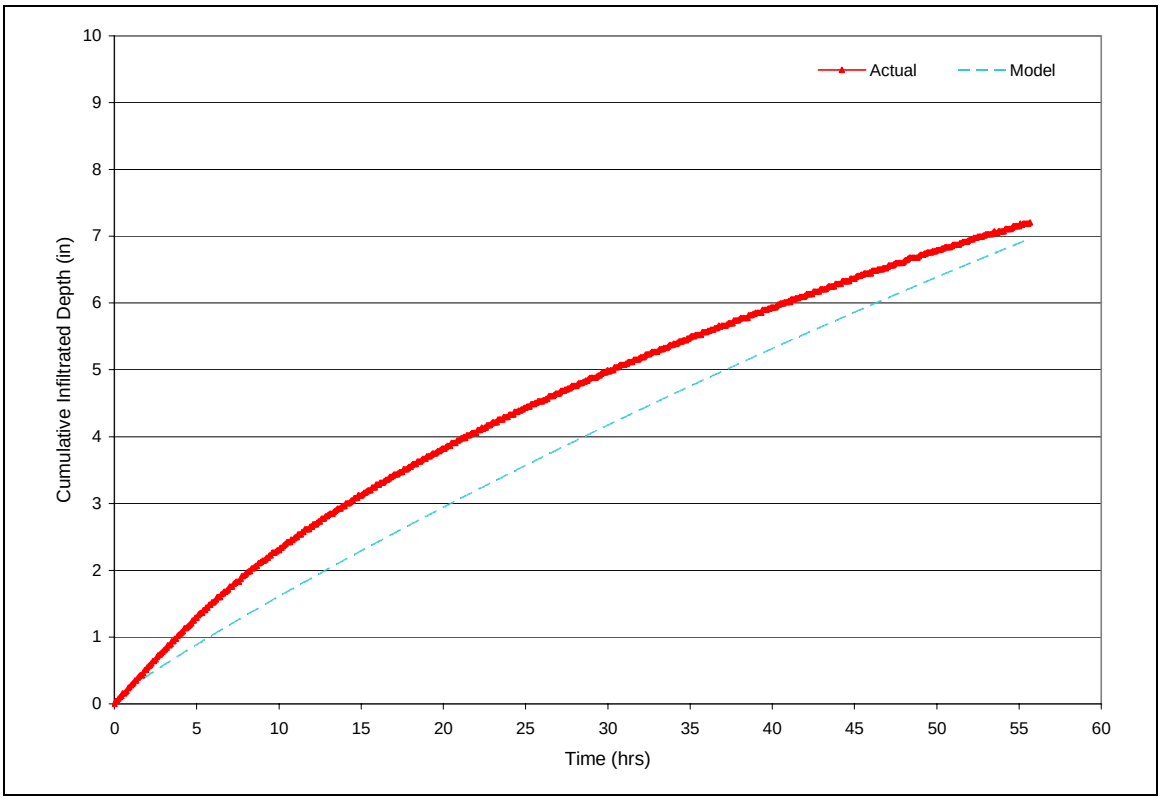

Figure M-9. Event 8/01/2004

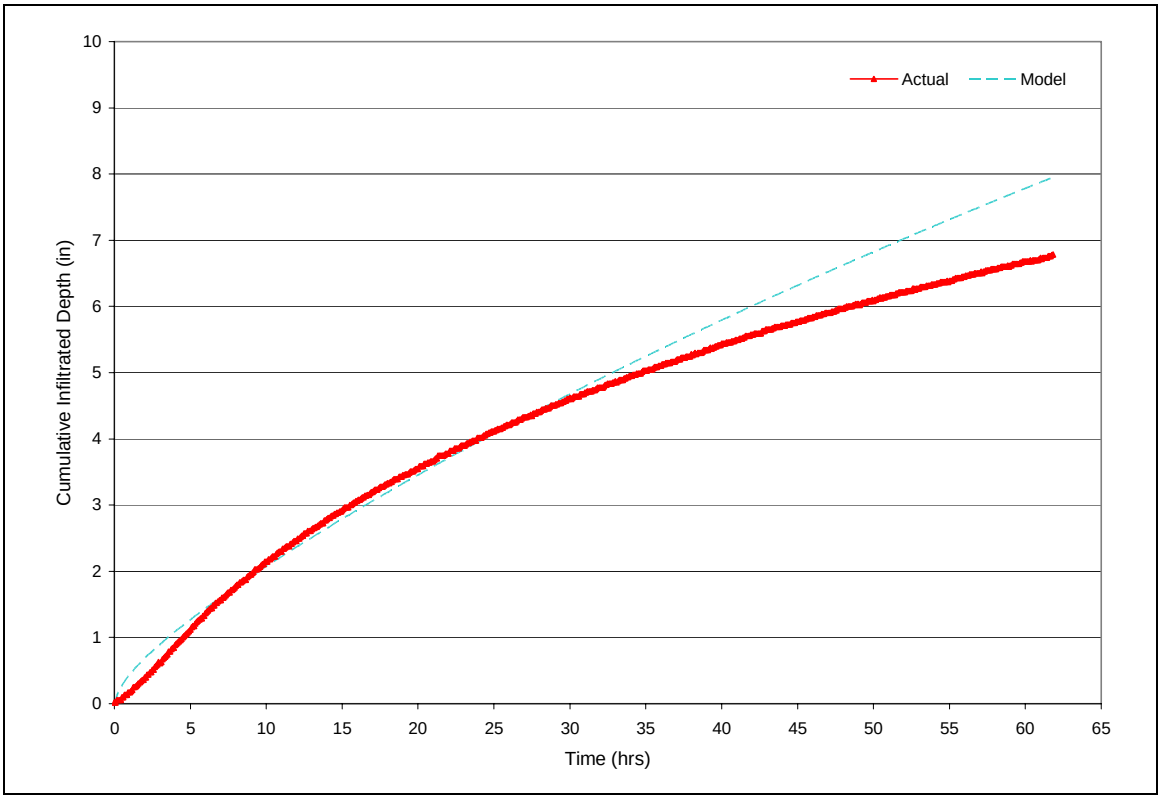

Figure M-10. Event 9/18/2004

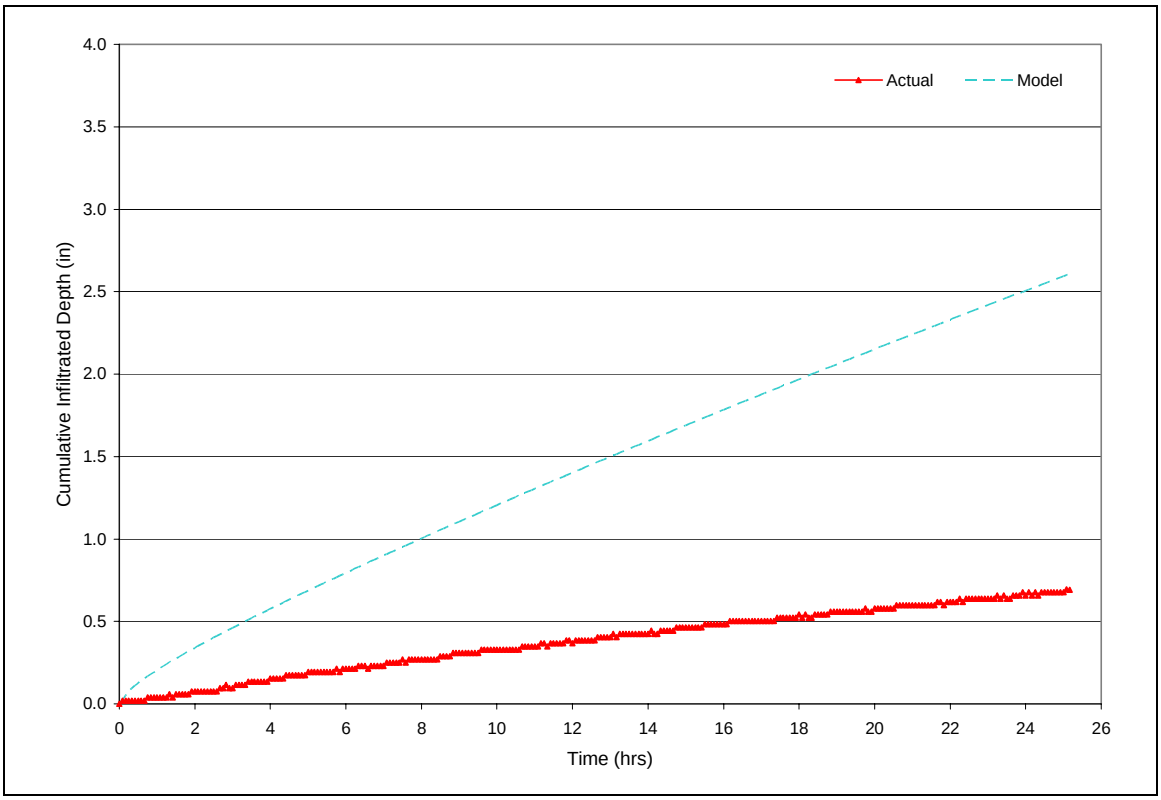

Figure M-11. Event 10/30/2004

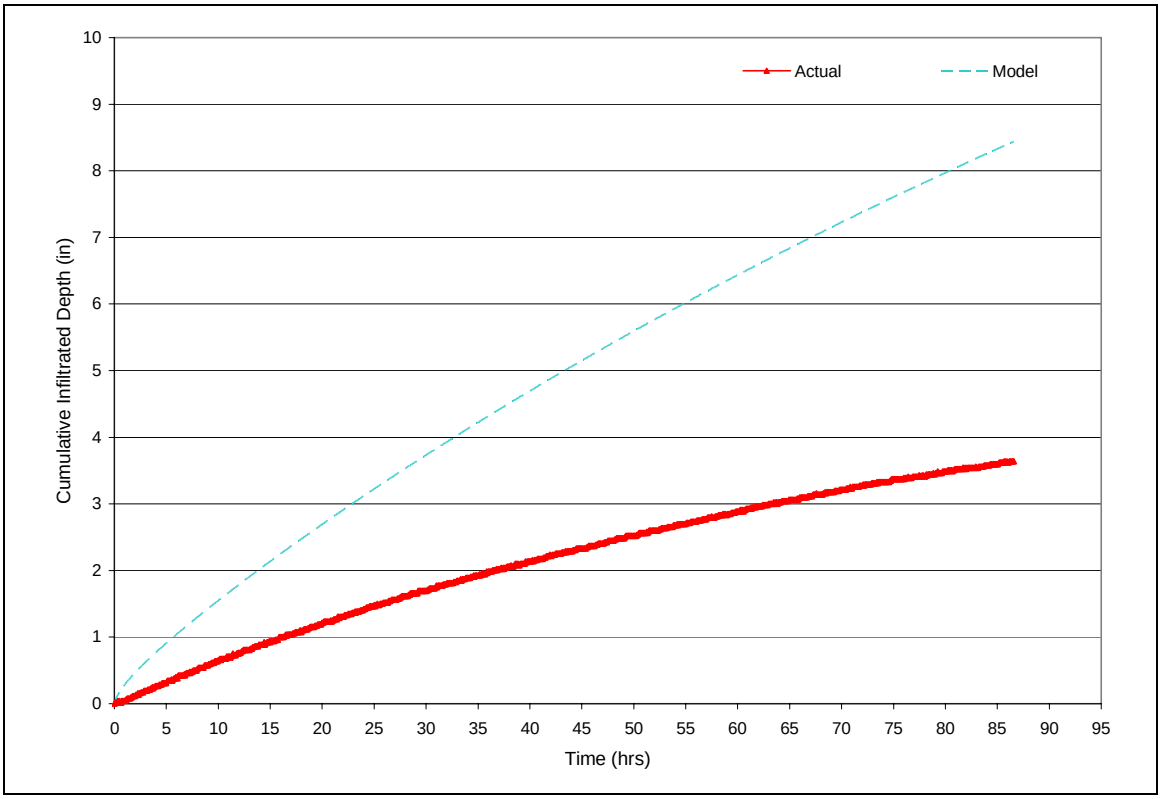

Figure M-12. Event 11/04/2004

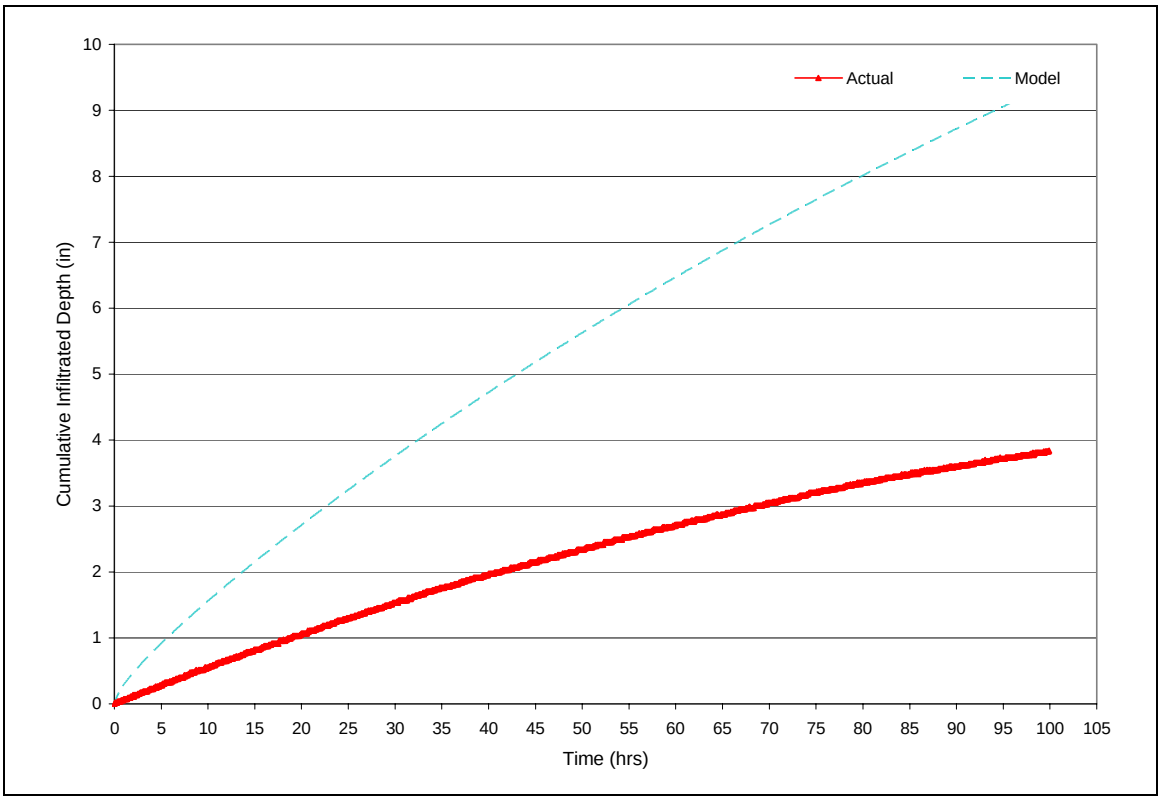

Figure M-13. Event 11/12/2004

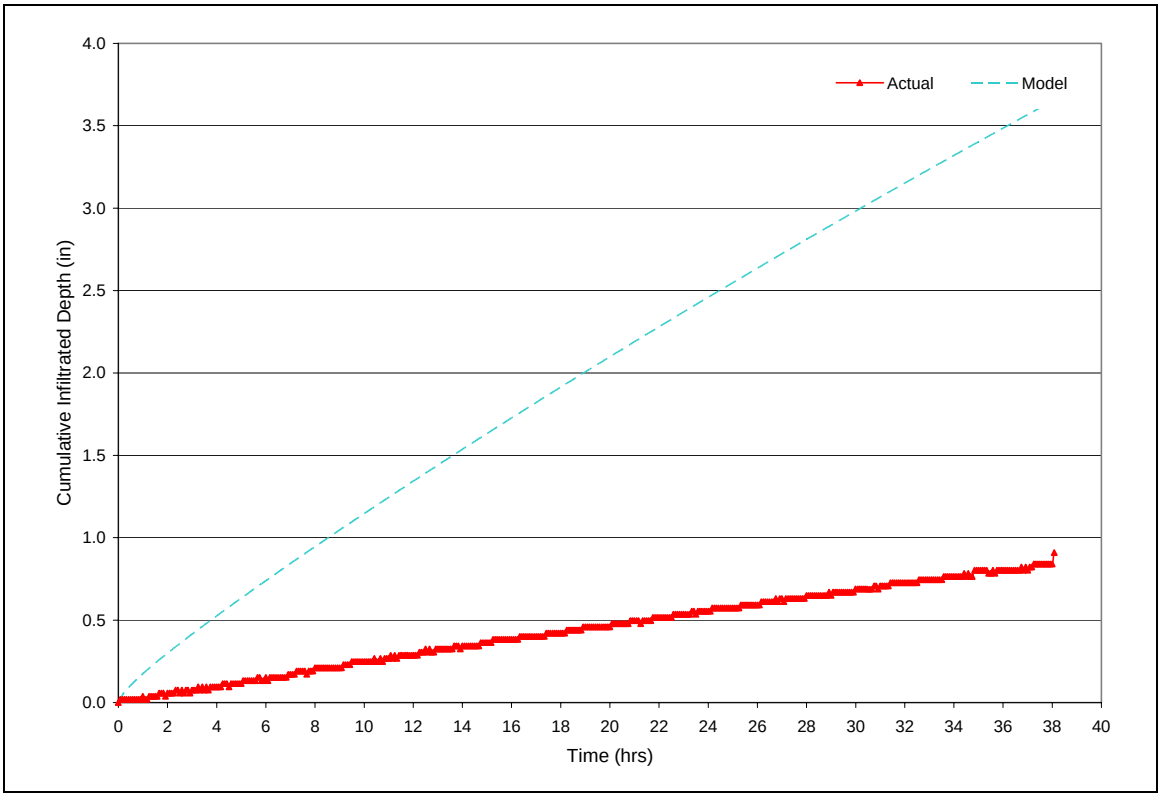

Figure M-14. Event 12/07/2004

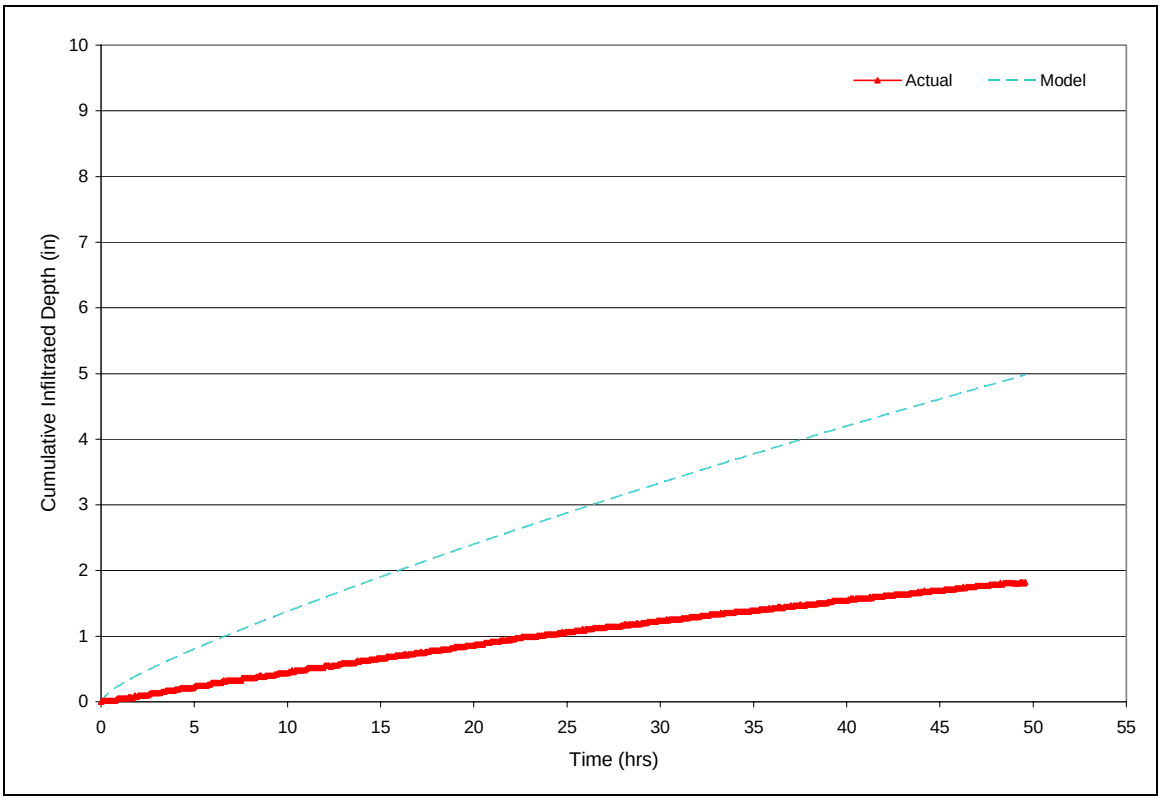

Figure L-15. Event 12/23/2004

Appendix N – Final Model Results: Recession Limb

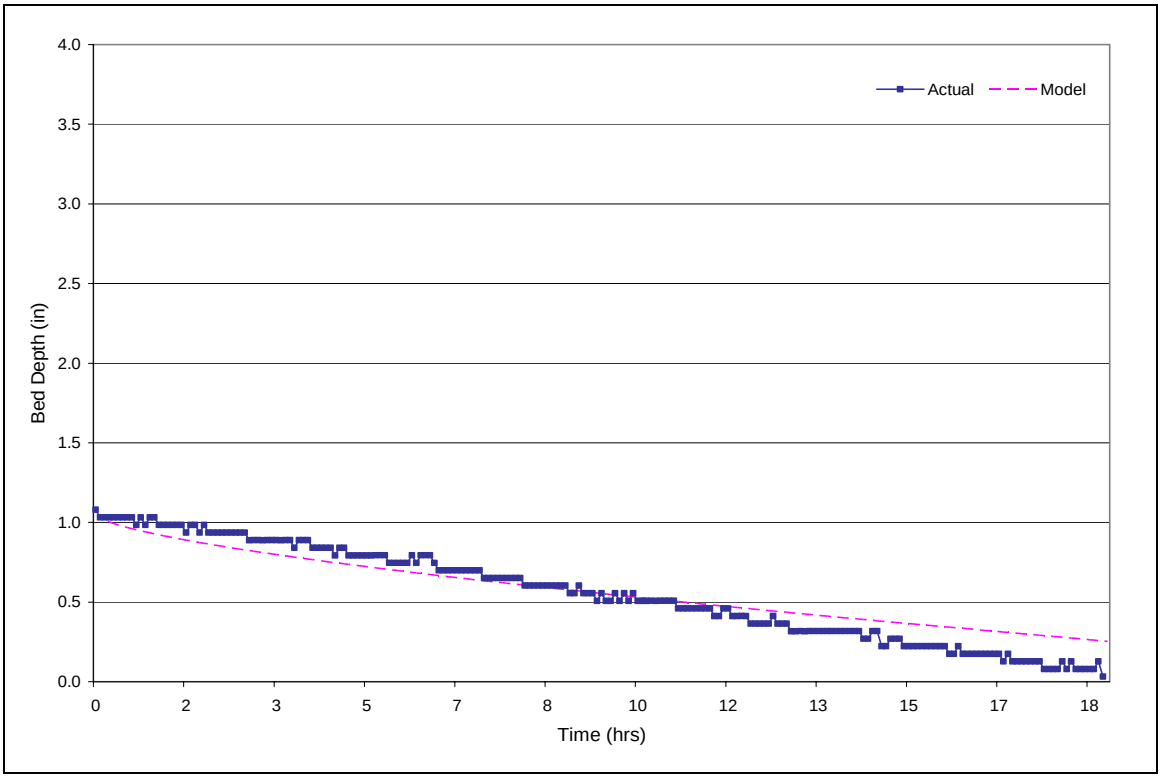

Figure N-1. Event 1/04/2004

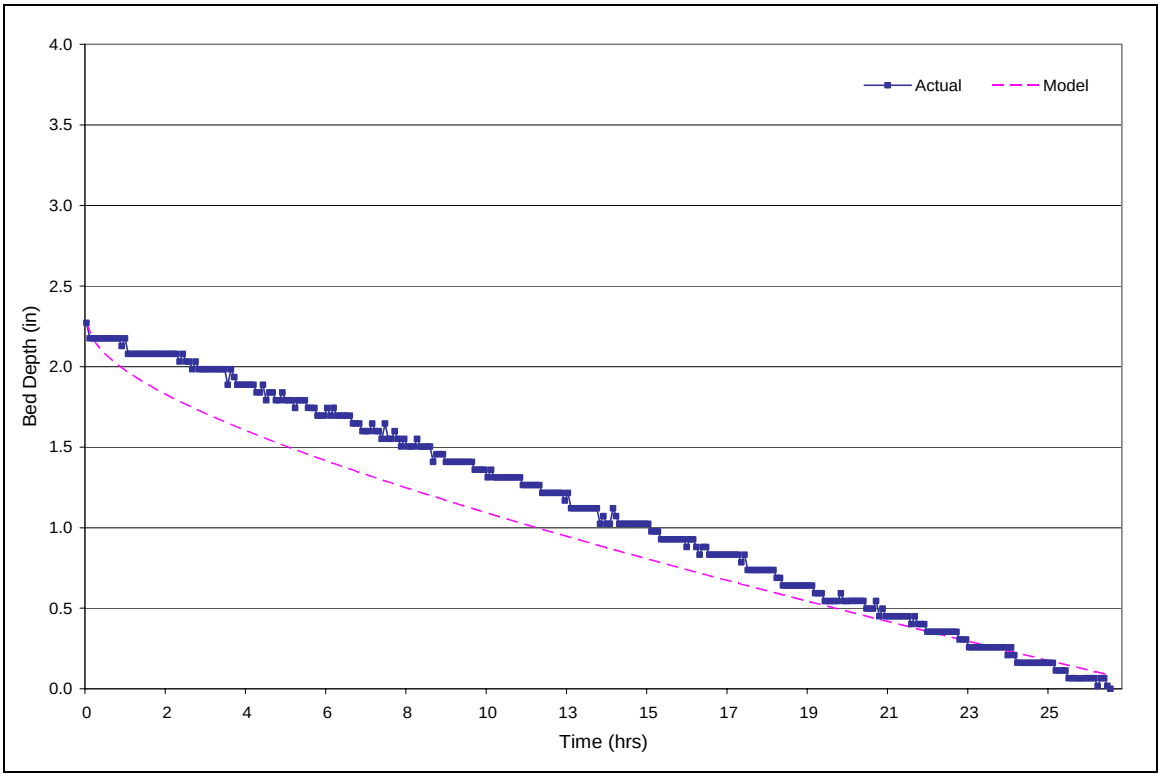

Figure N-2. Event 3/06/2004

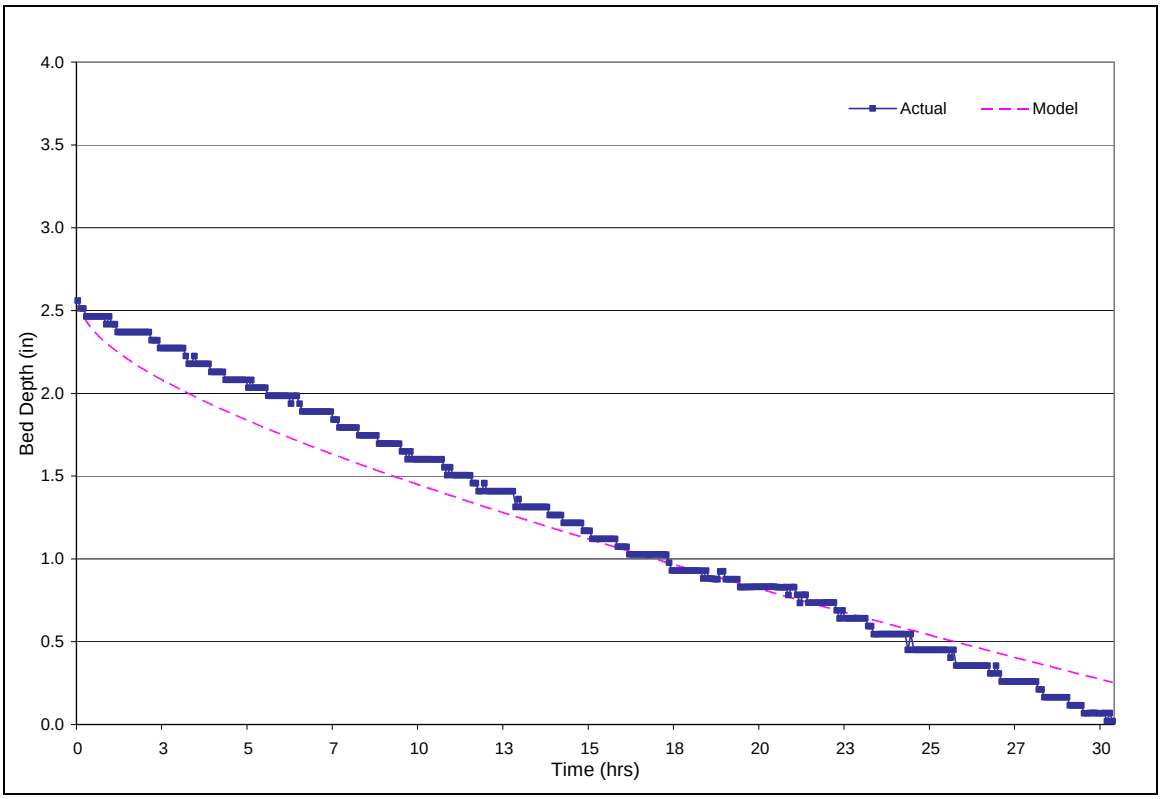

Figure N-3. Event 3/07/2004

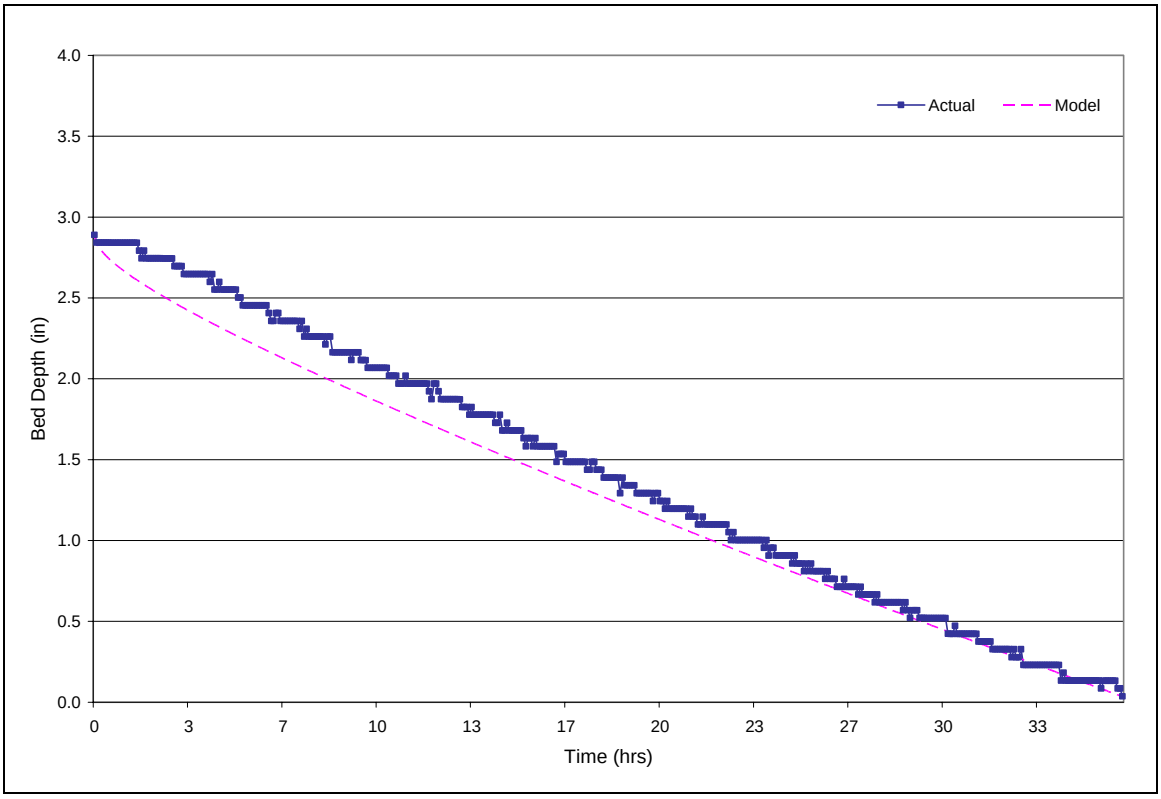

Figure N-4. Event 4/23/2004

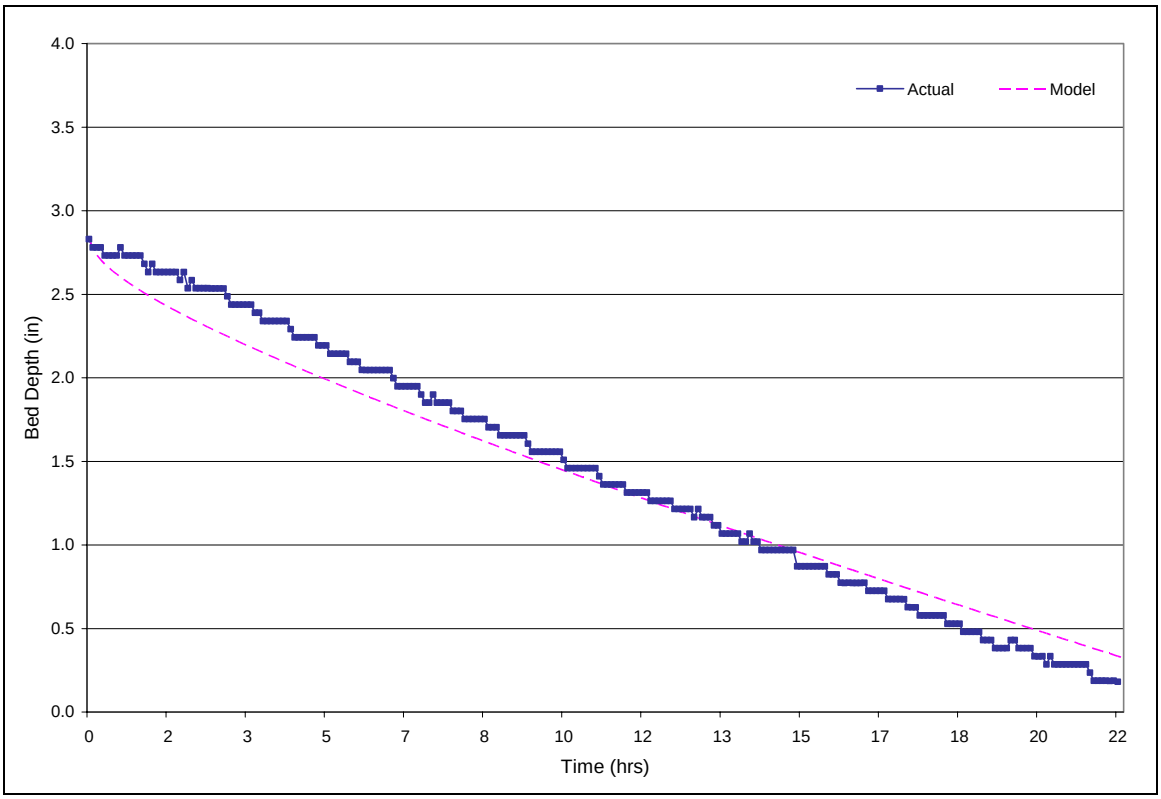

Figure N-5. Event 6/16/2004

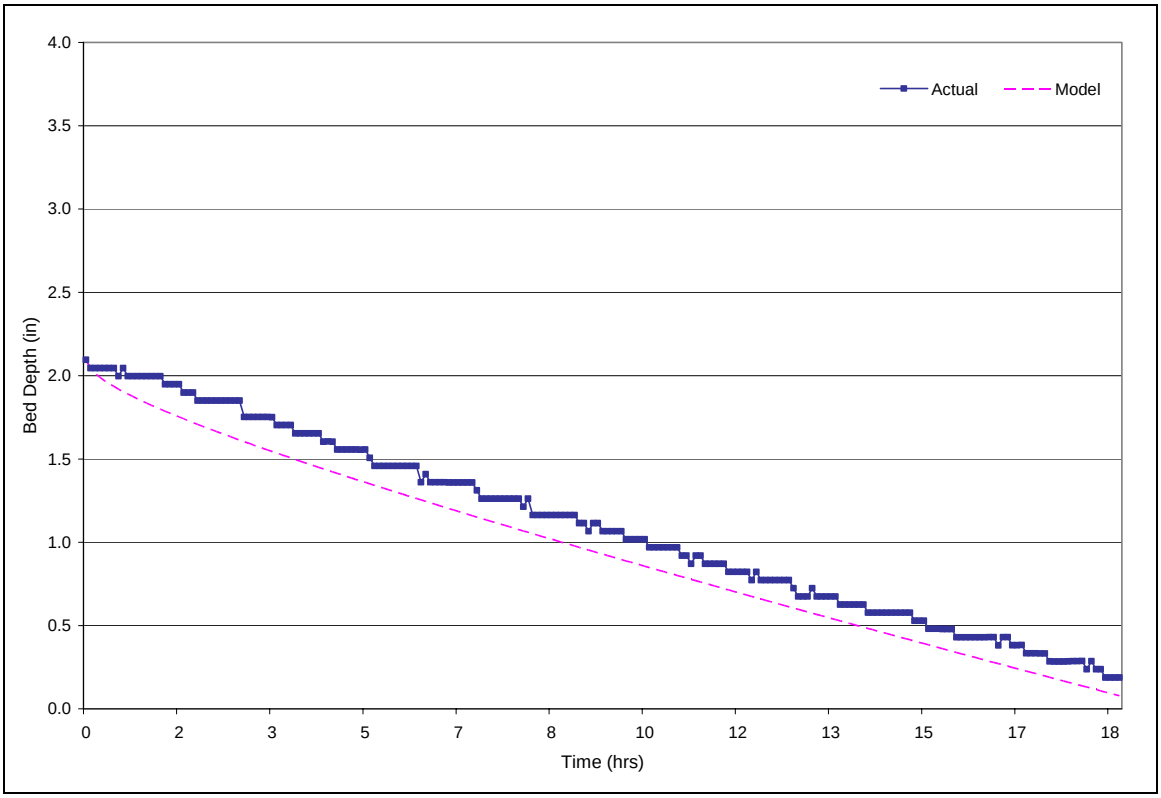

Figure N-6. Event 6/22/2004

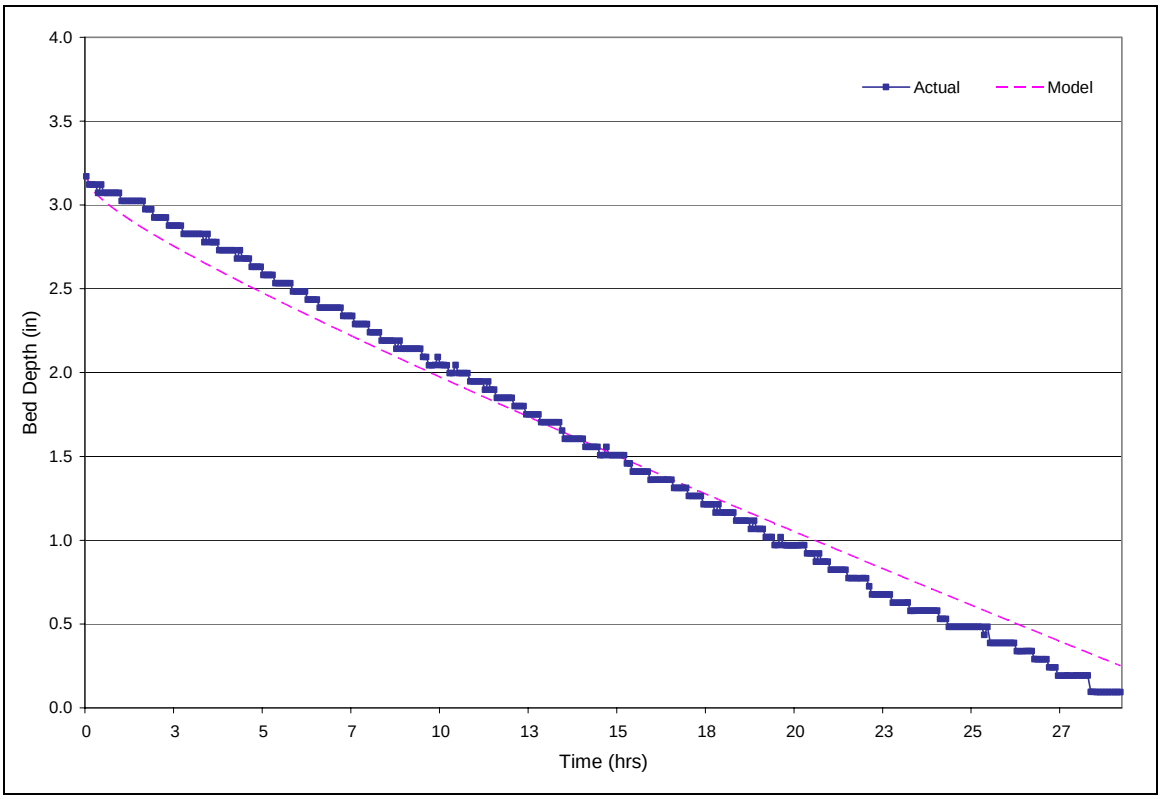

Figure N-7. Event 7/18/2004

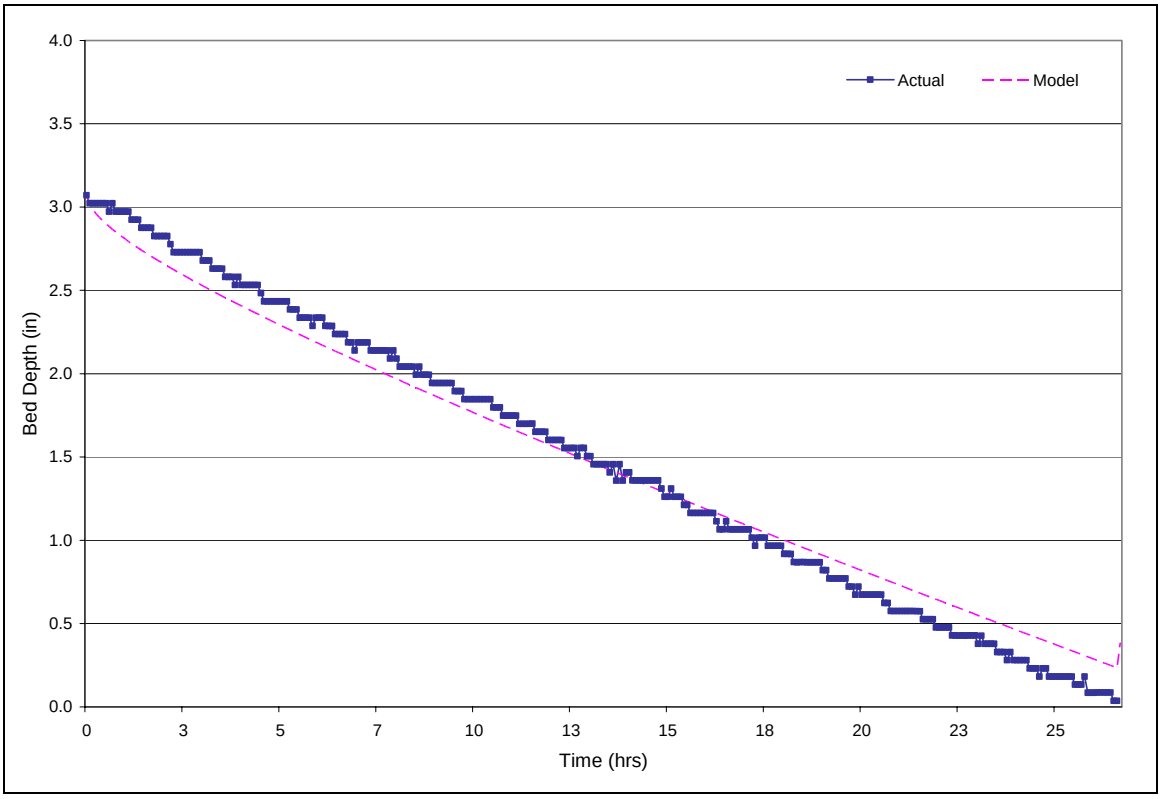

Figure N-8. Event 7/23/2004

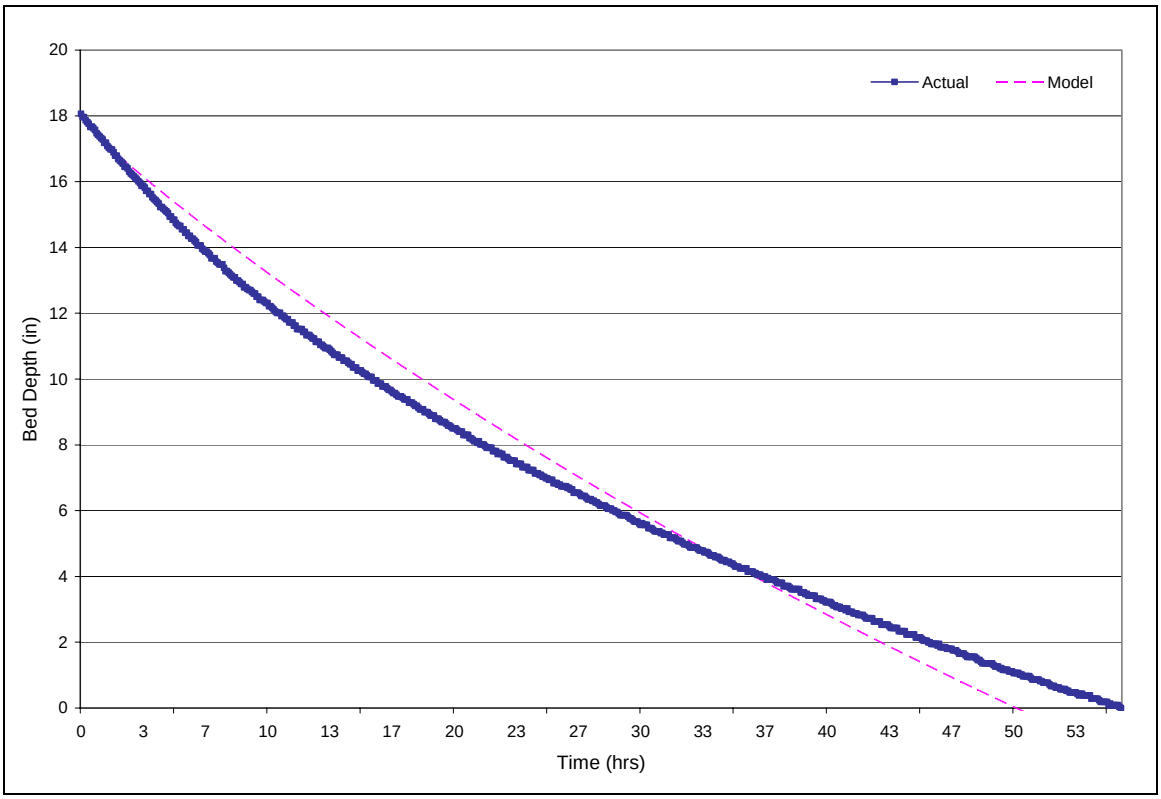

Figure N-9. Event 8/01/2004

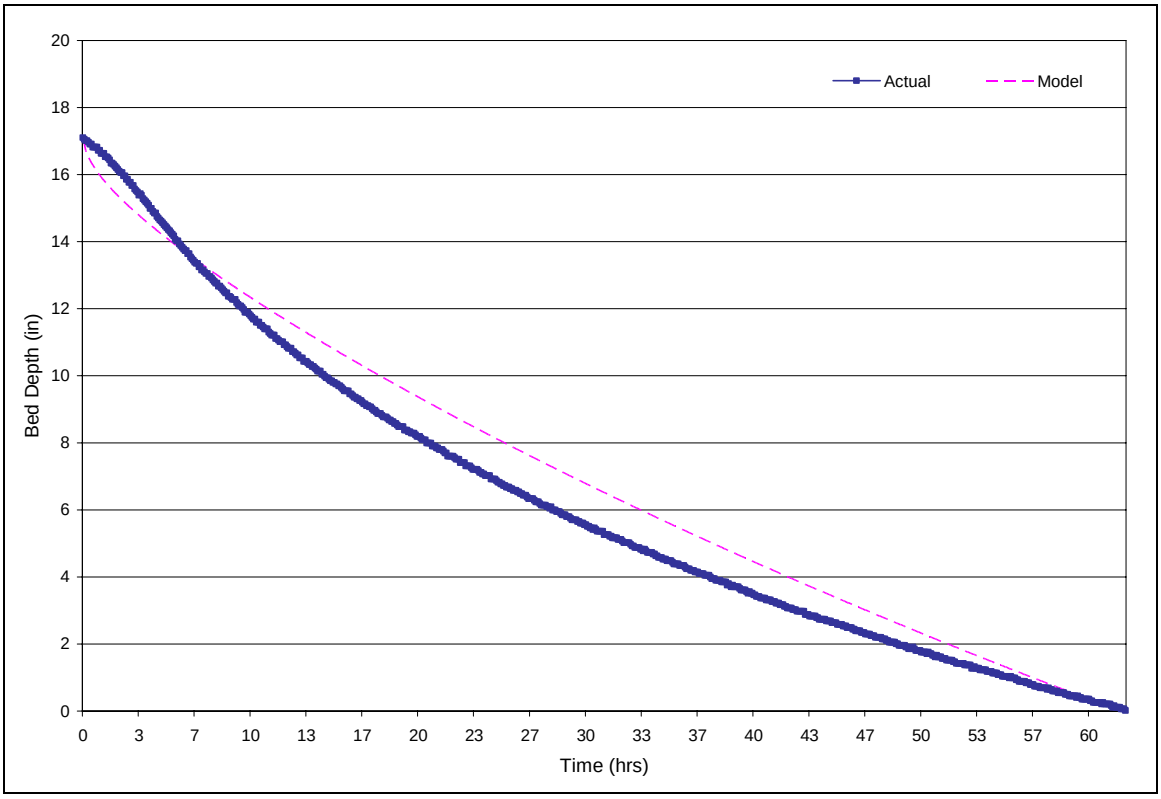

Figure N-10. Event 9/18/2004

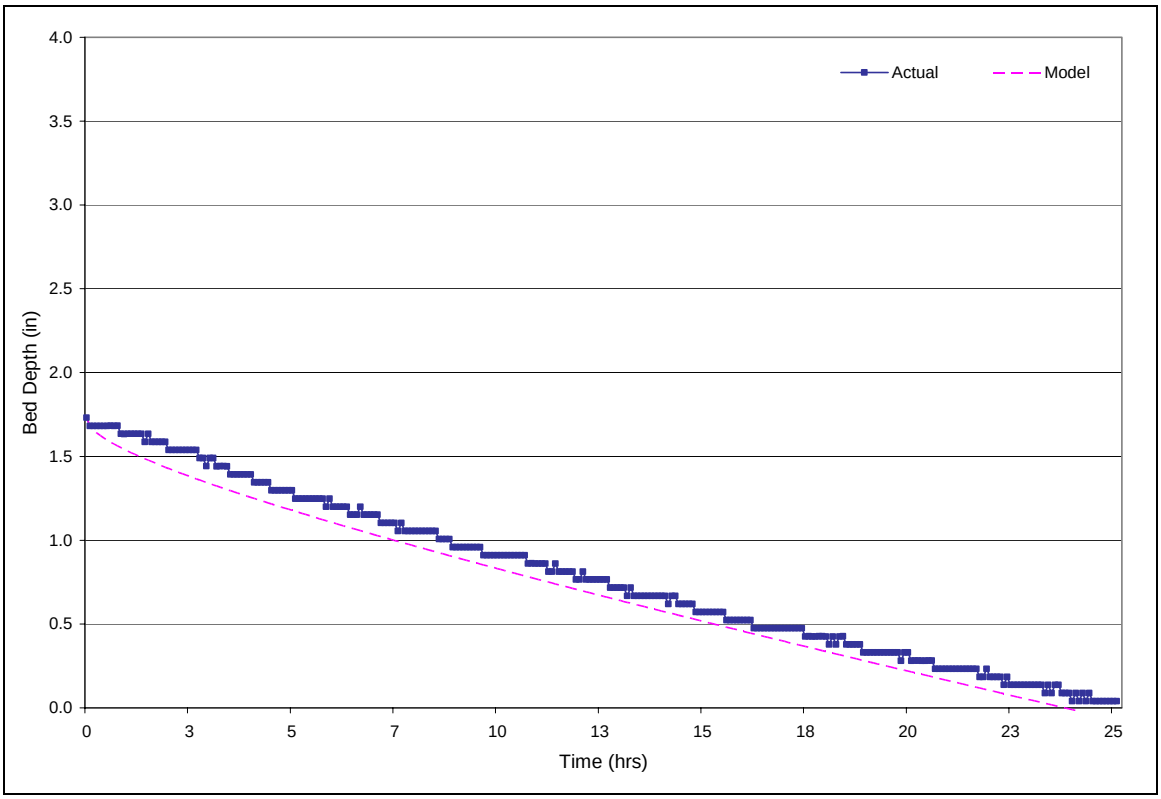

Figure N-11. Event 10/30/2004

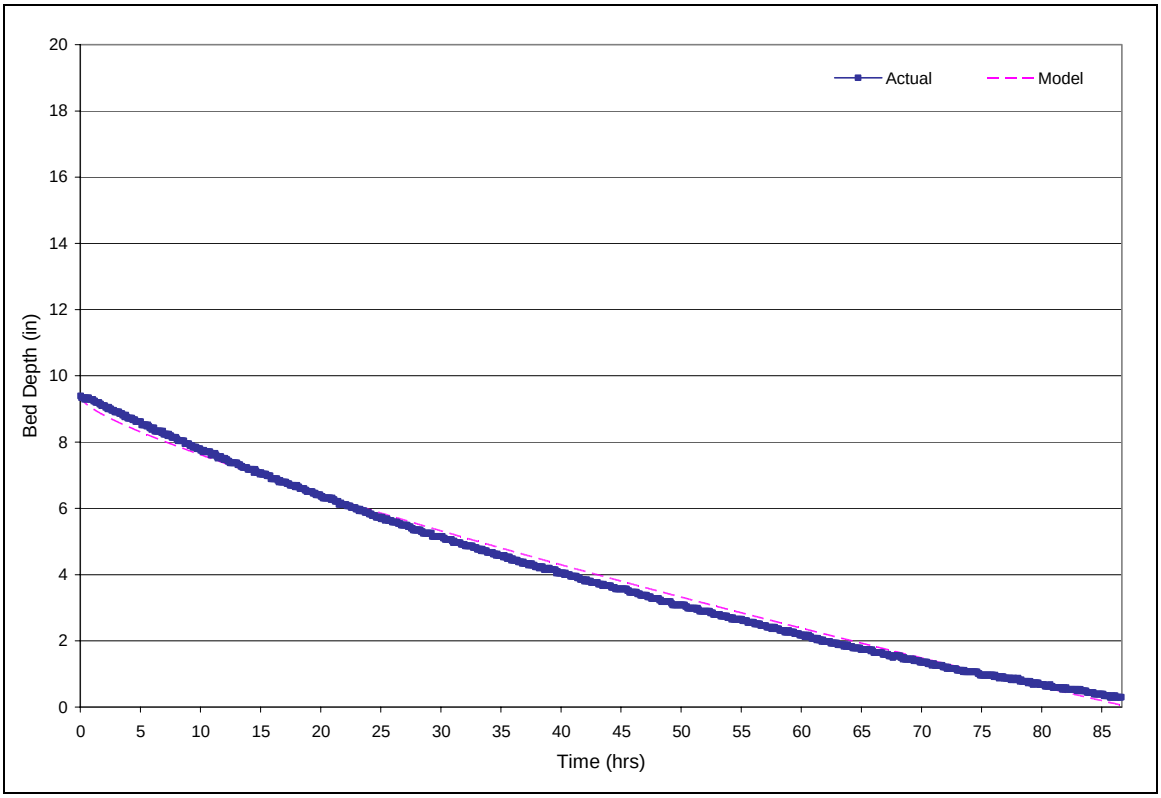

Figure N-12. Event 11/04/2004

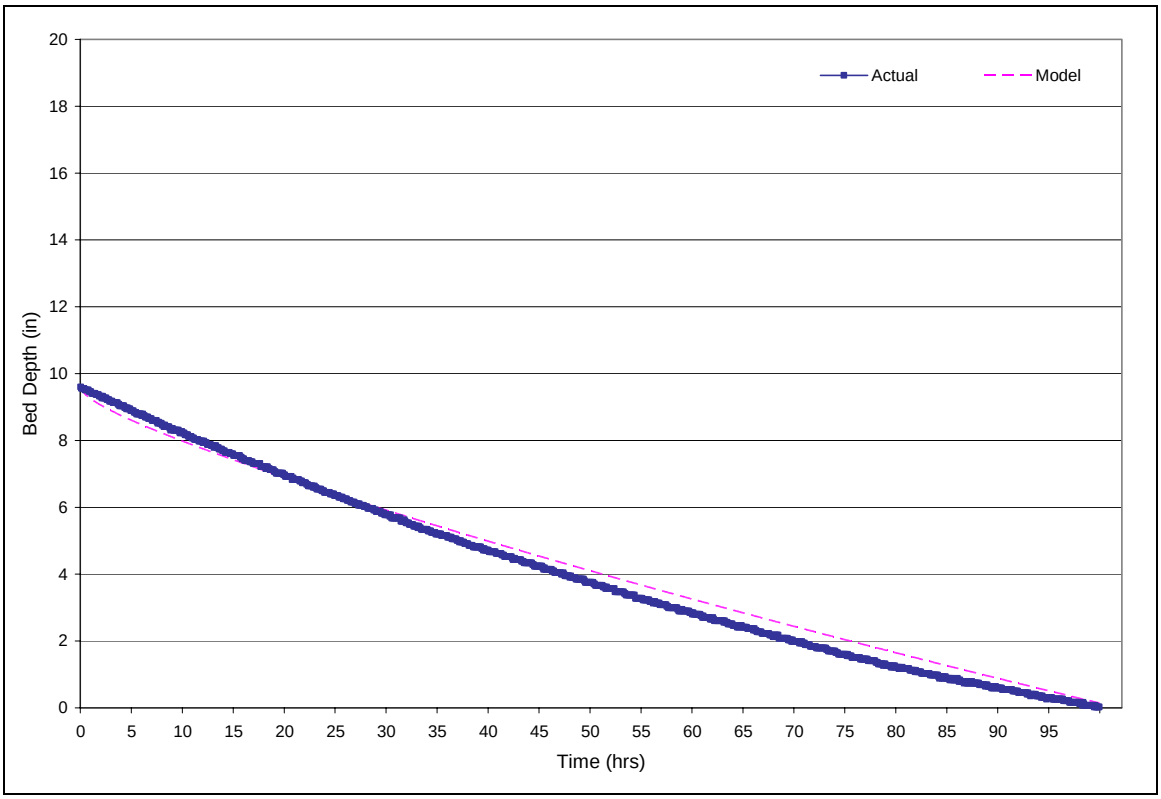

Figure N-13. Event 11/12/2004

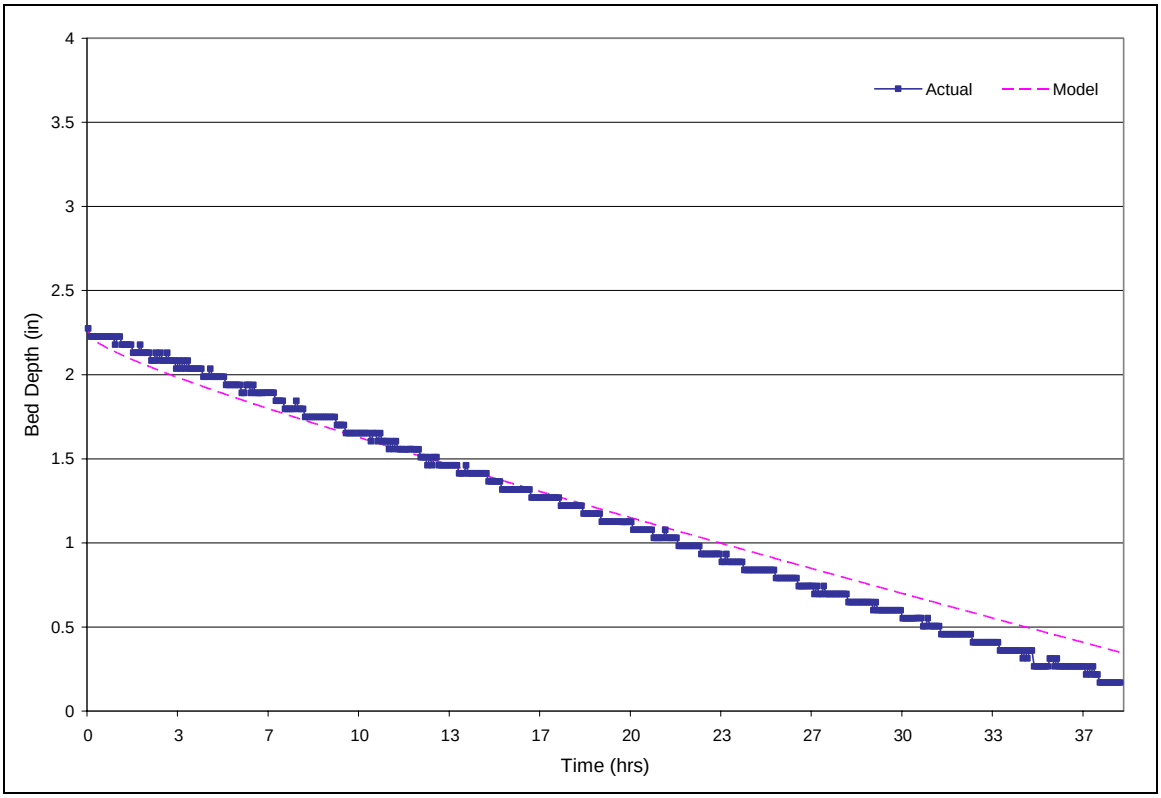

Figure N-14. Event 12/07/2004

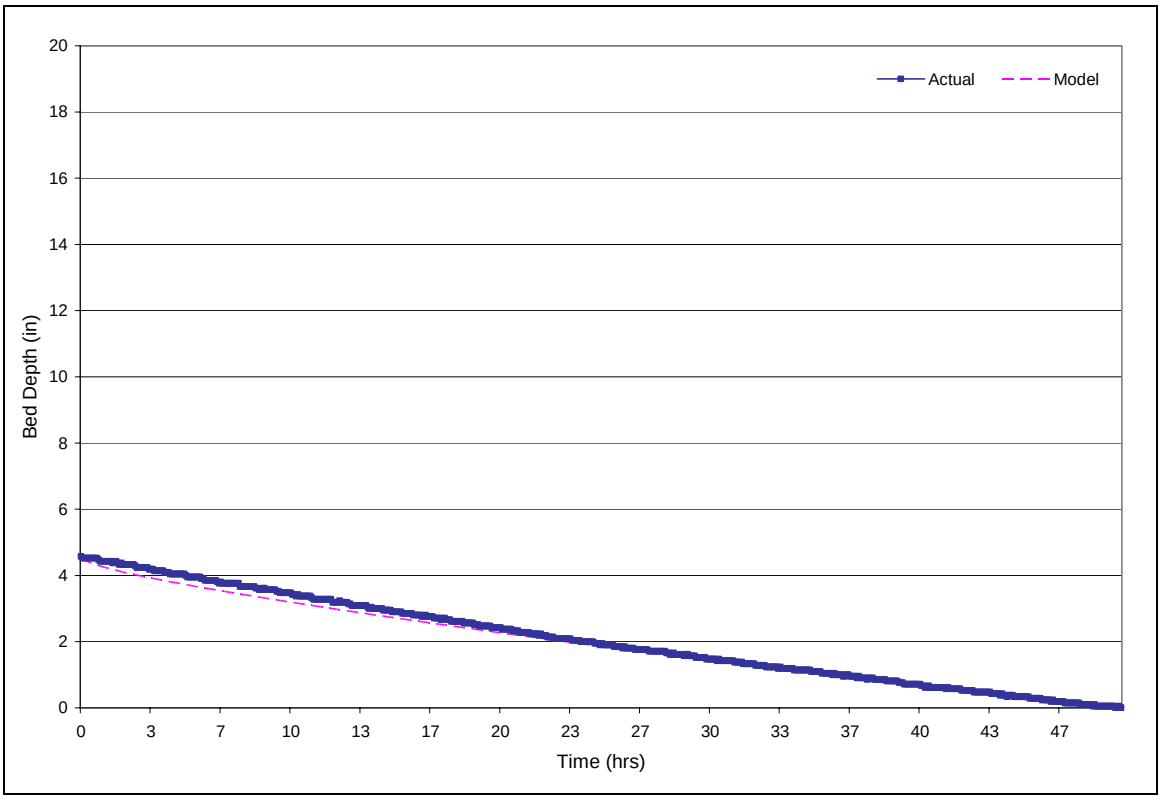

Figure N-15. Event 12/23/2004

Appendix O – Final Model Results: Cumulative Infiltrated Depth

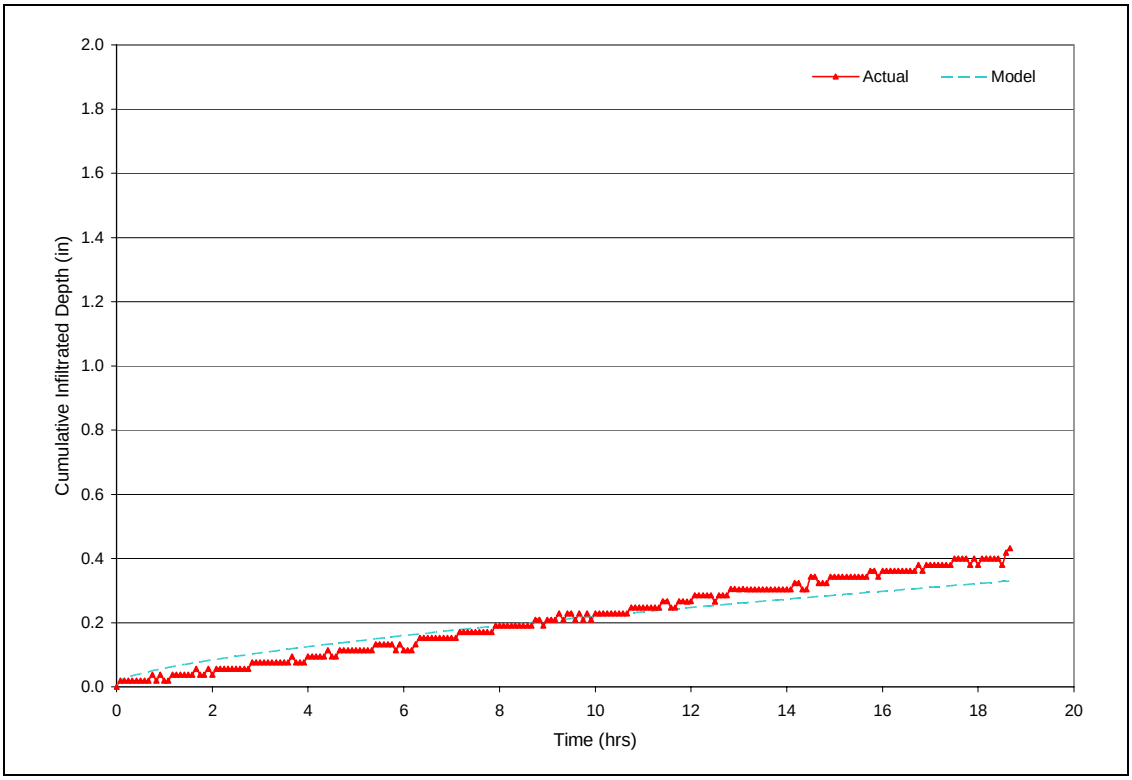

Figure O-1. Event 1/04/2004

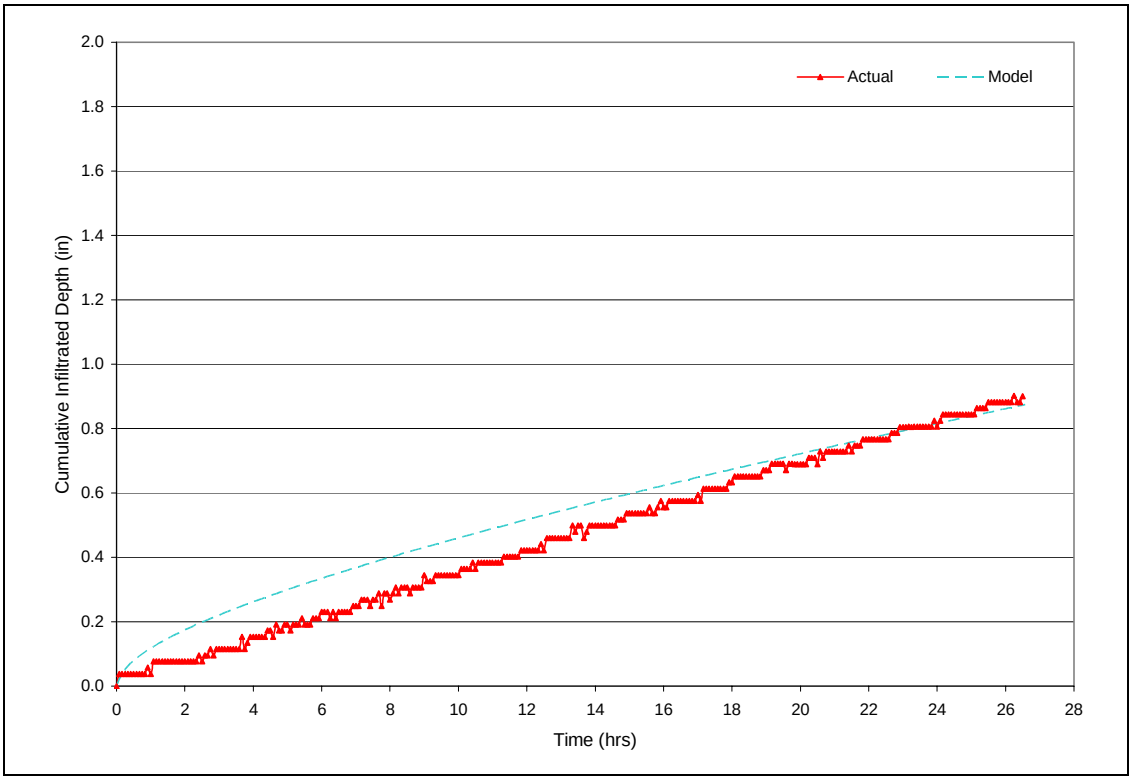

Figure O-2. Event 3/06/2004

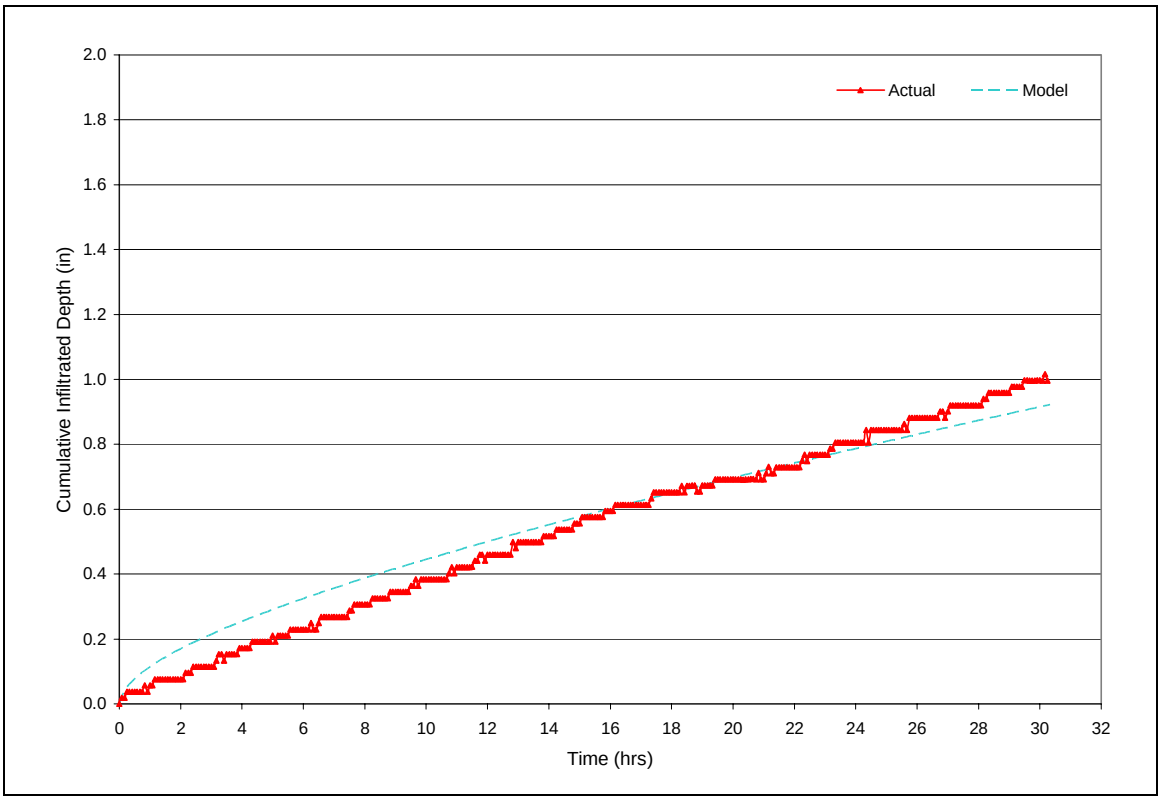

Figure O-3. Event 3/07/2004

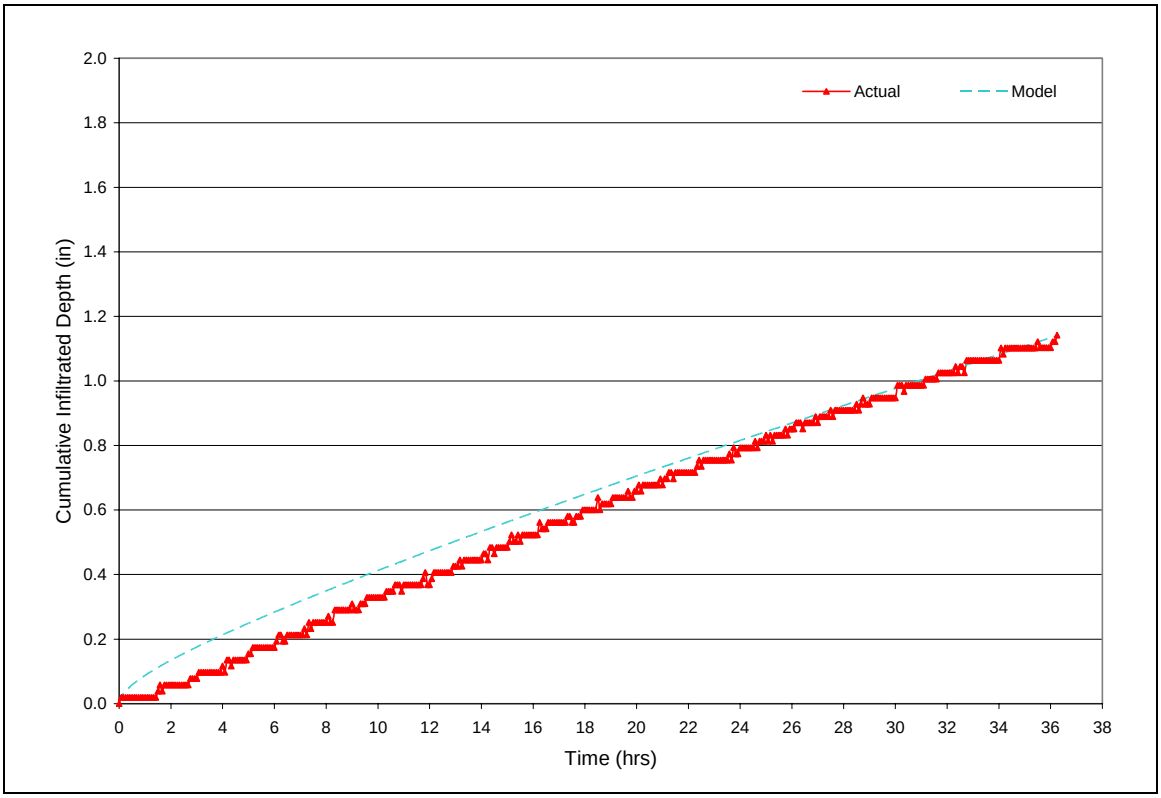

Figure O-4. Event 4/23/2004

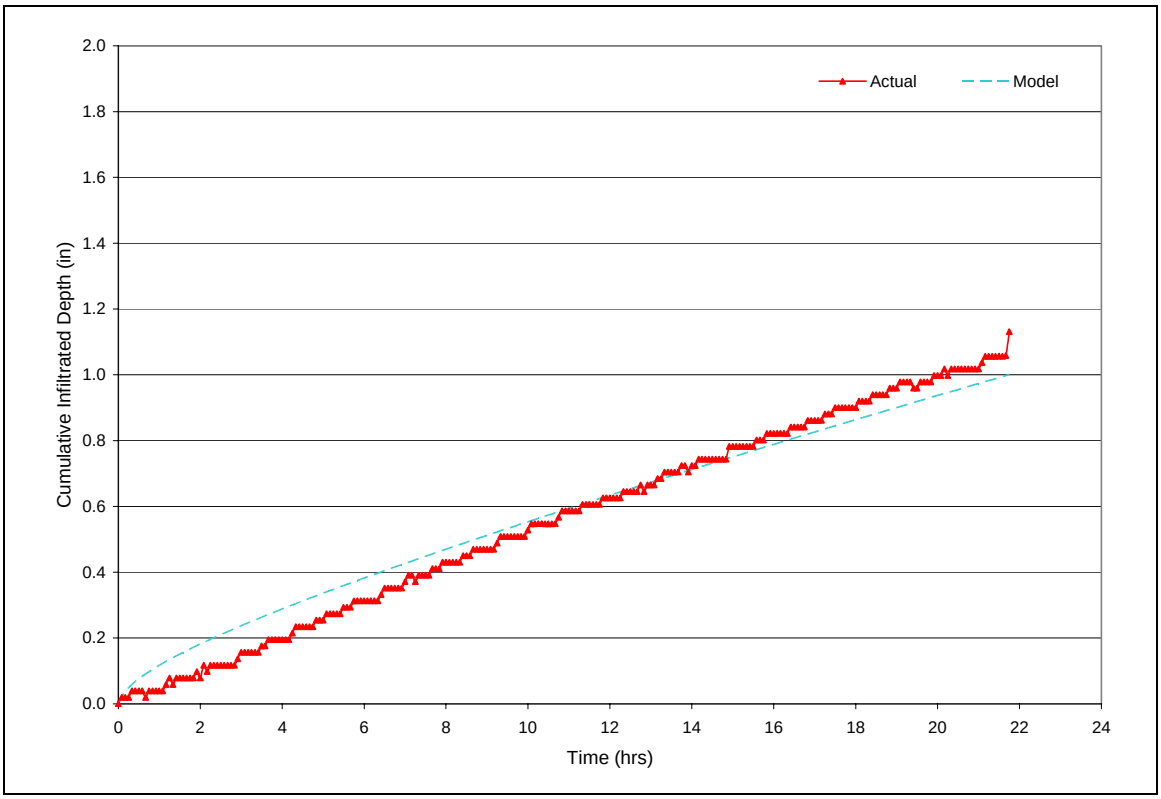

Figure O-5. Event 6/16/2004

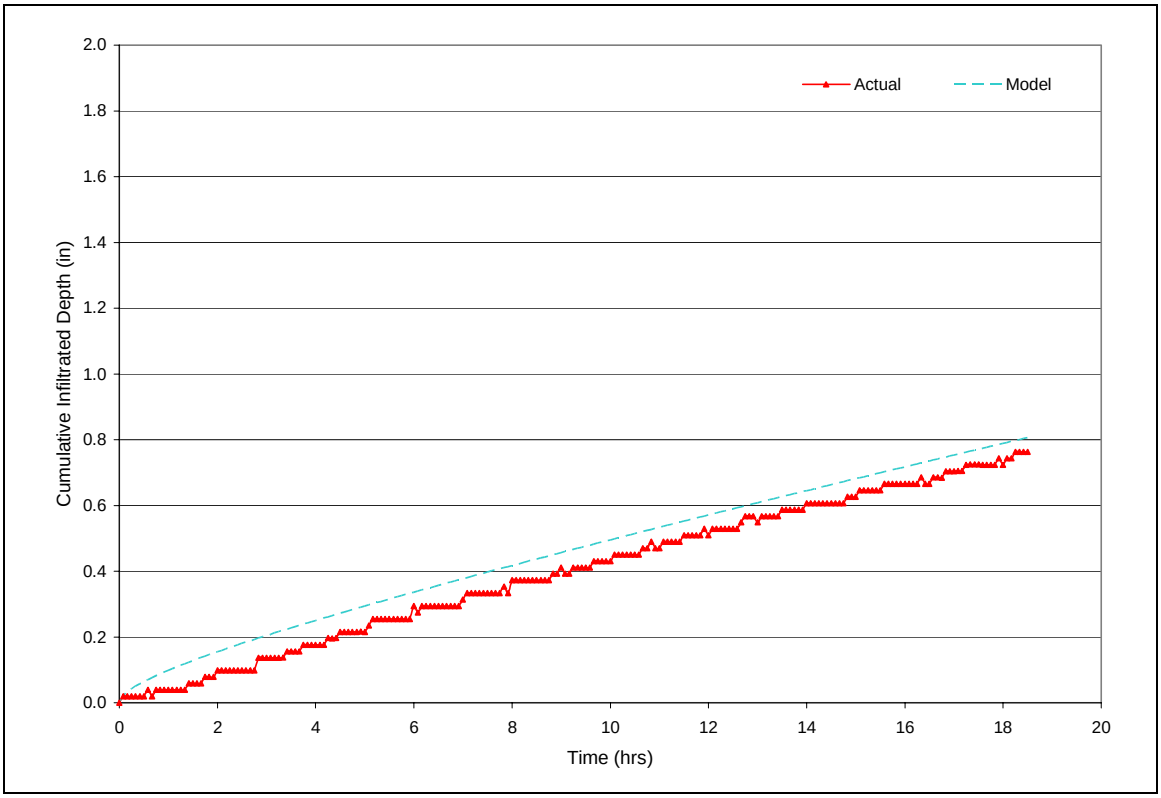

Figure O-6. Event 6/22/2004

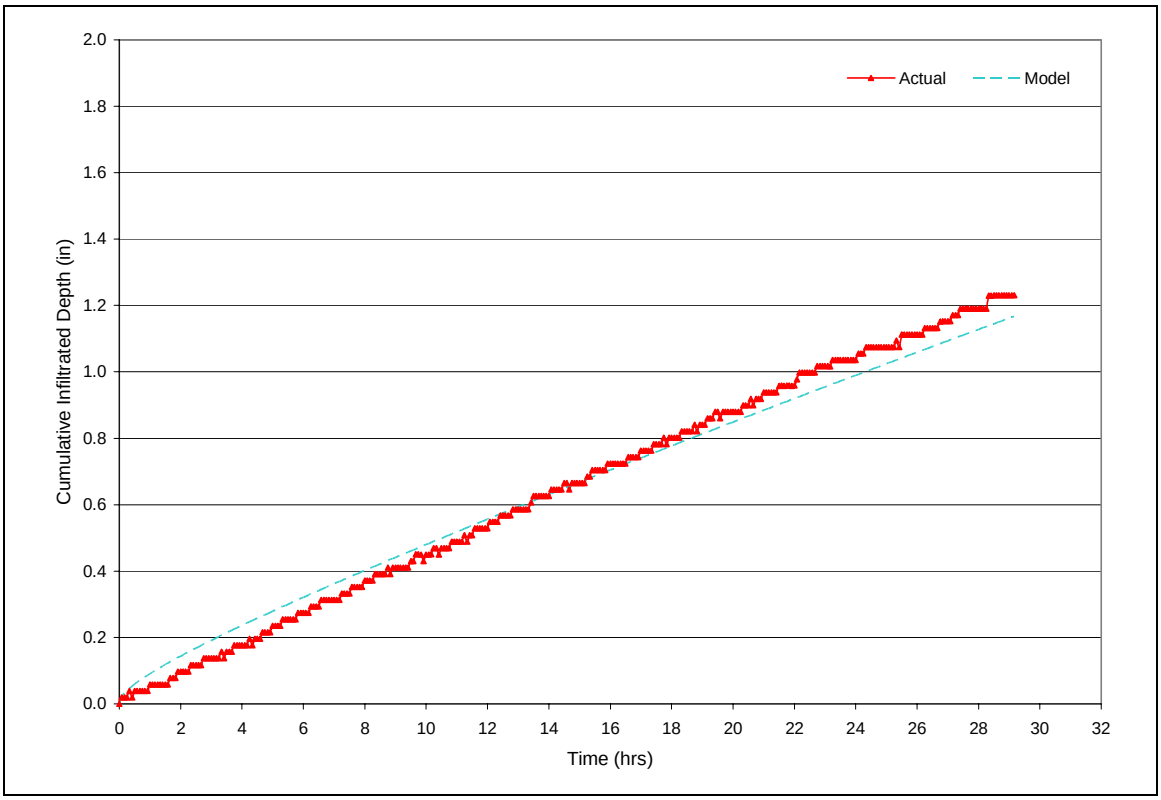

Figure O-7. Event 7/18/2004

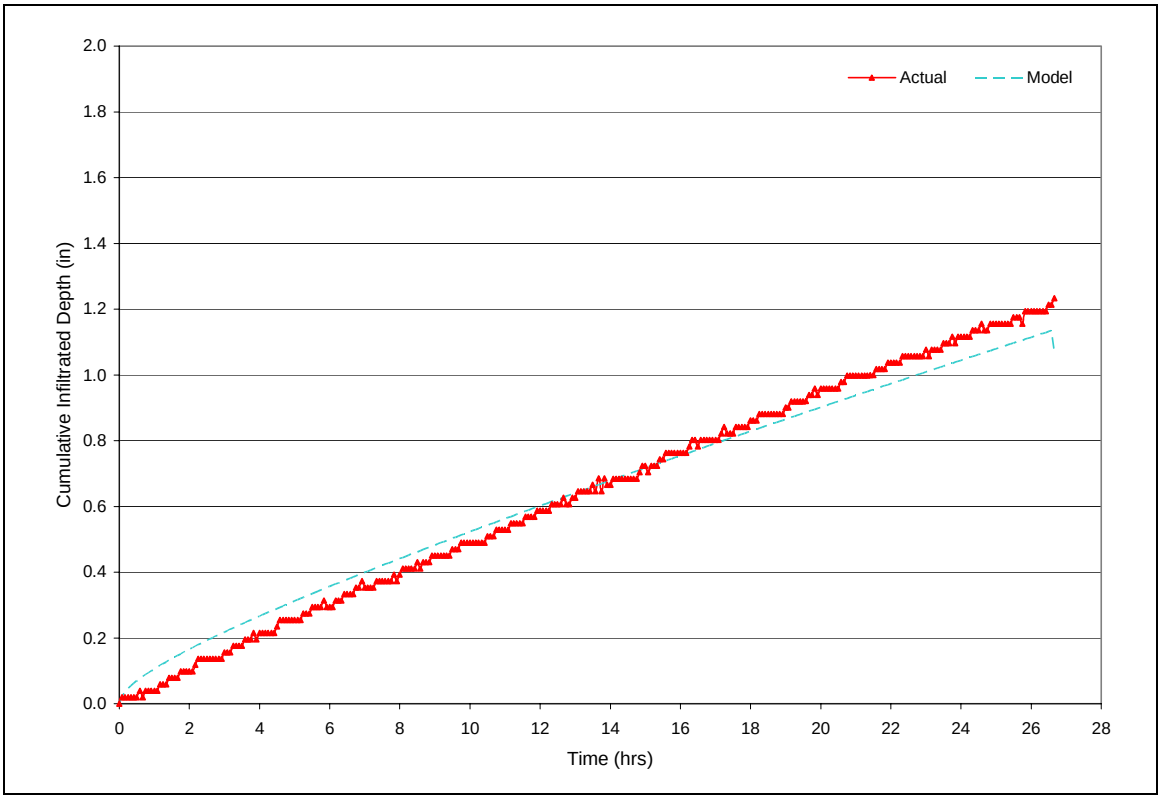

Figure O-8. Event 7/23/2004

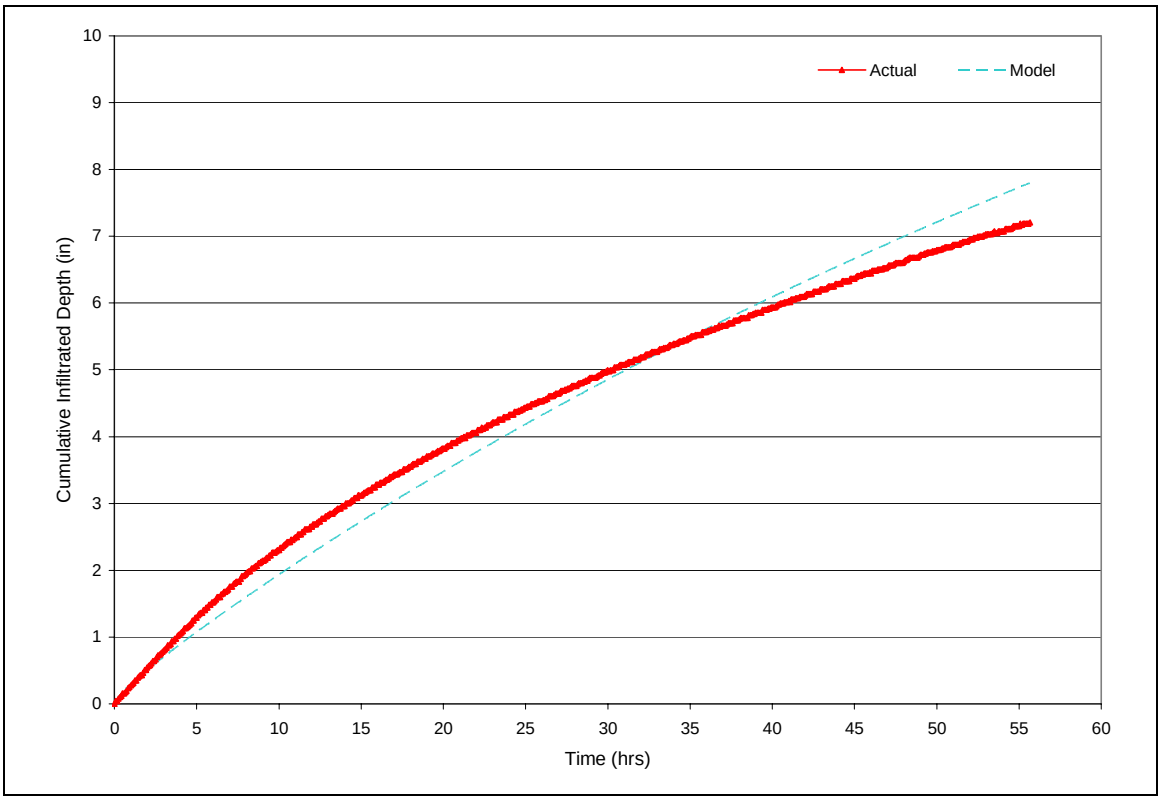

Figure O-9. Event 8/01/2004

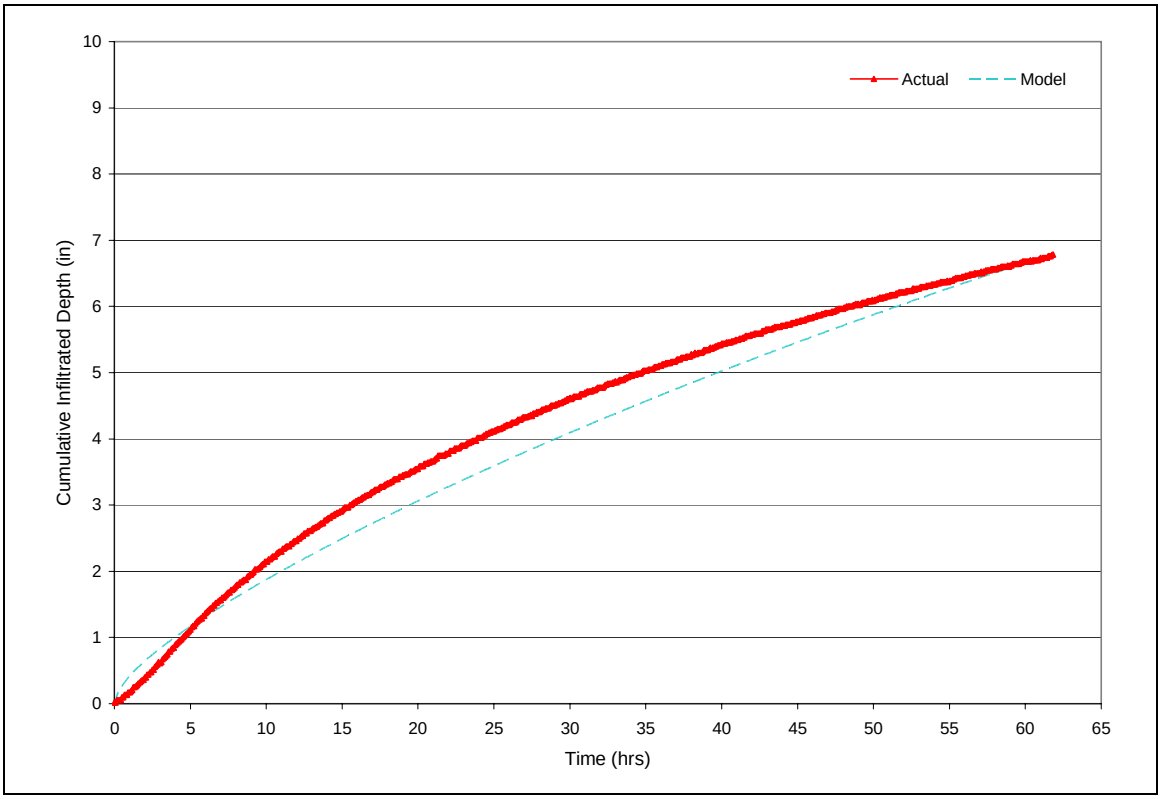

Figure O-10. Event 9/18/2004

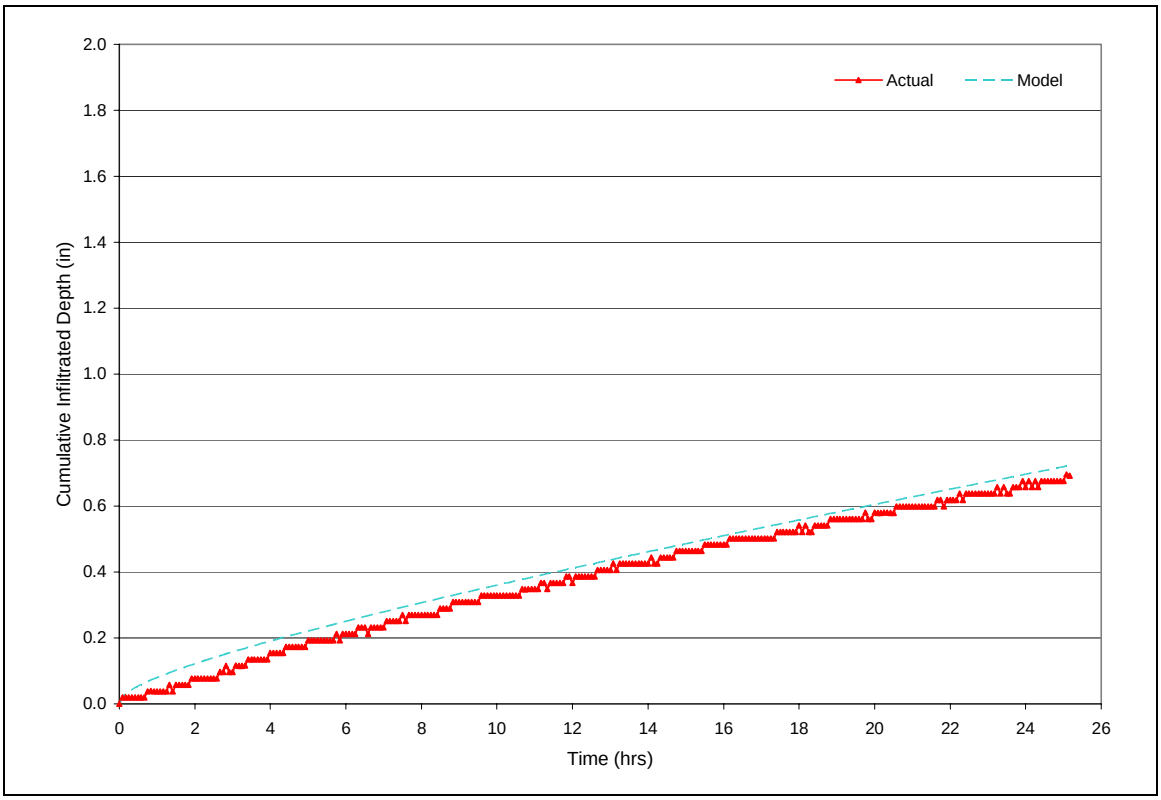

Figure O-11. Event 10/30/2004

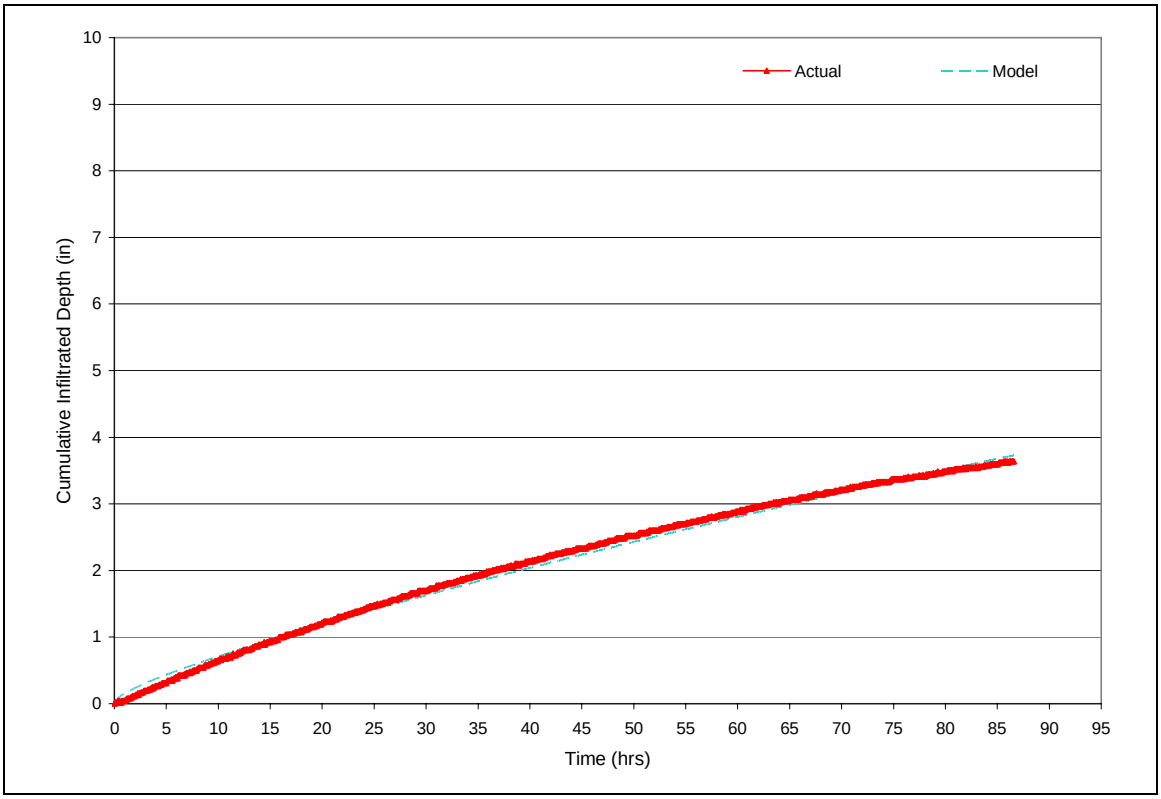

Figure O-12. Event 11/04/2004

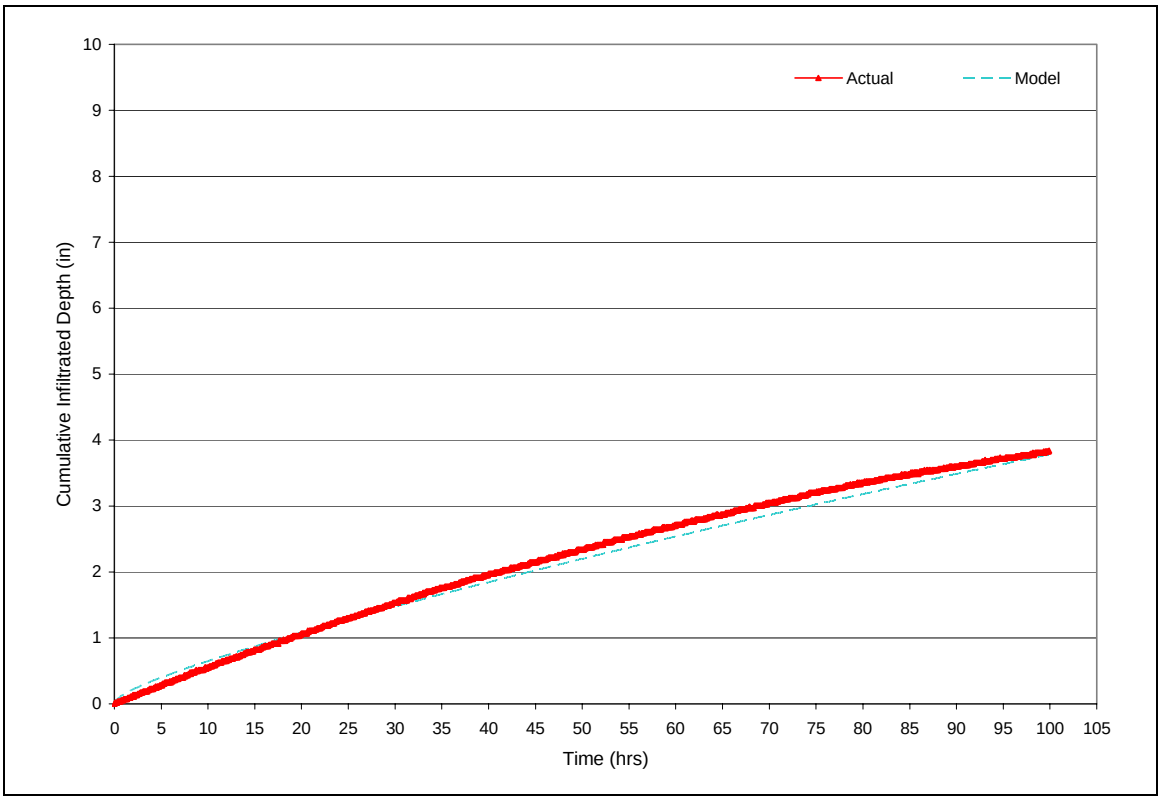

Figure O-13. Event 11/12/2004

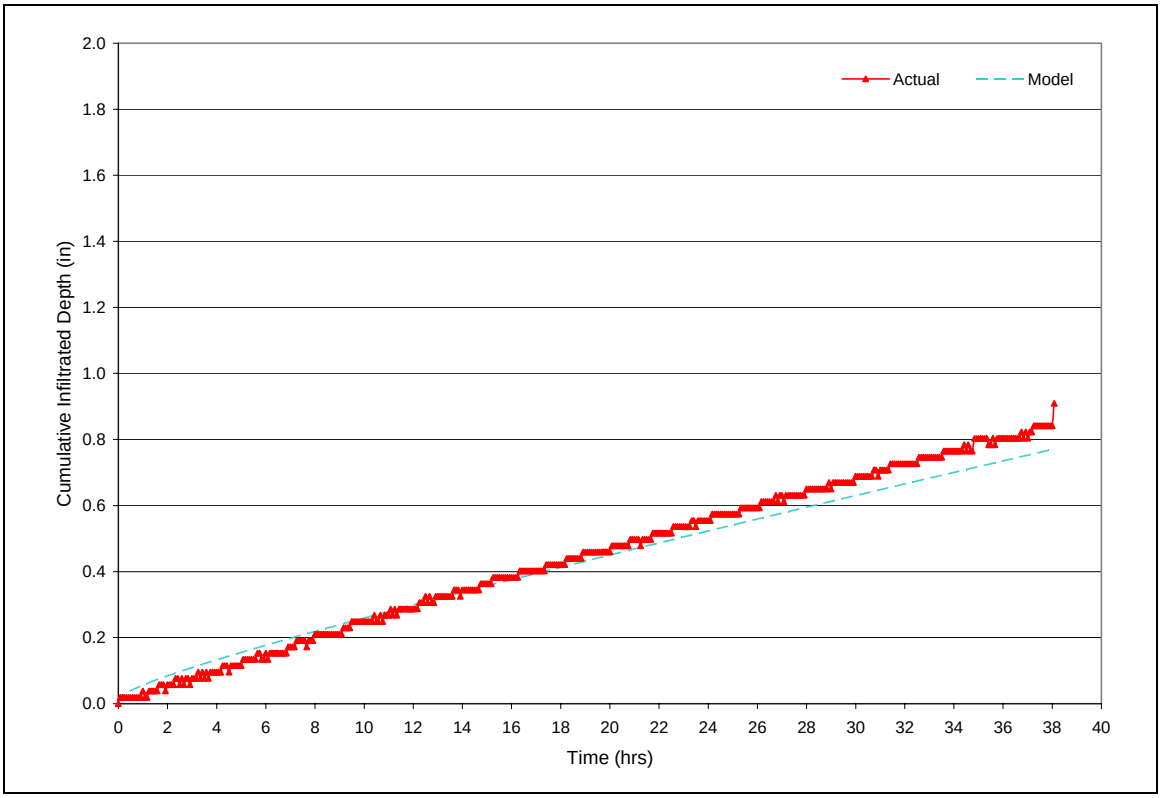

Figure O-14. Event 12/07/2004

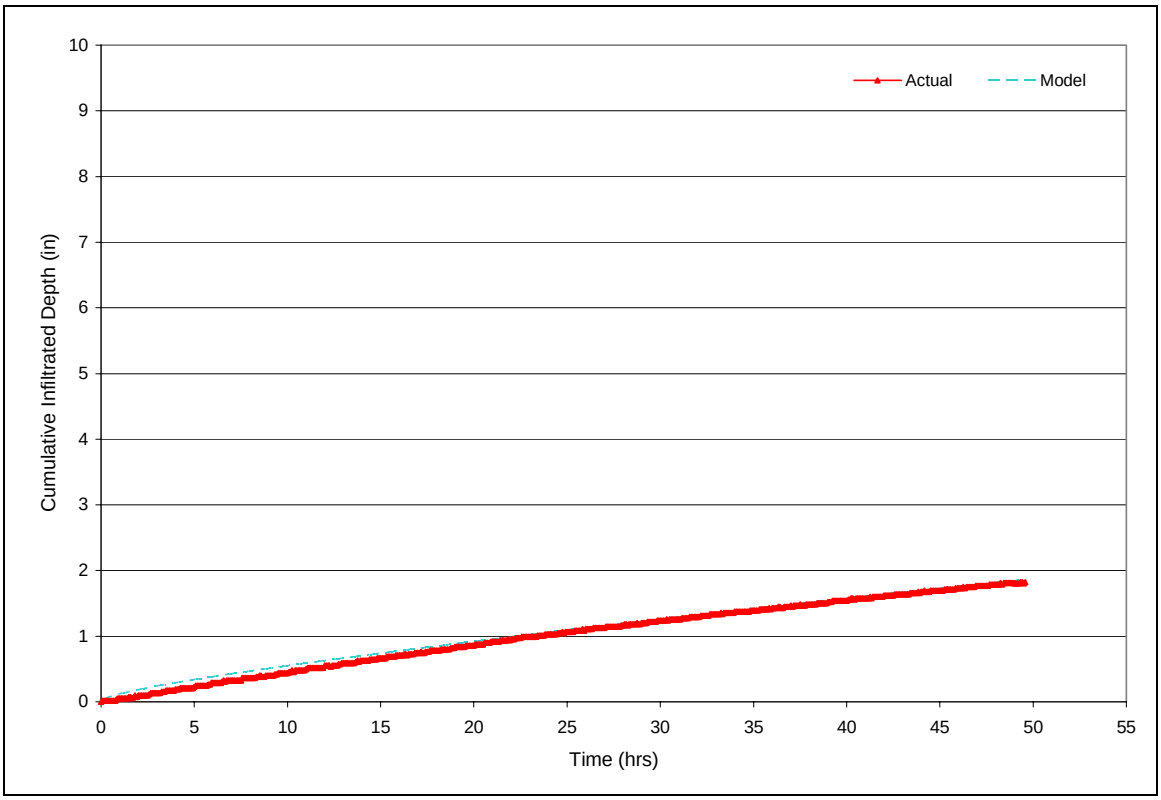

Figure O-15. Event 12/23/2004

Appendix P – Model Calibration: Additional Event Results

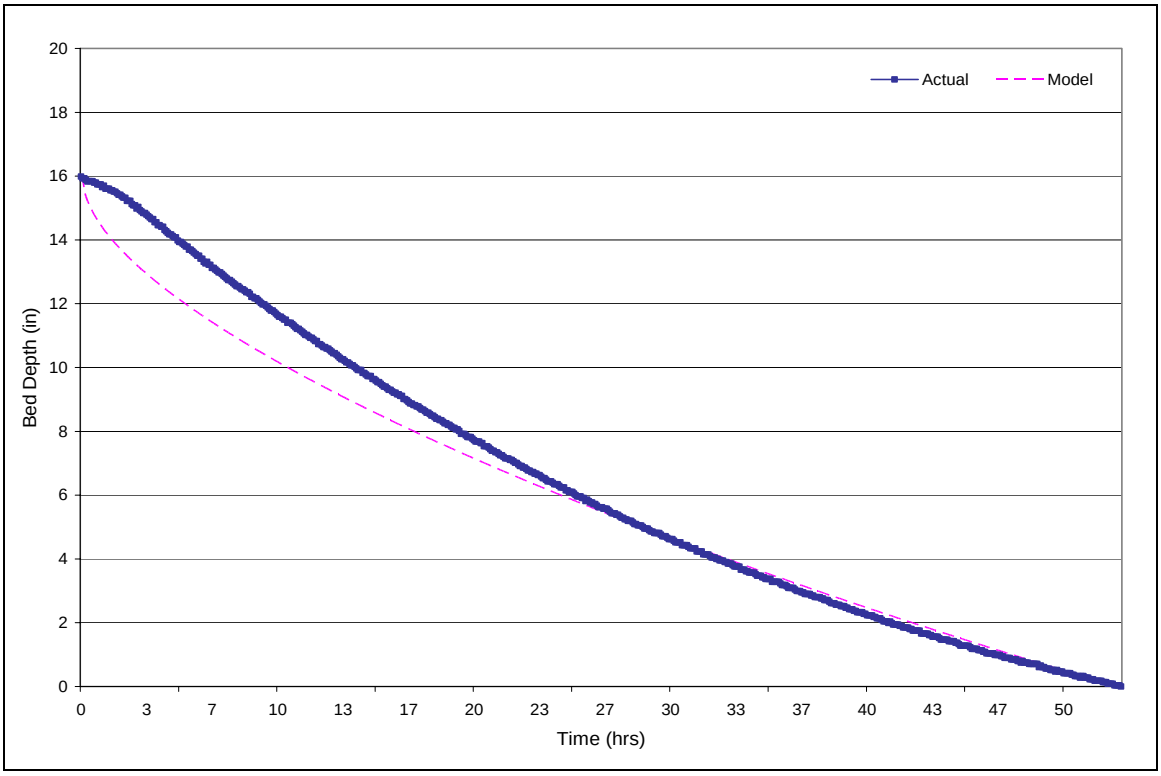

Figure P-1. Recession Limb Event 01/13/2005

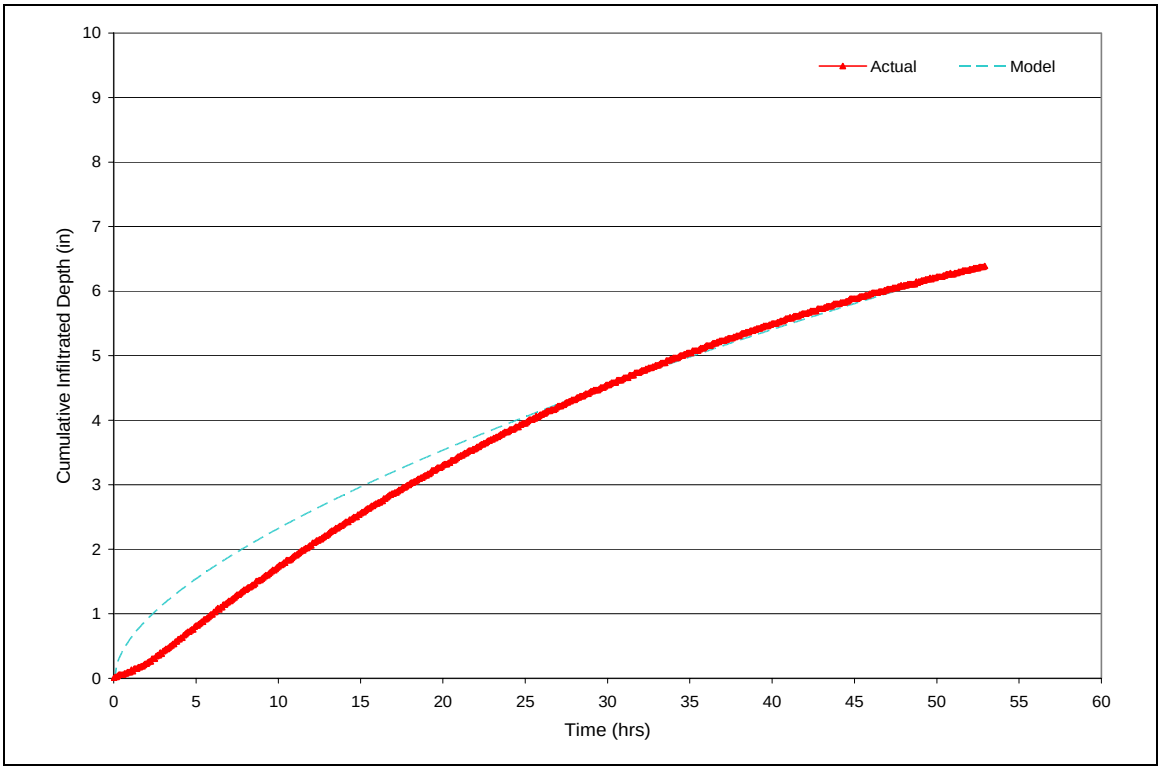

Figure P-2. Cumulative Infiltrated Depth Event 01/13/2005

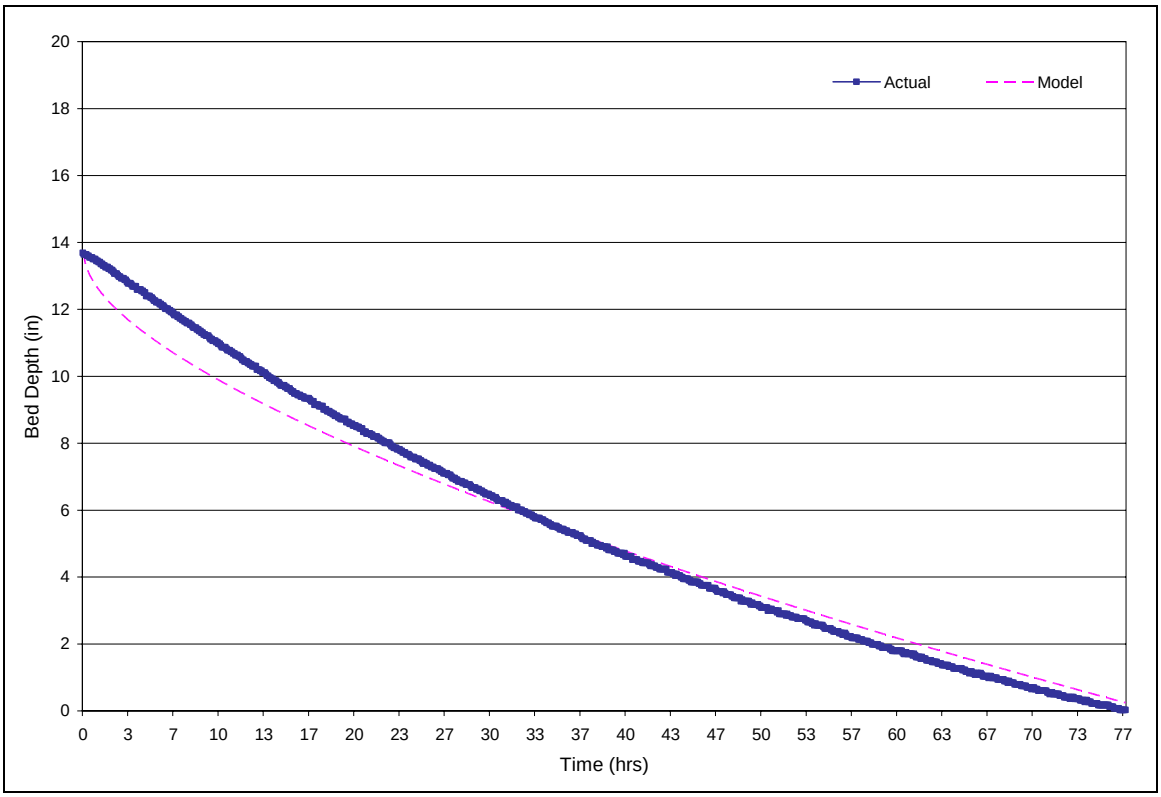

Figure P-3. Recession Limb Event 03/27/2005

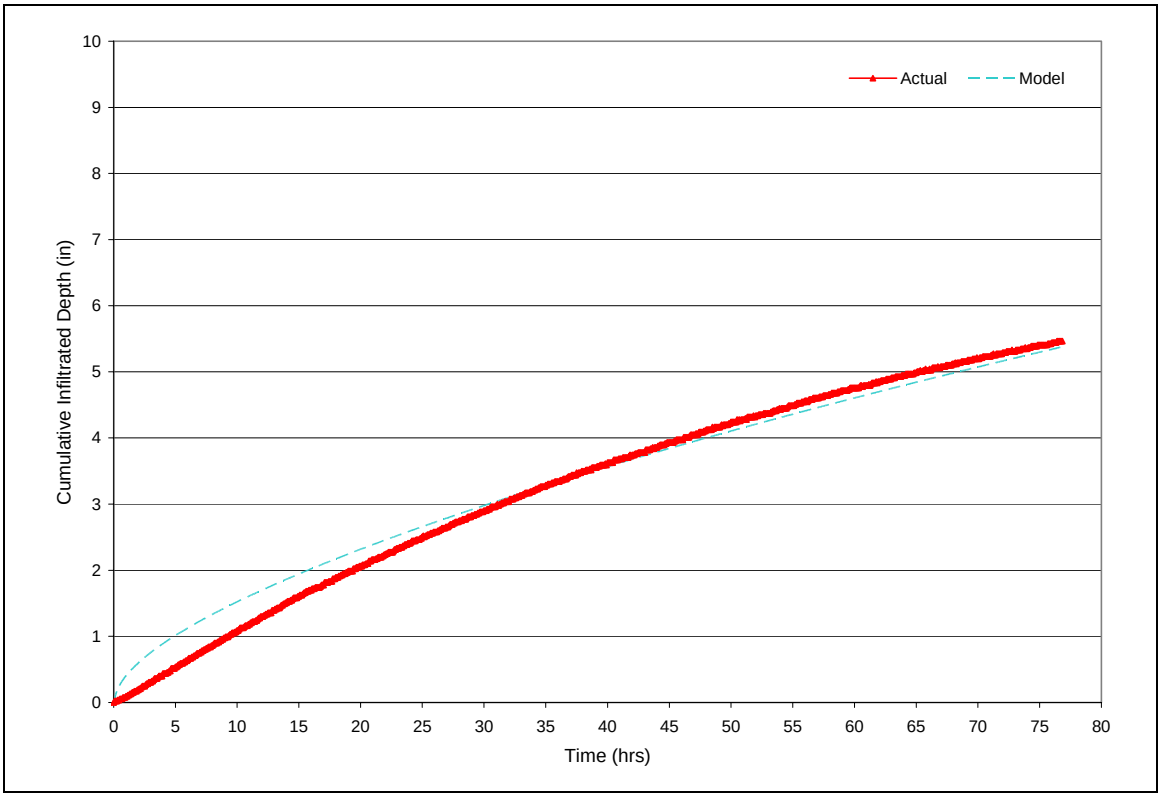

Figure P-4. Cumulative Infiltrated Depth Event 03/27/2005

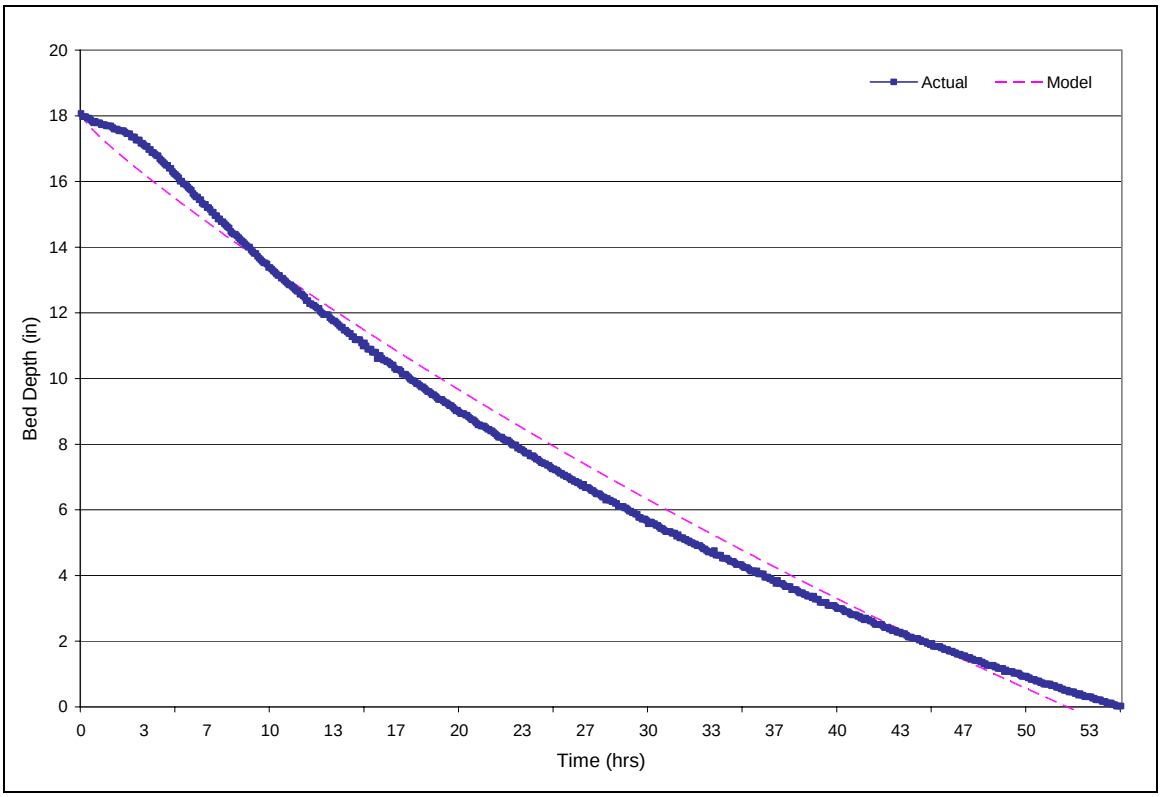

Figure P-5. Recession Limb Event 04/01/2005

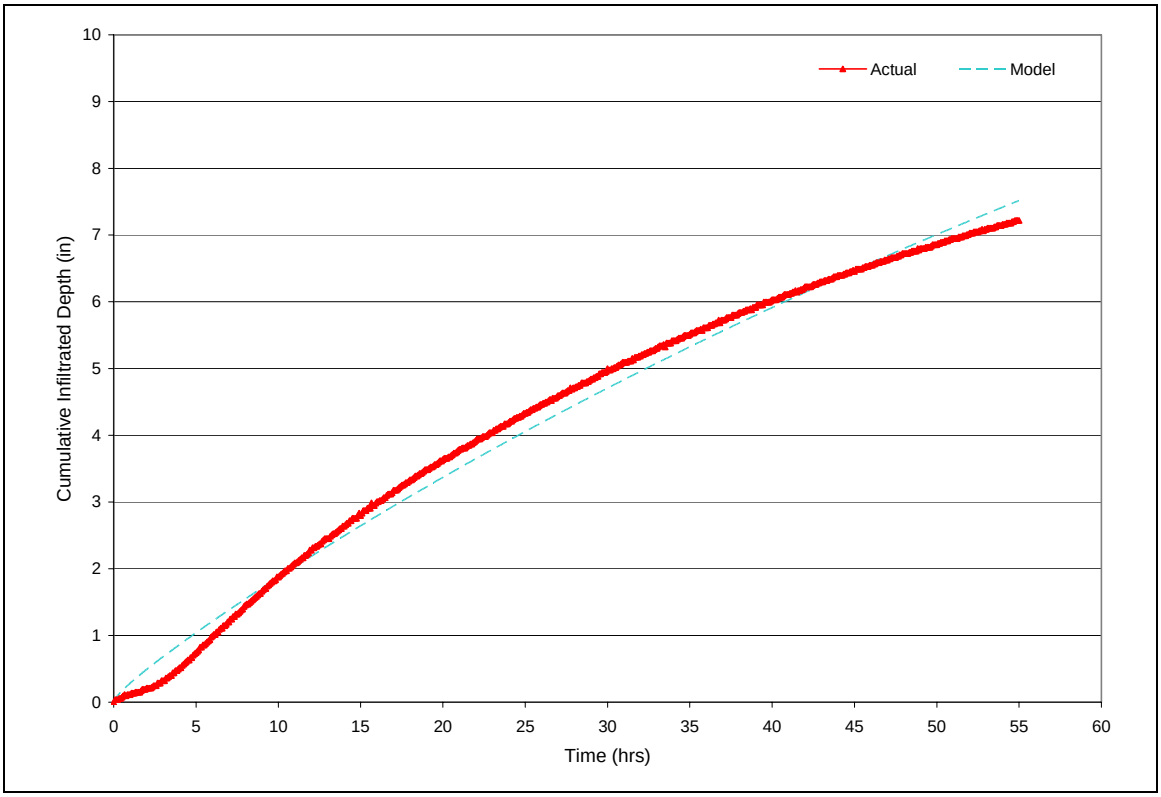

Figure P-6. Cumulative Infiltrated Depth Event 04/01/2005

Appendix Q – Model Verification: Small Event Results

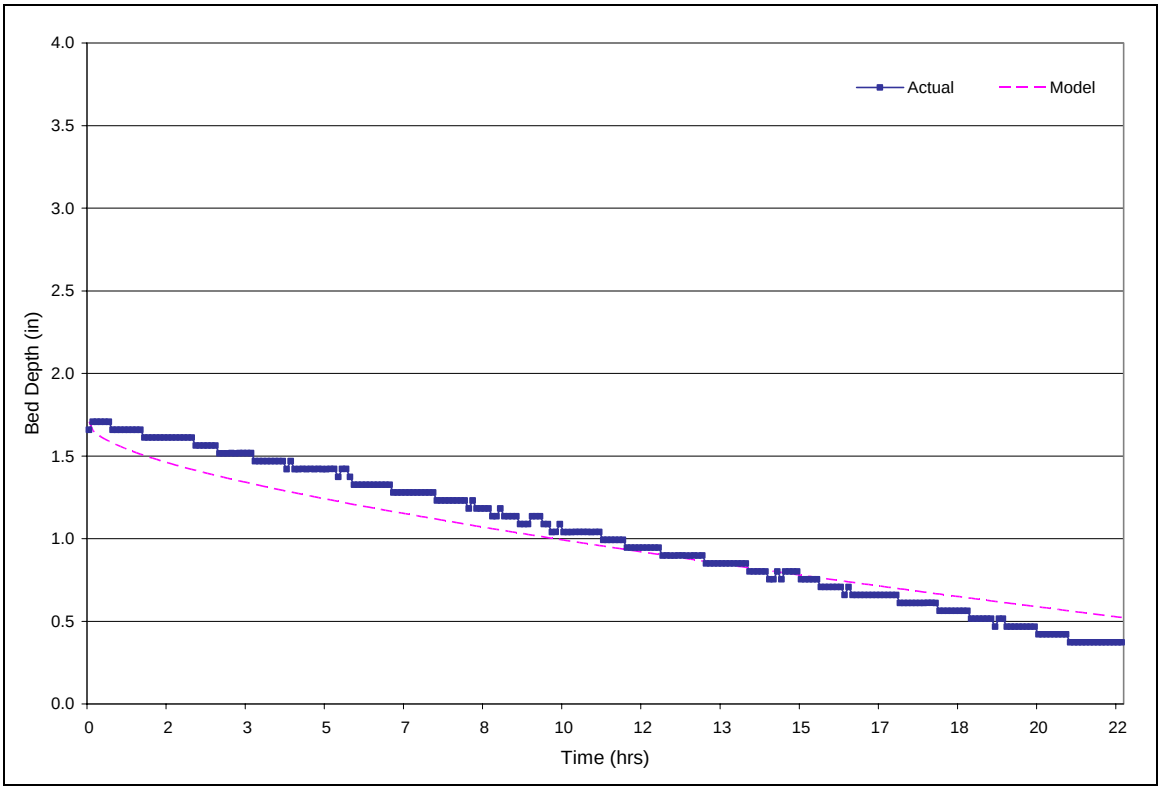

Figure Q-1. Recession Limb Event 01/15/2005

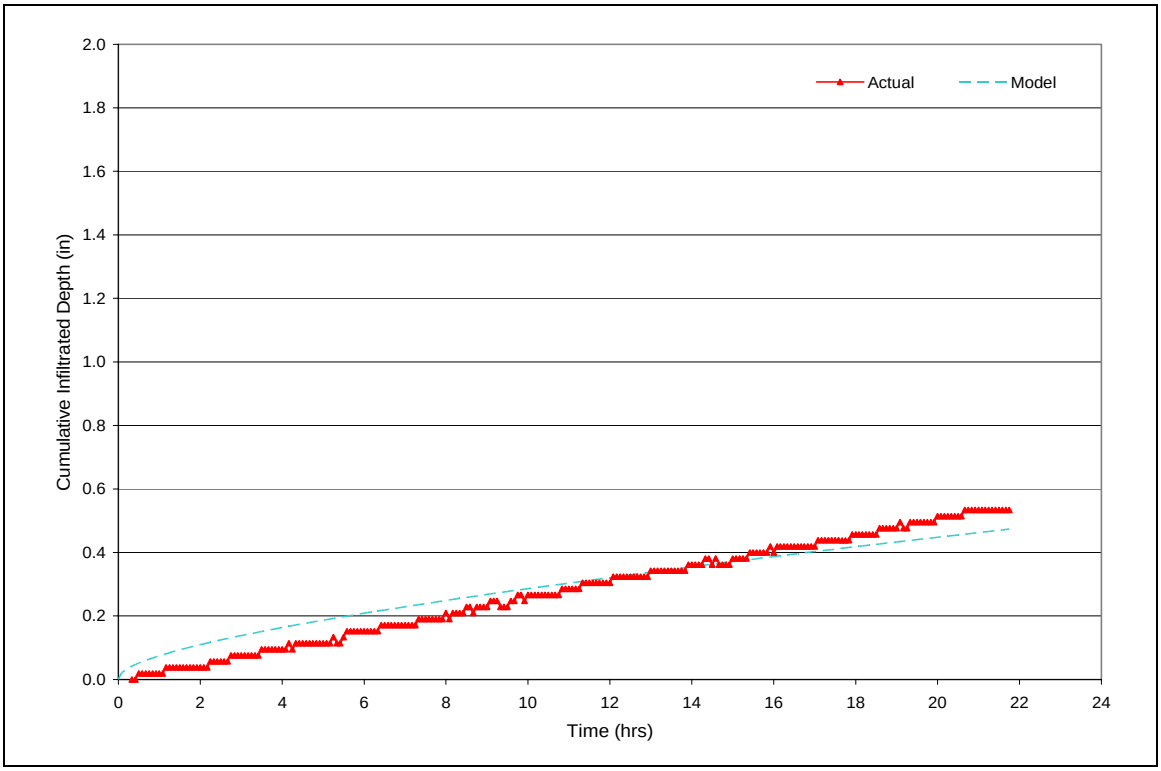

Figure Q-2. Cumulative Infiltrated Depth Event 01/15/2005

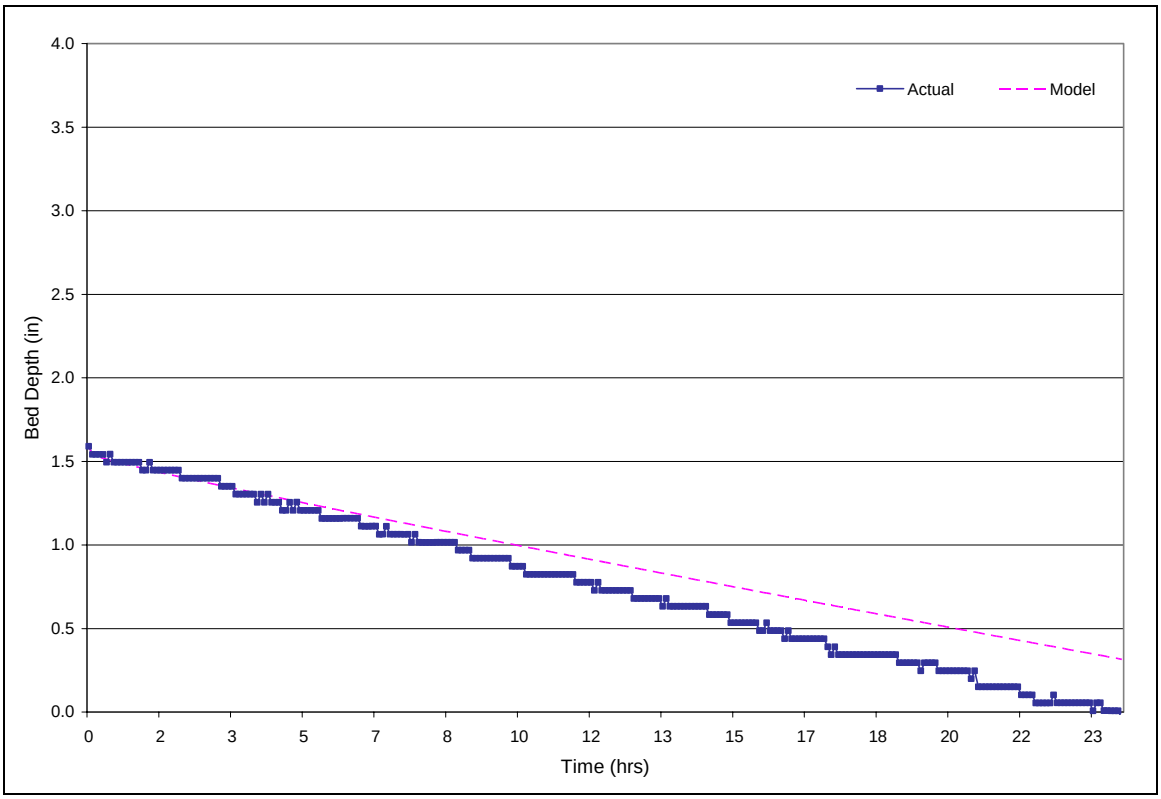

Figure Q-3. Recession Limb Event 04/07/2005

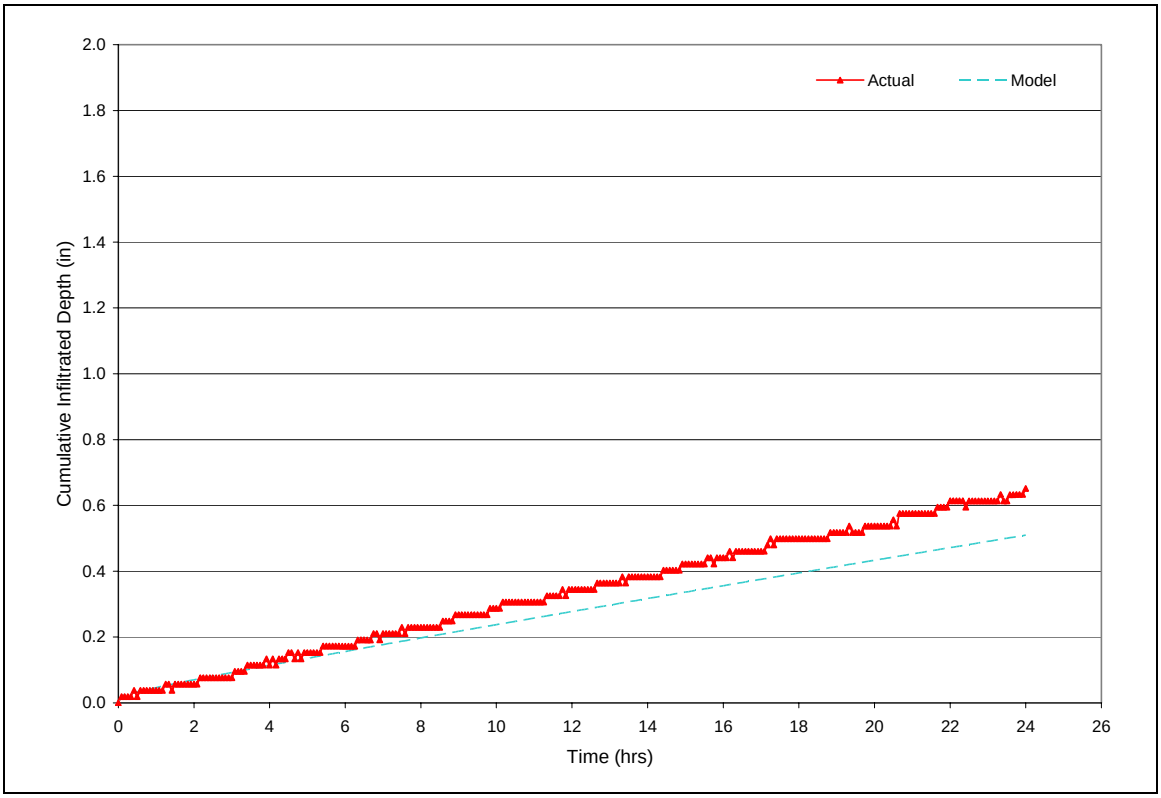

Figure Q-4. Cumulative Infiltrated Depth Event 04/07/2005

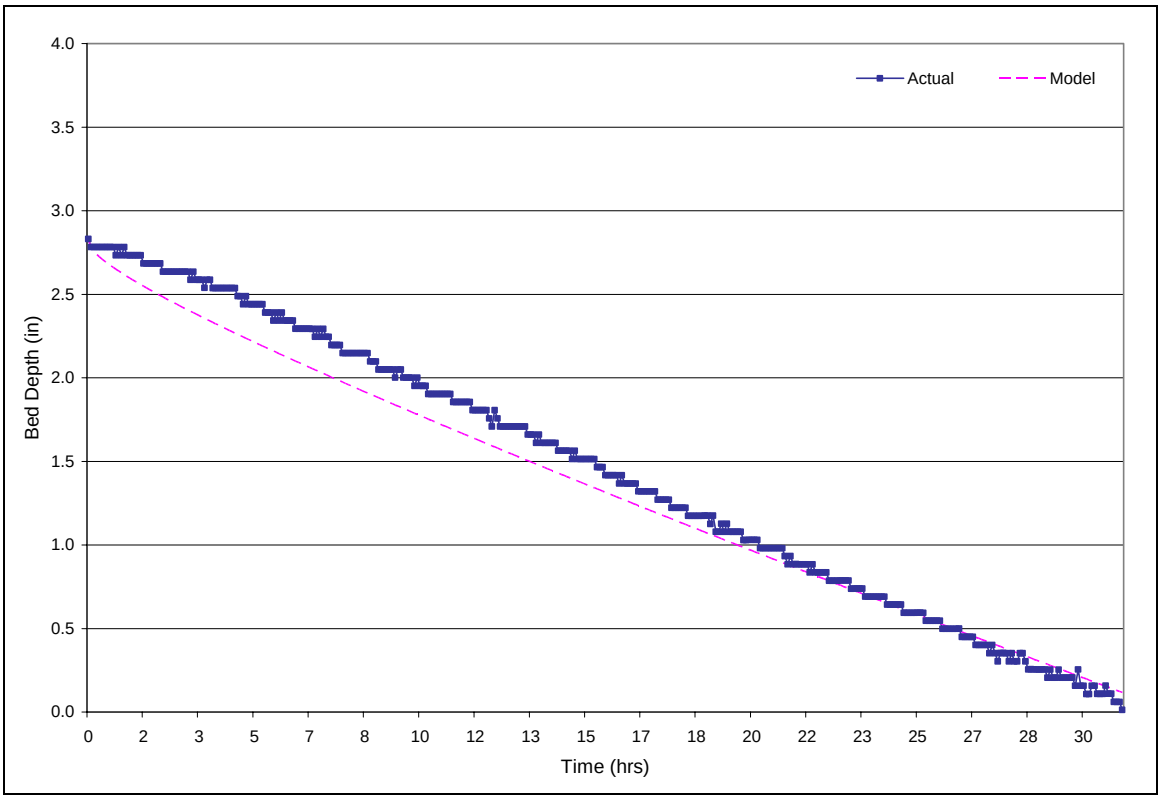

Figure Q-5. Recession Limb Event 09/27/2005

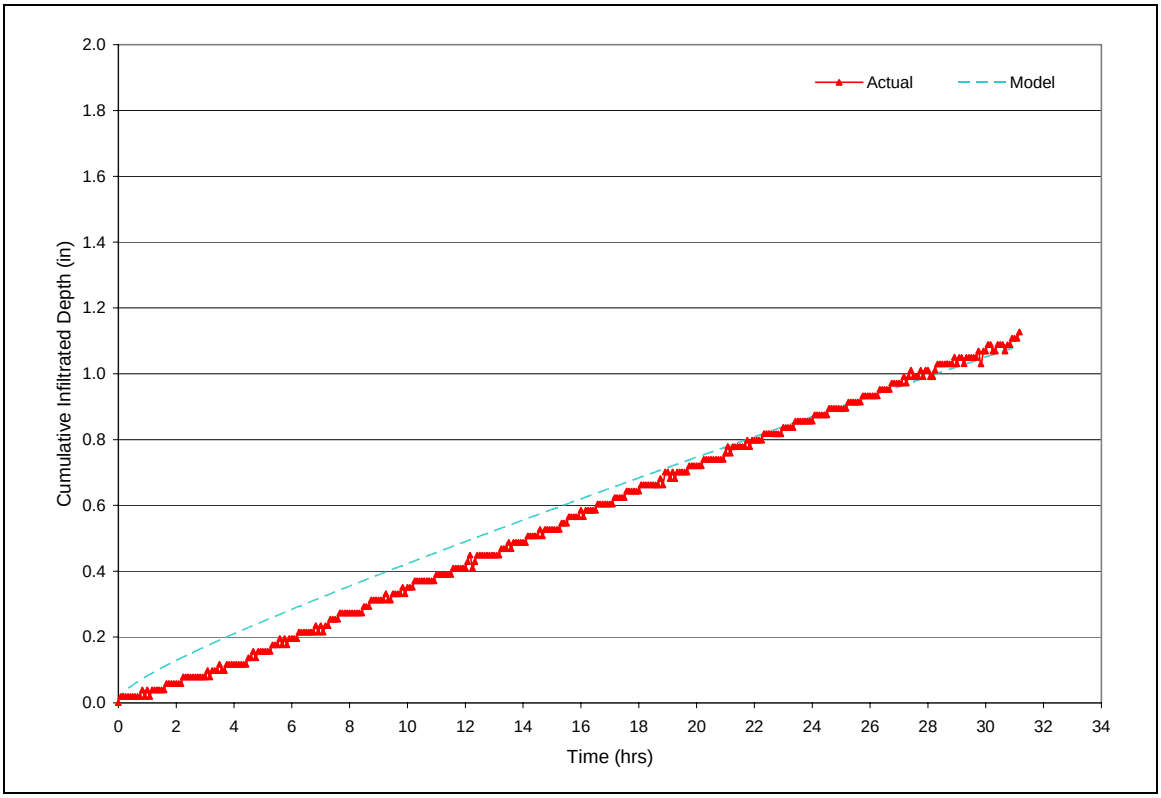

Figure Q-6. Cumulative Infiltrated Depth Event 09/27/2005

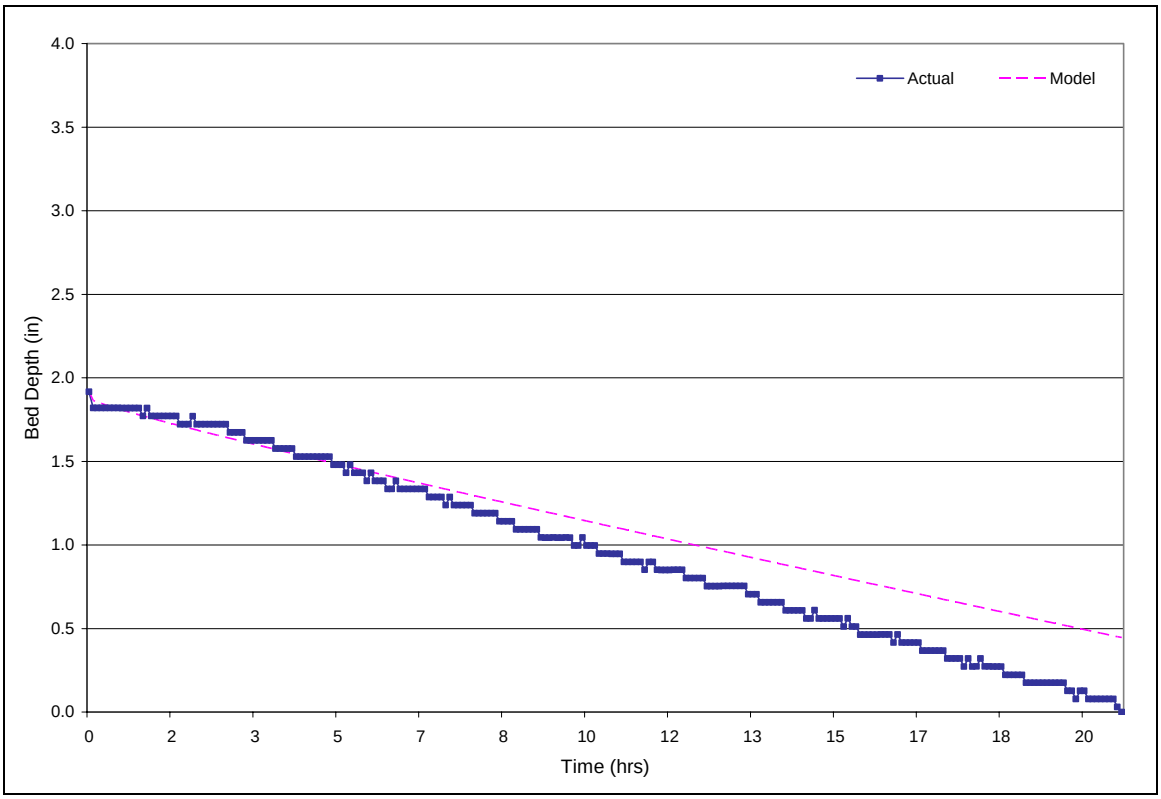

Figure Q-7. Recession Limb Event 10/17/2003

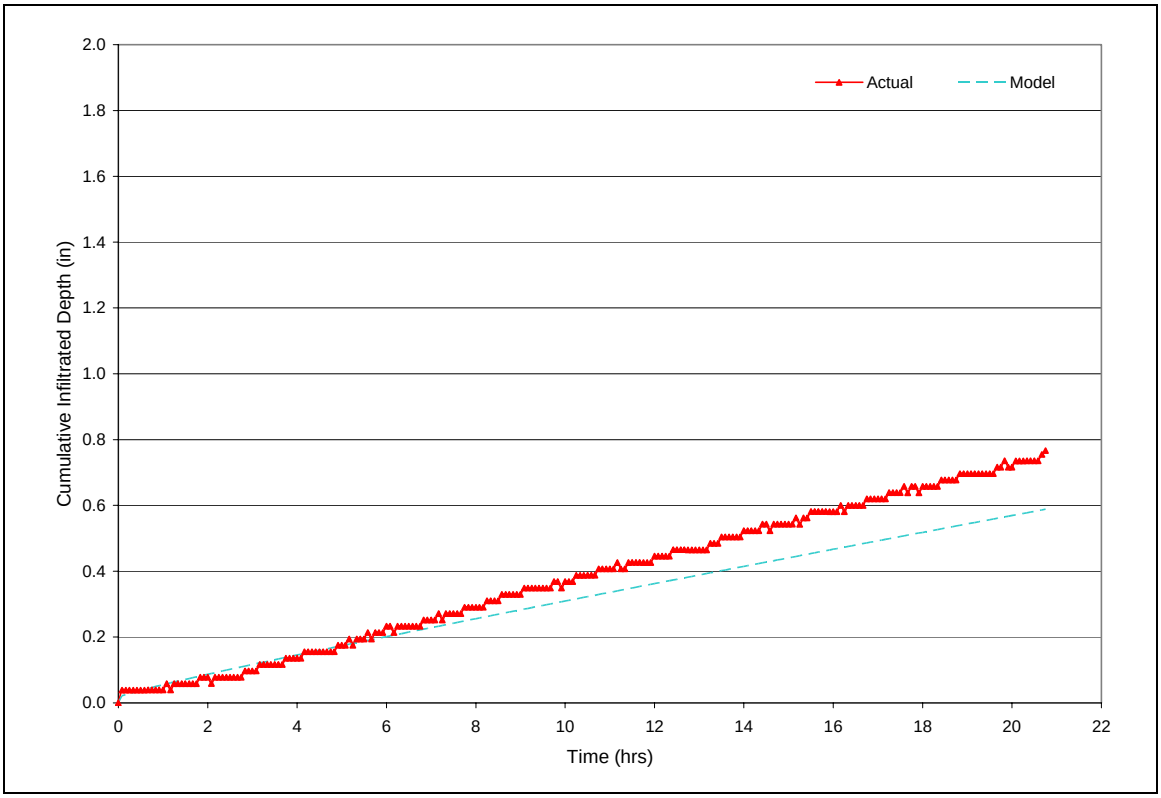

Figure Q-8. Cumulative Infiltrated Depth Event 10/17/2003

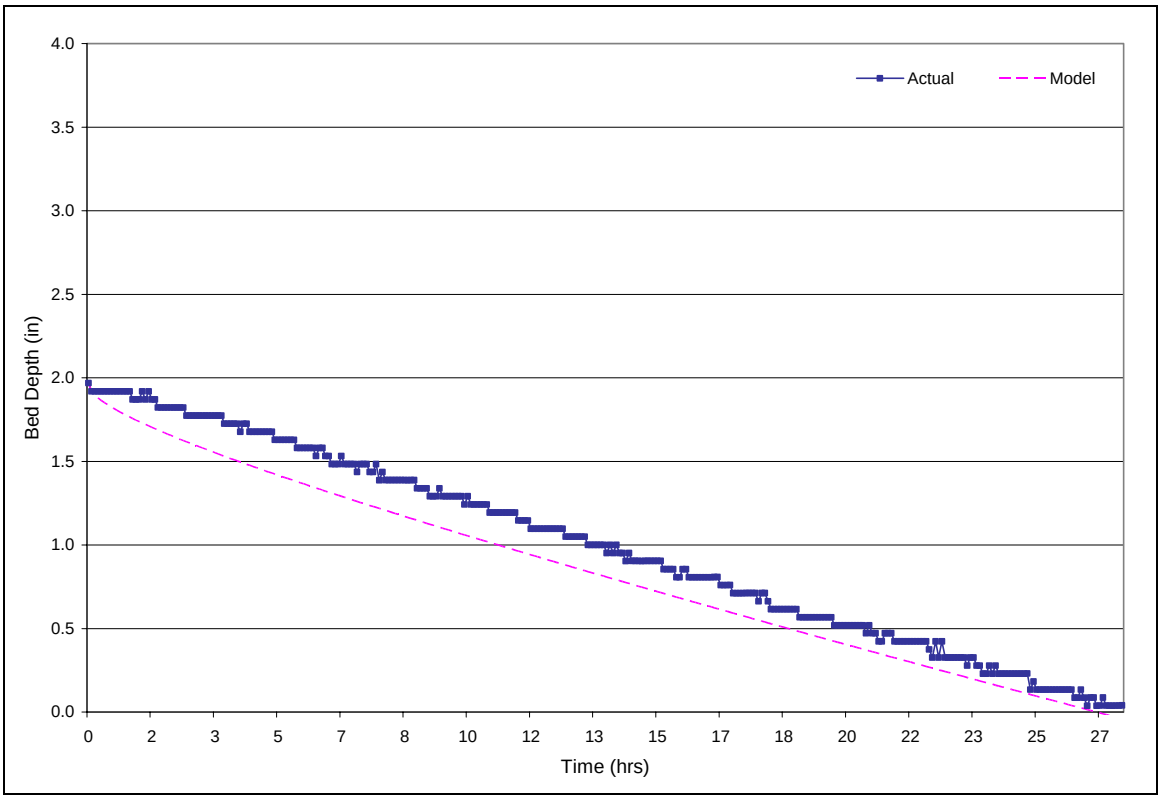

Figure Q-9. Recession Limb Event 11/04/2003

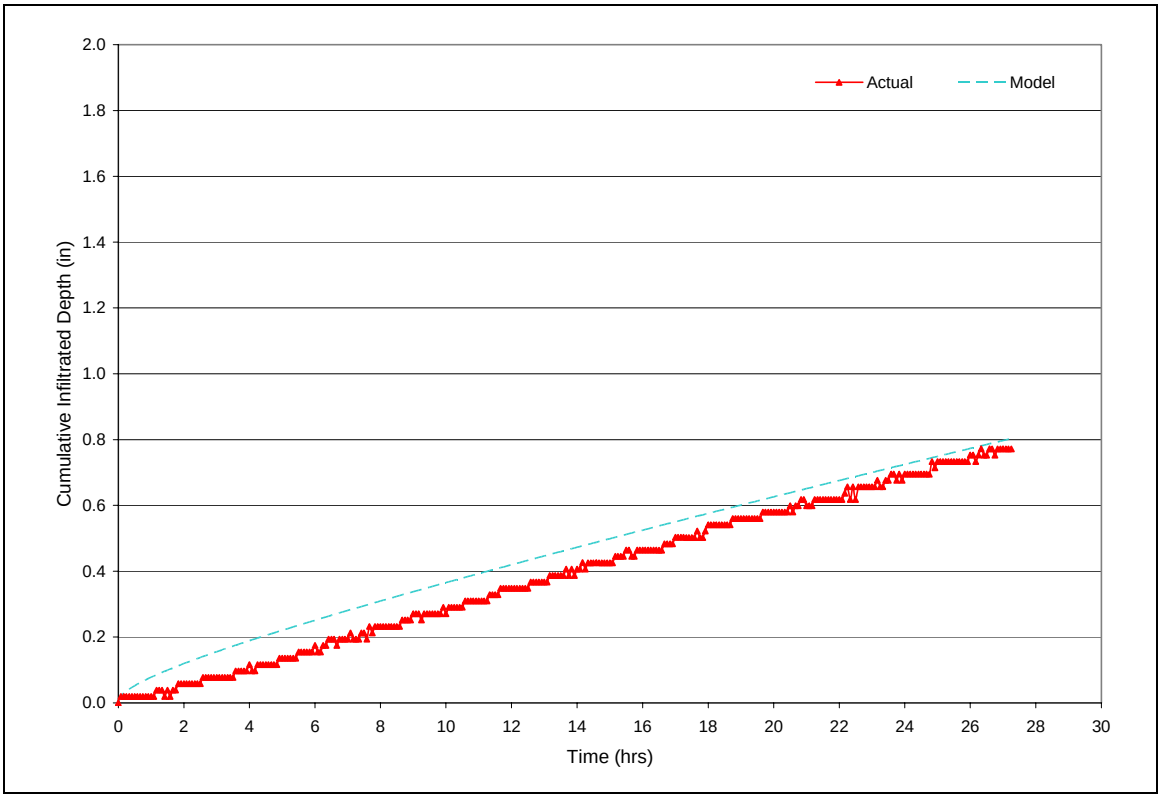

Figure Q-10. Cumulative Infiltrated Depth Event 11/04/2003

Appendix R – Model Verification: Large Event Results

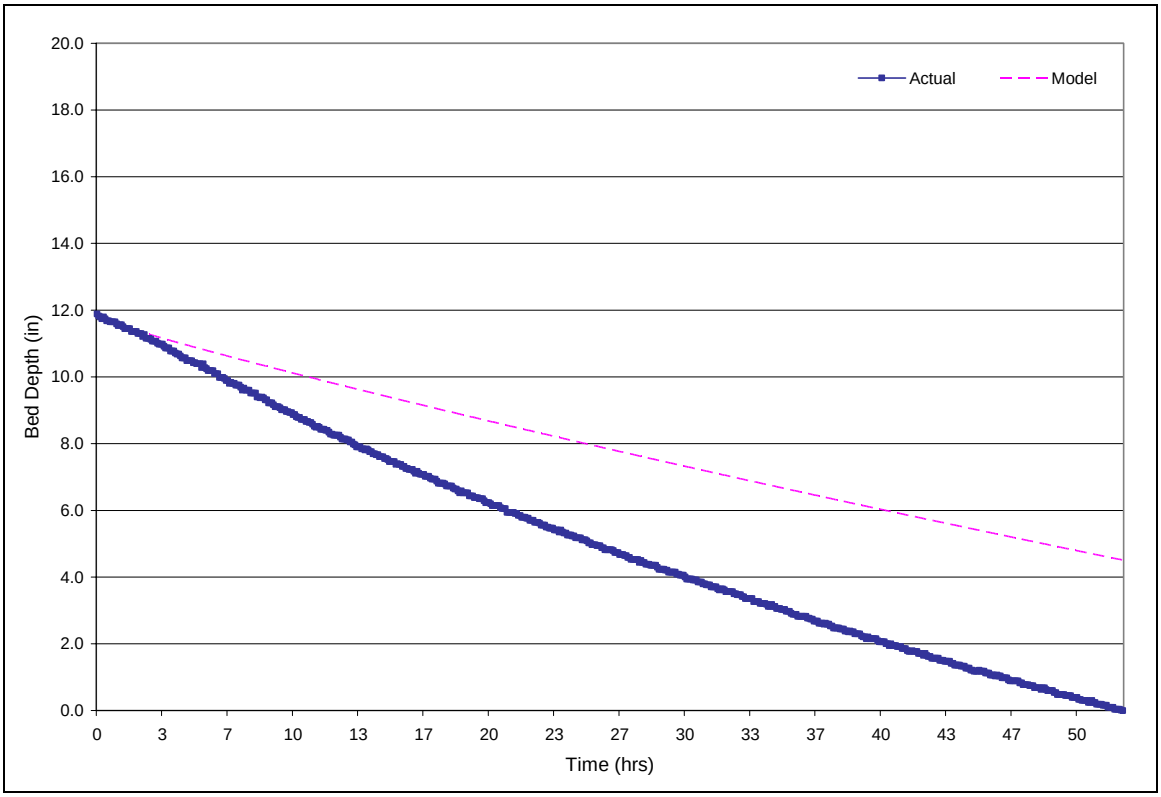

Figure R-1. Recession Limb Event 09/18/2003

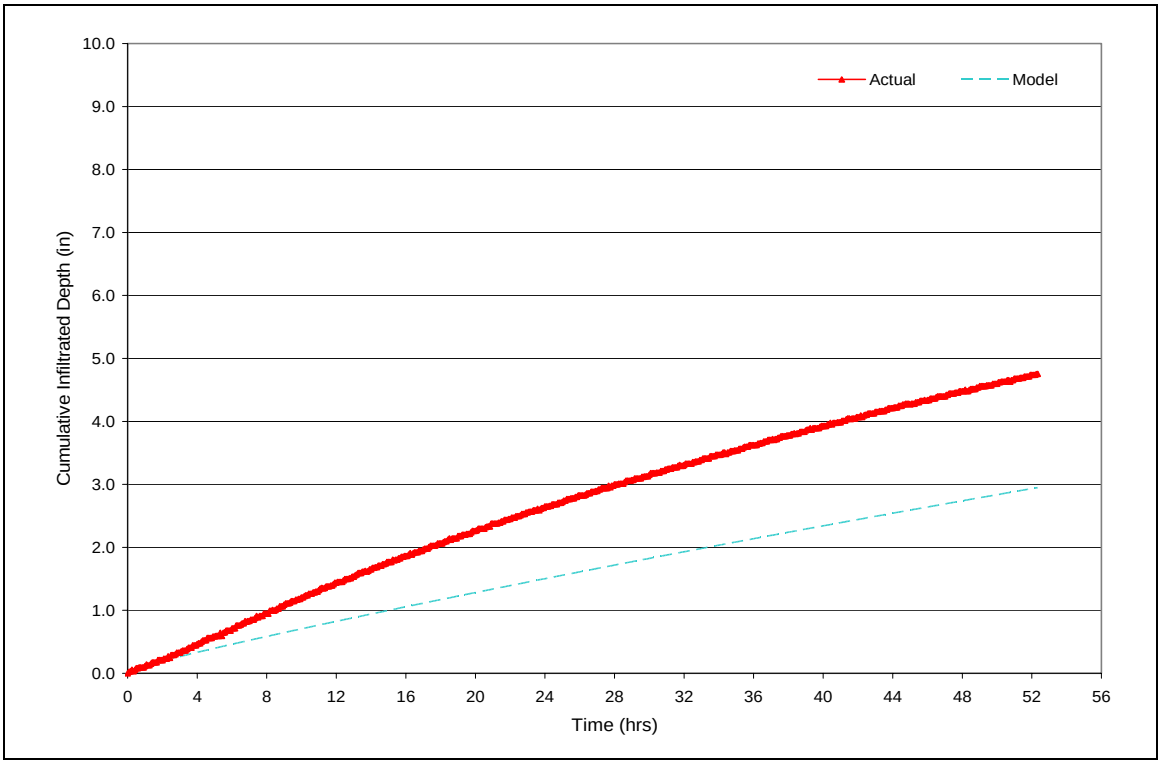

Figure R-2. Cumulative Infiltrated Depth Event 09/18/2003

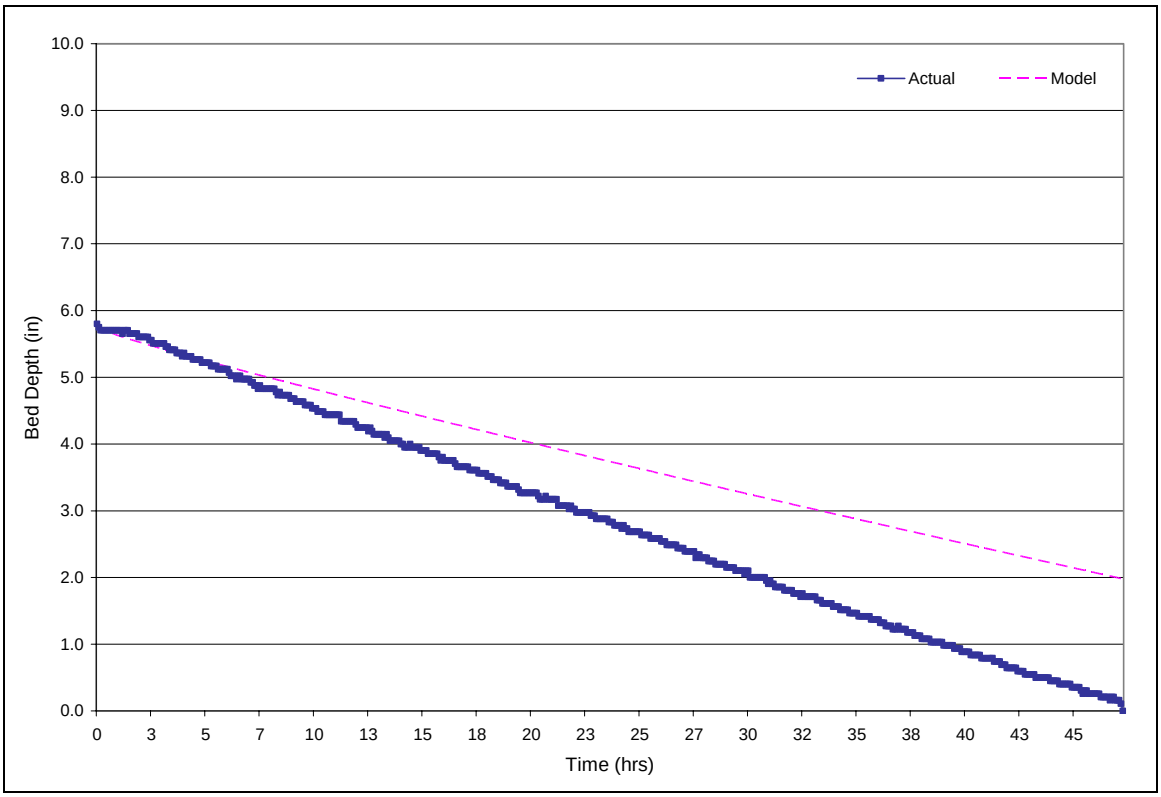

Figure R-3. Recession Limb Event 09/22/2003

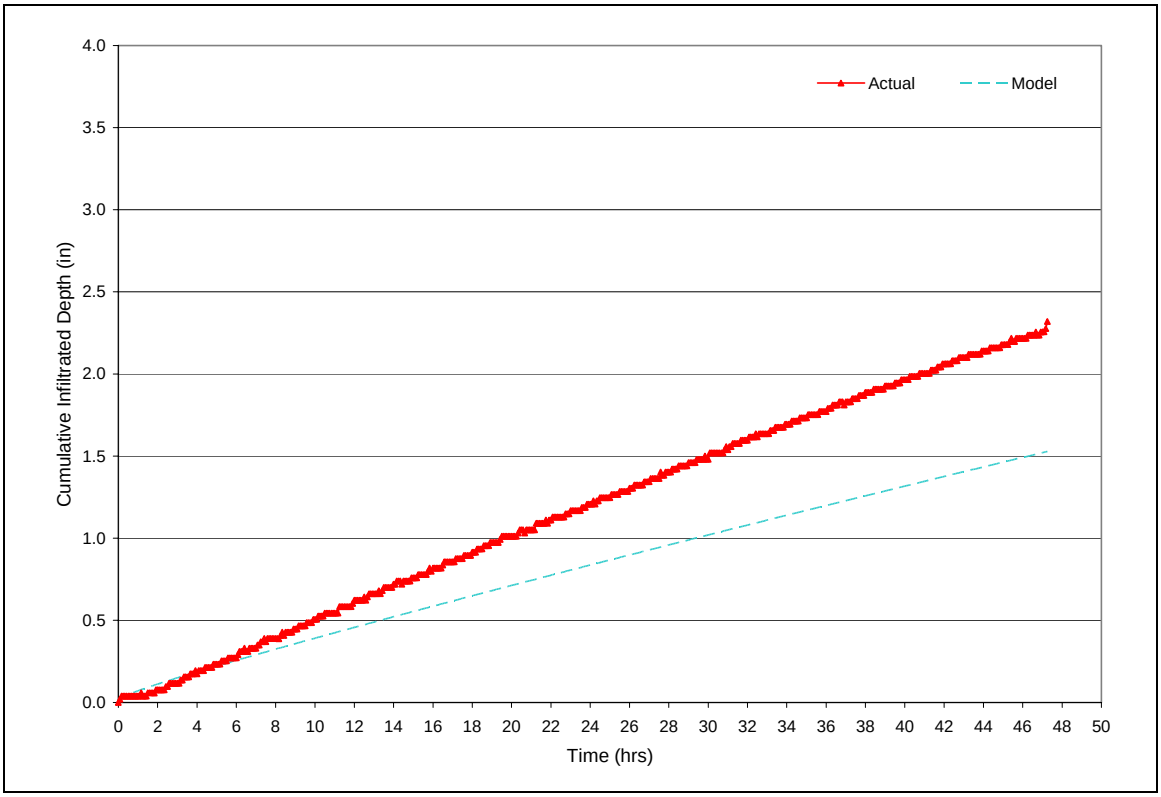

Figure R-4. Cumulative Infiltrated Depth Event 09/22/2003

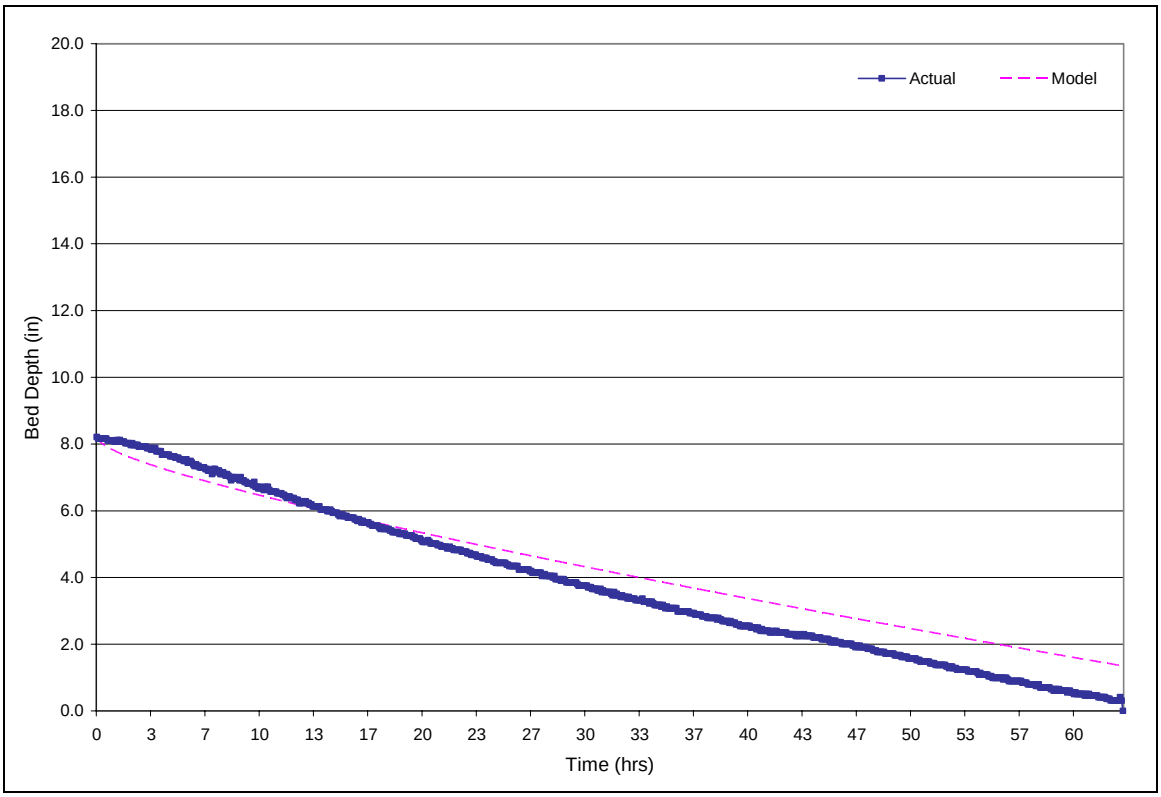

Figure R-5. Recession Limb Event 10/14/2003

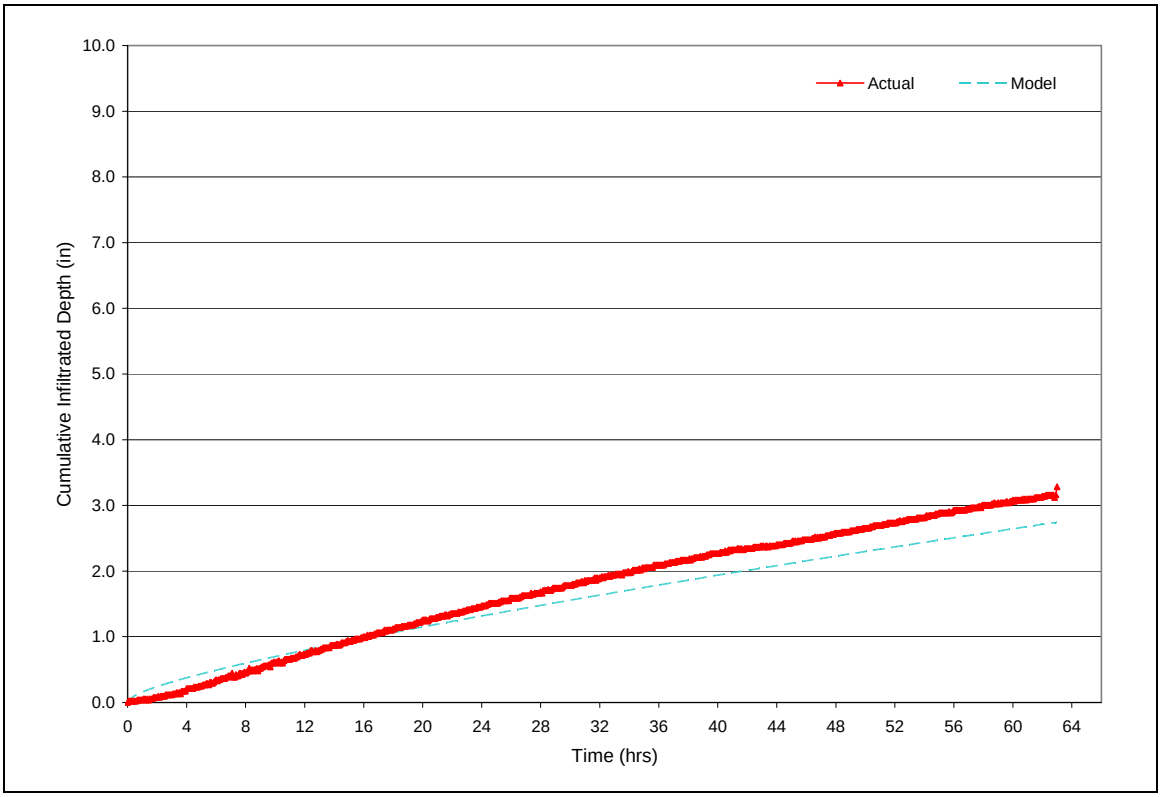

Figure R-6. Cumulative Infiltrated Depth Event 10/14/2003

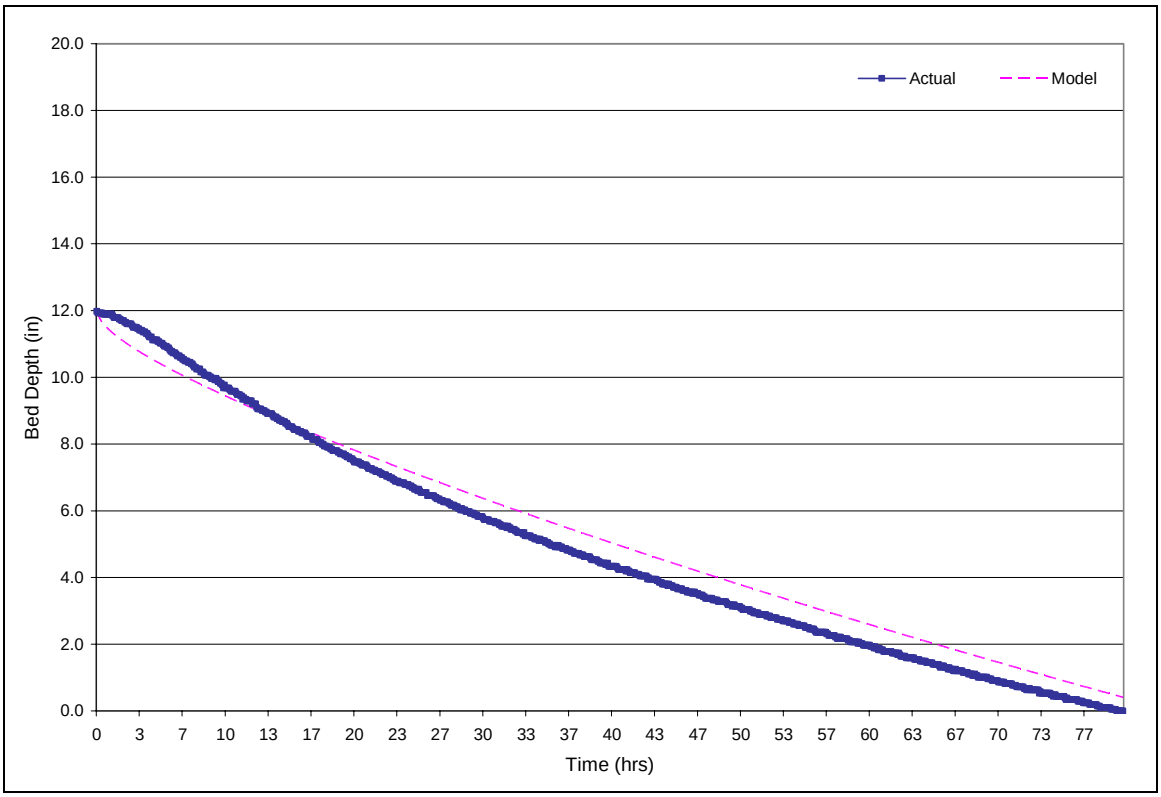

Figure R-7. Recession Limb Event 11/19/2003

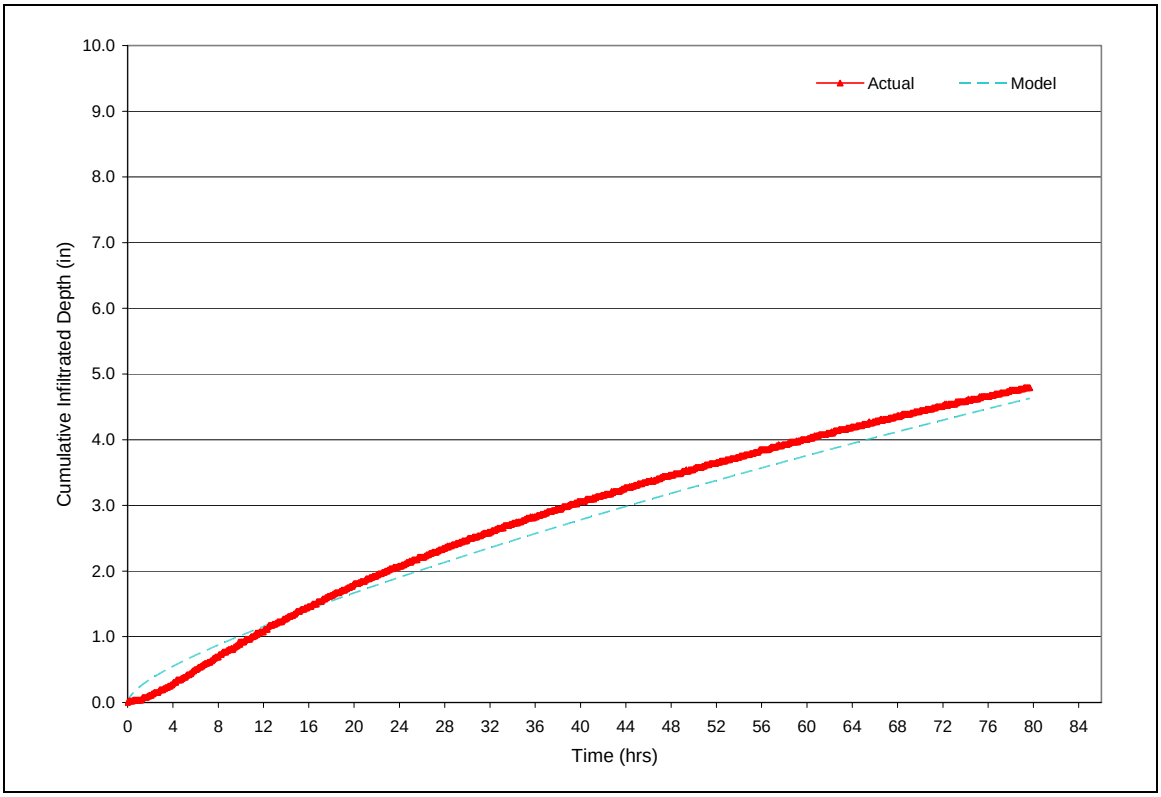

Figure R-8. Cumulative Infiltrated Depth Event 11/19/2003

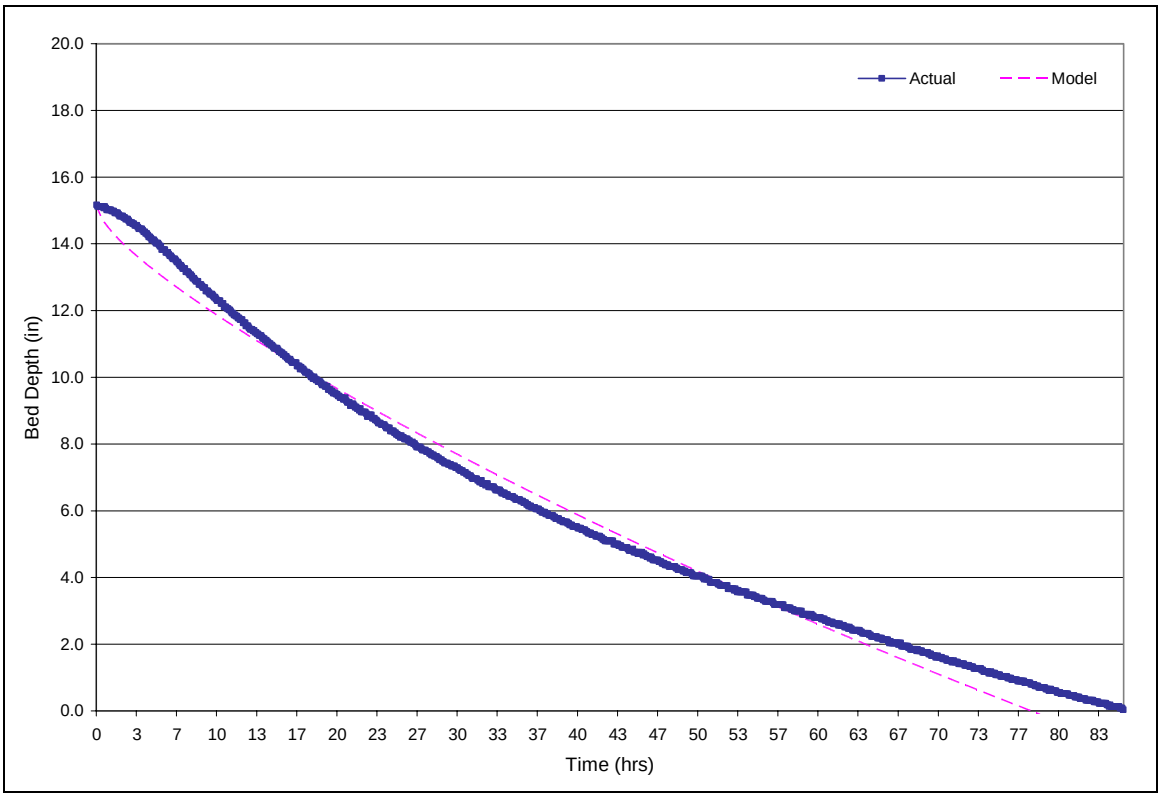

Figure R-9. Recession Limb Event 12/23/2003

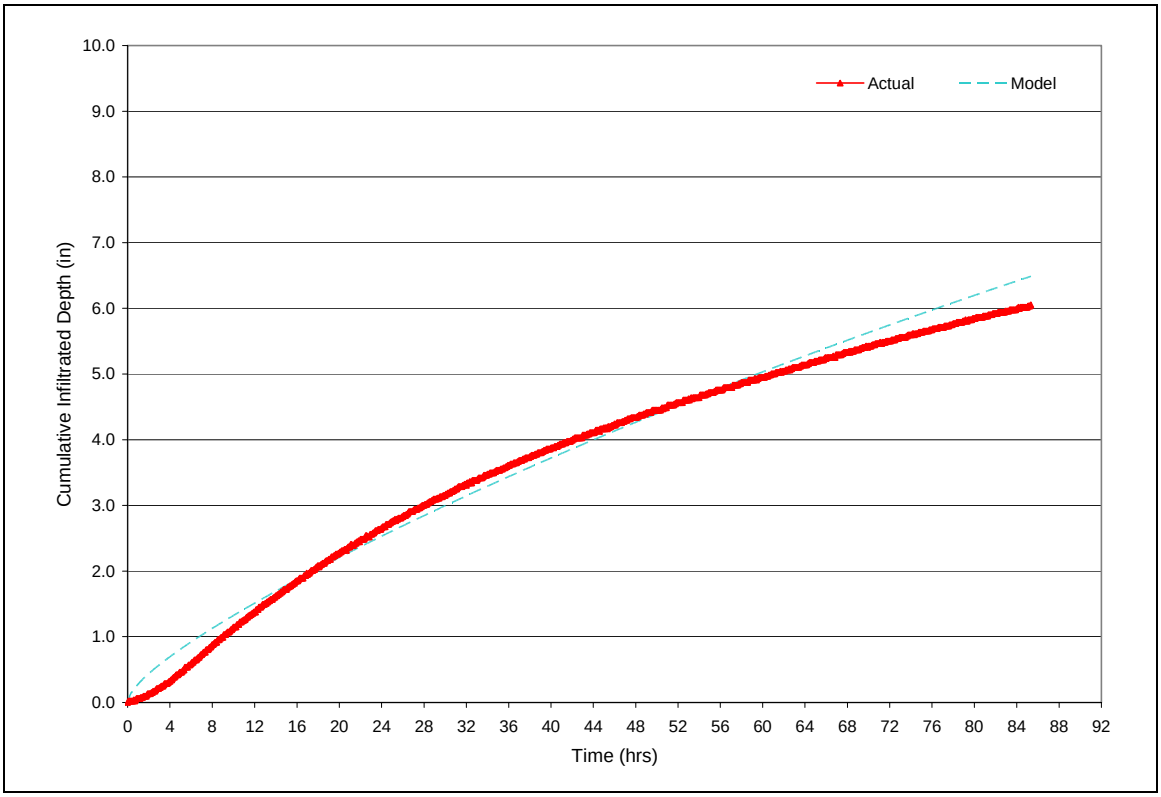

Figure R-10. Cumulative Infiltrated Depth Event 12/23/2003

Appendix S – Infiltration Rate Analysis: Small Event Results

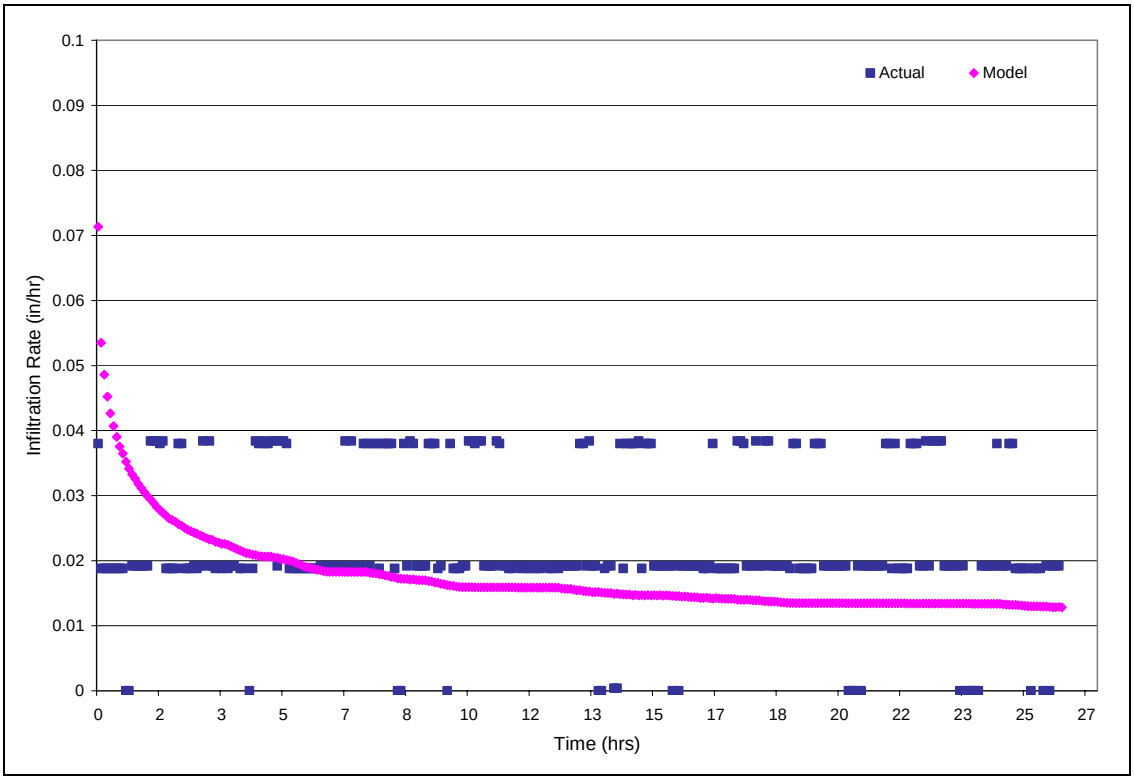

Figure S-1. Infiltration Rate vs. Time Event 01/11/2005

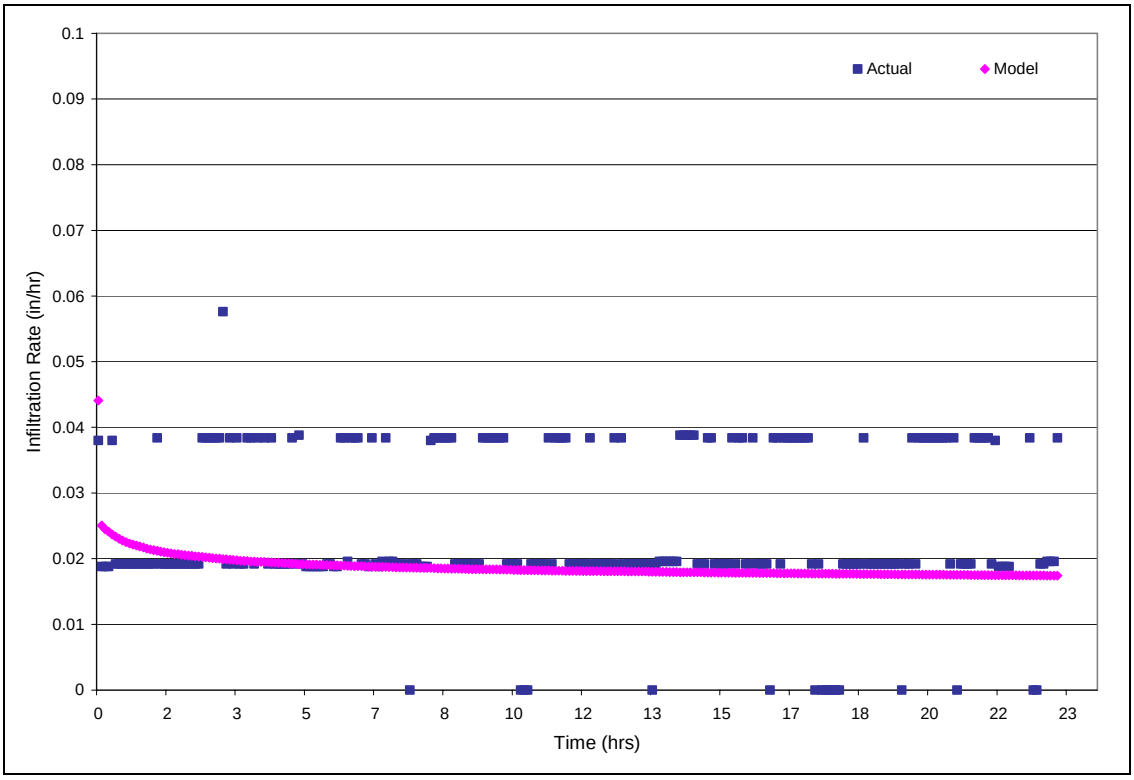

Figure S-2. Infiltration Rate vs. Time Event 04/07/2005

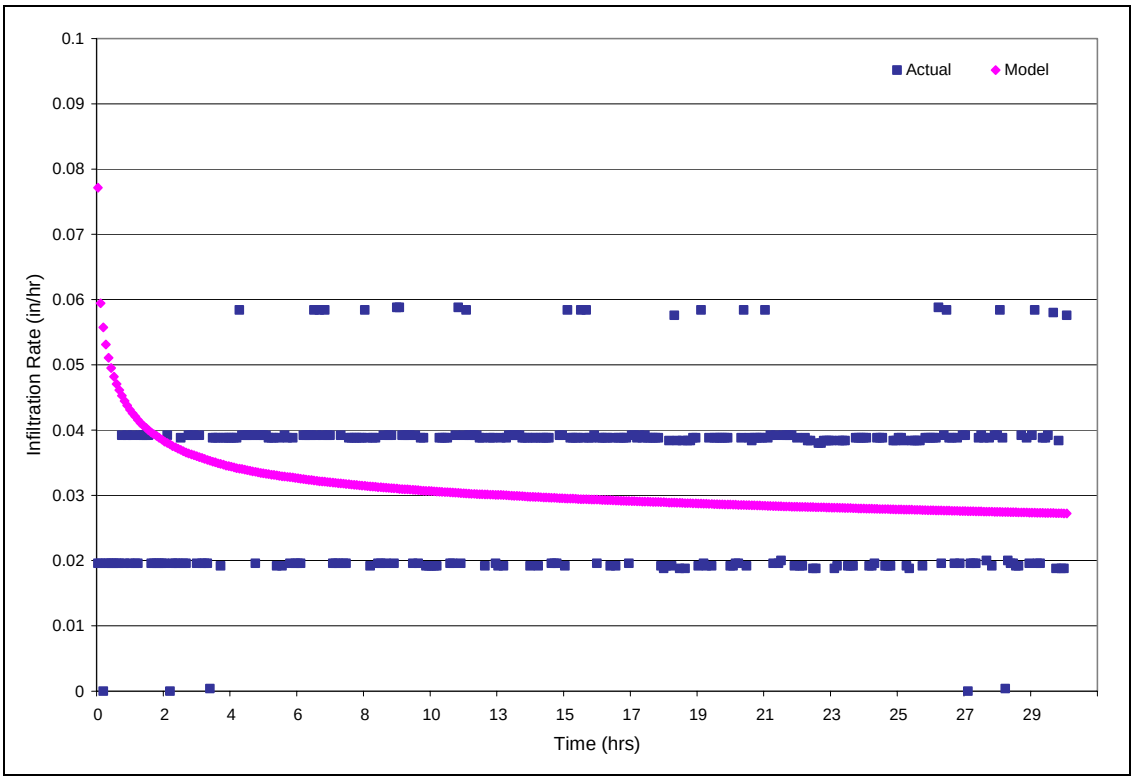

Figure S-3. Infiltration Rate vs. Time Event 09/27/2003

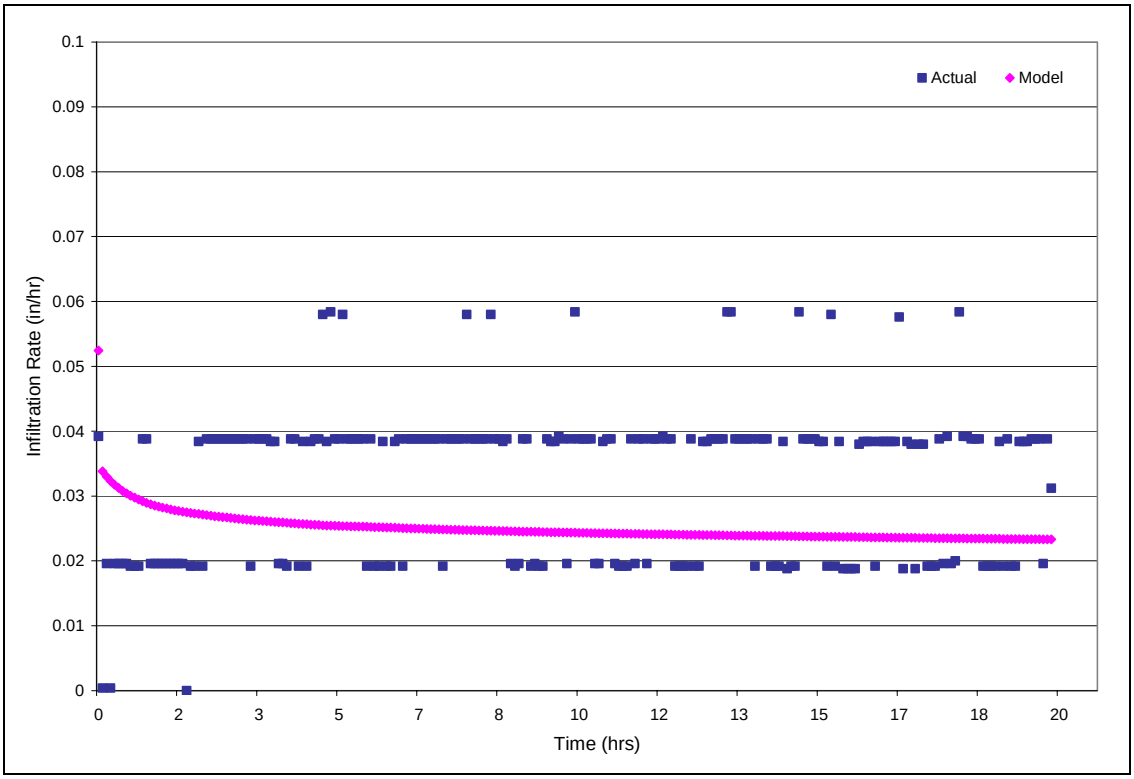

Figure S-4. Infiltration Rate vs. Time Event 10/17/2003

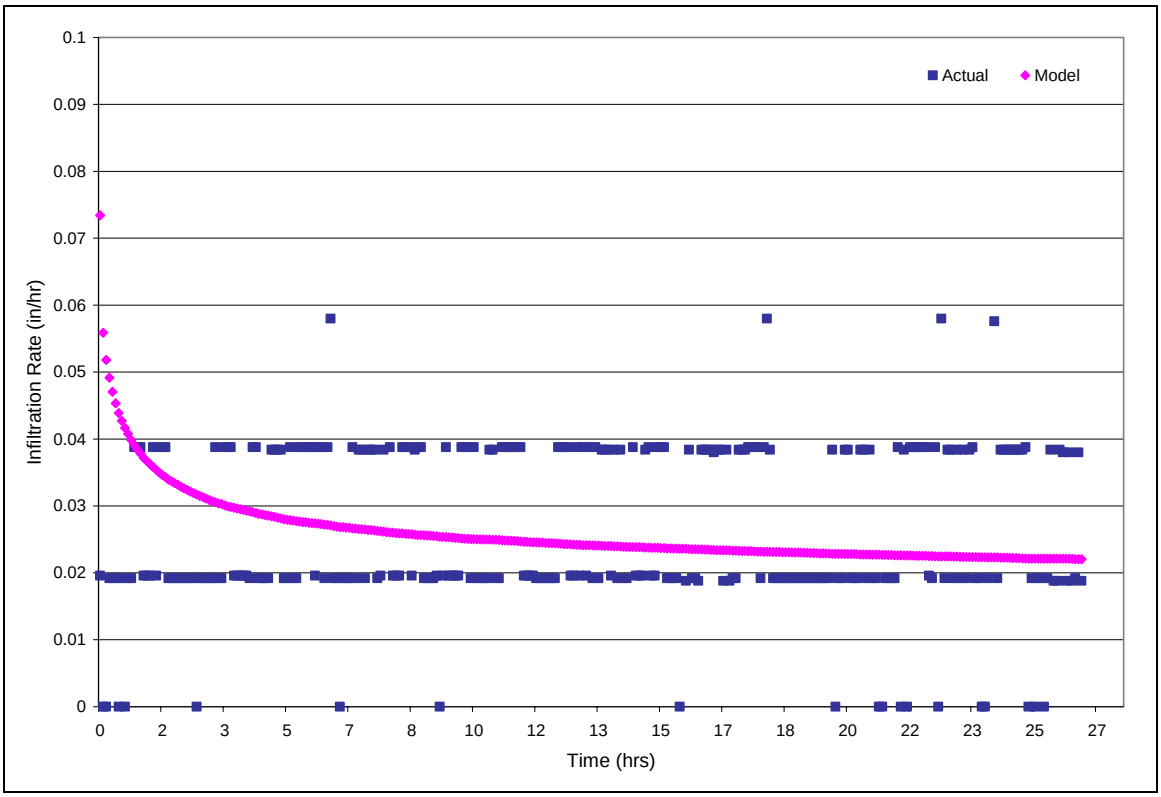

Figure S-5. Infiltration Rate vs. Time Event 11/04/2003

Appendix T – Infiltration Rate Analysis: Large Event Results

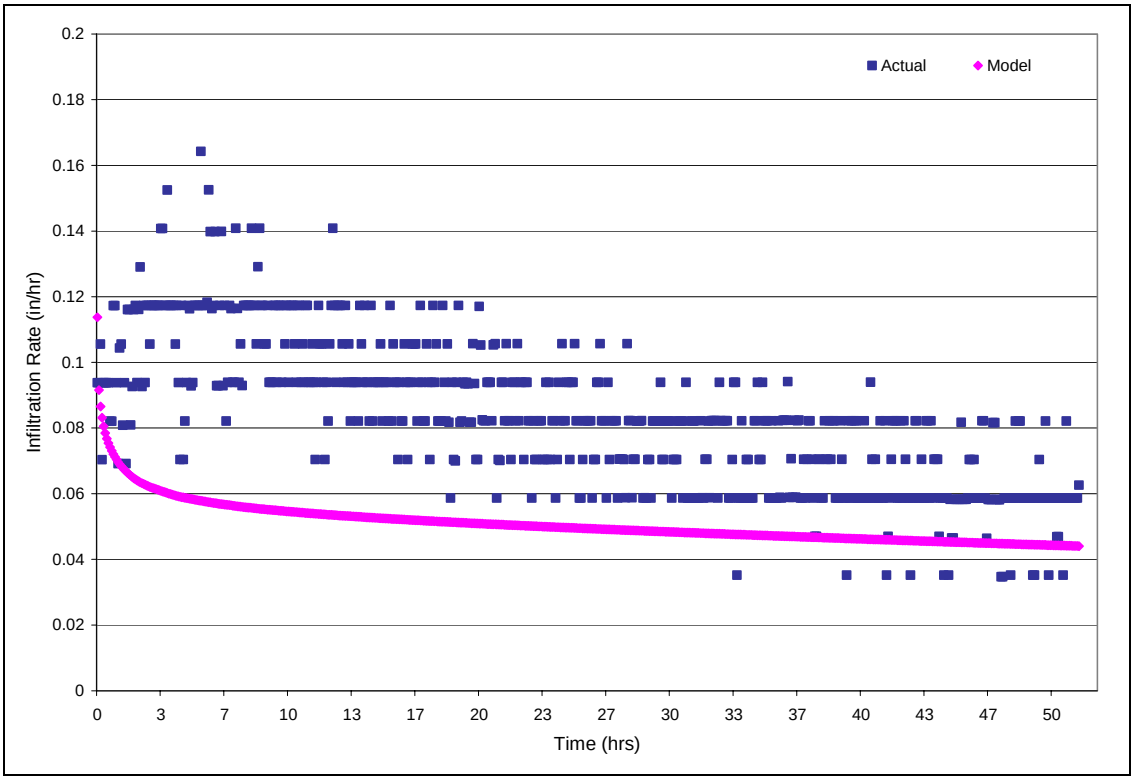

Figure T-1. Infiltration Rate vs. Time Event 09/18/2003

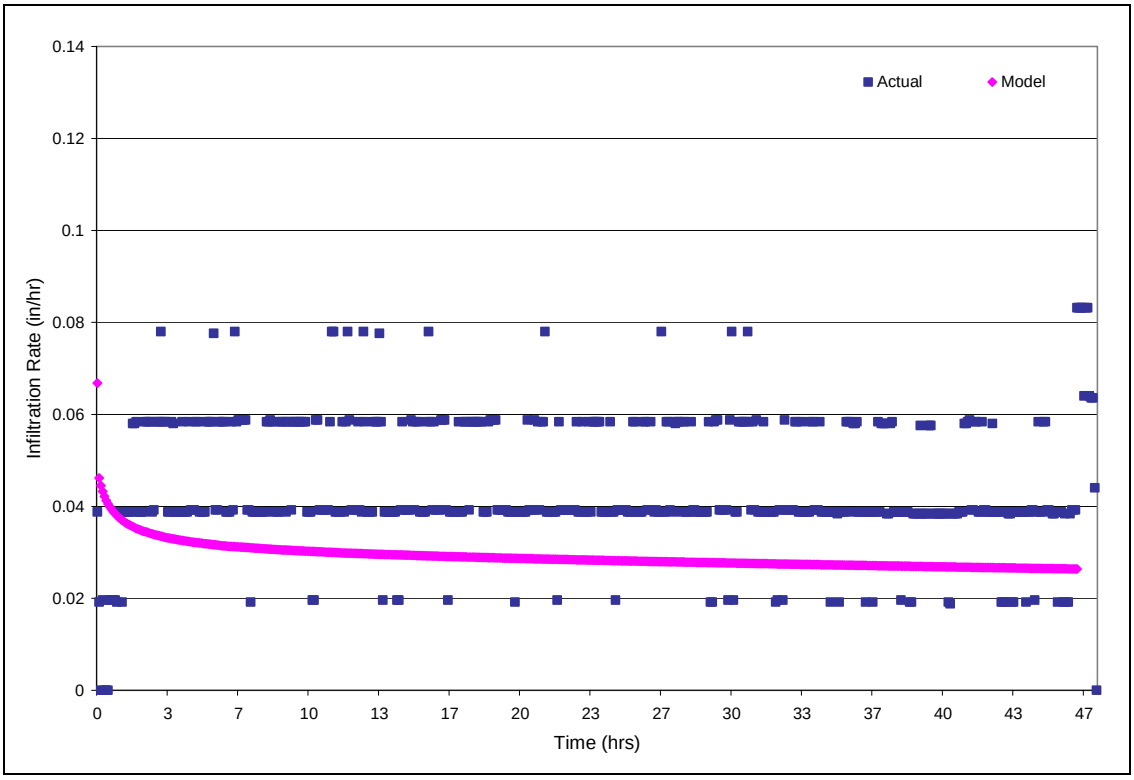

Figure T-2. Infiltration Rate vs. Time Event 09/22/2003

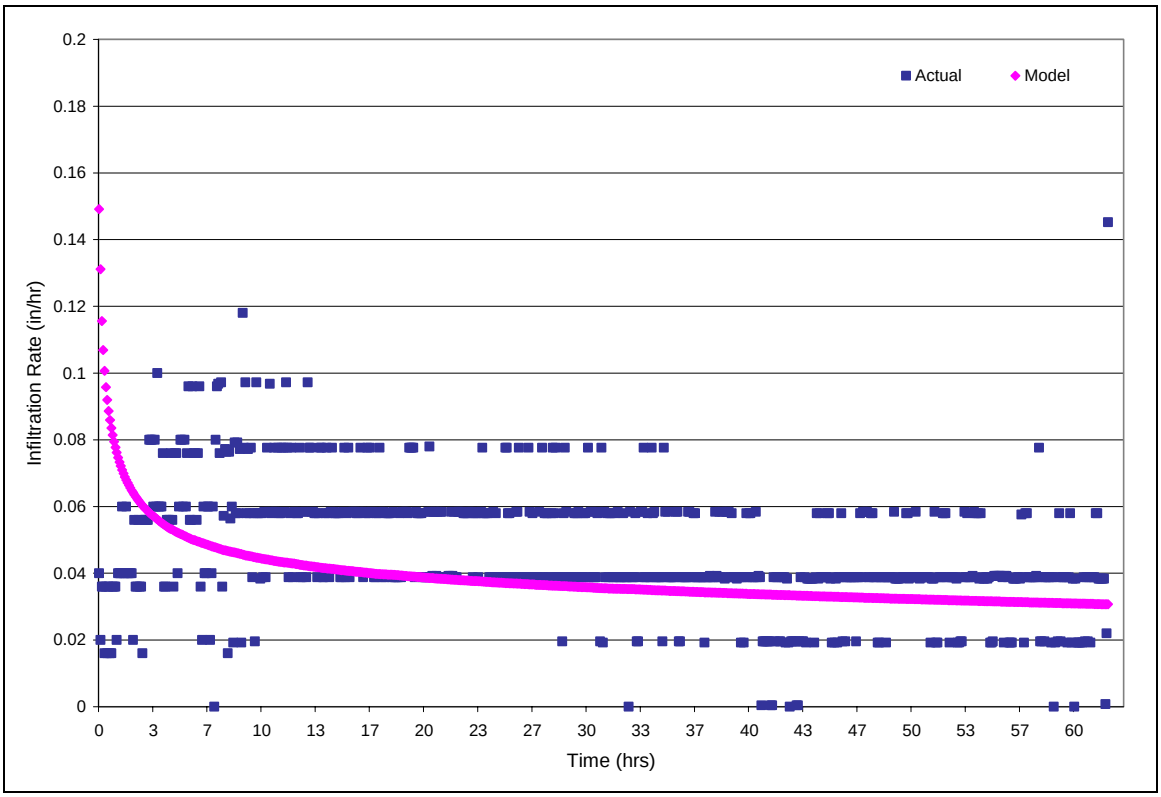

Figure T-3. Infiltration Rate vs. Time Event 10/14/2003

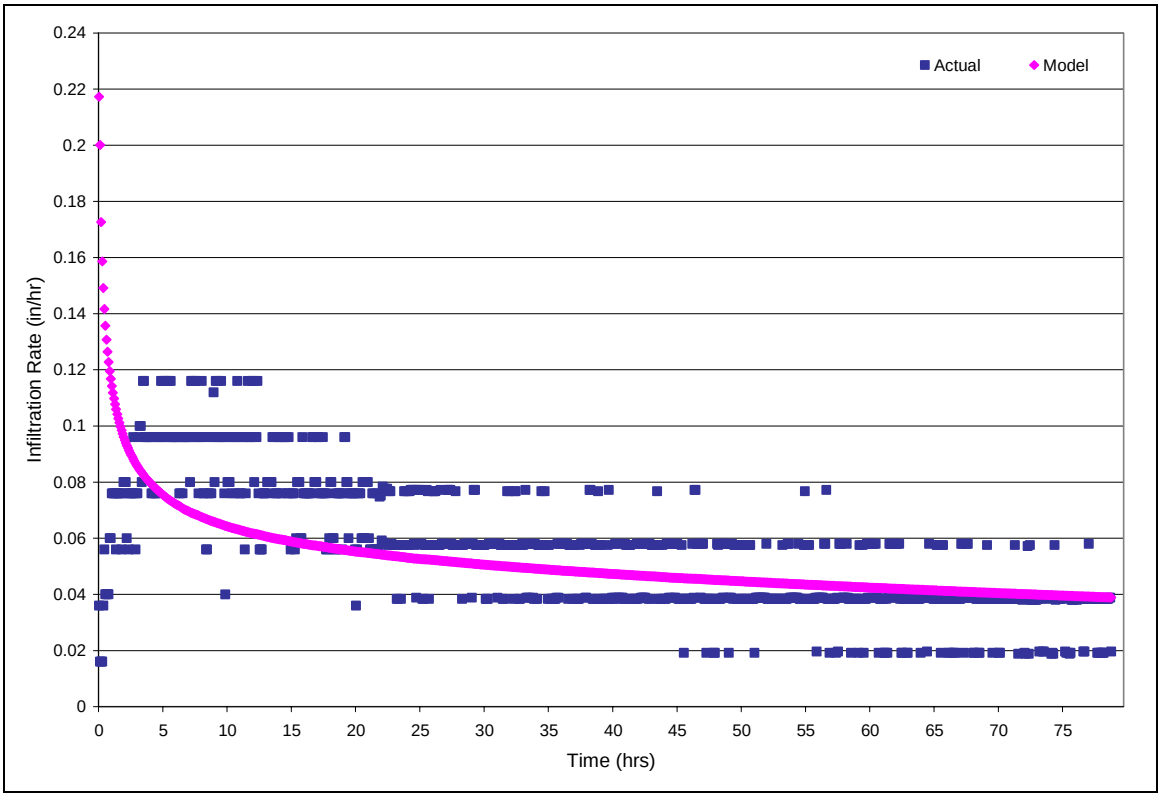

Figure T-4. Infiltration Rate vs. Time Event 11/19/2003

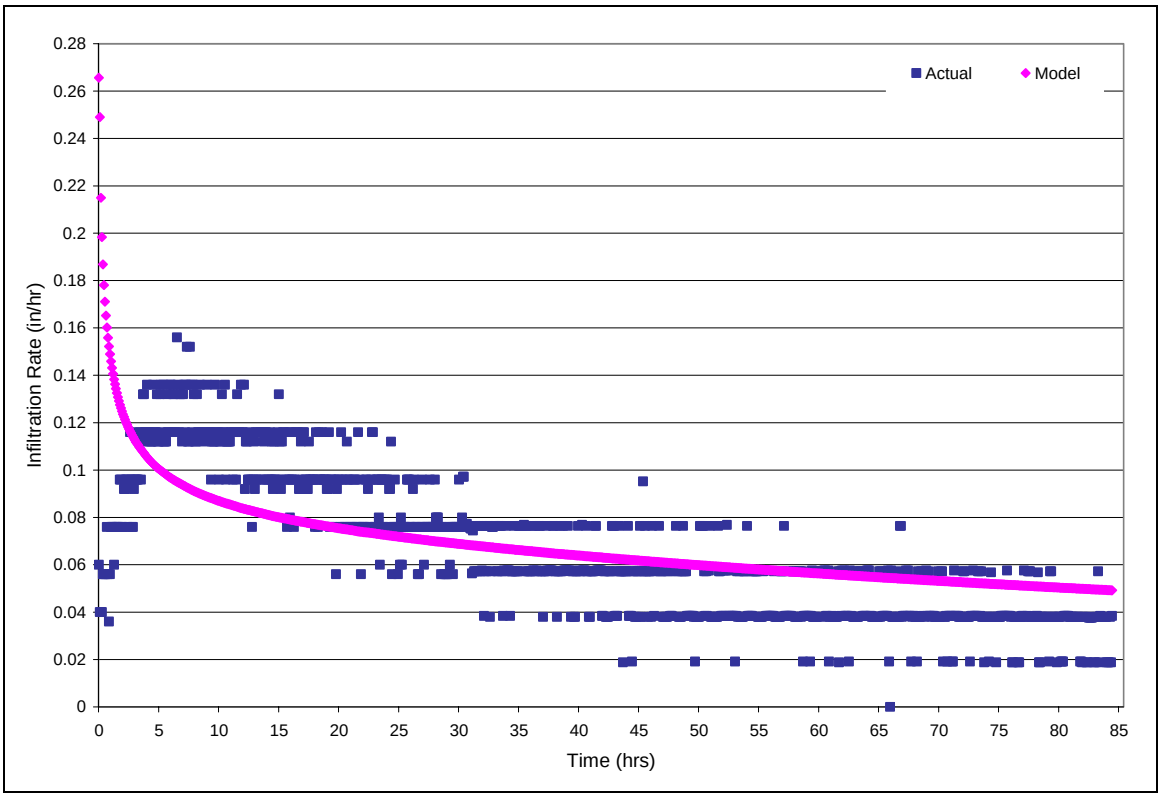

Figure T-5. Infiltration Rate vs. Time Event 12/24/2003